

**A GENERIC APPROACH FOR THE STUDY OF
HIGHER-ORDER MODE PROPAGATION IN
CIRCULAR DUCTS WITH SIMPLE APERTURE
DEVICES**

by


Yikun Hu

A Doctoral Thesis

*Submitted in partial fulfillment of the requirements
for the award of
Doctor of Philosophy of Loughborough University*

January 2007

© by Yikun Hu, 2007

 <p>Liverpool University Pilkington Library</p>
Date <i>July 2008</i>
Class <i>T</i>
Acc No. <i>0403474388</i>

ABSTRACT

The aim of the work reported in this thesis is to establish a generic approach for the study of the propagation of higher-order modes in ducts of circular cross section when a simple aperture device is installed in the duct. Additionally to describe the effects of the simple aperture device on the whole in duct acoustic field, especially in the frequency range after the first higher-order mode cuts on. The approach, which is based on approximating each higher-order mode as an uncoupled mode, requires an accurate and effective decomposition of the in duct field in the higher frequency range.

In the theoretical work for the propagation of the higher-order modes in circular ducts, one established model to describe the open end of the duct is considered. Another model to describe the sound source (both plane wave source and point source) and the boundaries between the aperture device and the main duct is proposed. Combining the two models together, a revised model to describe the whole acoustic system is obtained and used to carry out the in duct field decomposition in the higher frequency range. From this the amplitudes of various higher-order modes are obtained. Experimental investigations have also been carried out to determine the applicability of this model. The experimental work can be divided into two groups: reference measurements for the inputs to the models and direct measurements of the sound fields. The reference measurements are used to obtain the strength of the sound source. The direct measurements are used to compare with the results obtained from the theoretical calculations. Through the comparison, the errors and the applicability of the theoretical model are established. It is shown that this approach to the problem may be used in the normalized wave number region up to $k * R < 7$, which is nearly four times the plane wave region and includes sixteen propagating higher-order modes.

By determining the amplitudes of the higher-order modes, the whole in-duct acoustic field is fully decomposed into individual model contributions and can be reconstructed in detail. In order to get a complete and coordinate-independent description of the effects of installing different simple aperture devices, the power radiated out of the open end of

the duct is calculated in the form of different single modes. Additionally the insertion losses for different aperture device situations are also obtained. Then through the comparison of the powers and the insertion losses, it is possible to find an effective and direct way to express the effects of installing different simple aperture devices in a duct.

Key words: higher-order modes, simple aperture device, circular duct, normalized wave number, insertion loss (*IL*), radiated power.

Acknowledgements

This thesis is the final academic research report for my PhD registration at Loughborough University. I would like to thank my supervisor, Dr. Jane L. Horner, who introduced me to the subject of noise control in ducts. Thanks for Dr. Horner's great help and valuable comments.

I would also like to thank my family and friends for their consistent support and kindly help. Particularly, my mother and my parents-in-law gave me a lot of both material and spiritual support during my four years' hard work. I greatly appreciate everything they have done for me.

Thirdly, I gratefully acknowledge the Department of Aeronautics and Automotive Engineering of Loughborough University, for their generous financial aids during the four years of my research work.

Last but not least, I would like to thank my beloved wife Haiyan, my adorable daughters Xiaoyu and Xiaoyue, because of whom I am where I am today.

CONTENTS

Notation

Chapter

Page

1. Introduction	1
1.1 Background	1
1.2 Literature review	2
1.2.1 The plane wave propagation and reflection by duct termination	3
1.2.2 Analytical description of higher-order modes	4
1.2.3 Measurement methods for the acoustic properties in circular ducts	6
1.2.4 Higher-order mode experimental decomposition methods	9
1.2.5 Effects of the orifice plates on the acoustic field	11
1.2.6 Model for the description of the aperture device boundary condition	13
1.3 Present work	15
2. The plane wave propagation in a circular duct	19
2.1 Introduction	19
2.2 Theoretical derivation	19
2.3 Lumped-parameter model (acoustical two-ports system model)	22
2.3.1 Duct without simple aperture devices	22
2.3.2 Duct with simple aperture devices	24
2.4 Blocked particle velocity method	26
2.5 Two-different-inputs method	29
2.6 Discussion	34
3. Higher-order mode propagation in a circular duct and the reflection coefficients R_{mL} at the duct open end	35
3.1 Introduction	35

3.2 Higher-order mode in circular cross-section duct	36
3.3 Applicability of lumped-parameter model to higher-order modes in circular duct	41
3.4 Model to calculate the reflection coefficients R_{mnL} at the open end of the duct	44
3.5 Generalized impedances Z_{mnL} and reflection coefficients R_{mnL}	48
3.6 Discussion	58
4. The plane wave source and the point source	59
4.1 Introduction	59
4.2 The plane wave source	59
4.2.1 Configuration of the plane wave source	59
4.2.2 Description of the plane wave source boundary condition	60
4.3 The point source	65
4.3.1 Configuration of the point source	65
4.3.2 Description of the point source boundary condition	66
4.4 Discussion	72
5. Sound field produced by a point source propagating in a circular duct without simple aperture devices	73
5.1 Introduction	73
5.2 Experimental set-up	73
5.3 Experimental decomposition of the in duct acoustic field	75
5.3.1 Theoretical derivation for experimental decomposition approach	75
5.3.2 Experimental decomposition results	77
5.4 Theoretical decomposition approach of the in duct acoustic field	79
5.4.1 Theoretical derivation	81
5.4.2 Experiment measurements and results	83
5.4.3 Effects of the radial location of the sound source on prediction	87
5.4.4 Prediction for the different circumferential positions	90
5.5 Discussion	93

6. Sound wave produced by a plane wave source propagating in a circular duct without simple aperture devices	95
6.1 Introduction	95
6.2 Theoretical derivation	95
6.3 Experiment measurements and results	97
6.4 Difference between the coupled and uncoupled prediction	104
6.5 Effects of the length of the duct on prediction	107
6.6 Effects of the radial location of the sound source on the prediction	111
6.7 Predictions for different circumferential positions	112
6.8 Discussion	115
7. Sound field produced by a point source propagating in a circular duct with simple aperture devices	117
7.1 Introduction	117
7.2 Aperture device with a single orifice	117
7.2.1 Theoretical derivation	117
7.2.2 Experimental set-up and measurement results	128
7.2.3 Comparison of coupled and uncoupled predictions	131
7.2.4 Comparison of predictions with direct measurements for a device with single orifice	133
7.3 Aperture device with two orifices	139
7.3.1 Theoretical derivation	139
7.3.2 Experimental set-up	151
7.3.3 Comparison of predictions with direct measurements for a device with two orifices	151
7.4 Aperture device with several orifices	156
7.4.1 Theoretical derivation	156
7.4.2 Experimental set-up	157
7.4.3 Comparison of predictions with direct measurements for a device with several orifices	157
7.5 Error analysis	162
7.6 Discussion	165

8. Sound field produced by a plane wave source propagating in a circular duct with simple aperture devices	166
8.1 Introduction	166
8.2 Aperture device with a single orifice	166
8.2.1 Theoretical derivation	166
8.2.2 Experimental set-up and measurement results	168
8.2.3 Comparison of coupled and uncoupled predictions	171
8.2.4 Comparison of predictions with direct measurements for a device with single orifice	173
8.3 Aperture device with two orifices	178
8.3.1 Theoretical derivation	178
8.3.2 Experimental set-up	179
8.3.3 Comparison of predictions with direct measurements for a device with two orifices	179
8.4 Aperture device with several orifices	184
8.4.1 Theoretical derivation	184
8.4.2 Experimental set-up	184
8.4.3 Comparison of predictions with direct measurements for a device with several orifices	185
8.5 Error analysis	189
8.6 Predictions for different circumferential positions both before and after aperture device	191
8.7 Discussion	195
9. Radiated power and the insertion loss for different aperture devices	197
9.1 Introduction	197
9.2 Power radiated into and out of the main duct	198
9.2.1 Derivation of the power radiated from the open end of the duct	199
9.2.2 Approximate lumped-parameter model	206
9.2.3 Energy loss along z-axis in the main duct	208
9.2.4 Effects of the source location on the radiated power	210
9.3 Analysis of the radiated power of different single higher-order mode	212
9.3.1 Source concentric situation	212

9.3.2 Source eccentric situation	219
9.3.3 Applicability of the approximate lumped-parameter model	225
9.4 Effects of different configurations of the orifices on the insertion loss	226
9.4.1 Negative insertion loss (<i>IL</i>)	227
9.4.2 Source eccentric situation	229
9.4.3 Source concentric situation	238
9.5 Discussion	244
10. Conclusions and discussion	247
10.1 Conclusions	247
10.2 Discussion and future research suggestions	251
References	252
Appendices	258
Appendix A: Experiment equipments and set-up	258
Appendix B: Phase match of the microphone pair in the measurement	259
Appendix C: Derivation of pressure continuity boundary condition	261
Appendix D: Derivation of velocity continuity boundary condition	266
Appendix E: The procedure to calculate the amplitudes of the pressures by using reference measurement results (point source)	271
Appendix F: The procedure to calculate the amplitudes of the pressures by using reference measurement results (plane wave source)	273

Notation

A_{mn}, B_{mn}	Amplitudes of (m, n) mode in the main duct (without aperture device); Amplitudes of (m, n) mode in the before orifice field (with aperture device)
C_{mn}, D_{mn}	Amplitudes of (m, n) mode in the orifice
E_{mn}, F_{mn}	Amplitudes of (m, n) mode in the after orifice field (with aperture device)
c	Speed of sound
f	Frequency (Hz)
I	Sound intensity
IL	Insertion loss
J_m, N_m	Bessel function and Neumann function
k, k_r, k_z	Wave number, wave number along r and z -axis direction
k^*R	Normalized wave number
L	Length of the main duct
L_1, L_2, L_3	Length of the before orifice field; aperture device; after orifice field
LD	Level difference
N_{mn}	Normalized factor
P	Acoustic pressure
p_{mn}	Acoustic pressure of (m, n) mode
p_+, p_A	Acoustic pressure for incident wave
p_-, p_B	Acoustic pressure for reflected wave
Q	Source strength
Q_0	Directivity factor
R_0	Radius of the main duct
R_1, \dots, R_n	Radius of the orifice 1 to orifice n in the device
R_{mnL}	Complex reflection coefficients

R_p	Radius of the point source duct
r, θ	Coordinate of any point in the main duct coordinate system
r_1, φ	Coordinate of any point in the small duct coordinate system
SA_{mn}, SB_{mn}	Amplitudes of (m, n) mode in the source duct
S	The cross-section area of the main duct
S_1, \dots, S_n	The cross-section area of the orifice 1 to orifice n
TL	Transmission loss
U	Volume velocity
v	Particle velocity
v_r, v_z, v_φ	Particle velocity along r direction, z -axis, and circumference
v_{mn}	Particle velocity of (m, n) mode
W, W_r	Total power, radiated power
Z_{ii}, Z_{io}, Z_{oo}	The input, transfer and output impedance
Z_0, Z_l	Mechanic impedance at the coordinate $z=0$ and $z=L$
Z_{mnl}	Generalized impedances
β_b	Specific admittance of the duct wall
γ	Specific-heat ratio
δ_1, θ_0	The coordinate for the original point of the orifice in the main duct coordinate system
δ_{nL}	Kronecker Delta function
λ	Wave length
ρ	The density of air
ψ	Velocity potential
ψ_0	Driving force
ω	Angular frequency

Chapter 1 Introduction

1.1 Background

Many engineering products contain ducts of constant cross-section that conduct sound, such as mufflers and ventilation ducts. The acoustic properties in these ducts have been widely studied in the past and the laws governing sound propagation in such systems are very important in solving problems in acoustics. At the same time many engineering systems, such as ventilation ducts, require the installation of aperture devices, such as grilles or louvers in the straight duct. These devices are installed for the purpose of airflow control or merely as ornaments. Acoustically, the installation of these devices introduces a change in impedance to the whole system and may also give rise to excessive noise in different parts of the audio frequency range. Currently research on the acoustic performance of such devices has focused on the specific application for a specific device and no generic approach has been taken. Thus this limitation often prevents published data on a particular device being applied to other situations, such as a different installation or a different frequency range.

The lumped-parameter model, extended from the electrical representation, is very useful for the analysis of the acoustic properties of ducts or pipes and has been widely studied. This model uses a limited number of time-dependent aggregate variables rather than field variables varying with both position and time. However there is a limitation for the application of this model, the sound propagating in circular ducts should satisfy the condition that $k * R \ll 1$. Thus the lumped-parameter model is only applicable to the plane wave region. Once $k * R > 1.84$, higher-order modes begin to propagate in the duct and cross-coupling effects between these higher-order modes occur. Thus these higher-order modes cannot be simply represented by lumped parameters.

To consider the performance of the aperture devices over a wide frequency range, it is necessary to consider the propagation of higher-order modes in circular ducts. Thus an approach is sought to allow each higher-order mode to be approximated by using

lumped parameters in the same manner as the plane wave. Although the results will be approximate, it will extend the frequency range of this method.

In this project, both experimental and theoretical analyses of higher-order modes are carried out. For the theoretical analysis, two different types of the sound source, the plane wave source and the point source, will be considered and the relevant descriptions will be presented. Combining the descriptions of the sound source with that of the duct open end, the solution for the acoustic properties in circular ducts without an aperture device present will be obtained. Then the descriptions of the boundary conditions between the main duct and the aperture device will be also presented and from the consideration of all the boundary conditions together, the solution for the acoustic properties for both the before aperture device field and the after aperture device field will be obtained.

For the experimental work, a circular cross-section duct with a flanged end will be used as the main duct and aperture devices of different open area will be placed in the duct. Measurements will be made in different regions (source duct region, before aperture device field and after aperture device field). The measurement made in this work can be divided into two categories: the first one is reference measurements, which are used for the predictions of the acoustic properties in the duct; the second one is direct measurements, which are used for the comparison with the predictions obtained from the theoretical analysis.

Based on the results, the acoustic properties of the main duct without and with aperture devices will be studied respectively in both the plane wave region and the higher-order mode region, then the acoustic properties of the aperture devices will be separated from those of the main duct. Each higher-order mode will be decomposed to consider the individual effect on the whole in-duct acoustic field.

1.2 Literature review

Many authors have published works on the acoustic properties or measuring methods for circular ducts. Discussions of the most relevant publications are given below. The

basic and also the most important part for the study of the acoustic properties in circular ducts is the plane wave propagation in duct.

1.2.1 The plane wave propagation and reflection by duct termination

The theories, which govern the plane wave propagation in circular ducts, have been discussed in detail and fully presented in Ref [1] to Ref [8]. From the theoretical derivation to the acoustic performance, these references covered nearly every detail of the plane wave propagation in circular ducts. Also in Ref [4], the lumped-parameter model (acoustic two-ports system model) was introduced as well as its applications and limitations. For the plane wave propagation in circular ducts of finite length, the reflection from the open end played a very important role. So references, which focused on the sound radiation from the end of the duct when there was only the plane wave propagation in duct, are introduced below. Ref [9] gives the detailed information on the derivation of the equations for different Bessel functions. By adopting these equations, one can derive the equation groups which are used to describe the boundaries between the main duct and the sound source, as well as the main duct and the aperture devices.

For example, one rigorous solution for the sound radiation (plane wave only) from an un-flanged circular pipe was proposed in Ref [10]. In order to simplify the problem, it did not consider the wall thickness and only axially-symmetric excitation was considered. One approximate solution for the sound radiation from the semi-infinite circular pipe of certain wall thickness was presented in Ref [11]. It used the Laplace transform and Wiener-Hopf technique to get the reflection coefficient and end correction of the duct end.

One approximate method to calculate the reflection coefficient R in the low frequency range was proposed in Ref [12]. In this paper, the authors gave the low-frequency end correction length of 0.82159 radii of the duct, which was very close to Rayleigh's conjectured value of 0.82 radii. The authors also expressed the transmitted power as a function of angle from the axis of the duct.

A boundary element method was proposed in Ref [13] to study the wave reflection from different types of the duct termination, such as flanged, un-flanged, oblique duct extension and the reflection coefficient and end correction to each situation were also presented. Although it mainly dealt with the plane wave, it was still very useful in the analysis of the acoustic properties in the ducts with open end.

An alternative approach of the *CAA* (computational aero-acoustics) method was introduced in Ref [14] to calculate both near field and far field radiation from an un-flanged duct. The authors divided the whole domain into three regions: the wave admission and emission region, a propagation region around the edge of the duct and a radiation region outside the duct. The authors applied the *CAA* model to these three regions with different emphasis. For the admission and emission region, spurious waves are damped by using a buffer zone boundary condition. In the propagation region, the acoustic wave propagation was predicted by solutions of the Linear Euler Equation (*LEE*). An integral solution of the *FW-H* (Ffowcs-Williams Hawkins) equations was used to predict the far field radiation. Through the calculation, the authors found that the computation near the edge of the duct had a large influence on the far field directivity prediction, especially in the angle prediction.

Although the plane wave propagation remains the most important part for the acoustic properties studies in circular ducts, in recent years more and more attention has been paid to higher-order mode propagation in ducts. So in the next section, higher-order mode propagation in circular ducts will be introduced.

1.2.2 Analytical description of higher-order modes

Many works have discussed the propagating higher-order modes in circular ducts, but much of the literature concerned with higher-order modes dealt with the radiation from the end of the duct rather than the in-duct field.

For example, one model to calculate the generalized radiation impedances Z_{mnL} of all modes in circular ducts, which was terminated with an infinite baffle, was given in

Ref [15]. The equation for Z_{mnL} was reduced to a single infinite integral which was a function of the mode radiation directivity factors. Then an infinite matrix equation was derived to relate the generalized mode reflection coefficients R_{mnL} to the radiation impedances Z_{mnL} . By knowing the complex reflection coefficients R_{mnL} , one could easily relate the reflected amplitudes B_{mn} with the incident amplitudes A_{mn} and then it was possible to decompose the in-duct field into different higher-order modes and then to predict the acoustic properties in circular ducts precisely.

One theoretical study of non-dimensional directivity factor Q_0 for multi-modes sound radiation from the open end of a duct without a flange was presented in Ref [16]. In this paper, the authors used a single incident duct mode to calculate the single-mode sound power transmission coefficient and the multimode far field directivity factor. For the multimode calculation, the modes were assumed to be incoherent and three types of source were explored: (1) equal power per mode incident on the open end; (2) incoherent monopoles uniformly distributed over a duct cross-section; (3) incoherent axial dipoles uniformly distributed over a duct cross section. Conclusions of relationships between the directivity factor Q_0 and frequency, angle to the axis and the weighting models were obtained. These could then be used in the sound power measurement from exhaust pipes or ducts.

A quite different method to study the radiation from a flanged circular duct was developed in Ref [17]. Most previous works have used Bessel functions to decompose the field inside the duct, but in this paper, the authors used 'edge functions' (the velocity field near the corner yields a new family of functions). The authors compared the results obtained from the new functions with those from the traditional Bessel functions and found although the Bessel functions were composed of a complete basis, this basis had difficulty in describing the velocity field, due to its singularity at the wave guide/flange corner and so resulted in a large degree of ripple and poor convergence. But the edge functions could improve the convergence properties and reduce the ripple. Through the analysis, one could see that the behavior of the edge had quite a large effect on the whole orifice.

Not only are the theoretical derivations of the plane wave and higher-order modes in circular ducts important for the study of the acoustic properties, but also the measurement set-ups and measurement methods. Through the measurement, one can get the acoustic properties, such as pressure and particle velocity in the duct directly. Also through the measurement, one can justify the theoretical model construction and calculation results. So the measurement methods and experimental set-ups have also been widely studied and new methods and set-ups are proposed one by one. In the following section, these different set-ups and measurement methods will be introduced.

1.2.3 Measurement methods for the acoustic properties in circular ducts

There is a significant body of literature on the measurement of the sound wave propagation in circular ducts. In order to obtain the lumped parameters of the circular ducts, it was necessary to determine both acoustic pressure and particle velocity at any point. The following references presented different approaches to measure acoustic properties or transfer functions.

For example, compared with the measurement of acoustic pressure, the measurement of particle velocity was much more difficult and complicated, just because the particle velocity was a vector value. Several methods for particle velocity measurement were introduced in Ref [18]. In recent years, the method using two closely placed identical pressure transducers was widely adopted. The theory for this method was quite simple, which was, the particle velocity was a function of the local spatial gradient of the acoustic pressure. So through the measurement of two closely placed microphones, one could have the spatial gradient at that point and then the particle velocity at that point was obtained.

A cross-spectral method for the measurement of the acoustic intensity was discussed and methods to avoid the error caused by the instrument phase mismatch were also proposed in Ref [19]. In order to eliminate the instrument phase mismatch between

two channels, the author first measured cross-spectral G_{12} at one point, then switched two channels and measured cross-spectral G_{21} at the same point, and then multiplied them together. By doing so, one could avoid errors caused by these two channels. But this method had its limitation, which was the product of the wave number and the microphone space remains small. This method had been adopted in this project to calculate the particle velocity.

A transfer function method was introduced in Ref [20] and Ref [21] for the in-duct acoustic properties measurement. The authors mathematically decomposed the broadband stationary random acoustic wave in the duct into incident and reflected components by using a simple transfer-function relation between the acoustic pressures at two locations on the duct wall. By knowing the incident and reflected components, one could easily get the complex reflection coefficient and then the complex acoustic impedance. So the transmission loss of a silencer element or sound absorption coefficient of a material could be determined.

Two-microphones method (the method which used two closely placed microphones to measure acoustic properties, such as acoustic pressure and particle velocity), which was introduced in Ref [22] to Ref [23], has been widely studied for the measurement of acoustic properties in ducts. In Ref [22], the author discussed the possible errors introduced by this method, such as, the bias errors and random errors of transfer functions, the length measurement errors and the calculated quantity errors. In order to minimize the errors, it was suggested that the overall length of the duct be kept small, in practice, $L = 5-10$ diameters; the source end of the duct should be as non-reflective as possible; microphones should be high coherence and the separation between the microphone pairs should be small. By doing so, the authors reduced the possible errors introduced by this method. Discussions of the first helical mode's contribution to the plane wave were made in Ref [24]. In this paper, the authors placed two receiver microphones in the same plane with the speaker. This arrangement allowed a better measurement of the plane wave up to the cut-on frequency of the second higher-order mode and hence was able to isolate the first higher-order mode. From the comparison of those different measurement methods of

acoustic properties of the in-duct field, the two-microphones method has been proved to be the most widely used one, as well as the standard one. The two-microphones method was widely applied in current research work, so it was very important to reduce the errors caused by the microphone locations or even the space between these two microphones. One method was proposed in Ref [25] to determine the space between these two microphones accurately. By knowing the accurate space between those two microphones, one could get the accurate particle velocity through the measurement.

The multiple-microphones method was proposed in Ref [26] for the measurement of the acoustic properties in ducts and some guidelines for the selection of proper microphone positions were also provided. Although the two-microphones method was accepted as the standard method for the measurement of the in-duct acoustic properties, results on using the least square method with multiple measurement points have been reported for enhancing the frequency response of the two-microphones method. By increasing the number of the microphones, one could improve the measurement accuracy and increase the effective frequency range.

Several techniques used to measure the impedance were reviewed in Ref [27] and Ref [28]. In these papers, the author made an overview of the impedance measurement methods and discussed the advantages and disadvantages of each method. These methods included: two-pressure-transducers method, one-pressure-transducer method, one-pressure-transducer and one-volume-velocity-transducer method and other-transducers method. Especially for the two-pressure-transducers method, the author pointed out that it could only give satisfactory results for some parts of the frequency range. Measurements were not possible if the distance between two microphones was too small or close to a multiple of the half wavelength. The two-pressure-transducers method was adopted by this project to measure the particle velocity and hence establish the impedance of the ducts or aperture devices.

One multi-loads method was proposed in Ref [29] to measure the acoustic source parameters such as, source strength or source impedance, in duct systems. Because the input data, such as load pressure or impedance, were usually contaminated by

measurement error, this always resulted in errors in the calculated source parameters. So the authors tried a set of pipe lengths to make the calculated results least sensitive to the input data error, and then yielded the best results.

1.2.4 Higher-order mode experimental decomposition methods

The references discussed above provided some practical experimental set-ups or measurement methods for the acoustic properties in the ducts. There were also some published works dealing with the experimental methods to separate the higher-order modes propagating in circular ducts and hence experimentally separate the measured, summed higher-order modes into individual ones. Then it was possible to compare the experimentally separated duct modes with those theoretically predicted ones and to test the applicability of the theories used to separate higher-order modes.

A cross-correlation technique was used to separate the modes at the blade-passing frequencies of an axial fan and the effects of reflected waves were discussed in Ref [30]. Although the current work did not contain a fan, the technique of mode decomposition described was still applicable. The method of the measurement was using two probes (hot wire anemometers to measure the axial component of particle velocity), which were traversed in the circumferential direction at a given axial and radial position. One improved measurement method was proposed in Ref [31], in which the authors used the microphones rather than hot wire anemometers and the radial mode separation was achieved by traversing one of the microphones in the axial direction.

One new technique of measuring the reflection matrix for duct discontinuities with higher-order modes was discussed in Ref [32]. It was based on the measurement of the acoustic pressure by microphone pairs in two closed cross sections of the circular duct and separated incident and reflected modes by using a Fourier-Lommel transform. It generated enough independent incident fields by mounting two acoustic drivers on the duct wall that could rotate 360 degree in the same cross section or two different axial positions.

Direct modal decomposition was carried out in Ref [33]. In circular ducts, the circumferential analysis was simply a Fourier transform, but the radial analysis was in terms of Bessel functions. So the author mainly focused on the separation of the radial modes and made a comparison of three methods, the matrix inversion method, the integration method and the least squares method. Through the comparison, the author found the least squares method was the best one, because the matrix method was prone to instability and the integration method had a relatively high noise floor. According to the study, it was possible to separate the in-duct field into different modes even when there were a larger number of higher-order modes propagating in circular ducts. However it needed quite a lot of measuring points. Ideally, the number of the measuring points should be twice the product of the maximum number of propagating circumferential modes and the maximum number of propagating radial modes for any circumferential order. But in practice, many more points were needed to average out the measurements errors.

The instantaneous mode separation method, which could separate the broadband noise propagating inside circular ducts into different higher-order modes, was developed in Ref [34]. In this method, $2*n$ pressure transducers spaced evenly around the circumference of the duct were used to separate the $(n-1)$ order of circumferential modes. This method had one advantage, in that it did not need the circumferential traversing of the microphone array, and so the circumferential separation did not involve matrix solutions, which could be sensitive to small measurement inaccuracies. However it also had a limitation, which was it could only separate the circumferential modes.

One new in-duct modal decomposition technique, which is based on the transfer function measurements between microphone pairs, was described in Ref [35]. The rationale for using this method was because the transfer functions had two advantages: first, they were independent of the signal type in the ducts; secondly, transfer functions were in many cases less sensitive to bias and random errors than other spectral quantities. By using this method, one could separate the in-duct field into incident and reflected waves from measurements at two axial positions. This method was also only valid for the separation of the circumferential modes.

There are also other experimental set-ups and measurement methods which provided useful information or approaches to the decomposition of higher-order mode propagation in circular ducts. For example, one new experimental set-up was proposed in Ref [36] for measurement of acoustic power dissipation in lined ducts for higher-order mode propagation with air-mean flow conditions. Through the measurement of the acoustic pressure and axial particle velocity in the upstream and downstream section, the authors could deduce the modal acoustic powers. By adding the modal powers together and comparing it with directly measured total acoustic power, the authors found the method to get the modal intensity was effective. Although this literature mainly dealt with the higher-order modes propagation with air-mean flow, the method and conclusion obtained were applicable to the situation without air-mean flow.

From the references discussed above, it could be seen that the experimental decomposition of higher-order modes was very difficult and many methods were only practical for the circumferential modes. So it was important to find another way to carry on the modal decomposition in circular ducts, which was the theoretical decomposition method. The so-called theoretical decomposition method was through the modal construction and calculation to obtain the parameters for those higher-order modes rather than through the direct measurement. If one could achieve the theoretical separation of the higher-order modes, then it would be easier for the study of the acoustic performance of the aperture devices.

1.2.5 Effects of the orifice plates on the acoustic field

In order to study the effects of the simple aperture devices in circular duct, one should consider the scattering effects of an orifice plate, especially if the frequency range was high enough when the wavelength was smaller than or nearly equal to the size of the open area. Again there were many previous works, which had studied the effects of the orifices in aperture devices.

The transmission coefficient Q of a circular orifice in a thin panel was introduced in Ref [37]. Some ways to get the Q were discussed, such as through the diffraction by

the orifice, piston theory or complex impedance presented by the orifice. The transmission coefficient Q was meaningful only when the k^*r was small, which meant it was only applicable for the plane wave situation.

An acoustic impulse technique in Ref [38] was developed to separate the reflected waves from the incident waves for the purpose of the study of the internal acoustic energy distribution. One high intensity pulse generated by a spark charge used as the sound source. Placing the microphone a certain distance from the end of the duct, it could pick the incident impulse and impulse reflected by the orifice plate at the end of the duct separately. Through the research, the author found that the acoustic behaviour of the orifice plate and the perforated plate terminations was qualitatively similar to that of the conical nozzle termination. The author also found that some low frequency power for orifice plates and perforated plates was absorbed (dissipated) at the end of the duct. This phenomenon was caused by non-linearity or dissipated in the form of vortical energy at the orifice plate and perforated plate termination.

Acoustic scattering from orifices in the hard thick wall was studied in Ref [39]. The Hankel transform was applied to express the scattered field and the boundary conditions were enforced to obtain simultaneous equations for the transmitted field inside the thick hard screen. The simultaneous equations were solved to represent the transmitted and scattered fields in series forms. Based on these representations, one approximate method to calculate the modal coupling between higher-order modes in the orifice was studied in Ref [40] and Ref [41]. In these papers, the authors found that each (m, n) mode of the scattered field was dependent on the amplitude of the in-orifice waves and a driving term unique to each (m, n) mode. So it was easy to establish the amplitude of the in-orifice field and the effects of modal coupling. In these papers, useful information about the scattered field were provided, which could be referred in the research of higher-order modes propagation in the duct with simple aperture devices.

Acoustic scattering from two circular orifices in a thick hard screen had been studied in Ref [42]. The authors used the Hankel transform and modal matching to represent the scattered field in rapidly convergent series. Thus reflection coefficient and

transmission coefficient could be derived and calculated rigorously. The coupling effects between two orifices in terms of distance between two orifices ($k*L$), incident polar angle, azimuth angle and orifice radii were also discussed. The authors also proposed the possibility to extend this situation to the multiple-orifices scattering case. This had direct relevance to the study of multi-orifice aperture devices.

Sound attenuation in circular ducts using slit-like short expansion of concentric and serialized configuration was studied in Ref [43]. Through the study, the authors pointed out that first, this slit-like circular expansion chamber performed as a resonator muffler in the duct; secondly, the serialized slits shown the summative performance of each composing slit, a certain interaction among those slits occurred if those resonant frequency came close to each other. The reason why this paper is interesting is they studied the slit like expansion while this project is studying the 'slit-like' contraction.

1.2.6 Model for the description of the aperture device boundary condition

For the simple aperture devices in circular ducts, it was important to find a way to describe and resolve the boundary conditions between the aperture devices and the circular ducts. Considerable works have been done on this subject. Although most of them were for the circular expansion chamber of a muffler, the method provided a similar way for the research work of this paper.

When the duct was uniform, then at low frequency, there should be only the plane wave propagating in the duct. But if there was a junction or sudden area discontinuity in the duct, some higher-order, evanescent modes should also occur and then could be considered as acoustical impedance to the propagation of the plane wave. This acoustic impedance was analyzed in Ref [44]. At the sudden area discontinuity, the author listed the continuity of the pressure and particle velocity and then multiplied each side of the equation with weighting functions $J_{mn}(k_{r_{mn}}r) * \exp(jm\theta)$ and then integrated both sides. Then the author obtained equations to correctly model this discontinuity. After considering this approach, it is possible to increase the accuracy

of the analysis of the low frequency plane wave in a circular duct with a sudden discontinuity.

A similar method was also applied in several other papers for their study of the *discontinuities in circular duct*. The effects of the length of the concentric expansion chamber on the acoustic attenuation performance were studied in Ref [45]. The acoustic attenuation performance of circular expansion chambers with single-inlet and double-outlet was studied in Ref [46]. The acoustic attenuation performance of circular expansion chambers with offset inlet/outlet was studied in Ref [47] and Ref [48]. The circular unsymmetric Helmholtz resonators were studied in Ref [49]. In these papers, the authors made an assumption that only the plane wave is propagating in the expansion chamber and the small duct, all other higher-order modes were evanescent. Based on this method, those authors proposed one three-dimensional analytical approach to determine the relationships between the transmission loss (TL) and the length of the chamber, the relative offset distance of the inlet/outlet, radius of the chamber and the number of the outlet. Through their studies this method had been proved to be very effective in the study of the sudden area discontinuity in circular ducts.

Other methods were also proposed to study the effects of the sudden area discontinuity. A three-dimensional ($3D$) finite element analysis to verify the inertia of the higher-order modes in a sudden area change was proposed in Ref [50]. The duct was treated as a substructure and then further divided into an appropriate number of segments which should be met the convergence criterion that the maximum typical finite element dimension should be smaller than 0.52λ . The author found that when the length of the duct is larger than 3 times the diameter of the duct with more segments, the result would be inaccurate, which might be caused by the rounding-off errors. This will limit the applicability of this $3D$ finite element method.

Discussions about the acoustic properties of circular orifice in the ducts with mean flow were also made in Ref [51] to Ref [53]. These works provided revised experimental set-ups for the measurement of the impedance of the orifice in circular ducts. In Ref [53], the author pointed out that the sound absorption by an orifice plate

takes place as the acoustic field energizes a vortex field which is generated at the orifice rim.

Other works have been done on the study of the acoustic properties in circular ducts, such as Ref [55] to Ref [59]. Although the works mainly focused on the condition with axial flow in circular ducts, the methods or analysis could still be referred to the without axial flow condition. For example, in Ref [55] and Ref [56], the authors pointed out that the power radiated from the end of the duct showed strong dependence on the parameters such as, source locations, source frequency, flow Mach number and duct length. In Ref [58] and Ref [59], the author studied the sound generation and transmission in ducts with flow, especially the generation and transmission of the rotating pressure patterns in ducts.

1.3 Present work

The research work in this thesis can be divided into three stages.

1. The analysis of the plane wave propagation in circular ducts with simple aperture devices.
2. The analysis of the higher-order modes propagation in circular ducts without aperture devices.
3. The analysis of higher-order modes propagation in circular duct with simple aperture devices.

The thesis follows this order of investigation.

In Chapter 2, the lumped-parameter model or the acoustical two-ports system model for the plane wave propagation in circular ducts, as well as in ducts with simple aperture devices is introduced and experimentally verified. Also in this chapter, some measurement methods are discussed for the measurement of the lumped parameters such as acoustic pressure and volume velocity of the simple orifices or of the ducts.

In Chapter 3, the theoretical derivation for the higher-order modes in circular ducts is given. Discussion about the applicability of the lumped-parameter model to this

situation is also made. In order to justify the approximate lumped-parameter model, one method used to obtain the generalized radiation impedances Z_{mnL} and the general reflection coefficients R_{mnL} at the flanged open end of the circular duct is presented. The general reflection coefficients R_{mnL} are very important in the calculation of the in-duct field amplitudes. There are two approaches to use these coefficients R_{mnL} , first one is the uncoupled method, in which only the self coupling effect is considered ($B_{mn} = R_{mn} A_{mn}$). The second method is the standard fully coupled method, in which other cross coupling effects are also considered ($B_{mn} = \sum_L R_{mnL} A_{mL}$). Then one can get the estimates of in-duct field amplitudes A_{mn} and B_{mn} with these two methods.

In Chapter 4, two types of sound source are introduced. One is the plane wave source and the other is the point source in a hard plate. Different types of sound source give different types of boundary conditions in the model construction. The plane wave source is a common sound source for ducts, pipes and mufflers. The point source is a simple sound source and the component of many complicated sound sources. In this chapter, the theoretical descriptions are given for these two types of source as well as the experimental set-ups.

In Chapter 5, the acoustic performances of the sound field produced by a point source propagating along a circular duct without simple aperture devices are studied. Combining the point source boundary condition with the model proposed in Chapter 3, one can get the in-duct field amplitudes A_{mn} and B_{mn} , and then decompose the in-duct field into single higher-order modes theoretically. In this chapter, the experimental decomposition method is also introduced. Through the comparison, the experimental method is found to be ineffective in the decomposition of the higher-order modes in circular ducts. So in this chapter, attention is focused on the theoretical decomposition method based on the model proposed. Comparison is made between the direct measurements and theoretical predictions. Finally the effects of the source location on the in-duct field are also discussed.

In Chapter 6 the acoustic performances of the sound field produced by the plane wave source propagating along a circular duct without a simple aperture device are studied. Following the same procedure of the Chapter 5, one can decompose the in-duct field into different single higher-order modes. With these amplitudes A_{mn} and B_{mn} known, one can reconstruct the acoustic properties, such as the acoustic pressure, at any points in circular ducts. Then by comparing the predicted pressures with those directed measured ones, one can get the errors as well as the applicability of this model.

In Chapter 7, the acoustic performances of the sound field produced by a point source propagating along a circular duct with simple aperture devices are studied. Three different simple aperture device configurations, namely a device with a single orifice, a device with two orifices and a device with several orifices, are investigated. Combining the theoretical descriptions for the point source boundary, the simple aperture device boundaries with the open end boundary, one can develop an equation group for the solution of those amplitudes of A_{mn} , B_{mn} , E_{mn} and F_{mn} . By solving this equation group, those amplitudes are obtained. So both the before aperture device field and the after aperture device field have been decomposed. With these amplitudes known, one can get the acoustic properties, such as pressure and particle velocity, at any point in the whole duct. So comparisons are made between direct measured pressures with theoretical predicted pressures at appointed points to obtain the errors and applicability for each situation.

In Chapter 8, the acoustic performances of the sound field produced by the plane wave source propagating along a circular duct with simple aperture devices are studied. Again three different simple aperture device configurations, namely a device with a single orifice, a device with two orifices and a device with several orifices, are investigated. Following the same procedure of Chapter 7, one can also get those amplitudes of A_{mn} , B_{mn} , E_{mn} and F_{mn} for these different situations. Comparisons are also made between direct measured pressures with theoretical predicted pressures at appointed points to obtain the errors and applicability for each situation.

In Chapter 9, after achieving the decomposition of the in-duct field, one can analyze the power contributed by each higher-order mode for different situations. The power rather than the volume velocity is chosen as the approximate lumped parameter. Then the feasibility of the approximate lumped parameter model to higher normalized wave number range is discussed. Also another parameter, insertion loss (*IL*) is selected to show the effects of different simple aperture devices. Compared with the plane wave situation, the insertion loss (*IL*) for higher-order modes is difficult to measure. However with those amplitudes known, it is easy to calculate it. Through the analysis of each mode's power and the insertion loss (*IL*), one can have a clear and direct view of the acoustic performance for those simple aperture devices at different normalized wave number ranges.

Finally in Chapter 10, Conclusions of this generic approach for the higher order modes propagation in circular duct with simple aperture devices are obtained. The future possible research direction is also given.

Chapter 2 The plane wave propagation in a circular duct

2.1 Introduction

Considerable previous research, such as Ref [1] to Ref [8], has been done on the study of the wave propagation in circular ducts. They mainly focused on the frequency range lower than the cut-on frequency of the first higher-order mode and dealt with the plane wave situation. One important model (lumped-parameter model or acoustical two-ports system model) is introduced and discussed in this chapter. This model is widely accepted as a powerful tool for the research of the acoustic properties in circular ducts in the plane wave region. Because of the complication of the wave motion, there are no effective approximate methods to study the performance of the simple aperture devices in the higher-order modes propagation situation. So this model is considered in the plane wave region just before being approximated and extended to the higher-order modes region. Also in this chapter two measurement methods, *blocked particle velocity method* and *two-different-inputs method*, are introduced and compared. Through the measurement of the lumped parameters, such as the acoustic pressure and volume velocity, the input impedance, transfer impedance and output impedance of the component (aperture device) and the whole system are determined. Then the effects of the component on the system can be analyzed.

2.2 Theoretical derivation

Considering a wave propagating in a circular duct, as discussed in Ref [8] (chapter V), when the frequency of the wave is comparatively low, it can be treated as a plane wave. If the length of the duct is infinite, there are no reflected waves in the duct. The acoustic pressure at certain point with the coordinate z (ignore the friction) is

$$p(z, t) = p_+(z)e^{j\omega t} = A_{01}e^{j(\omega t - kz)}. \quad (2.1)$$

In a duct of finite length, assuming the duct is closed by an imaginary piston (a moving surface) with mechanical impedance Z_0 at the open end and a speaker placed at the other

end of the duct produces a sound, it has the mechanical impedance Z_{-L} and is driven by the force $\psi_{-L}e^{j\omega t}$ (for convenience, the origin point of the coordinate is taken at the open end of the duct). There will be an infinite number of positive and negative waves that are superimposed on each other. All the positive waves have the same frequency and the resulting negative waves will also have the same frequency. In general form the acoustic pressure can be written as

$$p(z,t) = (p_+(z) + p_-(z))e^{j\omega t} = (A_{01}e^{-jkz} + B_{01}e^{jkz})e^{j\omega t}. \quad (2.2)$$

According to the relation between the pressure and particle velocity

$$p = -\rho \int \partial v / \partial t dz. \quad (2.3)$$

The particle velocity in the duct should be

$$v(z,t) = (A_{01}e^{-jkz} - B_{01}e^{jkz})e^{j\omega t} / \rho c. \quad (2.4)$$

Then the boundary conditions of the duct are given as

$$\begin{aligned} Z_{-L}v_{-L} &= \psi_{-L}, \\ Z_0v_0 &= Sp_0, \end{aligned} \quad (2.5)$$

in which S is the cross section area of the circular duct.

The quantities of A_{01} and B_{01} can be obtained from the boundary conditions above.

Substituting $p(z,t)$ and $v(z,t)$ at $z=0$ and $z=-L$ into equation (2.5), one can get

$$\begin{aligned} (Z_{-L}A_{01}e^{jkl} - Z_{-L}B_{01}e^{-jkl}) / \rho c &= \psi_{-L}, \\ (Z_0 - S\rho c)A_{01} - (Z_0 + S\rho c)B_{01} &= 0. \end{aligned} \quad (2.6)$$

Two linear equations with two unknowns variables A_{01} and B_{01} are obtained above. The determinant of these equations is denoted by

$$\begin{aligned} \Delta &= \begin{vmatrix} Z_{-L} / \rho c e^{jkl}, -Z_{-L} / \rho c e^{-jkl} \\ (Z_0 - S\rho c), -(Z_0 + S\rho c) \end{vmatrix} = \\ &2SZ_{-L} \cos(kL) - 2j(Z_0Z_{-L} / \rho c) \sin(kL). \end{aligned} \quad (2.7)$$

From equation (2.6), one can get

$$\begin{aligned} A_{01} &= (Z_0 + S\rho c)\psi_{-L} / \Delta, \\ B_{01} &= (Z_0 - S\rho c)\psi_{-L} / \Delta. \end{aligned} \quad (2.8)$$

Substituting A_{01} and B_{01} in equation (2.2) and equation (2.4), one can get

$$\begin{aligned} v &= [(Z_0 + S\rho c)e^{jkL} - (Z_0 - S\rho c)e^{-jkL}] \psi_{-L} e^{j\omega t} / (\rho c \Delta), \\ p &= [(Z_0 + S\rho c)e^{jkL} + (Z_0 - S\rho c)e^{-jkL}] \psi_{-L} e^{j\omega t} / \Delta. \end{aligned} \quad (2.9)$$

In equation (2.9) the first term denotes the forward wave and the second term denotes the backward wave. It should also be noticed that the phase of the forward and backward waves are both functions of the quantity L , which is the distance from the end of the duct.

If there is a hard screen in the end of the duct which blocks the particle velocity, then $Z_0 \approx \infty$, compared with the Z_0 , it is possible to ignore the quantity of $S\rho c$, so

$$\begin{aligned} A_{01} &\approx \psi_{-L} / [-2j(Z_{-L} / \rho c) \sin(kL)], \\ B_{01} &\approx \psi_{-L} / [-2j(Z_{-L} / \rho c) \sin(kL)]. \end{aligned} \quad (2.10)$$

If the other end of the duct is open, then ignoring the end effect error, the impedance at that position is so small that it can be expressed as $Z_0 \approx 0$, such that

$$\begin{aligned} A_{01} &\approx \rho c \psi_{-L} / [2Z_{-L} \cos(kL)], \\ B_{01} &\approx -\rho c \psi_{-L} / [2Z_{-L} \cos(kL)]. \end{aligned} \quad (2.11)$$

By knowing this, one can get the acoustic pressure and particle velocity of the in duct field. Substituting equation (2.10) into equation (2.2) and (2.4), one can get the acoustic pressure and particle velocity when there is a hard screen at the end of the duct as follow,

$$\begin{aligned} v &= (e^{jkL} - e^{-jkL}) \psi_{-L} e^{j\omega t} / [-2jZ_{-L} \sin(kL)], \\ p &= (e^{jkL} + e^{-jkL}) \psi_{-L} e^{j\omega t} / [-2j(Z_{-L} / \rho c) \sin(kL)]. \end{aligned} \quad (2.12)$$

Also substituting equation (2.11) into equation (2.2) and (2.4), one can get the acoustic pressure and particle velocity when the duct end is left open as,

$$\begin{aligned} v &= (e^{jkL} + e^{-jkL}) \psi_{-L} e^{j\omega t} / [2Z_{-L} \cos(kL)], \\ p &= \rho c (e^{jkL} - e^{-jkL}) \psi_{-L} e^{j\omega t} / [2Z_{-L} \cos(kL)]. \end{aligned} \quad (2.13)$$

However normally, the driving force $\psi_{-L} e^{j\omega t}$ is hard to obtain directly. On the contrary, the acoustic pressure and particle velocity are quite easy to obtained through the direct measurement in the plane wave situation. Through the analysis of the change of the acoustic impedance of the system, one can get the effects of the different simple aperture

devices on the whole in duct field. So in next section, one model is introduced to study the impedances of the in duct system.

2.3 Lumped-parameter model (acoustical two-ports system model)

2.3.1 Duct without simple aperture devices

As discussed in Ref [7] (chapter 7), a lumped-parameter model uses a limited number of time-independent aggregate variables rather than field quantities varying with both position and time. In acoustics, the commonly used lumped-parameter variables are volume velocity and average acoustic pressure.

For a circular duct, if the wavelength is comparatively large compared to the cross section, it is treated as the plane wave. In the plane transverse to the axis of the duct, the pressure and particle velocity is equal everywhere. So the volume velocity U equals the particle velocity multiplied by the area S and average pressure P equals to the pressure measured at any point. In the description of this lumped-parameter model that uses these two variables, it is convenient to use the concept of the acoustic impedance Z that is defined as the ratio of P/U .

Suppose there are two surfaces S_i and S_o in an acoustical system and the propagating direction is defined as from S_i to S_o . The region between S_i and S_o can be regarded as a passive black box, which is referred to as a two-ports system. The acoustic boundary-value problem for the black-box region, given pressures P_i and P_o on surfaces S_i and S_o , should have a unique solution. The linear nature of the governing partial differential equations and boundary conditions require that P_i and P_o should be linear function of U_i and U_o , namely

$$\begin{aligned} P_i &= U_i Z_{ii} + U_o Z_{io} , \\ P_o &= U_i Z_{oi} + U_o Z_{oo} , \end{aligned} \tag{2.14}$$

in which U_i is the input volume velocity of the duct, U_o is the output volume velocity of the duct, Z_{ii} is the input acoustic impedance of the system, Z_{oo} is the output acoustic

2. The plane wave propagation in a circular duct

impedance of the system and Z_{io} is the transfer acoustic impedance of the system. Assuming reciprocity, there is $Z_{io} = -Z_{oi}$,

The analogous principle of equation (2.14) is shown in Fig 2.1. Through the measurement of P_i, U_i, P_o and U_o , it is possible to determine the input impedance Z_{ii} and the transfer impedance Z_{io} and the output impedance Z_{oo} of this system.

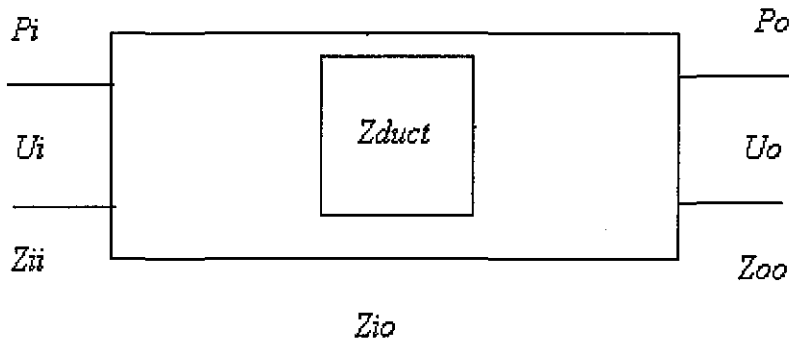


Fig 2.1 Layout of the acoustical two-ports system model for duct without aperture device

So for equation (2.14), when there is a hard screen at the end of the duct, there should be $Z_o = \infty$ and $U_o = 0$, then one can get

$$P_i = U_i Z_{ii} \Big|_{z=-L} \quad (2.15)$$

Substituting equation (2.12) into equation (2.15), there is

$$\begin{aligned} Z_{ii} &\approx \frac{\rho c (e^{jkL} + e^{-jkL})}{S((e^{jkL} - e^{-jkL}))} \\ &= -j\rho c \frac{\cos(kL)}{S \sin(kL)} \\ &= -j\rho c \cot(kL) / S. \end{aligned} \quad (2.16)$$

If the end of the duct is left open, there should be $Z_o \approx 0$. Substituting equation (2.13) and equation (2.16) into equation (2.14), Z_{io} is given below:

$$\begin{aligned}
 Z_{io} &\approx (P_i - U_i Z_{ii}) / U_o \\
 &= (p_{-L} - S * v_{-L} * Z_{ii}) / (S * v_o) \\
 &= \frac{\rho c [(e^{jkL} - e^{-jkL}) + j \cot(kL) (e^{jkL} + e^{-jkL})]}{2S} \\
 &= \frac{j \rho c}{S * \sin(kL)}
 \end{aligned}
 \tag{2.17}$$

2.3.2 Duct with simple aperture devices

The equations obtained above are only applicable for a duct without a simple aperture device. If there is an aperture device in the circular duct and, compared with the wavelength, the dimension of the aperture device is very small, then it can still be regarded as a passive black box. The acoustic boundary-value problem for this black-box region, given pressures P_i and P_o on two surfaces should also have a unique solution. So the linear nature of the governing partial differential equations and boundary conditions still require that P_i and P_o should be linear function of U_i and U_o , which is given in equation (2.14). The analogous principle for the duct with simple aperture devices is shown in the figure below.

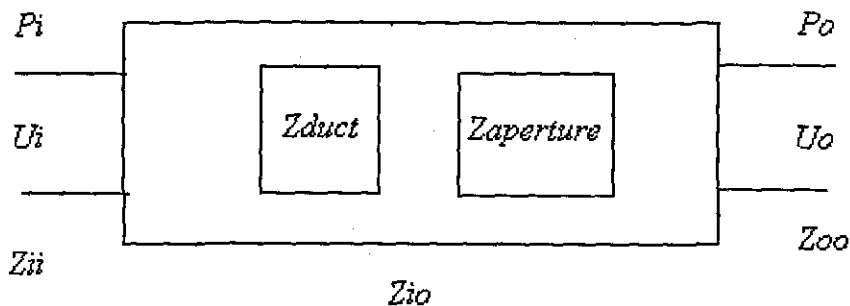


Fig 2.2 Layout of the acoustical two-ports system model for duct with aperture devices

According to the acoustical two-ports system theory, the circular duct and the aperture device can also be treated as the acoustical two-ports system individually. So the impedance of the duct Z_{duct} and aperture device $Z_{aperture}$ can be shown as below

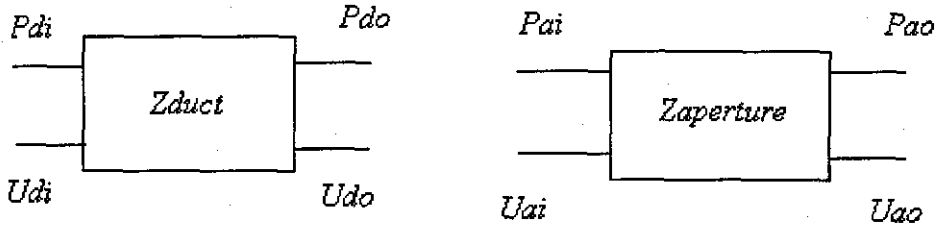


Fig 2.3 Layout of the acoustical two-ports subsystem for duct and aperture device

So for the combination of the duct and the aperture device, one can get equation (2.14).

But for the duct without aperture device, one can have

$$\begin{aligned} P_{di} &= U_{di} Z_{dii} + U_{do} Z_{dio} , \\ P_{do} &= U_{di} Z_{dio} + U_{do} Z_{doo} . \end{aligned} \quad (2.18)$$

For the simple aperture device only, one can have

$$\begin{aligned} P_{ai} &= U_{ai} Z_{aia} + U_{ao} Z_{aio} , \\ P_{ao} &= U_{ai} Z_{aio} + U_{ao} Z_{aoa} . \end{aligned} \quad (2.19)$$

For continuity, there should be

$$U_{do} = U_{ai} . \quad (2.20)$$

For equilibrium, there should be

$$\begin{aligned} P_{do} &= P_{ai} \\ P_i &= P_{di} \\ P_o &= P_{ao} \\ U_i &= U_{di} \\ U_o &= U_{ao} . \end{aligned} \quad (2.21)$$

Substituting equations (2.20) and (2.21) into equations (2.18) and (2.19), one can get

$$\begin{aligned} P_i &= \frac{(Z_{dii} Z_{doo} + Z_{dij} Z_{pii} - Z_{dio}^2)}{(Z_{doo} + Z_{pii})} U_i + \frac{[-(Z_{dio} Z_{pio})]}{(Z_{doo} + Z_{pii})} U_o , \\ P_o &= \frac{[-(Z_{dio} Z_{pio})]}{(Z_{doo} + Z_{pii})} U_i + \frac{(Z_{doo} Z_{poo} + Z_{pii} Z_{poo} - Z_{pio}^2)}{(Z_{doo} + Z_{pii})} U_o . \end{aligned} \quad (2.22)$$

Comparing equation (2.22) with equation (2.14), the following relationship can be obtained

$$\begin{aligned}
 Z_{ii} &= \frac{(Z_{dii}Z_{doo} + Z_{dii}Z_{pii} - Z_{dio}^2)}{(Z_{doo} + Z_{pii})}, \\
 Z_{io} &= \frac{[-(Z_{dio}Z_{pio})]}{(Z_{doo} + Z_{pii})}, \\
 Z_{oo} &= \frac{(Z_{doo}Z_{poo} + Z_{pii}Z_{poo} - Z_{pio}^2)}{(Z_{doo} + Z_{pii})}.
 \end{aligned}
 \tag{2.23}$$

After obtaining the relationships between the overall impedances with the impedances of the components (duct and aperture device), it is possible to get the overall impedances through the equation above (calculated results), as well as direct measurements (measured results). Then it is possible to compare the impedances obtained by these two ways to see the errors caused by the assumptions made in equation (2.10) and (2.11).

2.4 Blocked particle velocity method

In order to measure the input impedance Z_{ii} and the transfer impedance Z_{io} of the duct without aperture devices, the experimental set-up is adopted as shown in Fig 2.4. The list of instruments used in measurement and the connection of the equipments are given in Appendix A.

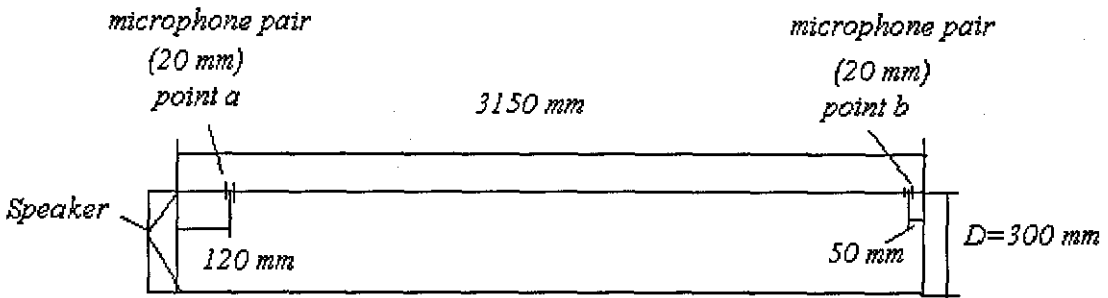


Fig 2.4 Experimental set-up for duct without aperture devices

Two phase matched microphone pairs are used to measure the acoustic pressure and particle velocity at point a and point b (The phase matched procedure is given in Appendix B). According to Ref [18] (chapter 5), the particle velocity along the line joining the acoustic center of two closely placed microphones can be obtained by employing a finite difference approximation to the local spatial gradient of acoustic

pressure. The Euler's equation shows: in a small amplitude sound field, the component of pressure gradient in any direction n is proportional to the component of fluid particle acceleration in that direction:

$$\rho_0 \frac{\partial v_n}{\partial t} = \frac{\partial p}{\partial n}. \quad (2.24)$$

The corresponding particle velocity is therefore given by the time integral

$$v_n(t) = -\frac{1}{\rho_0} \int_{-\infty}^t \left(\frac{\partial p(\tau)}{\partial n} \right) d\tau. \quad (2.25)$$

This is the particle velocity in the time domain, applying the Fourier transform it is easy to get the particle velocity in the frequency domain as

$$v(\omega) \approx \frac{1}{i\rho_0\omega d} [p_1(\omega) - p_2(\omega)]. \quad (2.26)$$

So equation (2.14) can be written as follow:

$$\begin{aligned} P_i(z)e^{j\phi_{pi}} &= U_i(z)e^{j\phi_{ui}} Z_{ii} + U_o(z)e^{j\phi_{uo}} Z_{io}, \\ P_o(z)e^{j\phi_{po}} &= U_i(z)e^{j\phi_{ui}} Z_{io} + U_o(z)e^{j\phi_{uo}} Z_{oo}, \end{aligned} \quad (2.27)$$

in which $P_i(z)$, $P_o(z)$, $U_i(z)$ and $U_o(z)$ are real space-dependent amplitudes of acoustic pressure and volume velocity at the input end and output end of the system. ϕ_{pi} , ϕ_{po} , ϕ_{Ui} and ϕ_{Uo} are space-dependent phases of acoustic pressure and volume velocity.

The measurement procedure is given below:

1. Place a hard screen at the output end of the duct and take the measurement of the input pressure and particle velocity. The purpose of using the hard screen at the output end is to block the particle velocity to zero, by doing so, according to equation (2.27), one can get the input impedance directly.
2. Remove the hard screen and measure the pressure and particle velocity individually at point a and point b .

This method will be referred as the *blocked particle velocity method*.

Through the measurements of the acoustic pressure and particle velocity at these two situations, then from equation (2.27) one can get the input impedance Z_{ii} and the transfer impedance Z_{io} of the duct without aperture devices. Also another group of the

2. The plane wave propagation in a circular duct

impedances are obtained from equation (2.10) and equation (2.11), which is an ideal condition.

The comparison of these two groups of the impedances is shown in Fig 2.5. The frequency range is taken as 200 – 600 Hz , which is transferred to the normalized wave number range $k * R$ as 0.55-1.66. In Fig 2.5, the left hand column shows the real part, imaginary part and amplitude of the input impedance Z_{ii} ; the right hand column shows the real part, imaginary part and amplitude of the transfer impedance Z_{io} . The ideal results are those given by equation (2.10) and equation (2.11).

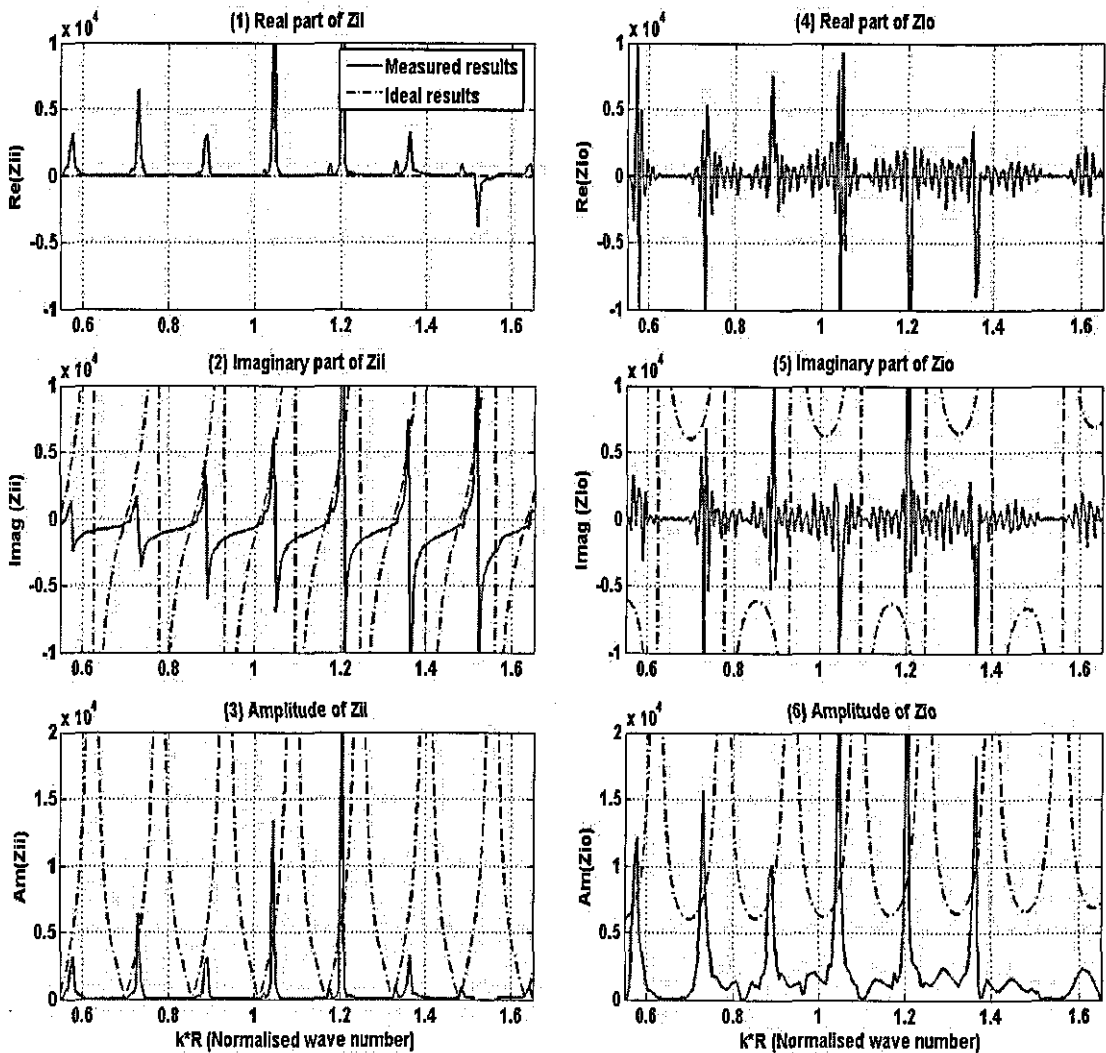


Fig 2.5 Comparison of the ideal results and the measured results for duct without aperture device situation

From Fig 2.5 and equation (2.28) and (2.29), it can be seen that

1. For the ideal condition, the real parts of the impedances Z_{ii} and Z_{io} are zero. However the measurements generate significant real part values rather than zero real part of theory.
2. For the ideal condition, the imaginary part of the input impedance Z_{ii} is a function of $\cot(k * L)$ and the imaginary part of the transfer impedance Z_{io} is a function of $1/\sin(k * L)$. However the measurements are not pure functions of $\cot(k * L)$ or $1/\sin(k * L)$.
3. The measured impedances agree with the ideal ones in period. However the amplitudes of those impedances have significant differences because it is difficult to acquire the ideal boundary condition. The hard screen used in measurement cannot give a perfect rigid boundary, which means the impedance Z_0 is not infinite and thus when ignoring the term $S\rho c$ in equation (2.10), there should be some errors. Also for the duct open end, for the ideal condition described in equation (2.11), it is assumed $Z_0 \approx 0$, which is not true for the real situation.
4. From Fig 2.5, it can be seen that there are too many sources of errors in *blocked particle velocity method* to make it a reliable method.

So from the comparison, it is easy to see that even for a duct without a simple aperture device, *the blocked particle velocity method* is not an accurate way for the analysis of the acoustic properties unless significant effort is spent on obtaining a purely rigid boundary. So there is no need to test this method for a duct with a simple aperture device. In order to avoid these errors introduced by this method, another widely adopted method, *two-different-inputs method*, is tested in the following section to obtain the transfer properties of the aperture device as well as the whole system.

2.5 Two-different-inputs method

As discussed above, the microphone pair method (which means two closely placed microphones) is now widely accepted as the acoustic impedance measurement standard, especially for the acoustic properties in ducts or pipes. In order to achieve a better

2. The plane wave propagation in a circular duct

understanding of the acoustic properties in ducts and to check the acoustical two-ports system's applicability in the acoustic system with an open end, another method (*Two-different-inputs* method) is adopted. The experimental set-up shown in Fig 2.6 is adopted and two phase matched microphone pairs are placed at point *a* and point *b* respectively.

According to equation (2.14), there are totally three unknown variables (Z_{ii} , Z_{io} and Z_{oo}), so there should be at least two different conditions available to get enough equations for those unknown values. The *blocked particle velocity method* acquires two different conditions by the presence and the absence of the hard screen. The *Two-different-inputs* method acquires two different conditions by applying two different input voltages to the speaker.

In this section four wooden simple aperture devices of thickness 25 mm are used for the study of the effects of the aperture devices. For each aperture device, there is a single concentric orifice drilled in it, the inner diameters of these orifices are 60 mm (4% of open area), 120 mm (16% of open area), 170 mm (32% of open area) and 210 mm (49% of open area) respectively. The experimental set-up is shown as below,

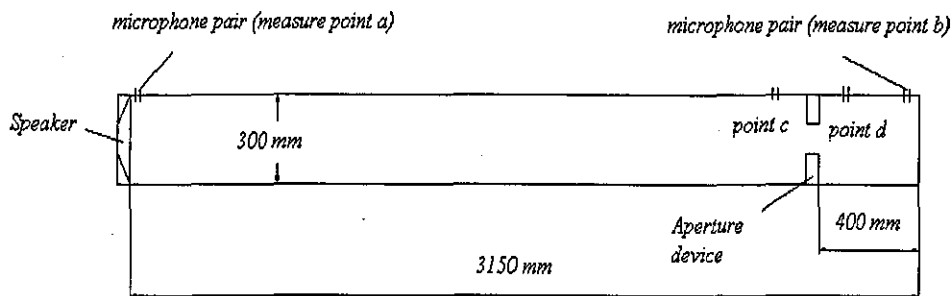


Fig 2.6 Experimental set-up for duct with simple aperture device situation

For the measurement of the impedances of the whole system, the experimental set-up is adopted as shown in Fig 2.6. First the aperture device is placed in and two microphone pairs situated at point *a* and point *b* can get one set of acoustic pressure and particle velocity. Then the input to the speaker is changed and another set of acoustic pressure

and particle velocity is obtained. Substituting these two sets of measurement results into equation (2.14), one can get the impedances Z_{ii} , Z_{io} and Z_{oo} directly (referred to as 'Measured results').

The procedures to measure the impedances of these two subsystems are given as below: First the measurement of the impedances for the duct without aperture device subsystem is carried on. Still the experimental set-up shown in Fig 2.6 is adopted. The aperture device is taken out and two microphone pairs are placed at point a and point b respectively to measure one set of the input and output acoustic pressure and particle velocity. Then the input to the speaker is changed and another set of measurement results is obtained. Substituting these two sets of measurement results into equation (2.18), the impedances of the duct without aperture device subsystem are obtained.

Secondly the measurement of the impedances for aperture device subsystem is carried on. The aperture device is placed in the duct and two microphone pairs are placed at point c and point d respectively to measure one set of the input and output acoustic pressure and particle velocity. Then the input to the speaker is changed and another set of measurement results is obtained. Substituting these two sets of measurement results into equation (2.19), the impedances of the aperture device subsystem are obtained.

Substituting the impedances of these two subsystems into equation (2.23), one can get the impedances Z_{ii} , Z_{io} and Z_{oo} for the whole system through the calculation (referred to as 'Calculated results').

The comparison of the results obtained by these two ways is shown below. Four different aperture devices with single concentric orifice are considered and two sets of results are shown for illustration. In these two figures, the left hand column shows the real part, imaginary part and amplitude of the input impedance Z_{ii} ; the middle column shows the real part, imaginary part and amplitude of the transfer impedance Z_{io} ; the right hand column shows the real part, imaginary part and amplitude of the output impedance Z_{oo} . Fig 2.7 shows the results when the diameter of the orifice is 210 mm (49% of open area).

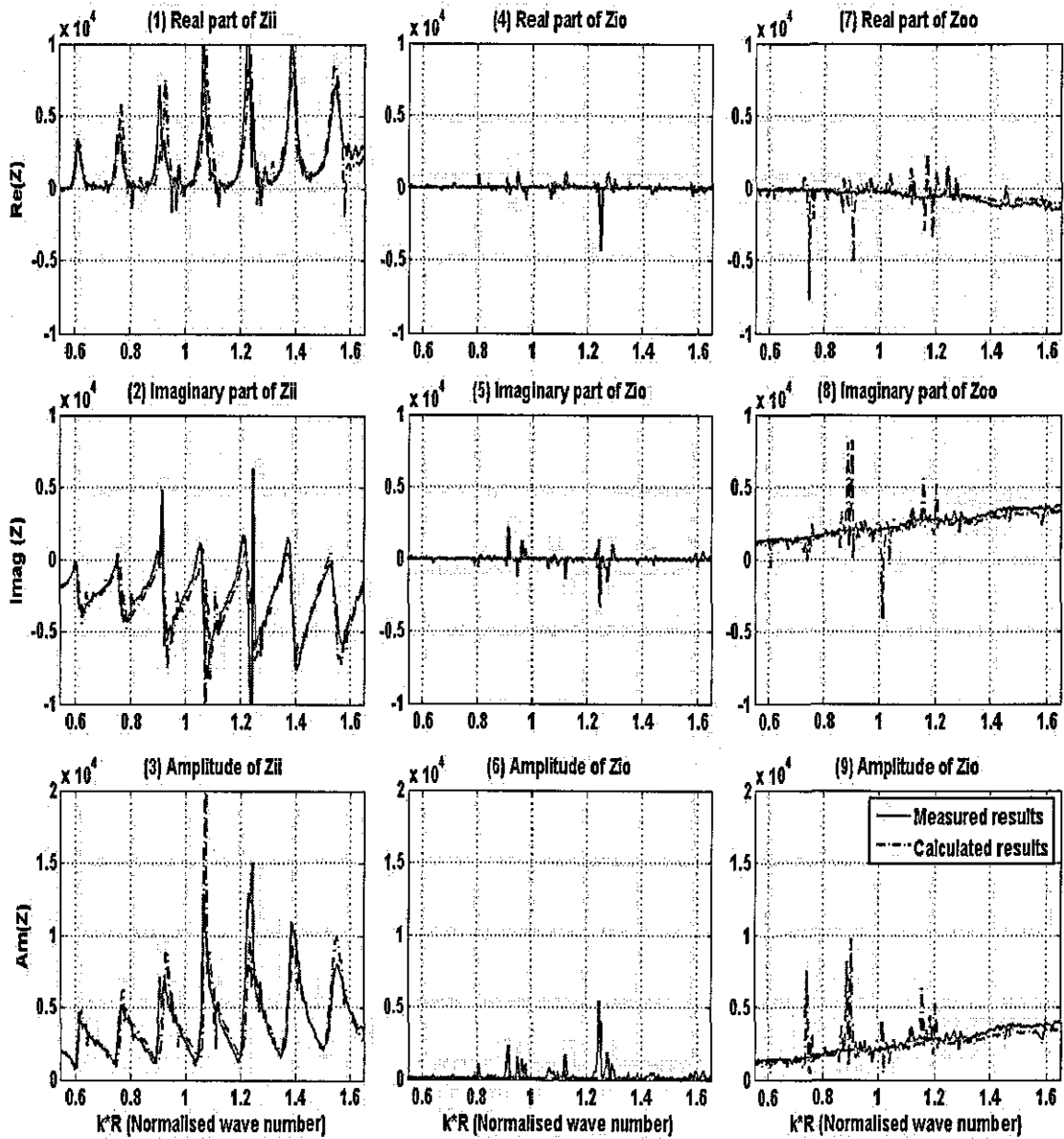


Fig 2.7 Comparison of impedances for aperture device with 49% of open area
(Two-different-inputs method)

Fig 2.8 shows the results when the diameter of the orifice is 60 mm (4% of open area).

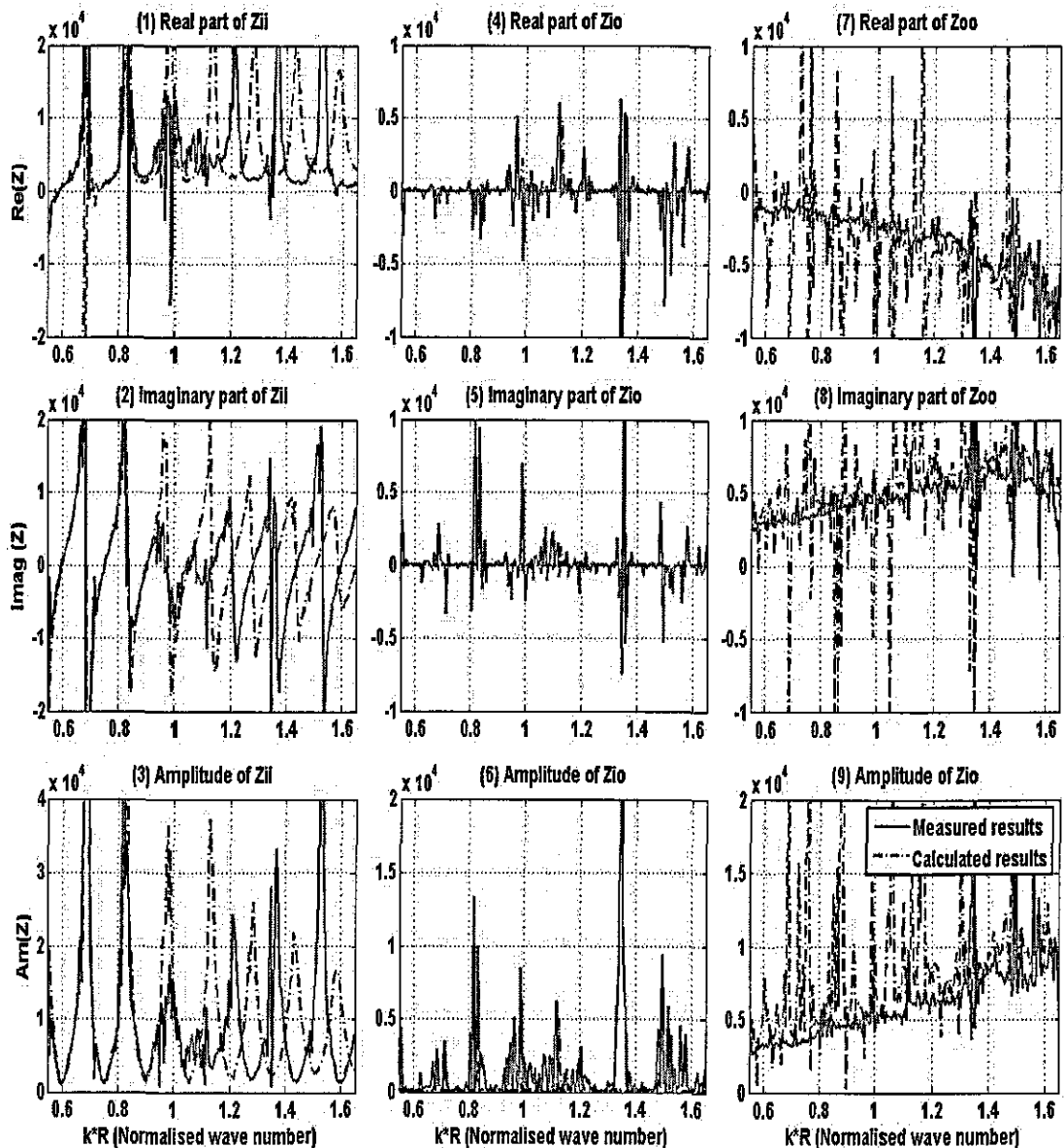


Fig 2.8 Comparison of impedances for aperture device with 4% of open area
(Two-different-inputs method)

Through the comparison of Fig 2.5, Fig 2.7 and Fig 2.8, it can be seen that

1. For the aperture device with 49% open area, the calculated results agree quite well with the measured results in the whole normalized wave number range shown in the figure. However for the aperture device with 4% open area, the calculated results agree quite well with the measured ones only in the normalized wave number range $k * R < 1$. In the normalized wave number range $k * R > 1$,

significant errors occur for the input impedance, which should be caused by the aperture device. By comparing Fig 2.7 with Fig 2.8, the effects of the open area on the calculation of the impedances through equation (2.23) can be seen. The larger the open area is, the smaller the errors are. For the other aperture devices, whose results are not shown, the results improved as the open area increased.

2. From Fig 2.5, it can be seen that the *blocked particle velocity method* is not an effective method, however from Fig 2.7 – 2.8, it can be seen that the *two-different-inputs method* is a reliable one for the aperture device with considerable open area.

2.6 Discussion

From the analysis above, one can see that, just as expected, the lumped-parameter model or the acoustical two-ports system is applicable at least to the plane wave situation in circular ducts. It is also often acknowledged by other researches as a powerful tool for the analysis of the acoustic properties in circular ducts. This model will be referred to in Chapter 3 and Chapter 9 and be approximated for the higher-order modes region, hence the reason for being introduced in this chapter.

Comparing these two measurement methods discussed above (*blocked particle velocity method* and *two-different-inputs method*), one can see that the *two-different-inputs method* is more accurate and effective than the *blocked particle velocity method*. So it will be applied in the investigation of the acoustic properties for higher-order modes propagation in circular ducts.

Compared with the wavelength, the dimension of the aperture devices used in this chapter are much smaller (the thickness of the aperture device is only 25 mm), so it is applicable to take it as lumped-parameter model. However if the frequency range is higher or the thickness of the aperture device is larger enough, the lumped-parameter model can not work any more and then the method provided in this chapter is not applicable for that situation. A new approach will be considered in the later chapters.

Chapter 3 Higher-order mode propagation in a circular duct and the reflection coefficients R_{mnl} at the duct open end

3.1 Introduction

In the previous chapter, the plane wave propagation in a circular duct has been discussed theoretically and experimentally. In this chapter, attention is given to the theoretical derivation of higher-order mode propagation in a circular duct without the presence of the aperture devices. Also the generalized impedance and the complex reflection coefficients at the open duct end are studied.

When considering the wave propagation in circular ducts, it is necessary to adopt the general three-dimensional (3D) wave equations. As discussed by M. L. Munjal in Ref [3] (chapter 1), in the ideal case of a rigid walled duct filled with stationary ideal (non-viscous) fluid and with only small amplitude waves travelling in it, the basic linear equations are given below.

Continuity equation:

$$\rho_0 \nabla \cdot u + \frac{\partial \rho}{\partial t} = 0. \quad (3.1)$$

Euler's equation:

$$\rho_0 \frac{\partial u}{\partial t} + \nabla p = 0. \quad (3.2)$$

State equation:

$$\frac{\partial p}{\partial \rho} \approx \frac{\gamma p_0}{\rho} = c^2. \quad (3.3)$$

From these three equations, the wave equation can be obtained

$$\left[\frac{\partial^2}{\partial t^2} - c^2 \nabla^2 \right] \psi = 0, \quad (3.4)$$

in which ψ is the velocity potential and the Laplacian ∇^2 for circular duct is given below:

$$\nabla^2 = \frac{\partial^2}{\partial r^2} + \frac{1}{r} \frac{\partial}{\partial r} + \frac{1}{r^2} \frac{\partial^2}{\partial \varphi^2} + \frac{\partial^2}{\partial z^2}. \quad (3.5)$$

3.2 Higher-order modes in circular cross-section duct

According to equation (3.4) and equation (3.5), the wave equation for the function velocity potential ϕ can be written in the form

$$\frac{1}{r} \frac{\partial}{\partial r} \left(r \frac{\partial \phi}{\partial r} \right) + \frac{1}{r^2} \frac{\partial^2 \phi}{\partial \varphi^2} + \frac{\partial^2 \phi}{\partial z^2} + k^2 \phi = 0, \quad (3.6)$$

where $\psi = \phi e^{j\omega t}$ and $k = \omega / c$. φ is the azimuthal angle.

Separating the variables by Fourier's method, it is possible to find the solution of this equation in the form

$$\phi(r, z, \varphi) = \sum_m R_m(r) e^{jm\varphi} Z(z), \quad (3.7)$$

in which the z-dependence function $Z(z)$ is given below

$$\frac{d^2 Z}{dz^2} = -k_z^2 Z. \quad (3.8)$$

Then substituting equation (3.7) and equation (3.8) in the wave equation (3.6), a Bessel function for r-dependence function $R_m(r)$ can be obtained

$$\frac{d^2 R_m}{dr^2} + \frac{1}{r} \frac{dR_m}{dr} + \left(k^2 - k_z^2 - \frac{m^2}{r^2} \right) R_m = 0. \quad (3.9)$$

The general solution for this function is

$$R_m = A_1 J_m(k_r r) + B_1 N_m(k_r r), \quad (3.10)$$

in which

$$k_r = \sqrt{k^2 - k_z^2}. \quad (3.11)$$

In equation (3.10), J_m and N_m are Bessel and Neumann functions of argument $(k_r r)$, k_r is the wave number. Since on the axis of the duct ($r = 0$), velocity potential ϕ should be finite, which means R_m should be also finite. But at the axis of the duct, if $r = 0$, $N_m(0) = -\infty$, this leads $R_m = -\infty$, which makes no sense for the velocity potential ϕ in the duct. So the index B_1 of the Neumann function N_m must be zero to make R_m sensible. If $B_1 = 0$, then the general solution of equation (3.10) can be written as,

$$R_m = A_1 J_m(k_r r) . \quad (3.12)$$

Again, if the wall of the duct is rigid, the radial velocity at the wall ($r = R_0$) should be zero. Therefore,

$$\frac{dJ_m(k_r r)}{dr} = 0 , \quad \text{when } r = R_0 . \quad (3.13)$$

so, k_r can only take discrete values, which satisfy the equation below:

$$J'_m(k_r R_0) = 0 . \quad (3.14)$$

By denoting the value of k_r corresponding to the n th root of this equation as $k_{r,m,n}$, one can get

$$\phi(r, z, \varphi) = \sum_{m=0}^{\infty} \sum_{n=1}^{\infty} J_m(k_{r,m,n} r) e^{jm\varphi} (A_{m,n} e^{-jk_{z,m,n} z} + B_{m,n} e^{jk_{z,m,n} z}) , \quad (3.15)$$

in which

$$k_{z,m,n} = \sqrt{k^2 - k_{r,m,n}^2} . \quad (3.16)$$

Introducing the harmonic multiplier $e^{j\omega t}$, the solution of the wave equation in the finite length circular duct is given as follow

$$(r, z, \varphi, t) = \sum_{m=0}^{\infty} \sum_{n=1}^{\infty} J_m(k_{r,m,n} r) e^{jm\varphi} e^{j\omega t} (A_{m,n} e^{-jk_{z,m,n} z} + B_{m,n} e^{jk_{z,m,n} z}) , \quad (3.17)$$

in which the first term is for forward propagating waves and the second term is for backward propagating waves reflected from the end of the duct.

Considering only forward propagating waves, one can get

$$\begin{aligned} \phi(r, z, \varphi, t) &= \sum_{m=0}^{\infty} \sum_{n=1}^{\infty} A_{m,n} J_m(k_{r,m,n} r) e^{jm\varphi} e^{j\omega t} e^{-jk_{z,m,n} z} , \\ p &= \rho \frac{\partial \phi}{\partial t} = j\rho\omega \sum_{m=0}^{\infty} \sum_{n=1}^{\infty} A_{m,n} J_m(k_{r,m,n} r) e^{jm\varphi} e^{j\omega t} e^{-jk_{z,m,n} z} , \\ v_z &= -\frac{\partial \phi}{\partial z} = jk_z \sum_{m=0}^{\infty} \sum_{n=1}^{\infty} A_{m,n} J_m(k_{r,m,n} r) e^{jm\varphi} e^{j\omega t} e^{-jk_{z,m,n} z} . \end{aligned} \quad (3.18)$$

If a sound wave produced at the source end can propagate along the z -axis, it should satisfy the condition below

$$\begin{aligned} k_{z,m,n} &> 0 , \\ k_{r,m,n} &< k . \end{aligned} \quad (3.19)$$

Otherwise $k_{z,m,n}$ is imaginary and can be written in the form,

$$k_{z,m,n} = \pm j\beta = \pm j\sqrt{k_{r,m,n}^2 - k^2} . \quad (3.20)$$

So $\phi(x, y, z, t)$ is given below

$$\phi(x, y, z, t) = e^{\pm\beta z} \sum_{m=0}^{\infty} \sum_{n=1}^{\infty} A_{m,n} J_m(k_{r,m,n}r) e^{jm\phi} e^{j\omega t} . \quad (3.21)$$

Taking the negative root of $k_{z,m,n}$ results in the amplitude of the wave diminishing exponentially with the increasing distance from the source end.

Thus, when $k = k_{r,m,n}$, there should be a corresponding cut-on frequency for this (m, n) mode.

$$f_{mn} = \frac{c * k_{r,m,n}}{2 * \pi} . \quad (3.22)$$

At a frequency below f_{mn} , the wave cannot propagate along the duct. This cut-on frequency corresponds to the frequency of the natural oscillations of the mode (m, n) in the direction transverse to z-axis.

According to the above discussion, one can get the cross-sectional spatial patterns of different modes (m, n) , shown in Fig 3.1 and Fig 3.2, for waves propagating in a circular duct (for convenience, the data is plotted on a Cartesian co-ordinate system). From these two figures, one can see that there are two different types of nodal lines in the plane transverse to z-axis. The first type nodal lines are the circumference nodal lines, which are corresponding to the Bessel function $J_m(k_{r,m,n}r)$ and on these nodal lines, there is $J_m(k_{r,m,n}r) = 0$, so the acoustic pressure p and the particle velocity v_z along z-axis on these nodal lines are zero. The second type nodal lines are the radial nodal lines, which are corresponding to the item $e^{jm\phi}$. It should also be noted that for circular duct that the first possible root of the differential of $J_m(k_{r,m,n}r)$ is $m = 0$ and $n = 1$, so the plane wave in circular duct is denoted to be $(0, 1)$ mode.

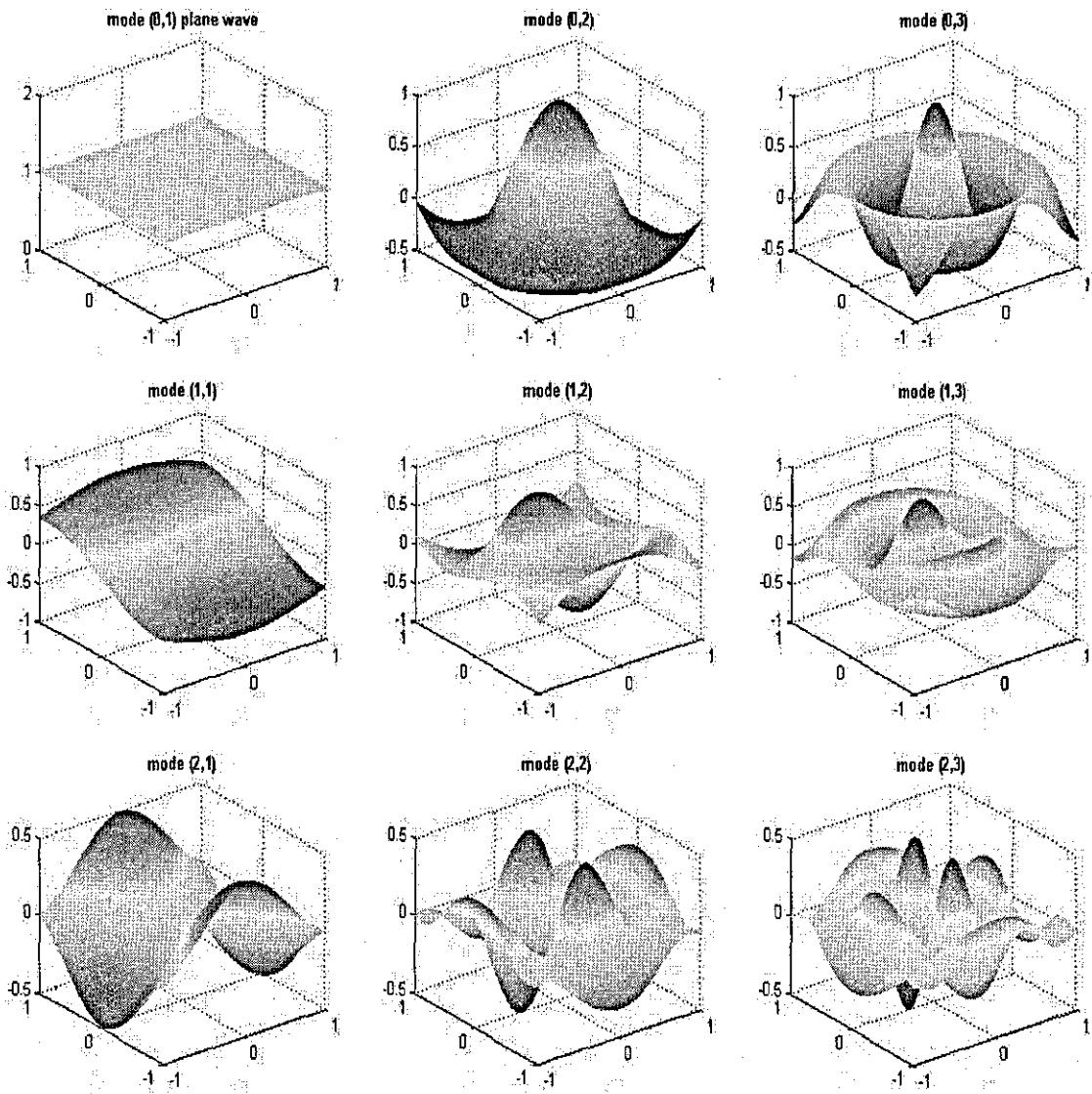


Fig 3.1 Normalised modal pattern of some higher-order modes in circular ducts (from (0, 1) mode to (2, 3) mode)

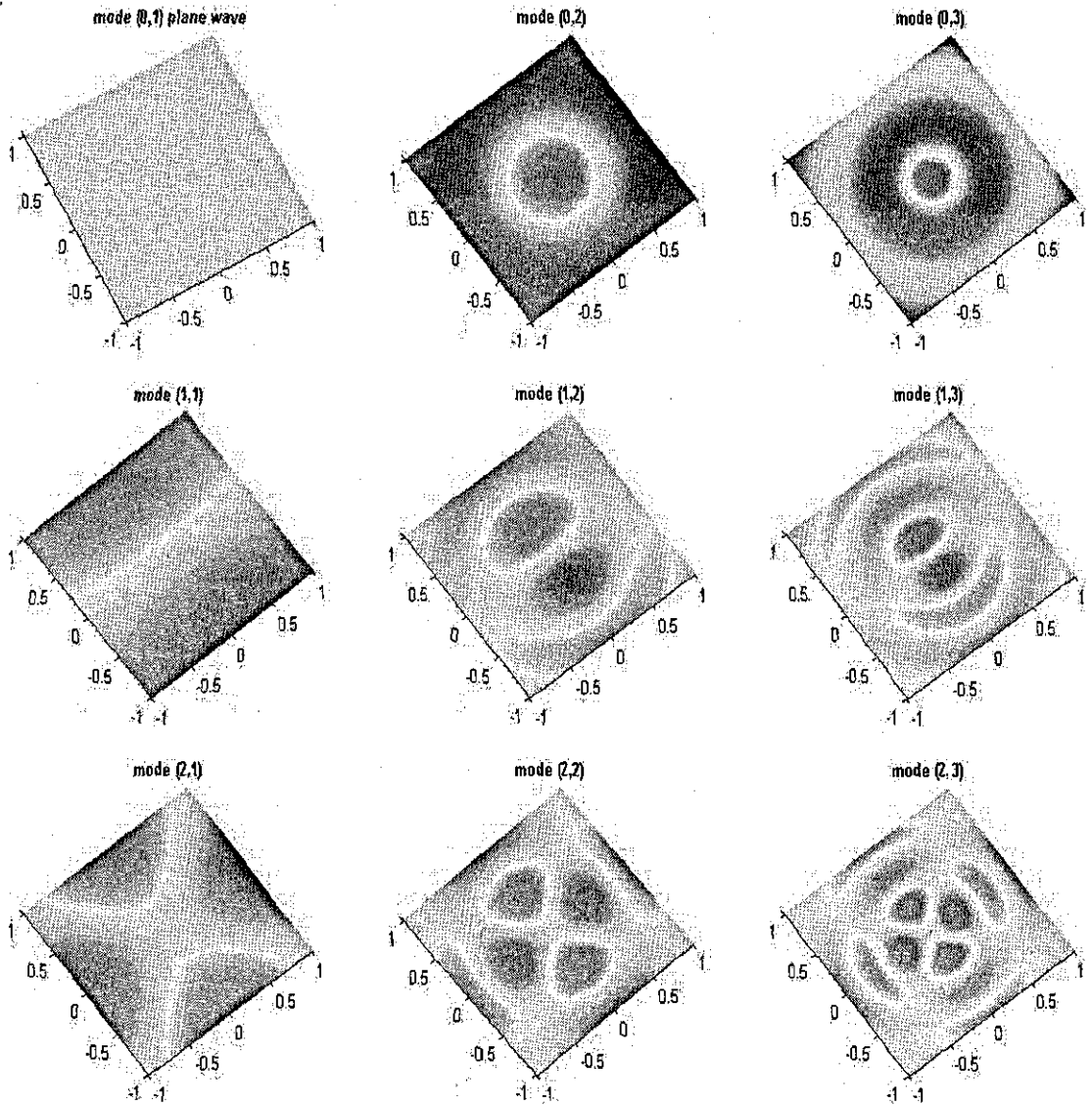


Fig 3.2 Surface of the modal patterns of some higher-order modes

From equation (3.18), one can also see that if the radius position and z-axis position stay unchanged, the acoustic pressure is a function of $\cos(m\varphi)$, which means that there is pressure difference between any two adjoining points with the same radius. This difference causes the spiral propagation pattern of those higher-order modes which agree $m \neq 0$.

3.3 Applicability of lumped-parameter model to higher-order modes in circular duct

In the previous chapter, when there was only the plane wave propagating in the circular duct, acoustic pressure and volume velocity were taken as two lumped parameters. Then the lumped-parameter model or the two ports system model was tested in the circular duct without and with simple aperture devices respectively. The results were considered satisfactory for orifice of significant open area. So in this section, the applicability of this model for higher-order mode propagation in a circular duct is discussed.

With the increasing of the frequency, higher-order modes begin to propagate along the duct. According to the equation (3.17), the acoustic pressure is given as follow:

$$p = \rho \frac{\partial \phi}{\partial t} = \sum_m \sum_n j\rho\omega (A_{mn} e^{-jk_{z,m,n}z} + B_{mn} e^{jk_{z,m,n}z}) J_m(k_{r,m,n}r) e^{jm\varphi} e^{j\omega t} \quad (3.23)$$

The particle velocities along z , r and φ are given as

$$v_z = -\frac{\partial \phi}{\partial z} = \sum_m \sum_n jk_{z,m,n} (A_{mn} e^{-jk_{z,m,n}z} - B_{mn} e^{jk_{z,m,n}z}) J_m(k_{r,m,n}r) e^{jm\varphi} e^{j\omega t} \quad (3.24)$$

$$v_r = -\frac{\partial \phi}{\partial r} = \sum_m \sum_n -k_{r,m,n} (A_{mn} e^{-jk_{z,m,n}z} + B_{mn} e^{jk_{z,m,n}z}) J'_m(k_{r,m,n}r) e^{jm\varphi} e^{j\omega t}, \quad (3.25)$$

$$v_\varphi = -\frac{\partial \phi}{\partial \varphi} = \sum_m \sum_n -jm (A_{mn} e^{-jk_{z,m,n}z} + B_{mn} e^{jk_{z,m,n}z}) J_m(k_{r,m,n}r) e^{jm\varphi} e^{j\omega t}.$$

In which the velocity along z -axis is of interest in this investigation. Then the volume velocity along z -axis is

$$\begin{aligned} U &= \int_0^R \int_0^{2\pi} v_z r dr d\varphi = \int_0^R \int_0^{2\pi} -\frac{\partial \phi}{\partial z} r dr d\varphi \\ &= \sum_m \sum_n jk_{z,m,n} (A_{mn} e^{-jk_{z,m,n}z} - B_{mn} e^{jk_{z,m,n}z}) e^{j\omega t} \int_0^R r J_m(k_{r,m,n}r) dr \int_0^{2\pi} e^{jm\varphi} d\varphi \quad (3.26) \\ &= 2\pi \sum_0 \sum_n jk_{z,0,n} (A_{0n} e^{-jk_{z,0,n}z} - B_{0n} e^{jk_{z,0,n}z}) e^{j\omega t} \int_0^R r J_0(k_{r,0,n}r) dr. \end{aligned}$$

It is well known that the relationship of Bessel function is

$$\int_0^R r J_0(kr) dr = \frac{R}{k} J_1(kR), \quad (3.27)$$

so applying equation (3.27) into equation (3.26), one can get

$$U = 2\pi R^2 (A_{01} e^{-jkz} - B_{01} e^{jkz}) e^{j\omega t} . \quad (3.28)$$

This equation equals to the volume velocity for the plane wave. Because for integration

$\int_0^{2\pi} e^{jm\varphi} d\varphi$, it is zero unless $m = 0$, which means that the volume velocity U_{mn} for (m, n)

mode equals zero unless $m = 0$. For integration $\int_0^R r J_0(k_{r,0,n} r) dr$, it is zero unless $n = 1$.

Combine them together, only (0, 1) mode (the plane wave) contributes to the volume velocity, which means the volume velocities of all higher-order modes are zero and have no significance.

Also the impedance along z-axis is given as follows:

$$\begin{aligned} Z_z = \frac{P}{v_z} &= \frac{\sum_m \sum_n j\rho\omega (A_{mn} e^{-jk_{z,m,n}z} + B_{mn} e^{jk_{z,m,n}z}) J_m(k_{r,m,n}r) e^{jm\varphi} e^{j\omega t}}{\sum_m \sum_n jk_{z,m,n} (A_{mn} e^{-jk_{z,m,n}z} - B_{mn} e^{jk_{z,m,n}z}) J_m(k_{r,m,n}r) e^{jm\varphi} e^{j\omega t}} \\ &= \frac{\sum_m \sum_n \rho\omega (A_{mn} e^{-jk_{z,m,n}z} + B_{mn} e^{jk_{z,m,n}z}) J_m(k_{r,m,n}r) e^{jm\varphi}}{\sum_m \sum_n k_{z,m,n} (A_{mn} e^{-jk_{z,m,n}z} - B_{mn} e^{jk_{z,m,n}z}) J_m(k_{r,m,n}r) e^{jm\varphi}} \end{aligned} \quad (3.29)$$

This impedance is so complicated that it cannot be expressed in an explicit form. From this equation, it is easy to see the impedance is not only a function of those coordinates z , r and φ , but also a function of the amplitudes of different higher-order modes A_{mn} and B_{mn} . In order to get the impedance along z-axis, it is necessary to know those amplitudes A_{mn} and B_{mn} first.

For the two ports system model, there is

$$\begin{aligned} P_i &= U_i Z_{ii} + U_o Z_{io} , \\ P_o &= U_i Z_{io} + U_o Z_{oo} . \end{aligned} \quad (3.30)$$

From this equation, one can see that it is impossible to apply this model for higher-order mode propagation in a circular duct. Because unlike the plane wave propagation in circular duct, the acoustic pressure and impedance along z-axis for higher-order modes are not constant in the plane transverse to z-axis of the duct. Also according to the lumped-parameter theory, the lumped-parameter model can only be applied to the situation when $k^* R \ll 1$. i.e. significantly below the first cut-on frequency. So it

appears that this model cannot directly apply to the higher-order mode propagation situation. However, if one can separate the in-duct field into a combination of different single higher-order modes, it is possible to treat each higher-order mode as an approximate lumped parameter. A schematic diagram for the approximate lumped-parameter model is shown below:

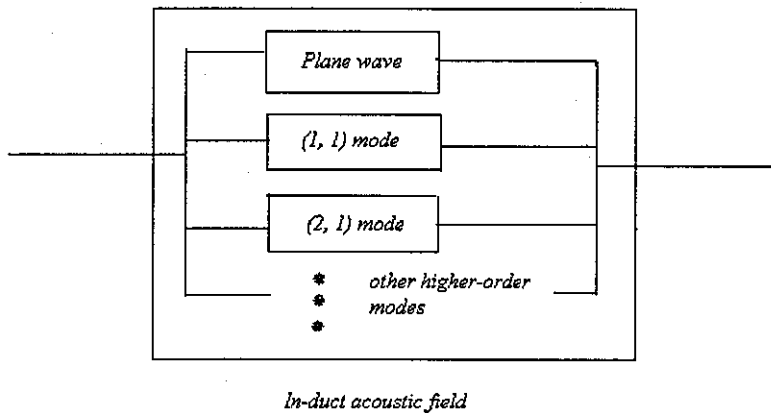


Fig 3.3 Schematic plot for the approximate lumped-parameter model

In order to justify the approximate lumped-parameter model, one should try to decompose the in-duct field into the combination of different single higher-order modes. This also requires knowledge of the coupling effects between different modes. In other words, one should try to get the complex amplitudes of different higher-order modes A_{mn} and B_{mn} . By knowing these amplitudes, one can not only analyse the distribution of the acoustic properties, such as, pressure, particle velocity, but also analyse the impedance or insertion loss (IL) of different simple aperture devices.

In the following section, one model is introduced to calculate the complex reflection coefficients R_{mnL} from the open end of the duct. From these coefficients, one can include the effects of the discontinuity at the open end of the duct, as well as the cross coupling effects between (m, n) mode and (m, L) mode.

3.4 Model to calculate the reflection coefficients R_{mL} at the open end of the duct

As shown in Fig 3.4, there is a circular duct of finite length and terminated with an infinite flange. Following the model proposed in Ref [15] by E. Z. William, the acoustic pressure at point A outside the duct ($z \geq 0$) with the coordinate (r, φ, z) is given by Helmholtz integral, which depends on the axial velocity v at the end of the duct.

$$p(r) = \frac{j\omega\rho}{2\pi} \int_0^{2\pi R} \int_0^{2\pi R} v(r_0) \frac{e^{-jkh}}{h} dr_0 d\varphi_0 . \quad (3.31)$$

In which h is the distance from the point A to the point x with the coordinate $(r_0, \varphi_0, 0)$ and is given by the equation below

$$h = [r^2 + r_0^2 - 2rr_0 \cos(\varphi - \varphi_0) + z^2]^{1/2} . \quad (3.32)$$

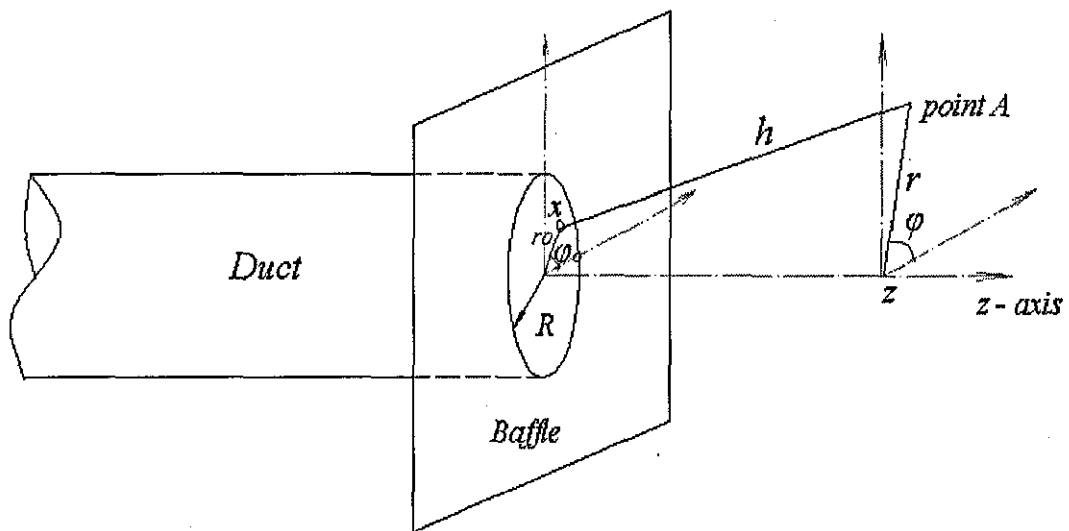


Fig 3.4 circular duct ended with infinite baffle

Equation (3.31) is the basis for the definition of generalized impedance of the duct termination.

The acoustic field in the duct ($z \leq 0$) is determined by the Helmholtz equation, the momentum equation and an admittance boundary condition of the duct walls:

$$\left. \begin{aligned} \nabla^2 p + k^2 p &= 0 \\ v &= \frac{j}{\rho\omega} \frac{\partial p}{\partial z} \end{aligned} \right|_{z \leq 0}, \quad (3.33)$$

$$\left. \beta_b p - \frac{j}{k} \frac{\partial p}{\partial r} = 0 \right|_{r=R}.$$

In this investigation, only the hard duct wall is considered, hence β_b , the specific admittance of the duct wall is zero. Then the equations above can be rewritten as:

$$\left. \begin{aligned} \nabla^2 p + k^2 p &= 0 \\ v &= \frac{j}{\rho\omega} \frac{\partial p}{\partial z} \end{aligned} \right|_{z \leq 0}, \quad (3.34)$$

$$\left. \frac{\partial p}{\partial r} = 0 \right|_{r=R}.$$

So the general solutions for the acoustic pressure and axial particle velocity of the in-duct fields are

$$p(r) = \rho c^2 \sum_{m=-\infty}^{\infty} e^{jm\phi} \sum_{n=1}^{\infty} (A_{mn} e^{-jk_{z,m,n}z} + B_{mn} e^{jk_{z,m,n}z}) J_m(k_{r,m,n}r) / N_{mn}, \quad (3.35)$$

$$v(r) = c \sum_{m=-\infty}^{\infty} e^{jm\phi} \sum_{n=1}^{\infty} \frac{k_{z,m,n}}{k} (A_{mn} e^{-jk_{z,m,n}z} - B_{mn} e^{jk_{z,m,n}z}) J_m(k_{r,m,n}r) / N_{mn}. \quad (3.36)$$

The radial modes are orthogonal and it is easy to choose the normalizing factor N_{mn}

$$k^2 \int_0^R r (J_m(k_{r,m,n}r) / N_{mn})^2 dr = 1. \quad (3.37)$$

Evaluating the resulting integral (Equation 11, Page. 135, Ref [9]) gives

$$N_{mn} = kR \left\{ 0.5 \left[1 - \left(\frac{m}{k_{r,m,n}R} \right)^2 \right] J_m(k_{r,m,n}R)^2 + J_m'(k_{r,m,n}R)^2 \right\}^{1/2}, \text{Re}(N_{mn}) > 0. \quad (3.38)$$

The acoustic pressure and particle velocity at the end of the duct (where $z = 0$) can be expressed in terms of the duct modes as

$$p(r) = \rho c^2 \sum_{m=-\infty}^{\infty} e^{jm\phi} \sum_{n=1}^{\infty} P_{mn} J_m(k_{r,m,n}r) / N_{mn}, \quad (3.39)$$

$$v(r) = c \sum_{m=-\infty}^{\infty} e^{jm\phi} \sum_{n=1}^{\infty} V_{mn} J_m(k_{r,m,n}r) / N_{mn}. \quad (3.40)$$

Substituting equation (3.40) into equation (3.31) gives the pressure

$$p(r) = \frac{j\omega\rho c}{2\pi} \sum_{m=-\infty}^{\infty} \sum_{n=1}^{\infty} V_{mn} \int_0^{2\pi} e^{jm\varphi_0} \int_0^R \frac{e^{-jkh}}{h} J_m(k_{r,m,n}r_0) / N_{mn} dr_0 d\varphi_0 . \quad (3.41)$$

In order to get the solution of the equation above, the function of h should be eliminated. According to the Sonine's infinite integral (Equation 4, Page 416, Ref [9]), this function can be expressed as follow:

$$\frac{e^{-jkh}}{h} = k \int_0^{\infty} \tau(\tau^2 - 1)^{-1/2} J_0(\tau kh) d\tau . \quad (3.42)$$

Using the Neumann's addition theorem

$$J_0(\tau kh) = \sum_{m=-\infty}^{\infty} J_m(\tau kr) J_m(\tau kr_0) e^{jm(\varphi-\varphi_0)} . \quad (3.43)$$

Substituting equation (3.43) into (3.42), one can get

$$\frac{e^{-jkh}}{h} = k \sum_{m=-\infty}^{\infty} e^{jm(\varphi-\varphi_0)} \int_0^{\infty} \tau(\tau^2 - 1)^{-1/2} J_m(\tau kr) J_m(\tau kr_0) d\tau . \quad (3.44)$$

Then equation (3.41) can be written as:

$$p(r) = j\rho c^2 \sum_{m=-\infty}^{\infty} e^{jm\varphi} \sum_{n=1}^{\infty} V_{mn} \int_0^{\infty} \tau(\tau^2 - 1)^{-1/2} J_m(\tau kr) D_{mn}(\tau) d\tau , \quad (3.45)$$

in which

$$D_{mn}(\tau) = k^2 \int_0^R J_m(\tau kr_0) J_m(k_{r,m,n}r_0) / N_{mn} dr_0 . \quad (3.46)$$

The integral relations of Bessel function is given as,

$$\int_0^R r J_m(\lambda r) J_m(\mu r) dr = \begin{cases} \frac{R}{\lambda^2 - \mu^2} [\mu J_m(\lambda R) J_m'(\mu R) - \lambda J_m(\mu R) J_m'(\lambda R)] & (\lambda \neq \mu) \\ \frac{R^2}{2} \left\{ (J_m'(\lambda R))^2 + \left(1 - \frac{m^2}{\lambda^2 R^2}\right) (J_m(\lambda R))^2 \right\} & (\lambda = \mu) . \end{cases} \quad (3.47)$$

Also according to equation (3.37), one can get the relationship as,

$$\sum_{L=1}^{\infty} k^2 \int_0^R (J_m(k_{r,m,L}r_0) / N_{mL})^* (J_m(k_{r,m,n}r_0) / N_{mn}) dr_0 = 1 . \quad (3.48)$$

So the modal velocity amplitude V_{mn} can be written as,

$$V_{mn} = \sum_{L=1}^{\infty} k^2 \int_0^R (J_m(k_{r,m,L}r_0) / N_{mL})^* (J_m(k_{r,m,n}r_0) / N_{mn}) dr_0 V_{mL} . \quad (3.49)$$

Then substituting equation (3.49) into equation (3.45), one can get,

$$\begin{aligned}
 p(r) &= j\rho c^2 \sum_{m=-\infty}^{\infty} e^{jm\varphi} \sum_{n=1}^{\infty} \left(\int_0^{\infty} \tau(\tau^2 - 1)^{-1/2} D_{mn}(\tau) d\tau * \right. \\
 &\quad \left. \sum_{L=1}^{\infty} k^2 \int_0^R J_m(\tau kr) (J_m(k_{r,m,L} r_0) / N_{mL}) dr_0 * (J_m(k_{r,m,n} r_0) / N_{mn}) V_{mL} \right) \quad (3.50) \\
 &= j\rho c^2 \sum_{m=-\infty}^{\infty} e^{jm\varphi} \sum_{n=1}^{\infty} (J_m(k_{r,m,n} r_0) / N_{mn}) \sum_{L=1}^{\infty} V_{mL} \int_0^{\infty} \tau(\tau^2 - 1)^{-1/2} D_{mn}(\tau) D_{mL}(\tau) d\tau \\
 &= \rho c^2 \sum_{m=-\infty}^{\infty} e^{jm\varphi} \sum_{n=1}^{\infty} (J_m(k_{r,m,n} r_0) / N_{mn}) \sum_{L=1}^{\infty} Z_{mnL} V_{mL} ,
 \end{aligned}$$

where the generalized impedance of the circular duct is given as,

$$Z_{mnL} = j \int_0^{\infty} \tau(\tau^2 - 1)^{-1/2} D_{mn}(\tau) D_{mL}(\tau) d\tau . \quad (3.51)$$

The modal pressure amplitudes can be got through equation (3.39) and equation (3.50)

$$P_{mn} = \sum_{L=1}^{\infty} Z_{mnL} V_{mL} . \quad (3.52)$$

From equation (3.35), it can be seen that the acoustic field in the duct is composed of sets of incident waves and reflected waves whose amplitudes have been designated by A_{mn} and B_{mn} . Comparing equations (3.35) and (3.36) with equations (3.39) and (3.40), one can see that A_{mn} and B_{mn} are related to the modal pressure and particle velocity amplitudes at the end of the duct by

$$P_{mn} = A_{mn} + B_{mn} , \quad (3.53)$$

$$V_{mn} = \frac{k_{z,m,n}}{k} (A_{mn} - B_{mn}) . \quad (3.54)$$

Substituting equations (3.53) and (3.54) into equation (3.51)

$$\sum_{L=1}^{\infty} (Z_{mnL} \frac{k_{z,m,L}}{k} + \delta_{nL}) B_{mL} = \sum_{L=1}^{\infty} (Z_{mnL} \frac{k_{z,m,L}}{k} - \delta_{nL}) A_{mL} , \quad (3.55)$$

in which δ_{nL} is Kronecker Delta function.

$$\delta_{nL} \equiv \begin{cases} 1 & n = L \\ 0 & n \neq L . \end{cases} \quad (3.56)$$

Then it is easy to get B_{mn} by the equation below

$$B_{mn} = \sum_{L=1}^{\infty} R_{mnL} A_{mL} . \quad (3.57)$$

In which R_{mnL} are the generalized reflection coefficients and can be obtained by the infinite matrix

$$[R_{mnL}] = [[Z_{mnL}] \left[\frac{k_{z,m,L}}{k} \right] + [I]]^{-1} [[Z_{mnL}] \left[\frac{k_{z,m,L}}{k} \right] - [I]], \quad (3.58)$$

in which $[I]$ is the unit matrix (identity matrix).

Then from the equations above, it is easy to get the complex reflection coefficients R_{mnL} and then A_{mn} and B_{mn} . So the in-duct fields are determined and predictable for this situation.

3.5 Generalized impedances Z_{mnL} and reflection coefficients R_{mnL}

From equation (3.51), one can get the generalized impedance Z_{0nL} as shown below. In Fig 3.5, Z_{011} , Z_{012} , Z_{013} , Z_{014} are generalized impedances which denote respectively (0, 1) to (0, 4) mode particle velocity driven by (0, 1) mode acoustic pressure. In Fig 3.6, Z_{012} , Z_{022} , Z_{032} , Z_{042} are generalized impedances which denote (0, 2) mode particle velocity driven by (0, 1) to (0, 4) mode acoustic pressure respectively. In Fig 3.7, Z_{111} , Z_{112} , Z_{113} , Z_{114} are generalized impedances which denote respectively (1, 1) to (1, 4) mode particle velocity driven by (1, 1) mode acoustic pressure, $k * R$ is the normalised wave number.

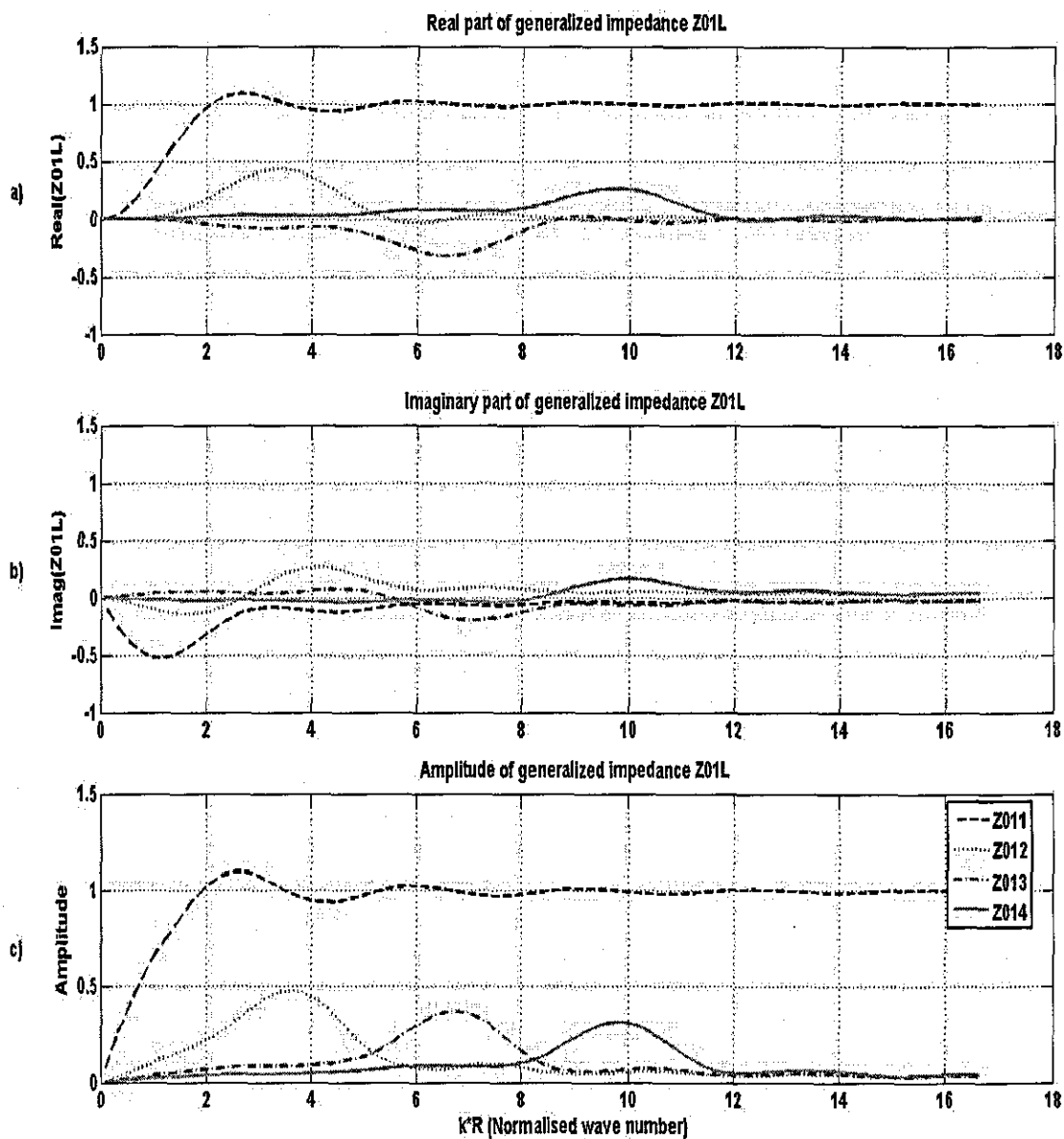


Fig 3.5 The generalized impedances Z_{01L} Vs $k * R$ (a) shows real parts of generalized impedance; b) shows imaginary parts of generalized impedance; c) shows amplitudes of generalized impedance)

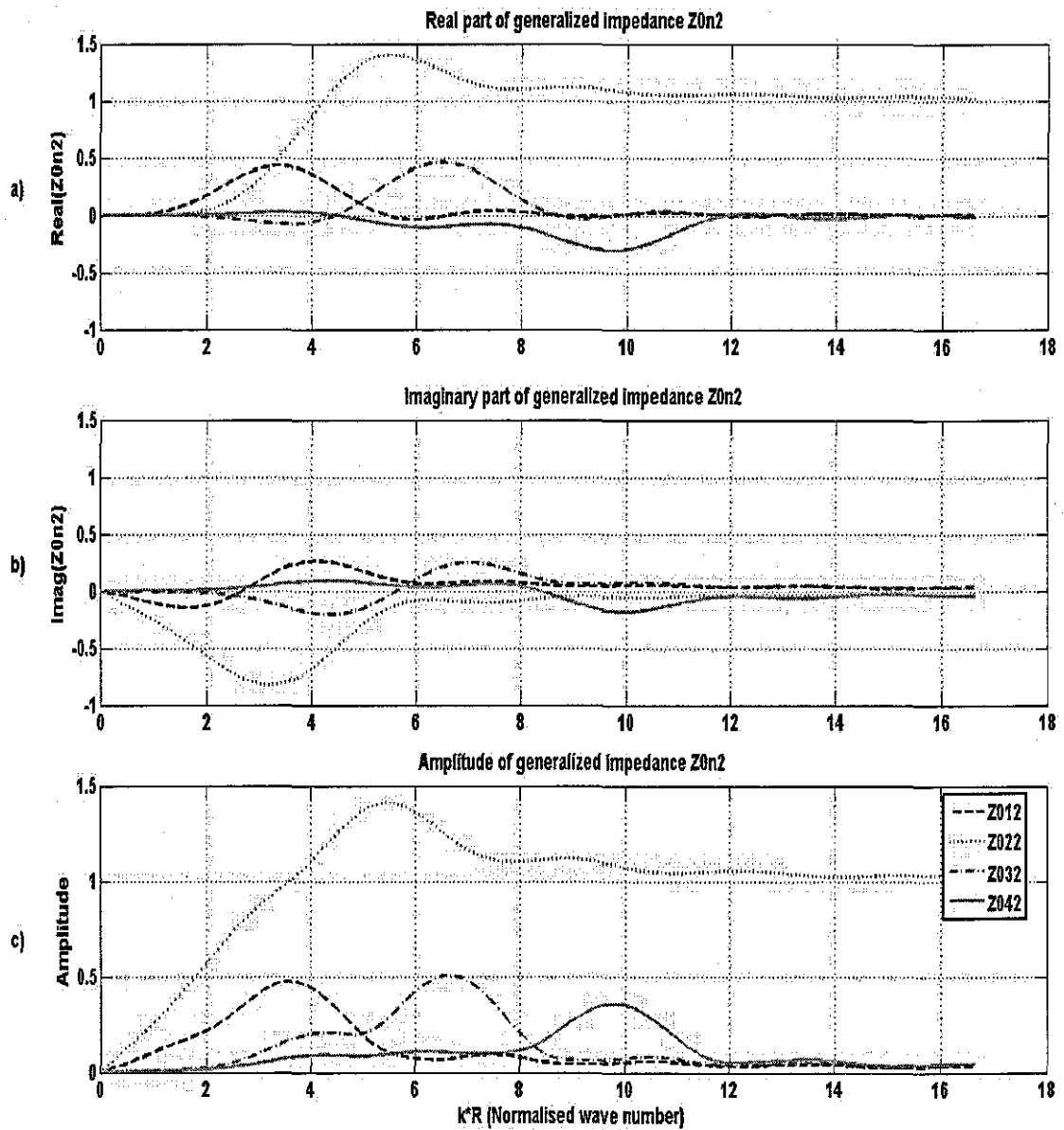


Fig 3.6 The generalized impedances Z_{0n2} Vs $k \cdot R$ (a) shows real parts of generalized impedance; b) shows imaginary parts of generalized impedance; c) shows amplitudes of generalized impedance)

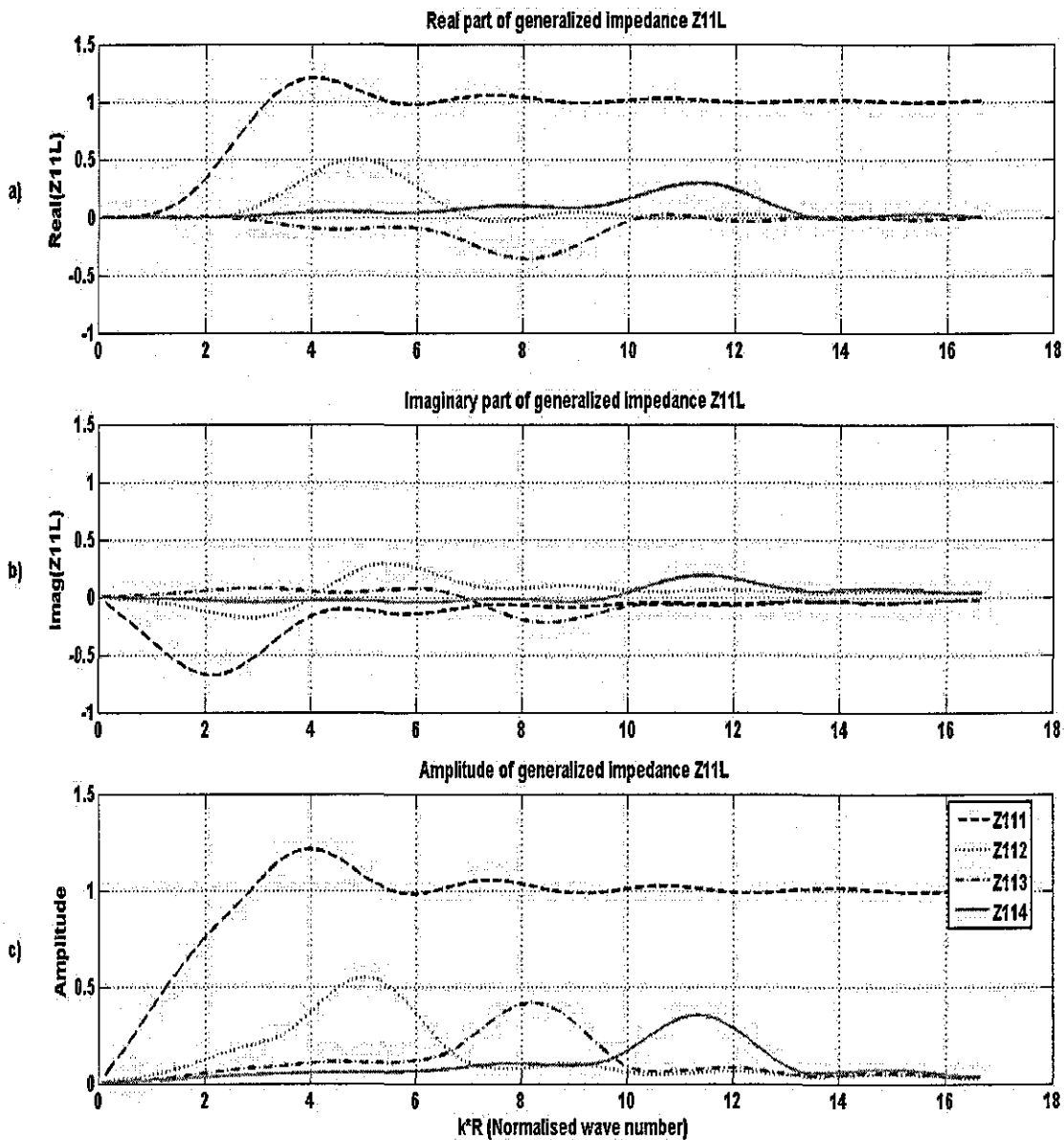


Fig 3.7 The generalized impedances Z_{11L} Vs $k \cdot R$ (a) shows real parts of generalized impedance; b) shows imaginary parts of generalized impedance; c) shows amplitudes of generalized impedance)

From Fig 3.5-3.7, it can be seen that

1. There are cross coupling effects between different higher-order modes. Take the Z_{11L} for example, which means the axially-unsymmetric 1st mode pressure distribution (P_{11}) caused by the axially-unsymmetric L^{th} mode velocity distribution (v_{1L}) at the end of the duct. The cross coupling impedances Z_{112} ,

Z_{113} , Z_{114} are largest when the L^{th} mode cuts on and then approach to zero with the increasing of the $k * R$ number. One can also see that the amplitudes of those cross coupling impedances are getting smaller with the increasing of the number $(L - n)$, which means the higher the number of the mode, the less cross coupling impedance Z_{1nL} . According to these figures, neglecting the coupling effects in the calculation of the acoustic properties of the in - duct field will introduce some errors to the results. So these effects will be considered in the calculation in this analysis.

2. For the direct impedances Z_{mm} , such as Z_{011} , Z_{022} and Z_{111} , are not largest at the cut on frequencies of those modes but they are approach unity with the increasing of the $k * R$ number. For example, the maximum of the impedance Z_{011} appears at $k * R \approx 2.5$, the maximum of the impedance Z_{022} appears at $k * R \approx 5.5$ and the maximum of the impedance Z_{111} appears at $k * R \approx 4$. However, it can be seen that the imaginary part of those impedances is largest around cut on frequencies of those modes, which means that around the cut on frequency, the acoustic pressure and particle velocity are out of phase and then they are in phase at the higher frequency range. From equation (3.51), it is easy to see that the matrix of the impedances Z_{mnL} is symmetric, which means

$$Z_{mnL} = Z_{mLn}.$$

3. The three figures show three different situations, Fig 3.5 shows the coupling impedances between other higher-order modes with the plane wave; Fig 3.6 shows the coupling impedances between those higher-order modes, which are axially-symmetric ($m = 0$); Fig 3.7 shows the coupling impedances between those higher-order modes, which are axially-unsymmetric ($m \neq 0$). No matter what situation, the modes follow the same trend. This means that the coupling impedances of all those higher-order modes are similar and can be explained by the equation (3.51).

Substituting the generalized impedance Z_{mnL} into equation (3.58), one can get the generalized reflection coefficients R_{mnL} . The following complex reflection coefficients R_{01L} , R_{0n2} , R_{11L} and R_{1nn} are shown from Fig 3.8 to Fig 3.11.

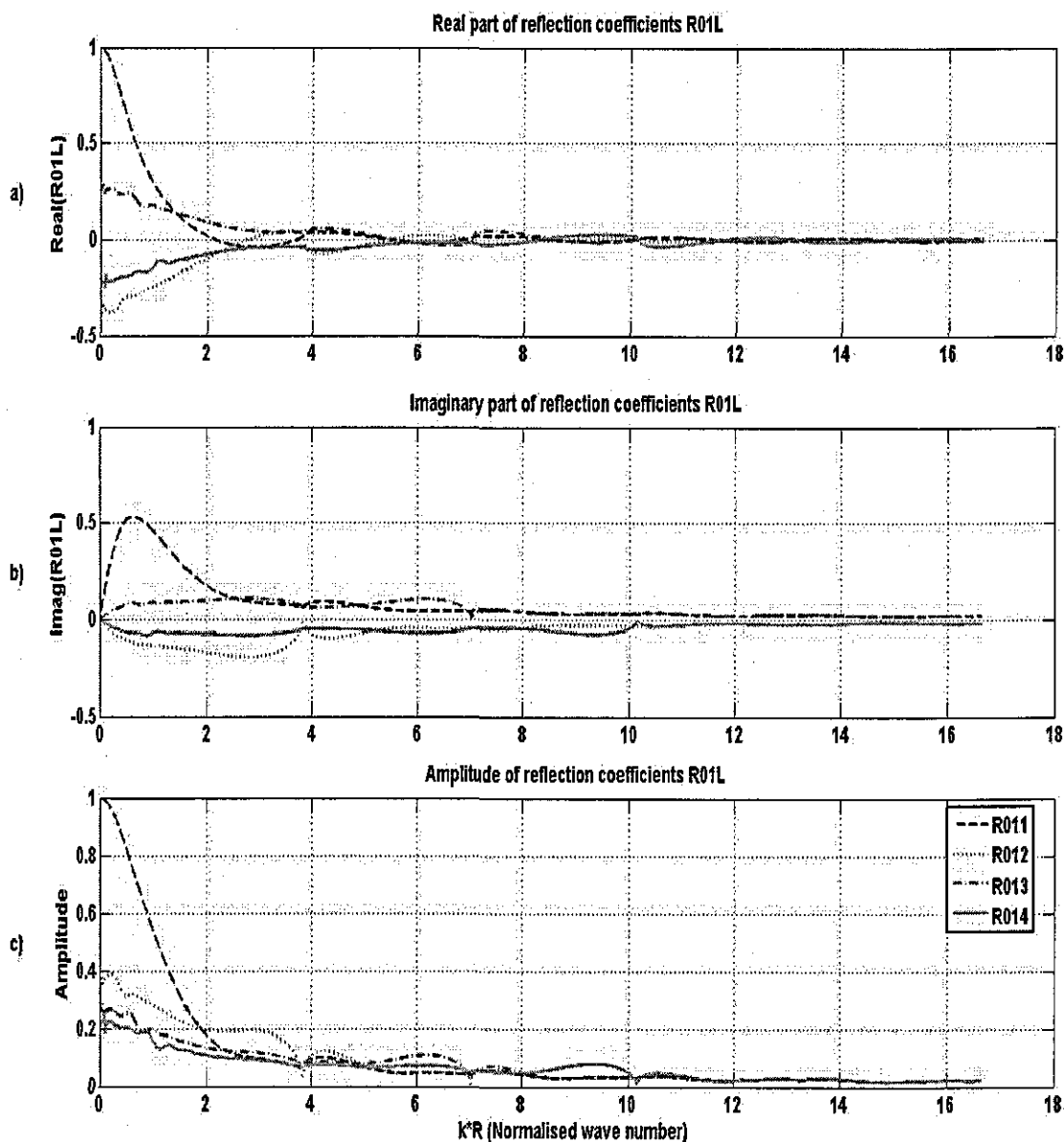


Fig 3.8 The reflection coefficients R_{01L} Vs $k \cdot R$ (a) shows real parts of reflection coefficients; b) shows imaginary parts of reflection coefficients; c) shows amplitudes of reflection coefficients)

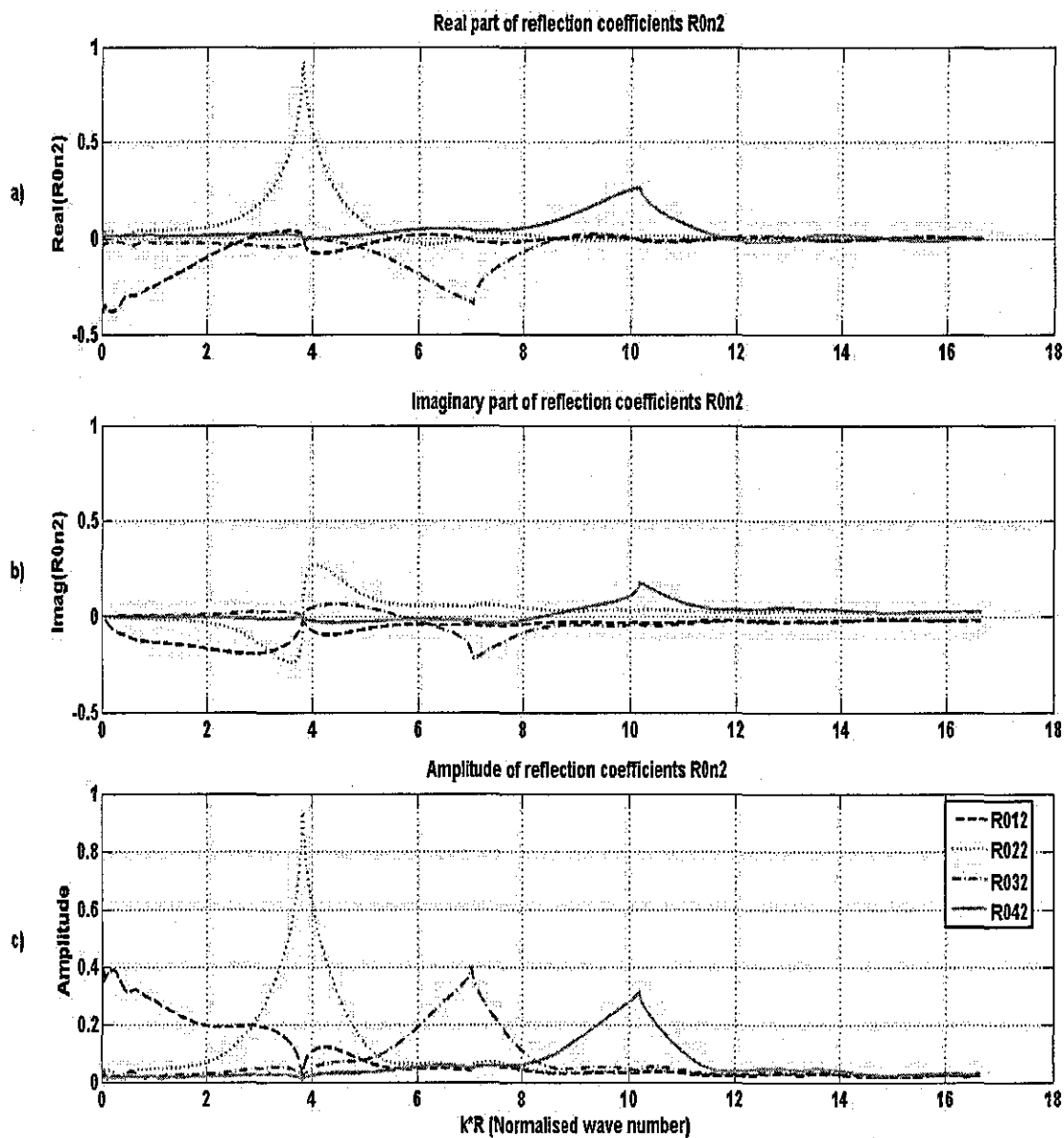


Fig 3.9 The reflection coefficients R_{0n2} Vs $k * R$ (*a*) shows real parts of reflection coefficients; *b*) shows imaginary parts of reflection coefficients; *c*) shows amplitudes of reflection coefficients)

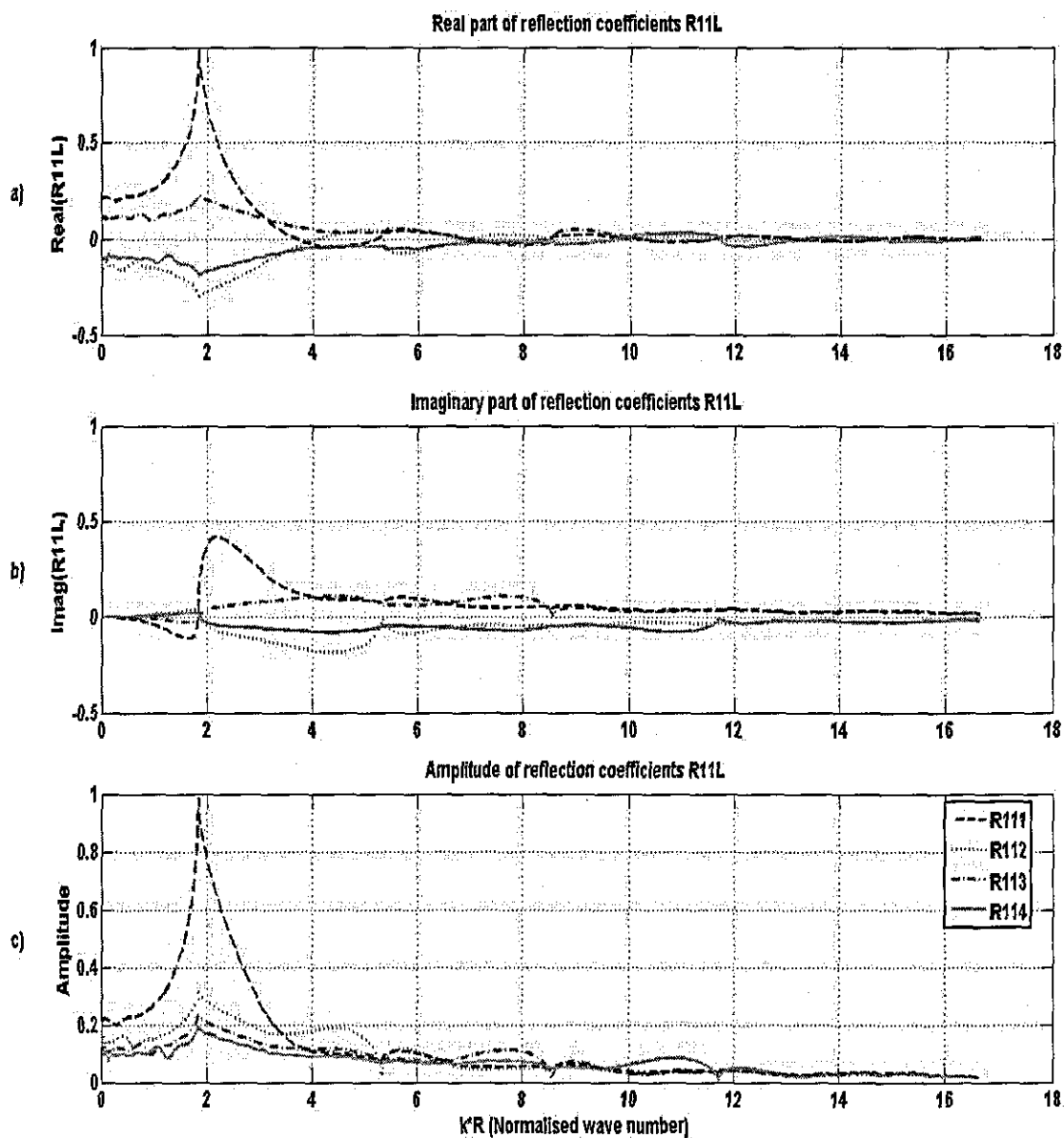


Fig 3.10 The reflection coefficients R_{11L} Vs $k * R$ (*a*) shows real parts of reflection coefficients; *b*) shows imaginary parts of reflection coefficients; *c*) shows amplitudes of reflection coefficients)

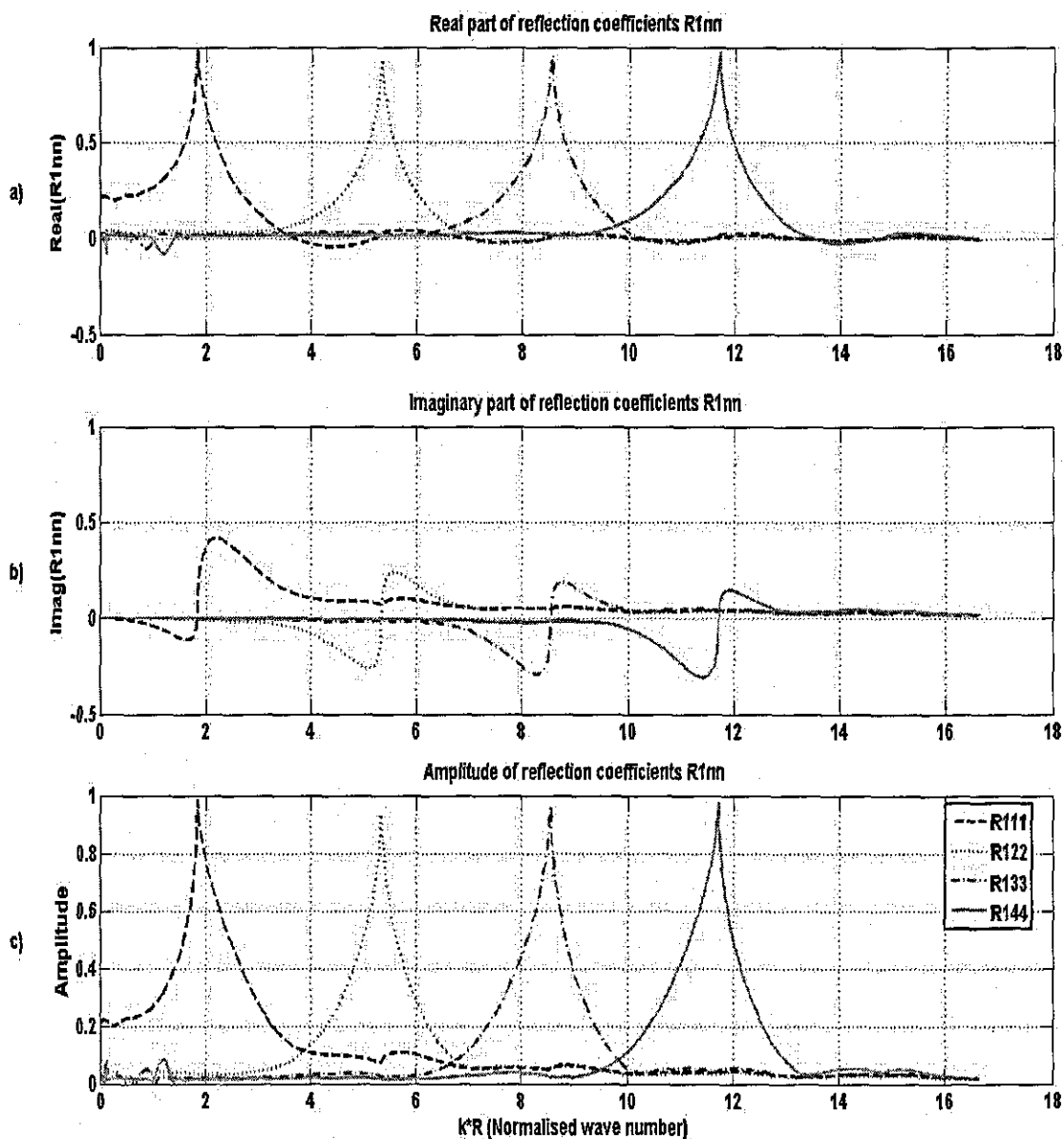


Fig 3.11 The reflection coefficients R_{1mn} Vs $k * R$ (a) shows real parts of reflection coefficients; b) shows imaginary parts of reflection coefficients; c) shows amplitudes of reflection coefficients)

From Fig.3.8 and Fig 3.10, one can see that for coefficients R_{mL} the maximum values appear when the (m, L) mode cuts on. From Fig 3.9 one can see that for coefficients R_{0n2} the maximum values appear when $(0, n)$ mode cuts on. Also one can see that R_{mnL} are not smooth curve lines. The discontinuity points occur when different higher-order modes cut on. For example, the coefficient R_{011} is biggest at zero frequency and then

discontinues at $k * R = 3.83$ ((0, 2) mode cuts on), $k * R = 7.02$ ((0, 3) mode cuts on) and $k * R = 10.17$ ((0, 4) mode cuts on). This phenomenon shows the contribution of other higher-order modes to the reflection coefficient of this model.

From Fig 3.8-3.11, it can be seen that:

1. As shown in Fig 3.8, at the plane wave cut on frequency (0 Hz), the coefficients $R_{011} = 1$, $R_{012} = -0.4$, $R_{013} = 0.25$ and $R_{014} = -0.21$, which means the amplitudes (absolute value) of these reflection coefficients are diminishing with the increasing of the number n . The same trend is also shown in Fig 3.10, which is $R_{111} > R_{112} > R_{113} > R_{114}$, when (1, 1) mode cuts on. This shows the higher number of the mode, the less contribution to those small number modes and vice versa.
2. At the low wave number range ($k * R < 1.84$), R_{011} is larger than any other coefficients R_{01n} and at this frequency range, other higher-order modes do not cut on, so the amplitudes of other higher-order modes should be nearly zero. The reflection coefficients of the even number modes, such as R_{012} and R_{014} are negative, but those of the odd number modes, such as R_{011} and R_{013} are plus. This means that the contributions of the odd number mode to odd number mode are constructive and the contributions of the even number mode to odd number mode are destructive.
3. From Fig 3.9, one can see that for R_{0n2} , the contributions of the (0, 2) mode to other (0, n) modes are significant only around the region when (0, n) mode cuts on. At all other wave number region, they are very small. Still the higher the number of (0, n), the less contribution of (0, 2) mode to it.
4. From Fig 3.11, one can see the direct reflection coefficients R_{1mn} are nearly the same. The coefficients are nearly equal to 1 at their cut on frequencies and are decreasing very quickly to a very small number - the real parts of those coefficients R_{1mn} are approaching zero, which means at the higher frequency range, the reflection coefficients are nearly purely imaginary. This means at the

higher frequency range, the backward waves are out of phase with those incident waves.

5. From all these four figures, one can also see the reflection coefficients of different types, which are coefficients of other higher-order modes with the plane wave R_{01n} , coefficients of axially-symmetric higher-order modes R_{0n2} ($m = 0$) and coefficients of axially-unsymmetric higher-order modes R_{mn1} ($m \neq 0$), are nearly the same and follow the same trend.

3.6 Discussion

In this chapter, the higher-order mode propagation in circular duct are introduced and the applicability of the lumped-parameter model is also presented. Then in order to break the limitation of the lumped-parameter model, the so-called approximate lumped-parameter model is proposed. In order to justify the approximate lumped-parameter model, the in-duct field should be decomposed into the combination of different higher-order mode. So one model to obtain the complex reflection coefficients at the open duct end is studied.

After knowing those reflection coefficients, combining with other boundary conditions, such as the sound source boundary condition, the aperture device boundary conditions, one can find an approach to construct enough equations for the decomposition. In the following chapters, two different types of sound source will be introduced and then the results will be compared.

Chapter 4 The plane wave source and the point source

4.1 Introduction

The acoustic field in a circular duct is determined not only by the type of aperture device and the condition of the open end, but also by the type of sound source. Different types of sound source can produce different acoustic waves, which can propagate along the duct. Two types of sound source, which are the point source and the plane wave source, are mainly considered for circular ducts. Indeed many other complicated sources can be treated as the combination of different point sources.

In order to predict or decompose the in-duct field, one should first decide which type of sound source is to be used and then describe it mathematically. Different types of sound source can produce different patterns of the higher-order modes in the duct, or even the same sound source located at different radial locations can produce different patterns of higher-order modes. In this chapter, the configurations of these two types of sound sources are introduced first. Then the descriptions of the sound source boundary conditions are also given. Combining the descriptions with other boundary conditions, one can easily construct the equations that are needed for the solution of the acoustic properties in circular duct.

4.2 The plane wave source

4.2.1 Configuration of the plane wave source

The first type of sound source to be introduced is the plane wave source. The configuration of this type of sound source is shown in Fig 4.1, in which a duct with a small diameter is used as the sound source. This type of sound source is quite common and widely adopted in the mufflers or the ventilation ducts which are composed of ducts with different radii. This is why the plane wave source is studied in this investigation.

The reason why it is called a plane wave source is given as follows. The frequency range which is of interest in this investigation is from 0 Hz to 2600 Hz . Because when the

radius of the duct is $0.15m$, the first higher-order mode is cut on around $640Hz$, so this frequency range is four times the first higher-order mode cut on frequency. And in this frequency range, there are altogether 17 modes propagating in the main duct (including the plane wave). The radius of the small duct (source duct) is only $0.024m$. So for this small duct at this frequency range,

$$0 \leq k * R \leq 1.15 . \quad (4.1)$$

This value of Helmholtz number is less than the first higher-order mode ($\pm 1,1$) cut on value of 1.84, which means that only the plane wave can propagate in this small duct (source duct). So this type of source is considered as a plane wave source. Actually on the boundary between these two ducts or even a very small distance from this boundary, there should be many other higher-order modes, which are attenuating in an exponential manner. So in order to get an accurate description of this boundary condition, those attenuating higher-order modes should also be considered.

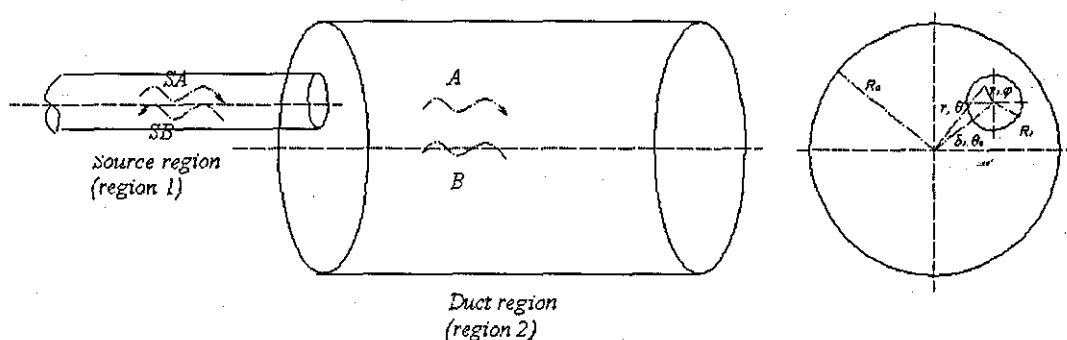


Fig 4.1 Configuration of the plane wave source in circular duct

4.2.2 Description of the plane wave source boundary condition

As discussed in Chapter 3, the acoustic pressure and particle velocity along the z -axis in one circular duct can be written as,

$$P(r, z, \varphi) = \sum_{m=-\infty}^{\infty} \sum_{n=1}^{\infty} J_m(k_{r,m,n} r) e^{jm\varphi} A_{m,n} e^{-jk_{z,m,n} z} , \quad (4.2)$$

4. The plane wave source and the point source

$$v_z(r, z, \varphi) = \frac{k_{z,m,n}}{\rho c k} \sum_{m=-\infty}^{\infty} \sum_{n=1}^{\infty} J_m(k_{r,m,n} r) e^{jm\varphi} A_{m,n} e^{-jk_{z,m,n} z}. \quad (4.3)$$

So as shown in Fig 4.1, for region 1 (source duct), one can write the acoustic pressure as follows, for positive direction propagating wave,

$$P_{SA} = SA_{01} e^{-jkz} + \sum_{n=2}^{\infty} SA_{0n} J_0(k_{r,0,n}^I r) e^{-jk_{z,0,n}^I z} \\ + \sum_{m=1}^{\infty} \sum_{n=1}^{\infty} J_m(k_{r,m,n}^I r) (SA_{mn}^+ e^{-jm\varphi} + SA_{mn}^- e^{jm\varphi}) e^{-jk_{z,m,n}^I z}. \quad (4.4)$$

For negative direction propagating wave,

$$P_{SB} = SB_{01} e^{jkz} + \sum_{n=2}^{\infty} SB_{0n} J_0(k_{r,0,n}^I r) e^{jk_{z,0,n}^I z} \\ + \sum_{m=1}^{\infty} \sum_{n=1}^{\infty} J_m(k_{r,m,n}^I r) (SB_{mn}^+ e^{-jm\varphi} + SB_{mn}^- e^{jm\varphi}) e^{jk_{z,m,n}^I z}. \quad (4.5)$$

For the positive and negative direction propagating waves in region 2 (main duct), the acoustic pressure can be written as

$$P_A = A_{01} e^{-jkz} + \sum_{n=2}^{\infty} A_{0n} J_0(k_{r,0,n}^{II} r) e^{-jk_{z,0,n}^{II} z} \\ + \sum_{m=1}^{\infty} \sum_{n=1}^{\infty} J_m(k_{r,m,n}^{II} r) (A_{mn}^+ e^{-jm\varphi} + A_{mn}^- e^{jm\varphi}) e^{-jk_{z,m,n}^{II} z}, \quad (4.6)$$

$$P_B = B_{01} e^{jkz} + \sum_{n=2}^{\infty} B_{0n} J_0(k_{r,0,n}^{II} r) e^{jk_{z,0,n}^{II} z} \\ + \sum_{m=1}^{\infty} \sum_{n=1}^{\infty} J_m(k_{r,m,n}^{II} r) (B_{mn}^+ e^{-jm\varphi} + B_{mn}^- e^{jm\varphi}) e^{jk_{z,m,n}^{II} z}, \quad (4.7)$$

in which, the parameters with superscript I, such as $k_{r,m,n}^I$, are the values for region 1 (source region) and the parameters with superscript II, such as $k_{r,m,n}^{II}$, are values for region 2 (main duct region).

Then at this boundary, the continuity conditions can be written as, for acoustic pressure,

$$P_{SA} + P_{SB} \Big|_{Z=-L} = P_A + P_B \Big|_{Z=-L} \quad (\text{over } S_1). \quad (4.8)$$

For particle velocity,

$$v_{SA} + v_{SB} \Big|_{Z=-L} = v_A + v_B \Big|_{Z=-L} \quad (\text{over } S_1), \quad (4.9)$$

$$v_A + v_B \Big|_{Z=-L} = 0 \quad (\text{over } (S - S_1)). \quad (4.10)$$

Here S is the cross sectional area of the main duct, S_1 is the cross sectional area of the source duct.

For pressure continuity condition, multiplying both sides of equation (4.8) by

$J_t(k_{r,t,s}^I r_1) e^{-jt\varphi}$ and integrating over the small duct region (S_1), for $t = 0, s = 1$, there is

$$\begin{aligned}
 & SA_{01} e^{jkL} + SB_{01} e^{-jkL} R_1 / 2 \\
 &= (A_{01} e^{jkL} + B_{01} e^{-jkL}) R_1 / 2 \\
 &+ \sum_{n=2}^{\infty} (A_{0n} e^{jk_{z,0,n}^I L} + B_{0n} e^{-jk_{z,0,n}^I L}) \frac{1}{k_{r,0,n}^I} J_0(k_{r,0,n}^I \delta_1) J_1(k_{r,0,n}^I R_1) \\
 &+ \sum_{m=1}^{\infty} \sum_{n=1}^{\infty} (((A_{mn}^+ e^{jk_{z,m,n}^I L} + B_{mn}^+ e^{-jk_{z,m,n}^I L}) e^{-jm\theta_0} + (A_{mn}^- e^{jk_{z,m,n}^I L} + B_{mn}^- e^{-jk_{z,m,n}^I L}) e^{jm\theta_0}) \\
 &\quad \frac{1}{k_{r,m,n}^I} J_m(k_{r,m,n}^I \delta_1) J_1(k_{r,m,n}^I R_1)) .
 \end{aligned} \tag{4.11}$$

For $t = 0, s = 2, 3, \dots, \infty$, there is

$$\begin{aligned}
 & (SA_{0s} e^{jk_{z,0,s}^I L} + SB_{0s} e^{-jk_{z,0,s}^I L}) J_0(k_{r,0,s}^I R_1) R_1 / 2 \\
 &= \sum_{n=2}^{\infty} (A_{0n} e^{jk_{z,0,n}^I L} + B_{0n} e^{-jk_{z,0,n}^I L}) \frac{k_{r,0,n}^I}{k_{r,0,s}^I{}^2 - k_{r,0,n}^I{}^2} J_0(k_{r,0,n}^I \delta_1) J_0'(k_{r,0,n}^I R_1) \\
 &+ \sum_{m=1}^{\infty} \sum_{n=1}^{\infty} (((A_{mn}^+ e^{jk_{z,m,n}^I L} + B_{mn}^+ e^{-jk_{z,m,n}^I L}) e^{-jm\theta_0} + (A_{mn}^- e^{jk_{z,m,n}^I L} + B_{mn}^- e^{-jk_{z,m,n}^I L}) e^{jm\theta_0}) \\
 &\quad \frac{k_{r,m,n}^I}{k_{r,0,s}^I{}^2 - k_{r,m,n}^I{}^2} J_m(k_{r,m,n}^I \delta_1) J_0'(k_{r,m,n}^I R_1)) .
 \end{aligned} \tag{4.12}$$

For $t = 1, 2, \dots, \infty, s = 1, 2, \dots, \infty$, there is

$$\begin{aligned}
 & (SA_{ts}^- e^{jk_{z,t,s}^I L_3} + SB_{ts}^- e^{-jk_{z,t,s}^I L_3}) (1 - \frac{t^2}{k_{r,t,s}^I{}^2 R_1^2}) J_t(k_{r,t,s}^I R_1) R_1 / 2 \\
 &= \sum_{n=2}^{\infty} (A_{0n} e^{jk_{z,0,n}^I L_3} + B_{0n} e^{-jk_{z,0,n}^I L_3}) J_t(k_{r,0,n}^I \delta_1) (\frac{k_{r,0,n}^I}{k_{r,t,s}^I{}^2 - k_{r,0,n}^I{}^2}) J_t'(k_{r,0,n}^I R_1) \\
 &+ \sum_{m=1}^{\infty} \sum_{n=1}^{\infty} ([(A_{mn}^+ e^{jk_{z,m,n}^I L_3} + B_{mn}^+ e^{-jk_{z,m,n}^I L_3}) (-1)^t J_{m-t}(k_{r,m,n}^I \delta_1) e^{-jm\theta_0} \\
 &\quad + (A_{mn}^- e^{jk_{z,m,n}^I L_3} + B_{mn}^- e^{-jk_{z,m,n}^I L_3}) J_{m+t}(k_{r,m,n}^I \delta_1) e^{jm\theta_0}] \\
 &\quad (\frac{k_{r,m,n}^I}{k_{r,t,s}^I{}^2 - k_{r,m,n}^I{}^2}) J_t'(k_{r,m,n}^I R_1)) .
 \end{aligned} \tag{4.13}$$

Multiplying both sides of equation (4.8) with $J_t(k_{r,t,s}^I r_1) e^{jt\phi}$ and integrating it over the small duct region (S_1), for $t = 1, 2, \dots, \infty, s = 1, 2, \dots, \infty$, there is,

$$\begin{aligned}
 & (SA_{ts}^+ e^{jk_{z,t,s}^I L} + SB_{ts}^+ e^{-jk_{z,t,s}^I L}) \left(1 - \frac{t^2}{k_{r,t,s}^I{}^2 R_1^2}\right) J_t(k_{r,t,s}^I R_1) R_1 / 2 \\
 &= \sum_{n=2}^{\infty} (A_{0n} e^{jk_{z,0,n}^I L} + B_{0n} e^{-jk_{z,0,n}^I L}) J_t(k_{r,0,n}^I \delta_1) \left(\frac{k_{r,0,n}^I}{k_{r,t,s}^I{}^2 - k_{r,0,n}^I{}^2}\right) J_t'(k_{r,0,n}^I R_1) \quad (4.14) \\
 &+ \sum_{m=1}^{\infty} \sum_{n=1}^{\infty} \left[(A_{mn}^+ e^{jk_{z,m,n}^I L} + B_{mn}^+ e^{-jk_{z,m,n}^I L}) J_{m+t}(k_{r,m,n}^I \delta_1) e^{-jm\theta_0} \right. \\
 &\quad \left. + (A_{mn}^- e^{jk_{z,m,n}^I L} + B_{mn}^- e^{-jk_{z,m,n}^I L}) (-1)^t J_{m-t}(k_{r,m,n}^I \delta_1) e^{jm\theta_0} \right] \\
 &\quad \left(\frac{k_{r,m,n}^I}{k_{r,t,s}^I{}^2 - k_{r,m,n}^I{}^2}\right) J_t'(k_{r,m,n}^I R_1) .
 \end{aligned}$$

The derivation procedure of equation (4.11) to equation (4.14) is given in Appendix C.

For two particle velocity continuity conditions, multiplying both equation (4.9) and equation (4.10) by $J_t(k_{r,t,s}^I r) e^{-jt\theta}$, integrating equation (4.9) over the small duct region (S_1) and integrating equation (4.10) over other region ($S - S_1$), adding them together, one can obtain the following equations.

For $t = 0, s = 1$, there is

$$(SA_{01} e^{jkl} - SB_{01} e^{-jkl}) R_1^2 = (A_{01} e^{jkl} - B_{01} e^{-jkl}) R_0^2 . \quad (4.15)$$

For $t = 0, s = 2, 3, \dots, \infty$, there is

$$\begin{aligned}
 & (SA_{01} e^{jkl} - SB_{01} e^{-jkl}) \frac{R_1}{k_{r,0,s}^I} J_0(k_{r,0,s}^I \delta_1) J_1(k_{r,0,s}^I R_1) \\
 &+ \sum_{n=2}^{\infty} \left(\frac{k_{z,0,n}^I}{k}\right) (SA_{0n} e^{jk_{z,0,n}^I L} - SB_{0n} e^{-jk_{z,0,n}^I L}) \\
 &\quad \frac{R_1 k_{r,0,s}^I}{k_{r,0,n}^I{}^2 - k_{r,0,s}^I{}^2} J_0(k_{r,0,s}^I \delta_1) J_0(k_{r,0,n}^I R_1) J_0'(k_{r,0,s}^I R_1) \quad (4.16) \\
 &+ \sum_{m=1}^{\infty} \sum_{n=1}^{\infty} \left(\frac{k_{z,m,n}^I}{k}\right) \left((SA_{mn}^+ e^{jk_{z,m,n}^I L} - SB_{mn}^+ e^{-jk_{z,m,n}^I L}) + (SA_{mn}^- e^{jk_{z,m,n}^I L} - SB_{mn}^- e^{-jk_{z,m,n}^I L}) \right) \\
 &\quad \frac{R_1 k_{r,0,s}^I}{k_{r,m,n}^I{}^2 - k_{r,0,s}^I{}^2} J_m(k_{r,0,s}^I \delta_1) J_m(k_{r,m,n}^I R_1) J_m'(k_{r,0,s}^I R_1)
 \end{aligned}$$

4. The plane wave source and the point source

$$= \frac{k_{r,o,s}^{II}}{k} (A_{0s} e^{jk_{z,o,s}^{II}L} - B_{0s} e^{-jk_{z,o,s}^{II}L}) \frac{R_0^2}{2} J_0^2(k_{r,o,s}^{II} R_0).$$

For $t = 1, 2, \dots, \infty, s = 1, 2, \dots, \infty$, there is,

$$\begin{aligned} & (SA_{01} e^{jkl} - SB_{01} e^{-jkl}) e^{-j\theta_0} J_t(k_{r,t,s}^{II} \delta_1) \frac{R_1}{k_{r,t,s}^{II}} J_1(k_{r,t,s}^{II} R_1) \\ & + \sum_{n=2}^{\infty} \left(\frac{k_{z,o,n}^I}{k} (SA_{0n} e^{jk_{z,o,n}^I L} - SB_{0n} e^{-jk_{z,o,n}^I L}) e^{-j\theta_0} \right. \\ & \quad \left. J_t(k_{r,t,s}^{II} \delta_1) \frac{R_1 k_{r,t,s}^{II}}{k_{r,o,n}^I - k_{r,t,s}^{II}} J_0'(k_{r,t,s}^{II} R_1) J_0(k_{r,o,n}^I R_1) \right) \\ & + \sum_{m=1}^{\infty} \sum_{n=1}^{\infty} \left[(SA_{mn}^+ e^{jk_{z,m,n}^I L} - SB_{mn}^+ e^{-jk_{z,m,n}^I L}) (-1)^m J_{t-m}(k_{r,t,s}^{II} \delta_1) \right. \\ & \quad \left. + (SA_{mn}^- e^{jk_{z,m,n}^I L} - SB_{mn}^- e^{-jk_{z,m,n}^I L}) J_{m+t}(k_{r,t,s}^{II} \delta_1) \right] \\ & \quad \frac{k_{z,m,n}^I}{k} \left(\frac{R_1 k_{r,t,s}^{II}}{k_{r,m,n}^I - k_{r,t,s}^{II}} \right) J_m'(k_{r,t,s}^{II} R_1) J_m(k_{r,m,n}^I R_1) e^{-j\theta_0} \\ & = \frac{k_{z,t,s}^{II}}{k} (A_{ts}^- e^{jk_{z,t,s}^{II} L} - B_{ts}^- e^{-jk_{z,t,s}^{II} L}) \frac{R_0^2}{2} \left(1 - \frac{t^2}{k_{r,t,s}^{II} R_0^2} \right) J_t^2(k_{r,t,s}^{II} R_0). \end{aligned} \tag{4.17}$$

Multiplying both equation (4.9) and equation (4.10) by $J_t(k_{r,t,s}^{II} r) e^{j\theta}$, integrating equation (4.9) over the small duct region (S_1) and equation (4.10) over other region ($S - S_1$), adding them together. One can get, for $t = 1, 2, \dots, \infty, s = 1, 2, \dots, \infty$,

$$\begin{aligned} & (SA_{01} e^{jkl} - SB_{01} e^{-jkl}) e^{j\theta_0} J_t(k_{r,t,s}^{II} \delta_1) \frac{R_1}{k_{r,t,s}^{II}} J_1(k_{r,t,s}^{II} R_1) \\ & + \sum_{n=2}^{\infty} \left(\frac{k_{z,o,n}^I}{k} (SA_{0n} e^{jk_{z,o,n}^I L} - SB_{0n} e^{-jk_{z,o,n}^I L}) e^{j\theta_0} \right. \\ & \quad \left. J_t(k_{r,t,s}^{II} \delta_1) \frac{R_1 k_{r,t,s}^{II}}{k_{r,o,n}^I - k_{r,t,s}^{II}} J_0'(k_{r,t,s}^{II} R_1) J_0(k_{r,o,n}^I R_1) \right) \\ & + \sum_{m=1}^{\infty} \sum_{n=1}^{\infty} \left[(SA_{mn}^+ e^{jk_{z,m,n}^I L} - SB_{mn}^+ e^{-jk_{z,m,n}^I L}) J_{m+t}(k_{r,t,s}^{II} \delta_1) \right. \\ & \quad \left. + (SA_{mn}^- e^{jk_{z,m,n}^I L} - SB_{mn}^- e^{-jk_{z,m,n}^I L}) (-1)^m J_{t-m}(k_{r,t,s}^{II} \delta_1) \right] \\ & \quad \frac{k_{z,m,n}^I}{k} \left(\frac{R_1 k_{r,t,s}^{II}}{k_{r,m,n}^I - k_{r,t,s}^{II}} \right) J_m'(k_{r,t,s}^{II} R_1) J_m(k_{r,m,n}^I R_1) e^{j\theta_0} \\ & = \frac{k_{z,t,s}^{II}}{k} (A_{ts}^- e^{jk_{z,t,s}^{II} L} - B_{ts}^- e^{-jk_{z,t,s}^{II} L}) \frac{R_0^2}{2} \left(1 - \frac{t^2}{k_{r,t,s}^{II} R_0^2} \right) J_t^2(k_{r,t,s}^{II} R_0). \end{aligned} \tag{4.18}$$

$$= \frac{k_{z,t,s}^{II}}{k} (A_{ts}^+ e^{jk_{z,t,s}^{II}L} - B_{ts}^+ e^{-jk_{z,t,s}^{II}L}) \frac{R_0^2}{2} \left(1 - \frac{t^2}{k_{r,t,s}^{II} R_0^2}\right) J_t^2(k_{r,t,s}^{II} R_0).$$

The derivation procedure of equation (4.15) to (4.18) is given in Appendix D.

By now one has sufficient equations for the plane wave source boundary condition from equation (4.11) to equation (4.18). For example, if $m = \pm 4$ and $n = 4$, there should be totally 144 ($2 * (2 * n + 4 * |m| * n)$) unknown amplitudes (SA_{mn}, SB_{mn}, A_{mn} and B_{mn}). At the same time, let $t = 4$ and $s = 4$, then from equation (4.11) to equation (4.18), one can get 72 ($2 * s + 4 * t * s$) independent equations. So combining with other boundary conditions, one can easily construct enough equations for those unknown amplitudes. These procedures will be adopted in the following chapters.

4.3 The point source

4.3.1 Configuration of the point source

The second type of sound source to be introduced is the point source. The configuration of the point source is shown in Fig 4.2. In which one small hole is opened on a hard baffle to act as a point source. In experimental set-up, one tube with very small inner radius R_p is used to act as this point source. In this situation, the radius of this tube is $R_p = 0.0075m$. The smaller the radius of the duct, the more it behaves like a point source. However it can never be a true point source and can only be treated as a good approximate one. In the frequency range which is of interest from 0 Hz to 2600 Hz, the value of Helmholtz Number $k * R_p \leq 0.36$, which is far less than the first higher-order mode $(\pm 1, 1)$ cut on value of 1.84. Also the ratio of these two radii is $0.0075m / 0.15m = 1/20 = 5\%$.

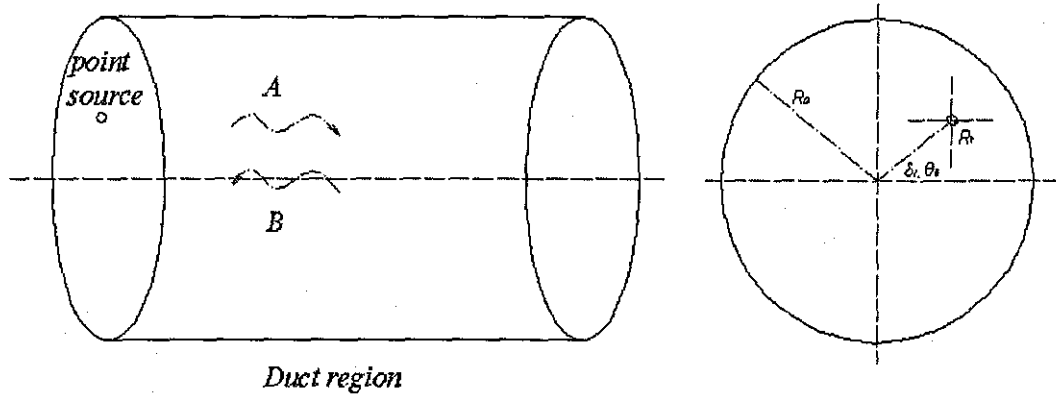


Fig 4.2 Configuration of the point source in circular duct

4.3.2 Description of the point source boundary condition

As discussed in Chapter IV of Ref [8] by S. N. Rschevkin, for a point source backed by a hard baffle, the particle velocity is related to acoustic pressure by

$$v_s = \frac{p(kl - j)}{\rho ckl}, \quad (4.19)$$

in which, l is the distance from the point source. If the radius of the source is very small, then the value of Helmholtz Number $k * l$ is nearly equal to zero, compared with unity, it can be ignored, so equation (4.19) can be expressed as

$$v_s \approx \frac{-jp}{\rho ckl} = \frac{Q}{2\pi l^2} e^{j(\omega t - kl)}, \quad (4.20)$$

in which Q is the source strength. If the radius l is very small, then the particle velocity should approach infinity. So the particle velocity continuity at the hard baffle can be written as,

$$v_A + v_B \Big|_{Z=-L} = v_s \Big|_{Z=-L} \quad (\text{over source region } S_1) \quad (4.21)$$

If the particle velocity is expressed as equation (4.20), the continuity equation (4.21) is impossible, because the particle velocity $v_A + v_B$ should be finite at that point.

Actually as discussed before, the ideal point source is replaced by a small duct of radius R_p . In the frequency range of interest, only the plane wave can propagate in this small tube. So it can be assumed that the particle velocity at this end of the duct is

$$v_s|_{z=-L} = v_0, \quad (4.22)$$

in which v_0 is constant that is decided only by the strength of the source. So the volume velocity for this situation is

$$U_0|_{z=-L} = \pi * R_p^2 * v_0. \quad (4.23)$$

The velocity boundary conditions of the plane wave source are shown by equation (4.9) and equation (4.10). For the point source, they can be written as

$$\begin{aligned} v_A + v_B|_{z=-L} &= v_0 \quad (\text{over } S_1), \\ v_A + v_B|_{z=-L} &= 0 \quad (\text{over } (S - S_1)), \end{aligned} \quad (4.24)$$

where S_1 is the area of the source duct and S is the area of the main duct. To implement these boundary conditions, multiply both sides with $J_l(k_{r,t,s}^{II} r) e^{-jt\theta}$ and integrate over their respective domains, finally add them together, one can get

$$\begin{aligned} & \int_0^{2\pi} \int_0^{R_p} v_0 J_l(k_{r,t,s}^{II} r) e^{-jt\theta} r_1 dr_1 d\varphi \\ &= \int_0^{2\pi} \int_0^{R_0} ((A_{0l} e^{jkL} - B_{0l} e^{-jkL}) \\ & \quad + \sum_{n=2}^{\infty} \frac{k_{z,0,n}^{II}}{k} (A_{0n} e^{jk_{z,0,n}^{II} L} - B_{0n} e^{-jk_{z,0,n}^{II} L}) J_0(k_{r,0,n}^{II} r) \\ & \quad + \sum_{m=1}^{\infty} \sum_{n=1}^{\infty} \frac{k_{z,m,n}^{II}}{k} [(A_{mn}^+ e^{jk_{z,m,n}^{II} L} - B_{mn}^+ e^{-jk_{z,m,n}^{II} L}) e^{-jm\theta} + \\ & \quad (A_{mn}^- e^{jk_{z,m,n}^{II} L} - B_{mn}^- e^{-jk_{z,m,n}^{II} L}) e^{jm\theta}] J_m(k_{r,m,n}^{II} r) J_l(k_{r,t,s}^{II} r) e^{-jt\theta} r dr d\theta). \end{aligned} \quad (4.25)$$

This means for the main duct region, the integration is over the whole duct region, but for the point source region the integration is over the source duct region, which is the volume velocity.

For $t = 0, s = 1$, equation (4.25) can be written as,

$$\begin{aligned}
 & \int_0^{2\pi} \int_0^{R_0} v_0 r_1 dr_1 d\varphi \\
 &= \int_0^{2\pi} \int_0^{R_0} ((A_{01} e^{jkL} - B_{01} e^{-jkL}) \\
 & \quad + \sum_{n=2}^{\infty} \frac{k_{z,0,n}^{II}}{k} (A_{0n} e^{jk_{z,0,n}^{II}L} - B_{0n} e^{-jk_{z,0,n}^{II}L}) J_0(k_{r,0,n}^{II} r) \\
 & \quad + \sum_{m=1}^{\infty} \sum_{n=1}^{\infty} \frac{k_{z,m,n}^{II}}{k} J_m(k_{r,m,n}^{II} r) [(A_{mn}^+ e^{jk_{z,m,n}^{II}L} - B_{mn}^+ e^{-jk_{z,m,n}^{II}L}) e^{-jm\theta} \\
 & \quad + (A_{mn}^- e^{jk_{z,m,n}^{II}L} - B_{mn}^- e^{-jk_{z,m,n}^{II}L}) e^{jm\theta}] r dr d\theta .
 \end{aligned} \tag{4.26}$$

The left hand side of this equation is equal to the volume velocity U_0 . For the right hand side of this equation, as discussed before, the volume velocities of those $m \neq 0$ higher-order modes are 0. Applying the Bessel function relationships to the right hand side of this equation,

$$\int_0^R r J_0(kr) dr = \frac{R}{k} J_1(kR) . \tag{4.27}$$

One can get,

$$U_0 = \pi * R_0^2 * (A_{01} e^{jkL} - B_{01} e^{-jkL}) . \tag{4.28}$$

For $t = 0, s = 2, 3, \dots, \infty$,

$$\begin{aligned}
 & \int_0^{2\pi} \int_0^{R_0} v_0 J_0(k_{r,0,s}^{II} r) r_1 dr_1 d\varphi \\
 &= \int_0^{2\pi} \int_0^{R_0} ((A_{01} e^{jkL} - B_{01} e^{-jkL}) \\
 & \quad + \sum_{n=2}^{\infty} \frac{k_{z,0,n}^{II}}{k} (A_{0n} e^{jk_{z,0,n}^{II}L} - B_{0n} e^{-jk_{z,0,n}^{II}L}) J_0(k_{r,0,n}^{II} r) \\
 & \quad + \sum_{m=1}^{\infty} \sum_{n=1}^{\infty} \frac{k_{z,m,n}^{II}}{k} J_m(k_{r,m,n}^{II} r) [(A_{mn}^+ e^{jk_{z,m,n}^{II}L} - B_{mn}^+ e^{-jk_{z,m,n}^{II}L}) e^{-jm\theta} \\
 & \quad + (A_{mn}^- e^{jk_{z,m,n}^{II}L} - B_{mn}^- e^{-jk_{z,m,n}^{II}L}) e^{jm\theta}] J_0(k_{r,0,s}^{II} r) r dr d\theta .
 \end{aligned} \tag{4.29}$$

The Graf's addition theorem of Bessel function is given below and the relationship between the coordinates is shown in Fig C.1.

$$J_m(\mu r) e^{-jm\theta} = \sum_{p=-\infty}^{\infty} J_{m+p}(\mu \delta_1) J_p(\mu r_1) e^{-j(p\varphi + m\theta_0)} . \tag{4.30}$$

Applying equation (4.30) and equation (4.27) to the left hand side of equation (4.29), it can be written as,

$$\begin{aligned}
 & \int_0^{2\pi R_p} \int_0^R v_0 J_0(k_{r,0,s}^H r) r_1 dr_1 d\varphi \\
 &= \int_0^{2\pi R_1} \int_0^R v_0 J_0(k_{r,0,s}^H \delta_1) J_0(k_{r,0,s}^H r_1) r_1 dr_1 d\varphi \quad (4.31) \\
 &= 2 * \pi * v_0 * J_0(k_{r,0,s}^H \delta_1) * R_p * \frac{J_1(k_{r,0,s}^H R_p)}{k_{r,0,s}^H} .
 \end{aligned}$$

In equation (4.31), if the radius of the point source R_p is very small (compared with the radius of the main duct), according to the properties of the Bessel function, one can get

$$J_1(k_{r,0,s}^H R_p) \approx k_{r,0,s}^H R_p . \quad (4.32)$$

So equation (4.31) can be written as,

$$\begin{aligned}
 & 2 * \pi * v_0 * J_0(k_{r,0,s}^H \delta_1) * R_p * \frac{J_1(k_{r,0,s}^H R_p)}{k_{r,0,s}^H} \\
 & \approx 2 * \pi * v_0 * J_0(k_{r,0,s}^H \delta_1) * R_p * k_{r,0,s}^H * R_p / k_{r,0,s}^H \quad (4.33) \\
 & = 2 * \pi * R_p^2 * v_0 * J_0(k_{r,0,s}^H \delta_1) \\
 & = 2U_0 * J_0(k_{r,0,s}^H \delta_1) .
 \end{aligned}$$

$$\int_0^R r J_m(\lambda r) J_m(\mu r) dr = \begin{cases} \frac{R}{\lambda^2 - \mu^2} [\mu J_m(\lambda R) J_m'(\mu R) - \lambda J_m(\mu R) J_m'(\lambda R)] & (\lambda \neq \mu) \\ \frac{R^2}{2} \left\{ (J_m'(\lambda R))^2 + \left(1 - \frac{m^2}{\lambda^2 R^2}\right) (J_m(\lambda R))^2 \right\} & (\lambda = \mu) . \end{cases} \quad (4.34)$$

Applying the integral relations of Bessel function (4.34) to the right hand side of the equation (4.29), one can get

$$\begin{aligned}
 & \int_0^{2\pi R_0} \int_0^R ((A_{01} e^{jkL} - B_{01} e^{-jkL}) \\
 & + \sum_{n=2}^{\infty} \frac{k_{z,0,n}^H}{k} (A_{0n} e^{jk_{z,0,n}^H L} - B_{0n} e^{-jk_{z,0,n}^H L}) J_0(k_{r,0,n}^H r) \\
 & + \sum_{m=1}^{\infty} \sum_{n=1}^{\infty} \frac{k_{z,m,n}^H}{k} J_m(k_{r,m,n}^H r) [(A_{mn}^+ e^{jk_{z,m,n}^H L} - B_{mn}^+ e^{-jk_{z,m,n}^H L}) e^{-jm\theta} \\
 & + (A_{mn}^- e^{jk_{z,m,n}^H L} - B_{mn}^- e^{-jk_{z,m,n}^H L}) e^{jm\theta}] r dr d\theta \quad (4.35) \\
 & = \frac{k_{z,0,s}^H}{k} (A_{0s} e^{jk_{z,0,s}^H L} - B_{0s} e^{-jk_{z,0,s}^H L}) R_0^2 J_0^2(k_{r,0,s}^H r) J_0(k_{r,0,s}^H r) .
 \end{aligned}$$

Let equation (4.33) equal equation (4.35), one can get

$$2 * U_0 * J_0(k_{r,0,s}^H \delta_1) = \frac{k_{z,0,s}^H}{k} (A_{0,s} e^{jk_{z,0,s}^H L} - B_{0,s} e^{-jk_{z,0,s}^H L}) R_0^2 J_0^2(k_{r,0,s}^H r) . \quad (4.36)$$

For $t = 1, 2, \dots, \infty, s = 1, 2, \dots, \infty,$

$$\begin{aligned} & \int_0^{2\pi R_p} \int_0^0 v_0 J_t(k_{r,t,s}^H r) e^{-jt\theta} r_1 dr_1 d\varphi \\ &= \int_0^{2\pi R_0} \int_0^0 ((A_{01} e^{jkL} - B_{01} e^{-jkL}) \\ &+ \sum_{n=2}^{\infty} \frac{k_{z,0,n}^H}{k} (A_{0n} e^{jk_{z,0,n}^H L} - B_{0n} e^{-jk_{z,0,n}^H L}) J_0(k_{r,0,n}^H r) \\ &+ \sum_{m=1}^{\infty} \sum_{n=1}^{\infty} \frac{k_{z,m,n}^H}{k} J_m(k_{r,m,n}^H r) [(A_{mn}^+ e^{jk_{z,m,n}^H L} - B_{mn}^+ e^{-jk_{z,m,n}^H L}) e^{-jm\theta} \\ &+ (A_{mn}^- e^{jk_{z,m,n}^H L} - B_{mn}^- e^{-jk_{z,m,n}^H L}) e^{jm\theta}] e^{-jt\theta} J_t(k_{r,t,s}^H r) r dr d\theta . \end{aligned} \quad (4.37)$$

Applying equation (4.27) and equation (4.30) to the left hand side of this equation, there is,

$$\begin{aligned} & \int_0^{2\pi R_p} \int_0^0 v_0 J_t(k_{r,t,s}^H r) e^{-jt\theta} r_1 dr_1 d\varphi \\ &= \int_0^{2\pi R_p} \int_0^0 v_0 e^{-jt\theta_0} J_t(k_{r,t,s}^H \delta_1) J_0(k_{r,t,s}^H r_1) r_1 dr_1 d\varphi \\ &= 2 * \pi * v_0 * e^{-jt\theta_0} * J_t(k_{r,t,s}^H \delta_1) * R_p * \frac{J_1(k_{r,t,s}^H R_p)}{k_{r,t,s}^H} . \end{aligned} \quad (4.38)$$

Still equation (4.32) is applicable here, so equation (4.38) can be written as

$$\begin{aligned} & 2 * \pi * v_0 * e^{-jt\theta_0} * J_t(k_{r,t,s}^H \delta_1) * R_p * \frac{J_1(k_{r,t,s}^H R_p)}{k_{r,t,s}^H} \\ & \approx 2 * \pi * v_0 * e^{-jt\theta_0} * J_t(k_{r,t,s}^H \delta_1) * R_p^2 \\ & = 2 * U_0 * e^{-jt\theta_0} * J_t(k_{r,t,s}^H \delta_1) . \end{aligned} \quad (4.39)$$

Applying equation (4.34) to the right hand side of equation (4.37), one can get

$$\begin{aligned}
 & \int_0^{2\pi} \int_0^{R_0} (A_{01} e^{jkL} - B_{01} e^{-jkL}) \\
 & + \sum_{n=2}^{\infty} \frac{k_{z,0,n}^{\parallel}}{k} (A_{0n} e^{jk_{z,0,n}^{\parallel} L} - B_{0n} e^{-jk_{z,0,n}^{\parallel} L}) J_0(k_{r,0,n}^{\parallel} r) \\
 & + \sum_{m=1}^{\infty} \sum_{n=1}^{\infty} \frac{k_{z,m,n}^{\parallel}}{k} J_m(k_{r,m,n}^{\parallel} r) [(A_{mn}^+ e^{jk_{z,m,n}^{\parallel} L} - B_{mn}^+ e^{-jk_{z,m,n}^{\parallel} L}) e^{-jm\theta} \\
 & + (A_{mn}^- e^{jk_{z,m,n}^{\parallel} L} - B_{mn}^- e^{-jk_{z,m,n}^{\parallel} L}) e^{jm\theta}] J_t(k_{r,t,s}^{\parallel} r) e^{-jt\theta} r dr d\theta \\
 & = \frac{k_{z,t,s}^{\parallel}}{2k} (A_{ts}^- e^{jk_{z,t,s}^{\parallel} L} - B_{ts}^- e^{-jk_{z,t,s}^{\parallel} L}) R_0^2 J_t^2(k_{r,t,s}^{\parallel} r) (1 - \frac{t^2}{k_{r,t,s}^{\parallel 2} R_0^2}) .
 \end{aligned} \tag{4.40}$$

So let equation (4.39) equal equation (4.40), one can get

$$2 * U_0 * e^{-jt\theta} * J_t(k_{r,t,s}^{\parallel} \delta_1) = \frac{k_{z,t,s}^{\parallel}}{2k} (A_{ts}^- e^{jk_{z,t,s}^{\parallel} L} - B_{ts}^- e^{-jk_{z,t,s}^{\parallel} L}) R_0^2 J_t^2(k_{r,t,s}^{\parallel} r) (1 - \frac{t^2}{k_{r,t,s}^{\parallel 2} R_0^2}) . \tag{4.41}$$

Multiplying both sides of equation (4.24) with $J_t(k_{r,t,s}^{\parallel} r) e^{jt\theta}$ and integrating the first one of equation (4.24) over point source region and integrating the second one of equation (4.24) over other region, adding them together, for $t = 1, 2, \dots, \infty, s = 1, 2, \dots, \infty$, there is,

$$2 * U_0 * e^{jt\theta} * J_t(k_{r,t,s}^{\parallel} \delta_1) = \frac{k_{z,t,s}^{\parallel}}{2k} (A_{ts}^+ e^{jk_{z,t,s}^{\parallel} L} - B_{ts}^+ e^{-jk_{z,t,s}^{\parallel} L}) R_0^2 J_t^2(k_{r,t,s}^{\parallel} r) (1 - \frac{t^2}{k_{r,t,s}^{\parallel 2} R_0^2}) . \tag{4.42}$$

So equation (4.28), (4.36), (4.41) and (4.42) provide one group of equations for the description of the point source boundary condition. Let $m = \pm 4$ and $n = 4$, there are altogether $72 (2 * n + 4 * |m| * n)$ unknown amplitudes of A_{mn} and B_{mn} . At the same time, let $t = 4$ and $s = 4$, there are $36 (s + 2 * t * s)$ independent equations. Combining them with other boundary conditions, for example, for the boundary condition of the open duct end, as discussed in Chapter 3, there is

$$B_{mn} = \sum_{L=1}^{\infty} R_{mLn} A_{mLn} . \tag{4.43}$$

Let $m = \pm 4$ and $n = L = 4$, it can give $36 (n + |m| * n)$ independent equations. So one can get 72 independent equations for those 72 unknown amplitudes A_{mn} and B_{mn} . So

through these 72 independent equations one can get the solution for those unknown amplitudes A_{mn} and B_{mn} , then the in-duct field can be decomposed.

4.4 Discussion

Two different types of sound source are introduced in this chapter. Also the descriptions of the relevant boundary conditions are discussed. Combining with the open end boundary condition of the circular duct introduced in Chapter 3, one can get the unknown amplitudes A_{mn} and B_{mn} , and then the acoustic properties in circular duct without an aperture device presented can be obtained. As stated before, the effects of the source radius location on the acoustic properties in the duct will also be investigated in Chapter 5 and Chapter 6.

Chapter 5 Sound field produced by a point source propagating in a circular duct without simple aperture devices

5.1 Introduction

In order to study the acoustic properties in circular ducts in the higher normalized wave number range, it is necessary to decompose the in-duct field into the different single higher-order modes, in other words, to get the amplitudes of A_{mn} and B_{mn} in the circular duct. Once these amplitudes are determined, it is possible to analyse the acoustic properties of the in-duct field or the acoustic properties of the components (such as baffles, aperture devices). There are two approaches to decompose the in-duct field, which are the experimental decomposition approach and the theoretical decomposition approach. Significant research works, such as Ref [27] to Ref [33], have been done on the decomposition of the in-duct field into higher normalized wave number range and mainly considered the experimental decomposition approaches.

Both experimental and theoretical decomposition approaches will be discussed in this chapter. However experimental decomposition approaches are always complicated and it is difficult to achieve the accurate decomposition of higher-order modes. So one experimental decomposition approach is demonstrated for the purpose of comparison with the theoretical approach and attention is mainly focused on the theoretical decomposition approach in this chapter. Based on the descriptions of the sound source boundary condition and the open end boundary condition, one theoretical approach is proposed. For this theoretical approach, only two reference measurements in the main duct region are required for the decomposition of the in-duct field.

5.2 Experimental set-up

As discussed in Chapter 4, a 0.9 m long copper duct with radius 0.0075 m is used as the point source. At one end it is connected to a speaker and at other end, it is connected to a rigid plate and then this plate is placed at the end of the main duct. A 3 m long duct of

internal radius 0.15 m is used as the main duct and is terminated with a large rigid baffle whose dimensions are $1.2 \times 1.2\text{ meter}$. The experimental set-up is shown in Fig 5.1. Taking the baffled end of the duct as the origin of the coordinate system, along the z -axis of the duct, two different locations $z = -0.54\text{ m}$ and $z = -0.18\text{ m}$ are taken. At each location, along the circumference of the duct, there are six equally positioned points, which are shown in Fig 5.2. Ideally more points mean greater measurement accuracy of the circumferential distribution. However too many drilled holes on the duct wall will affect the in-duct acoustic field. At each point, two closely placed holes are drilled to accommodate the microphone pair to measure particle velocity along the z -axis at that point (in this investigation, only this velocity is of interest). Using these positions, one can get the circumferential distribution of the acoustic pressure, as well as the circumferential distribution of the particle velocity. Another two pairs of holes, located at $(0.15\text{ m}, 0, -2.33\text{ m})$ and $(0.15\text{ m}, 3 * \pi / 4, -1.5\text{ m})$ respectively, are drilled and used for reference measurements. The detailed information of the experimental set-up is shown in Fig 5.2. The whole system is then placed in the middle of an anechoic room. The experiment equipments and connections are given in Appendix A.

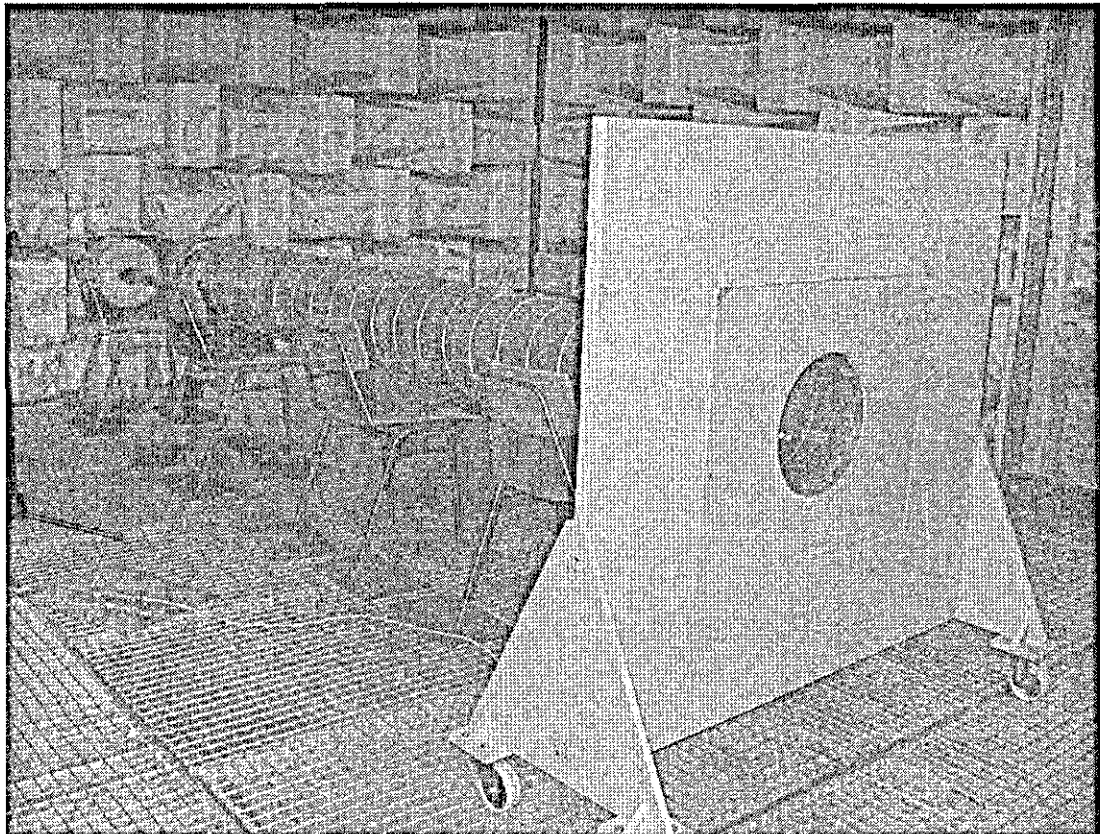


Fig 5.1 Picture of the experimental set-up for the measurement

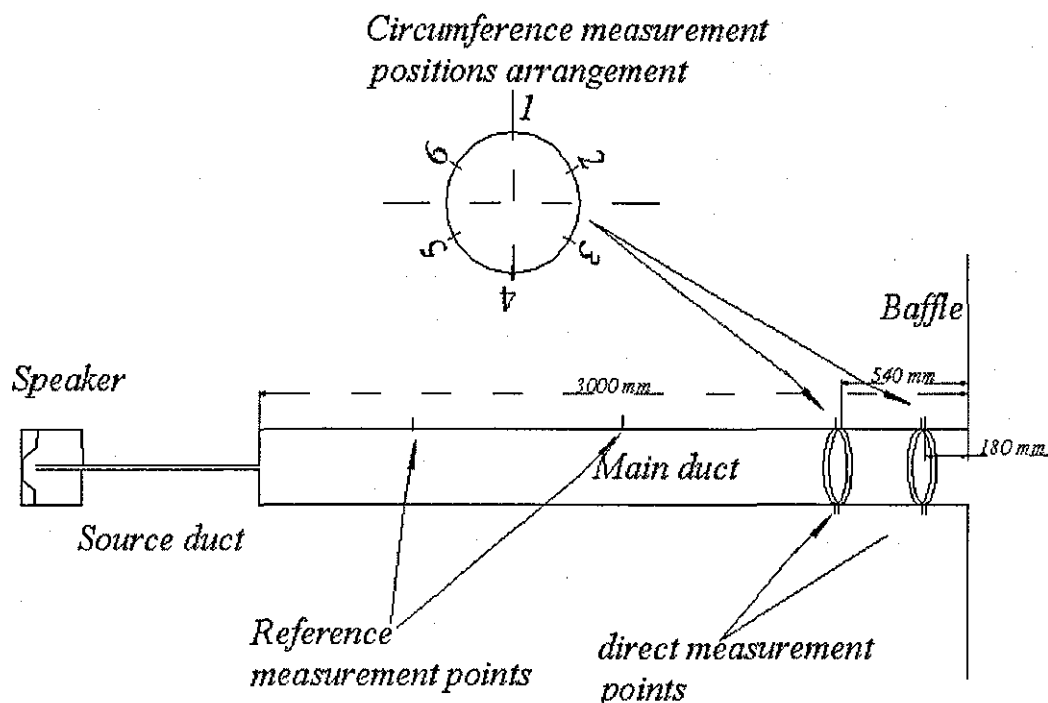


Fig 5.2 Detailed sketch of the point source measurement set-up

5.3 Experimental decomposition of the in duct acoustic field

5.3.1 Theoretical derivation for experimental decomposition approach

Some previous research introduced in Chapter 1 studied experimental approaches to decompose the in-duct field into single higher-order modes. As discussed by M. Åbom in Ref [35], the decomposition approaches discussed before can be divided into two main types: *direct approaches* and *correlation approaches*. The basis for the *direct approaches* is simultaneous measurements of an acoustic field quantity, such as, acoustic pressure, at a number of measurement positions. If the in-duct field is a steady one, one can measure at these different positions one by one (by doing so, it doesn't need so many microphones to do the measurement simultaneously). The basis for the *correlation approaches* is the space-time correlation of an acoustic field quantity between several pairs of measurement points. These two *approaches* basically perform the modal decomposition either by a two-dimensional spatial Fourier transforms over the duct cross-section or by the solution of a linear equation system that is formed by using measured data from a number of independent positions. Now one *direct approach* is reviewed in this section to test the applicability of the experimental approach.

For acoustic wave propagation in a circular duct with constant cross section, at those positions that are not close to any sources or obstructions, there should be only a finite number of modes that can give significant contributions to the acoustic field. So one can have

$$p(r, z, \varphi) = \sum_{m=-M}^M \sum_{n=1}^N J_m(k_{r,m,n}r) e^{jm\varphi} (A_{m,n} e^{-jk_{z,m,n}z} + B_{m,n} e^{jk_{z,m,n}z}), \quad (5.1)$$

in which M and N are finite integer numbers.

Because the length of the main duct is finite and the in-duct field includes both incident waves and reflected waves, at least two z -axis measurement positions are needed to separate the incident waves from the reflected ones. According to the experimental set-up shown in Fig 5.2, at each location, there are only six measurement points along the circumference, which limits the number of higher-order modes decomposable to a maximum of six experimentally. In the frequency range from 600–1400 Hz, only five higher-order modes: $(\pm 1, 1)$ modes, $(\pm 2, 1)$ modes and $(0, 2)$ mode are cut on in the duct (including the plane wave, there are six modes propagating in the duct). So equation (5.1) can be written as below:

Error! Objects cannot be created from editing field codes. . (5.2)

From the equation above, it can be seen that there are altogether $A_{0,1}$, $B_{0,1}$, $A_{\pm 1,1}$, $B_{\pm 1,1}$, $A_{\pm 2,1}$, $B_{\pm 2,1}$, $A_{0,2}$ and $B_{0,2}$, i.e. twelve unknown amplitudes. So if one can construct a set of twelve independent equations through the measurement at no fewer than twelve different positions, then one can get these twelve amplitudes. After these twelve amplitudes are obtained, the whole in-duct field can be expressed as the sum of these single modes. This is the theoretical basis for the experimental decomposition approach. So one can get the equation matrix as following:

$$\begin{bmatrix} e^{-ik_1 z_1} & e^{ik_1 z_1} & J_1(k_{r,1,1}R) e^{j\varphi_1} e^{-jk_{z,1,1}z_1} & \dots & J_0(k_{r,0,2}R) e^{jk_{z,0,2}z_1} \\ e^{-ik_1 z_2} & e^{ik_1 z_2} & J_1(k_{r,1,1}R) e^{j\varphi_2} e^{-jk_{z,1,1}z_2} & \dots & J_0(k_{r,0,2}R) e^{jk_{z,0,2}z_2} \\ \vdots & \vdots & \ddots & \ddots & \vdots \\ e^{-ik_2 z_1} & e^{ik_2 z_1} & J_1(k_{r,1,1}R) e^{j\varphi_1} e^{-jk_{z,1,1}z_1} & \dots & J_0(k_{r,0,2}R) e^{jk_{z,0,2}z_1} \\ e^{-ik_2 z_2} & e^{ik_2 z_2} & J_1(k_{r,1,1}R) e^{j\varphi_2} e^{-jk_{z,1,1}z_2} & \dots & J_0(k_{r,0,2}R) e^{jk_{z,0,2}z_2} \end{bmatrix}_{12 \times 12} * \begin{bmatrix} A_{0,1} \\ B_{0,1} \\ \vdots \\ A_{0,2} \\ B_{0,2} \end{bmatrix}_{12 \times 1} = \begin{bmatrix} p_1 e^{j\theta_1} \\ p_2 e^{j\theta_2} \\ \vdots \\ p_{11} e^{j\theta_{11}} \\ p_{12} e^{j\theta_{12}} \end{bmatrix}_{12 \times 1}, \quad (5.3)$$

in which p_1 to p_{12} are acoustic pressure amplitudes measured at the twelve positions, φ_1 to φ_{12} are angle coordinates of the twelve measurement positions, θ_1 to θ_{12} are phase angles between the measurement microphone and the reference microphone.

Then substituting the coordinates, such as z , φ and r , of these twelve measurement positions into equation (5.3), one can get these unknown amplitudes through the equation below:

$$\begin{bmatrix} A_{0,1} \\ B_{0,1} \\ \vdots \\ A_{0,2} \\ B_{0,2} \end{bmatrix}_{12 \times 1} = [X]_{12 \times 12}^{-1} * \begin{bmatrix} p_1 e^{i\theta_1} \\ p_2 e^{i\theta_2} \\ \vdots \\ p_{11} e^{i\theta_{11}} \\ p_{12} e^{i\theta_{12}} \end{bmatrix}_{12 \times 1}, \quad (5.4)$$

in which X is the index matrix in equation (5.3). By solving equation (5.4), one can get these amplitudes respectively and so the in-duct field can be decomposed.

5.3.2 Experimental decomposition results

Based on the analysis above, one can use the experimental set-up shown in Fig 5.1 and Fig 5.2. One reference microphone is placed at position $(0.15m, 0, -2.33m)$. Take the sound source located at $\delta = 0.06m(40\%R)$ for example, one can first take twelve different measurements, six each at two different z -axis locations $z = -0.54m$ and $z = -0.18m$ (shown in Fig 5.2). The frequency range is set from $600Hz$ to $1400Hz$, in which there are $(0, 1)$, $(\pm 1, 1)$, $(\pm 2, 1)$ and $(0, 2)$ six modes propagating in the duct. The measurement microphones are all nearly flush mounted at the duct wall. Because it is a circular duct, it is difficult to flush mount $1/2''$ microphone on the duct wall and this causes some errors in the measurement result.

Substituting these twelve positions' coordinates and measurement results into equation (5.4), the results are shown in Fig 5.3. Note the figure is plotted against normalised wave number $k * R$ rather than frequency, the $(+1, 1)$ mode cuts on at $k * R$ value of 1.84. Fig 5.3 a) shows the decomposed amplitudes of $A_{0,1}$, and $B_{0,1}$; Fig 5.3 b) shows

decomposed amplitudes of $A_{+1,1}$ and $B_{+1,1}$; Fig 5.3 c) shows acoustic pressure measured at two of the twelve different positions (position 1 and position 2 located at $z = -0.54m$).

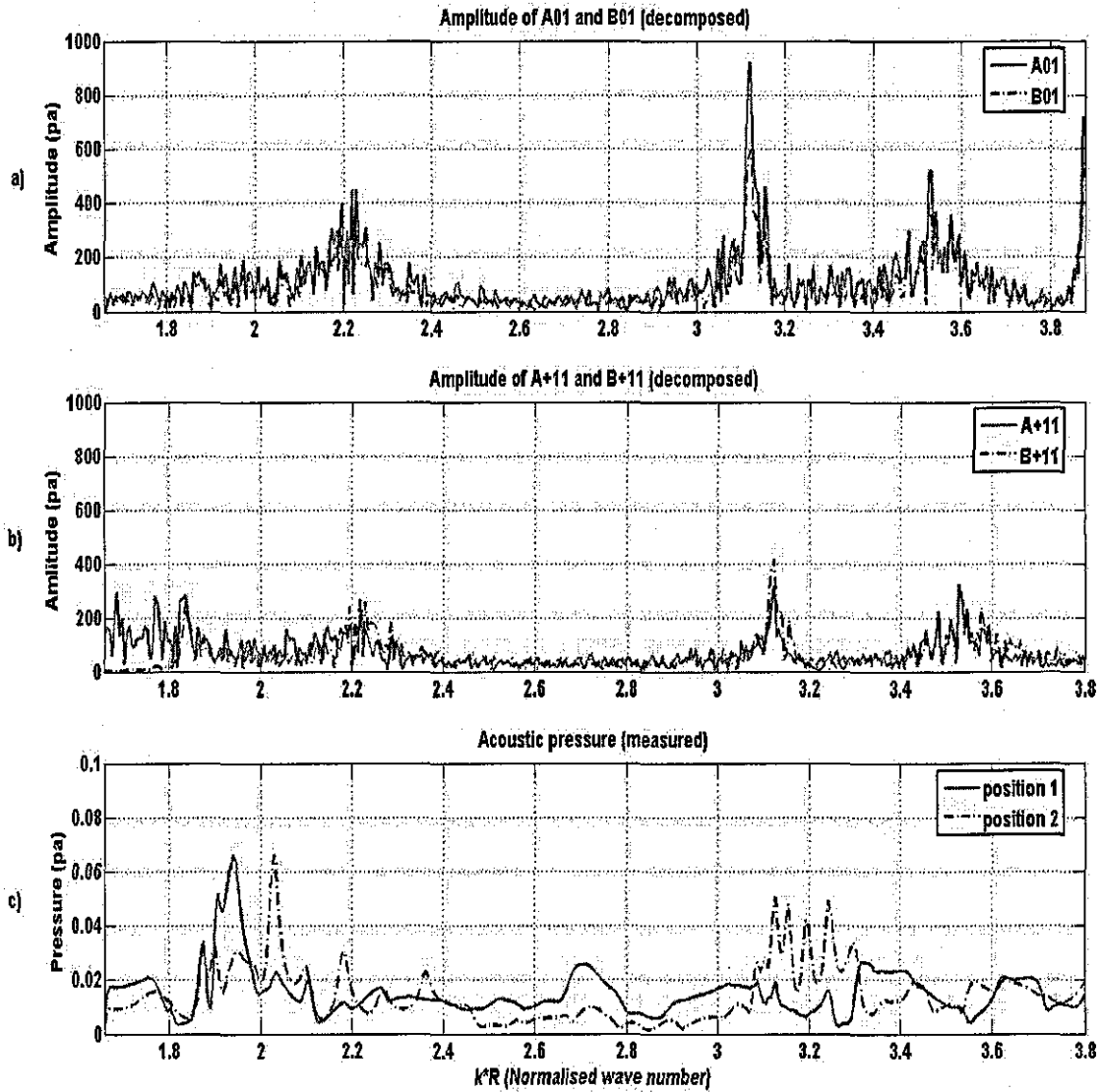


Fig 5.3 Experimentally decomposed amplitudes of (0, 1) mode and (+1,1) mode

From the results shown in this figure, it can be seen that the results obtained by equation (5.4) are absolutely wrong, because the amplitudes of directly measured acoustic pressure are around 0.02 pa , however the amplitudes decomposed by equation (5.4) are around 100 pa . So this means the results obtained from equation (5.4) is unacceptable and so this experimental decomposition method is also unacceptable. The reason for the large errors may come from two aspects: first, these twelve measurement positions are not fully independent, which makes the matrix X badly constructed; secondly, this

matrix is sensitive to those small measurement errors, which can cause a large error in the final results.

According to the analysis above, this experimental decomposition approach of the in-duct field is not an effective one. Because it needs a significant number of measurement positions especially when there are many higher-order modes propagating in duct. To make the result sensible, at least $2 * N$ (N is the number of the higher-order modes propagating in duct) independent measurement positions are required. Sometimes it is quite difficult to get so many independent measurement positions practically (as shown in Fig 5.2, those 12 positions are not fully independent). Also as discussed by M. Åbom in Ref [35], there is another limitation, which is the approaches can only effectively decompose those axially-unsymmetric modes, for these experimental decomposition approaches. For those axially-symmetric higher-order modes, most experimental methods cannot work properly.

So in order to decompose the in-duct field effectively and conveniently, other approaches, such as theoretical decomposition approaches, should be introduced. In the following section, one theoretical decomposition approach, based on both coupled and uncoupled assumptions will be discussed and comparisons will be also made between theoretical predicted results and directly measured results.

5.4 Theoretical decomposition approach of the in duct acoustic field

For the open ended boundary of a circular duct, if the length of the duct is infinite and there are no other obstacles, such as aperture devices or baffles in it, the in-duct field only contains forward propagating waves. At this situation, every mode is independent of each other and there is no energy transferring between different higher-order modes. So there is no cross coupling effects appear in the equation below:

$$p_A = j\rho\omega \sum_{m=0}^{\infty} \sum_{n=1}^{\infty} J_m(k_{r,m,n}r) (A_{m,n}^+ e^{-jm\varphi} + A_{m,n}^- e^{jm\varphi}) e^{j\omega t} e^{-jk_{z,m,n}z} \quad (5.5)$$

But if the length of duct is finite or there are some discontinuities in the duct, then at these points, there should be reflection of the incident wave, and the in-duct field at this situation is composed of both incident and reflected waves. So for the reflected field, the reflected waves can be written in the form:

$$p_B = j\rho\omega \sum_{m=0}^{\infty} \sum_{n=1}^{\infty} J_m(k_{r,m,n}r) (B_{m,n}^+ e^{-jm\phi} + B_{m,n}^- e^{jm\phi}) e^{j\omega t} e^{-jk_{z,m,n}z} \quad (5.6)$$

In the reflected field, for example, the particle velocity of (+2,1) mode v_{21}^+ is not only caused by (+2,1) mode acoustic pressure p_{21}^+ , but also caused by other higher-order modes such as, p_{22}^+ , p_{23}^+ ... p_{2n}^+ (the acoustic pressures of (+2,n) mode). Then the intensity of this mode can be written as

$$I_{21}^+ = \sum_n (p_{2n}^+ * v_{21}^+) \quad (5.7)$$

There should be some energy transfer from other higher-order modes to this one resulting from the discontinuities of the duct and also some energy transfer from this mode to other higher-order modes. Writing these in the form of the complex reflection coefficients, then as in equation (3.57), one has

$$B_{mn} = \sum_{L=1}^{\infty} R_{mLn} A_{mL} \quad (5.8)$$

This equation is called the fully coupled equation. For an uncoupled equation, one makes the assumption that the cross coupling effects between higher-order modes are so weak that the energy transferring between different modes is too small to be considered. So the amplitude of each reflected mode B_{mn} consists only of the reflection of its own incident mode A_{mn} , which can be written as

$$B_{mn} = R_{mnn} A_{mn} \quad (5.9)$$

However for the fully coupled calculation, according to equation (5.8), the amplitude of B_{mn} should include contributions of all other higher-order modes with the same value m. Actually, only a finite number of higher-order modes are considered in the subsequent prediction. For example, if $m=5$ in this equation, then only coupling effects between these five modes are considered, all other higher-order modes contributions are

neglected. So at this situation, the coupled equation can be called the partially coupled equation.

5.4.1 Theoretical derivation

The description of the point source boundary condition is given in equation (4.28), (4.36), (4.41) and (4.42). Combining these equations with the open end boundary condition given in equation (5.8) and equation (5.9), one can get both the coupled and uncoupled calculation. In either case, one can get a matrix equation of the general form:

$$[X]_{D \times D} \begin{bmatrix} A_{01} \\ A_{11}^+ \\ \vdots \\ B_{m(n-1)}^- \\ B_{nm}^- \end{bmatrix}_{D \times 1} = \begin{bmatrix} U \\ U \\ \vdots \\ 0 \\ 0 \end{bmatrix}_{D \times 1}, \quad (5.10)$$

in which X is the coefficient matrix for these amplitudes. Its dimension D is decided by how many higher-order modes are considered. For example, in this work, 17 modes cut on in the frequency range that is of interest. The mode with highest m value is $(\pm 5, 1)$ mode; the mode with highest n value is $(0, 3)$ mode. So $m = \pm 5$ and $n = 5$ should be enough for the calculation (it includes 17 cut on modes and other 38 cut off higher-order modes).

If $m = \pm 5$ and $n = 5$, the dimension of the matrix X is 110×110 ($2 * n + 4 * |m| * n$). That means the matrix X is a very large matrix. In order to get the solution of these amplitudes, one should first try to invert the matrix X :

$$\begin{bmatrix} A_{01} \\ A_{11}^+ \\ \vdots \\ B_{m(n-1)}^- \\ B_{nm}^- \end{bmatrix}_{D \times 1} = [X]_{D \times D}^{-1} * \begin{bmatrix} U \\ U \\ \vdots \\ 0 \\ 0 \end{bmatrix}_{D \times 1}. \quad (5.11)$$

But during the inversion, it is noted that the matrix is ill conditioned and is nearly singular. That means it is impossible to get the correct solution for this matrix. The reason, which causes the singularity of the matrix X , is there are many indexes contain

exponential items $e^{-jk_{z,m,n}^H L}$. For this item, if $L = -3m$ and $f = 1000 \text{ Hz}$, one can get $e^{-jk_{z,4,4}^H L} = e^{-47.22}$ and $e^{-jk_{z,5,5}^H L} = e^{-62.57}$ for (+4, 4) mode and (+5, 5) mode respectively. If the frequency is even lower, this value will be even smaller. Another reason is these items happen to appear on the leading diagonal of matrix X . So when one tries to invert the matrix, these items approach infinite and the matrix approaches singularity.

Several possible approaches to overcome the singularity problem are considered as follow.

1. The first one is re-arrangement of the matrix X . If one can move those items containing $e^{-jk_{z,m,n}^H L}$ from the leading diagonal of the matrix or make the elements on the leading diagonal similar scaled, the matrix X will be well conditioned. However, this approach is hardly achieved because from (4.28), (4.36), (4.41) and (4.42), one can see for most of those items that are non-zero contain this exponential item $e^{-jk_{z,m,n}^H L}$. This means on the leading diagonal of this matrix, there should be either these exponential style items or zero, but both of these two options will cause the singularity of the matrix. So this approach is not an ideal one.
2. The second approach tries to move the original point of the coordinate system to the plane where the source is located. As known for those exponential items $e^{-jk_{z,m,n}^H L}$, if L equals zero, those exponential items should all equal 1. However, as discussed in Chapter 3, the original point of the coordinate system is taken at the open end of the duct. By doing so, the complex reflection coefficients R_{mnL} are independent to the length of the duct. If one moves the original point into somewhere in the duct, it will cause the reflection coefficients changing as the length of the duct. This is also not possible.
3. The third approach is the one that is adopted by this work. From those exponential items $e^{-jk_{z,m,n}^H L}$, it can be seen that the reason why it causes the singularity of the matrix is before that mode cuts on, the wave number along z -axis $k_{z,m,n}^H$ is imaginary and multiplied by j , it becomes a real number, subsequently this real number causes $e^{-jk_{z,m,n}^H L}$ to be exponential decaying. But if

one can keep the value of $k_{z,m,n}^{II}$ always real, the values of these exponential items $e^{-jk_{z,m,n}^{II}L}$ will be complex numbers, then these terms only change phases of those indexes rather than amplitudes of those indexes. The only way to keep $k_{z,m,n}^{II}$ always real is at the boundary condition, only those modes that can be propagating along the duct are considered and all other cut off higher-order modes are neglected. Thus contributions from all cut-off modes are ignored.

For the main duct region, at different frequency ranges, there are different higher-order modes propagating in it, so one should just consider those modes that have been cut on. For example, at frequency 500Hz, only (0, 1) mode is considered and included in matrix X , at frequency 1000Hz, three modes (0, 1), (+1, 1) and (-1, 1) are considered and at frequency 2600Hz, totally 17 cut on modes (from (0, 1) to ... (+2, 2), (-2, 2) and (0, 3)) are included in matrix X . So for matrix X , its dimension D is not a constant one, it is dependent on the number of the cut on modes and increasing with the frequency.

At this situation, the neglecting of those cut off higher-order modes will bring some errors to the prediction results. In the following sections, comparison would be made between the actual results (direct measurements) and results obtained from calculation by using equation (5.11) (predictions).

5.4.2 Experiment measurements and results

The experimental set-up is shown in Fig 5.1 and Fig 5.2. The frequency range is set from 0–2600Hz (frequency step for the measurement is 4Hz). For convenience four microphones are used to measure the acoustic pressures and particle velocities. One pair is used to measure the acoustic pressure and particle velocity at the appointed positions (direct measurements); the other two microphones are used to measure at the two reference positions in the main duct, which are located at $(0.15m(100\%R), 0, -2.33m(-74.3\%L))$ and $(0.15m(100\%R), 3 * \pi / 4, -1.5m(-50\%L))$ respectively (reference measurements). The reasons to use two-reference positions measurement are:

1. utilising different circumferential angles, it is possible to catch information for the spiralling higher-order modes;
2. utilising different z -axis values, it is possible to separate incident waves and reflected waves more accurately;
3. through two positions measurement, one can reduce those random measurement errors introduced by using only one position measurement.

According to equation (5.12), if one wants to get the actual values of the amplitudes, the amplitude of the volume velocity U must be determined first. So the two reference measurement results are used to obtain the volume velocity of the point source. The procedure to calculate the amplitudes of the pressures by using the reference measurement results is given in Appendix E. Following this procedure, the amplitude of the volume velocity U , as well as the actual amplitudes of A_{mn} and B_{mn} are determined. After determining the actual amplitudes of different modes, the in-duct field is successfully decomposed.

First, before considering the comparison between the predicted results with direct measurement, comparison is made between coupled and uncoupled predictions for the amplitudes of a single higher-order mode. Take $(\pm 1, 1)$ modes for example, in Fig 5.4, three comparisons are plotted, Fig 5.4 a) shows the comparison between the amplitude of incident mode A_{11}^+ and reflected mode B_{11}^+ ; Fig 5.4 b) shows the comparison between the amplitude of A_{11}^+ and A_{11}^- ; Fig 5.4 c) shows the comparison between the amplitude of A_{11}^+ obtained from the coupled prediction and the uncoupled prediction.

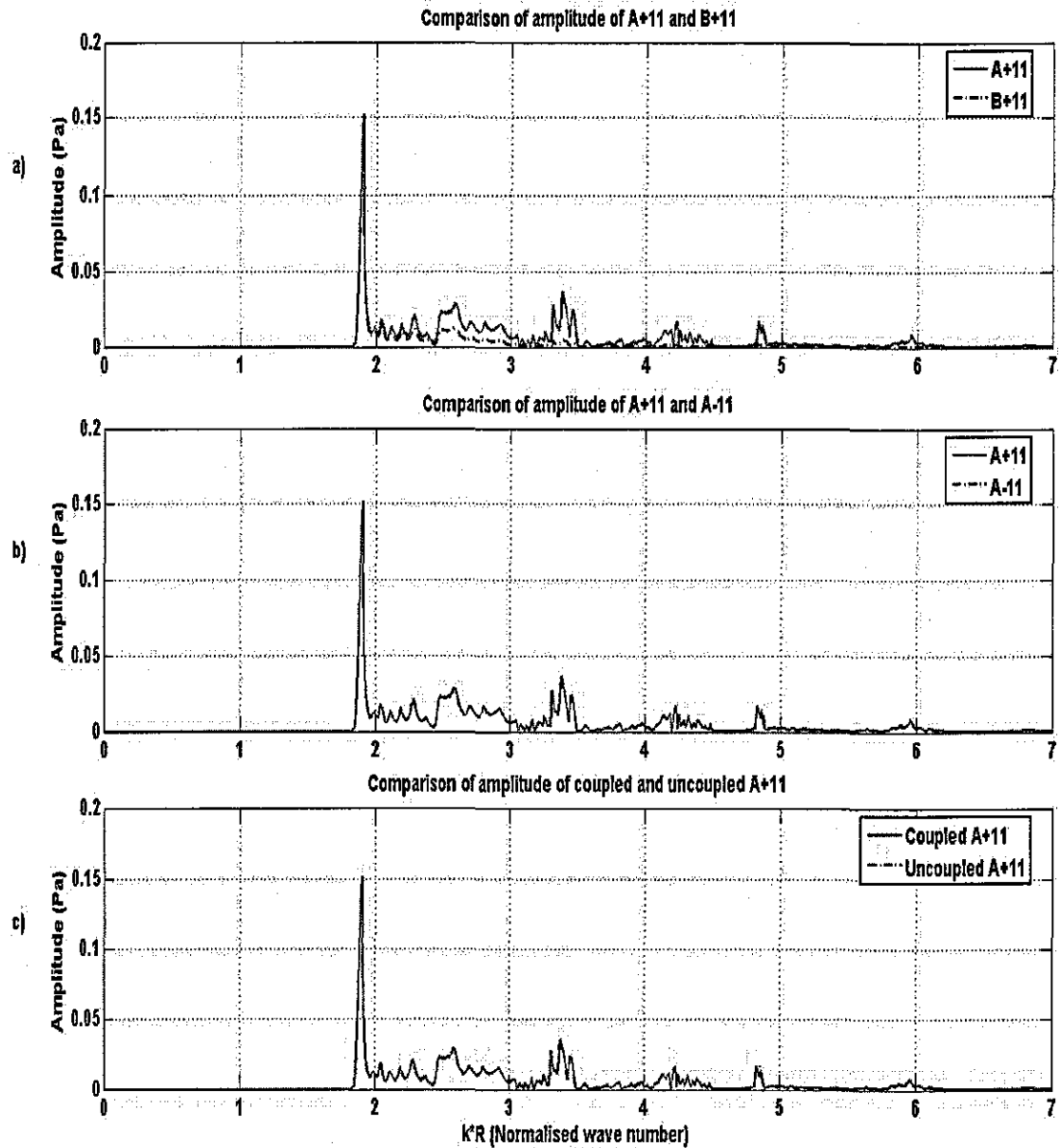


Fig 5.4 Comparison of the amplitudes of $(\pm 1,1)$ modes obtained by theoretical prediction

Based on the amplitudes obtained, it is possible to predict the acoustic pressure at any point in the main duct. So before discussing the results shown in Fig 5.4, position 1 located at $z = -0.54m$ is taken as an example. The coupled predicted pressure, uncoupled predicted pressure and directly measured pressure at this point are shown in Fig 5.5 (sound source located at $\delta = 0.06m(40\%R)$). In order to show the results clearly, in Fig 5.5 b) and Fig 5.5 c), the linear frequency data is transferred to 1/6 octave

band (compared with 1/3 octave band, 1/6 octave band can give more detailed information at higher normalised wave number range). Fig 5.5 c) shows the comparisons of coupled predictions, uncoupled predictions with direct measurements.

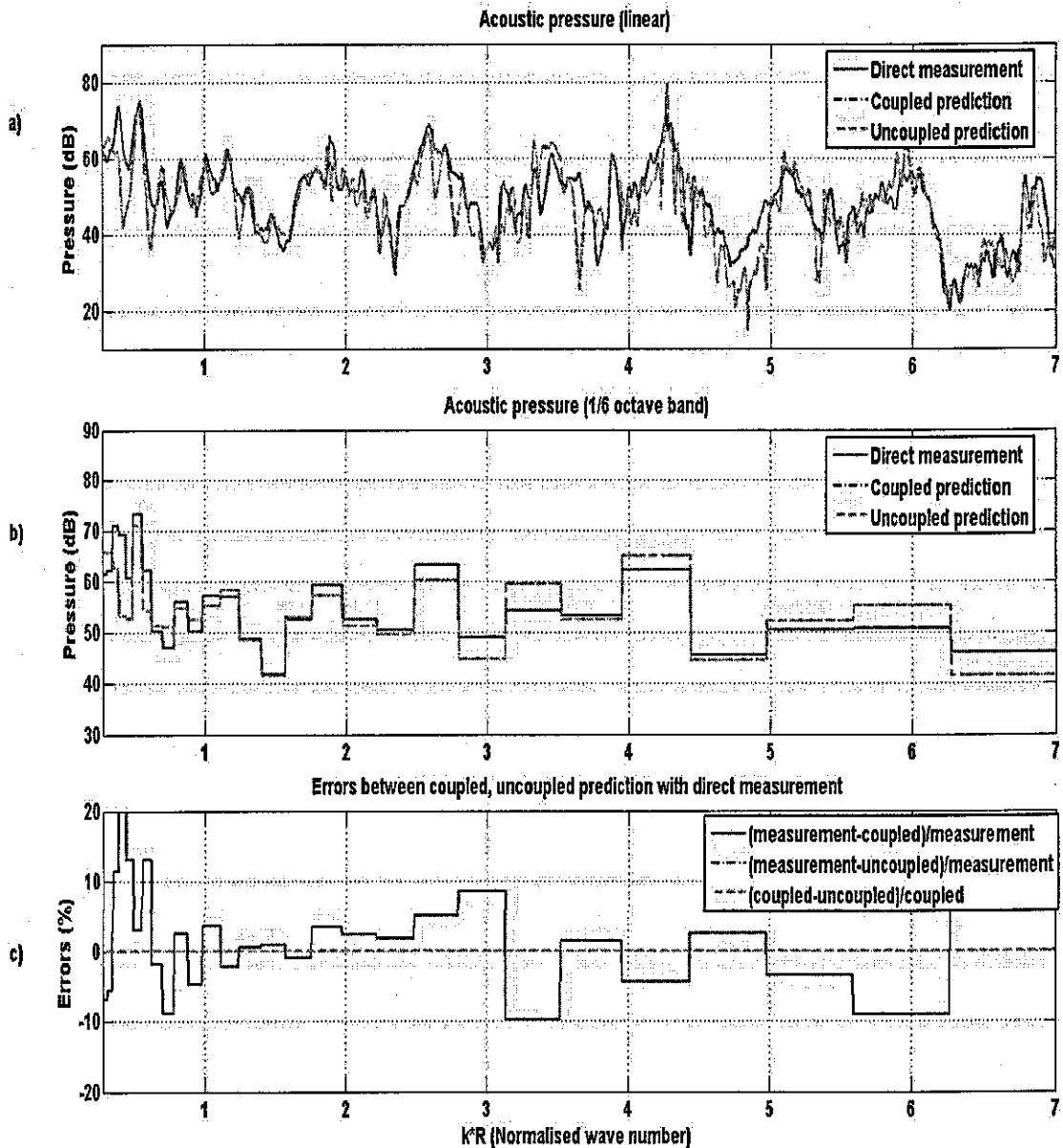


Fig 5.5 Comparison between coupled, uncoupled predictions with the direct measurements (sound source located at $\delta = 0.06m(40\%R)$)

From Fig 5.4 - 5.5, it can be seen that,

1. The amplitude of A_{11}^+ equals to amplitude of A_{11}^- . Which means the amplitudes of mode $(+m,n)$ and mode $(-m,n)$ are equal. From this figure, it can also be

seen that the amplitudes of those higher-order modes cut on at the respective cut on frequencies and then decay very quickly.

2. The coupling effects at the open end of the duct can be neglected, because the amplitudes obtained from partially coupled prediction are equal to those got from uncoupled prediction. From Fig 5.4, it can also be seen that the amplitudes of A_{11}^+ obtained from partially coupled prediction and uncoupled prediction are equal. Also from Fig 5.5, it can be seen that the partially coupled predicted acoustic pressure equals to uncoupled predicted acoustic pressure.
3. The errors between those partially coupled prediction and direct measurement mainly fall into the range $\pm 10\%$ of direct measurement (or even smaller), which are considered to be acceptable.

5.4.3 Effects of the radial location of the sound source on prediction

After discussing the difference between coupled and uncoupled predictions, in this section, the effects of the radial location of the sound source on the predictions are discussed. Two sound sources located at $\delta = 0m$ and $\delta = 0.06m(40\%R)$ are selected. The comparison of the errors between partially coupled predictions and direct measurement of these two sound sources are made.

Fig 5.6 shows the coupled predictions, uncoupled predictions and the direct measurements when the sound source is located at $\delta = 0m$ and $\delta = 0.06m(40\%R)$ respectively. For clarity, the linear frequency data is transferred to 1/6 octave band and then the relative error is plotted in Fig 5.7.

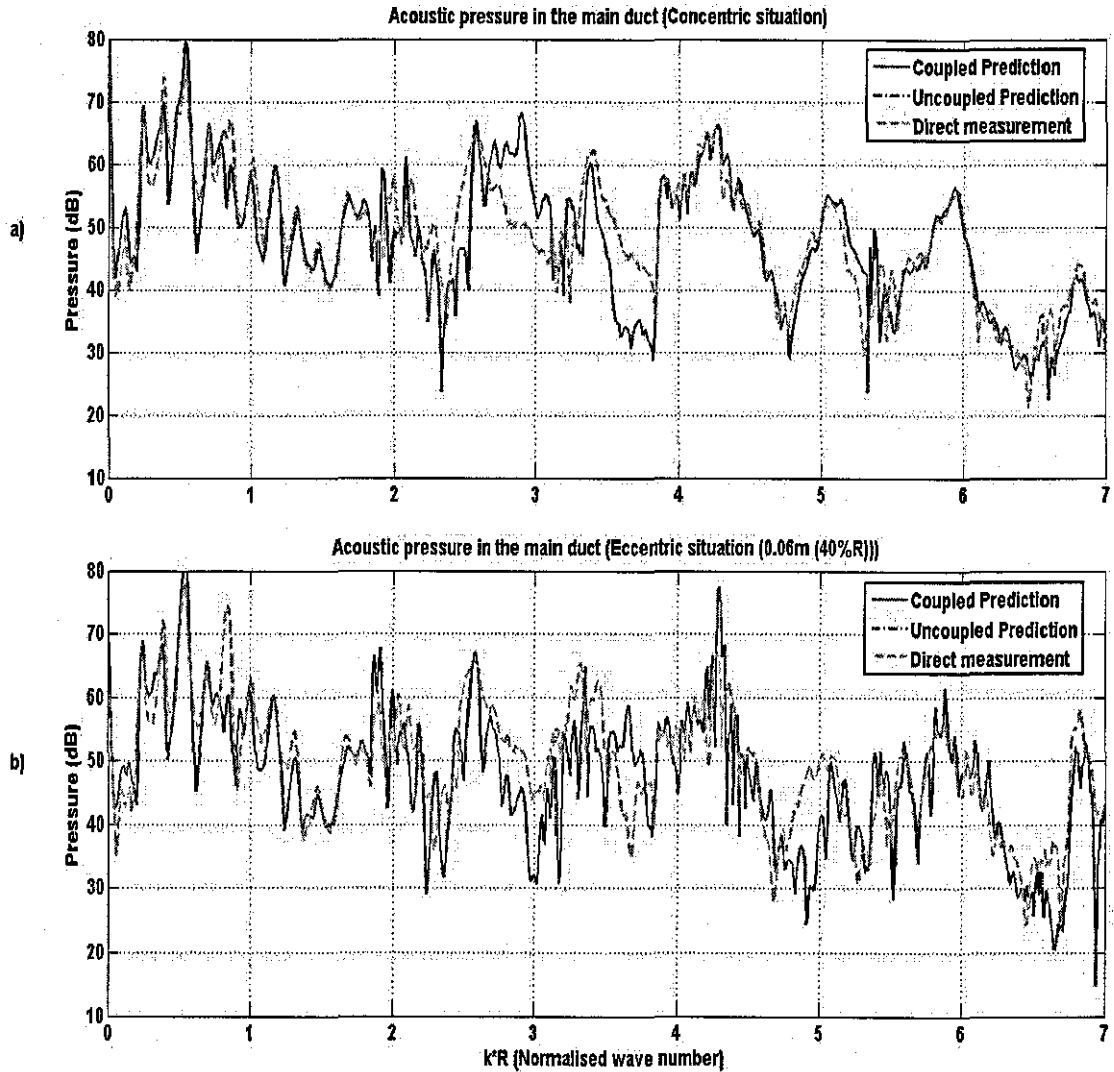


Fig 5.6 Comparison between the coupled predictions and the direct measurements
(a) shows the point source is concentric to the main duct situation ($\delta = 0m$); b)
shows the point source is eccentric to the main duct situation ($\delta = 0.06m (40\%R)$))

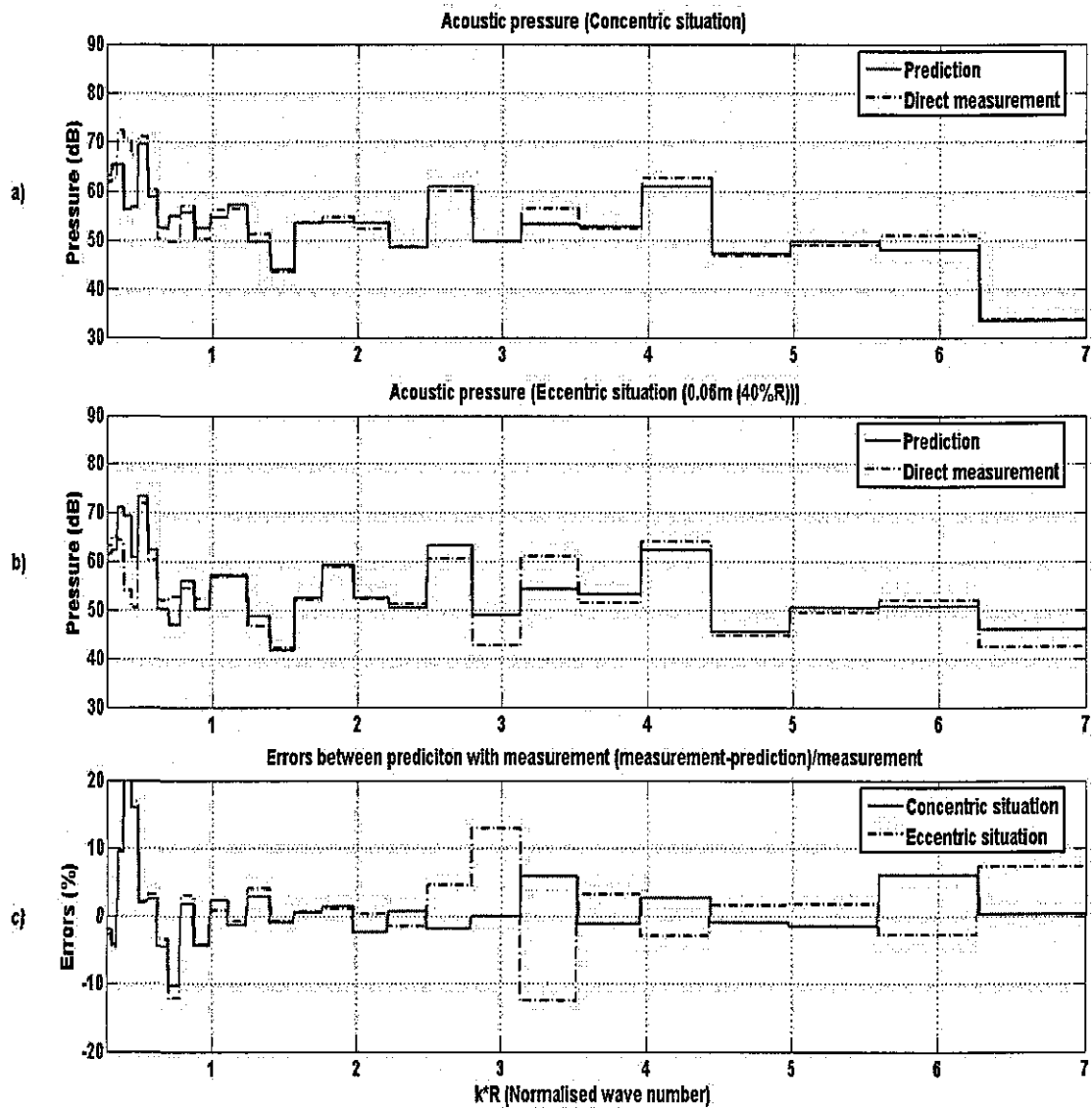


Fig 5.7 Comparison of the prediction made for $\delta = 0m$ and $\delta = 0.06m(40\%R)$ (a) shows the acoustic pressure when the point source is concentric to the main duct situation; b) shows the acoustic pressure when the point source is eccentric to the main duct situation; c) shows the errors between the predictions and the direct measurements for both situations)

From Fig 5.6 -5.7, it can be seen that

1. For both $\delta = 0m$ and $\delta = 0.06m(40\%R)$, the biggest error appears at the very low normalized wave number range $k * R < 0.8$, which means this model is inapplicable to the very low normalized wave number range. This error could be caused by a resonance in the source duct, because the length of the source duct is

not considered in the theoretical calculation. However the length of the source duct affects the acoustic field in the main duct, especially in the low normalized wave number range.

2. Other than $k^*R < 0.8$, the errors for $\delta = 0m$ fall into $\pm 5\%$ of the direct measurement and the errors for $\delta = 0.06m(40\%R)$ mainly fall into $\pm 10\%$ of the direct measurement. It is apparently the errors for $\delta = 0m$ are less than those errors for $\delta = 0.06m(40\%R)$. Because when the sound source is located at $\delta = 0m$, those axially-symmetric modes, such as (0, 1) mode and (0, 2) mode, are dominant in duct; but when the sound source is located at $\delta = 0.06m(40\%R)$, other higher-order modes appear and dominate in the respective cut on frequency ranges. So these higher-order modes bring extra errors to prediction. For example, one can see from Fig 5.7, for $\delta = 0.06m(40\%R)$, at frequency range $2.5 < k^*R < 3.5$, the errors are very large, because at this frequency, $(\pm 1, 1)$ mode and $(\pm 2, 1)$ mode cut on and these four spiralling higher-order modes dominate in this frequency range.

5.4.4 Prediction for the different circumferential positions

From Fig 5.7, one can see the effects of those spiralling higher-order modes on the prediction. In order to test whether or not this model can catch those spiralling higher-order modes, in this section, predictions for the different points along the circumference of the main duct will be made. To some extent this highlights the possible errors due to the spiralling wave front of those axially-unsymmetric higher-order modes. As shown in Fig 5.2, in the main duct, there are two rings of measurement points. Take the first ring for example, there are six equally distributed measurement positions. Along this ring, point 1, point 3 and point 5 are taken and named as position 1, position 2 and position 3 respectively in the following two figures.

Fig 5.8 shows the pressures when the source duct is concentric to the main duct ($\delta = 0m$) and Fig 5.9 shows the pressures when the source duct is eccentric to the main duct ($\delta = 0.06m(40\%R)$).

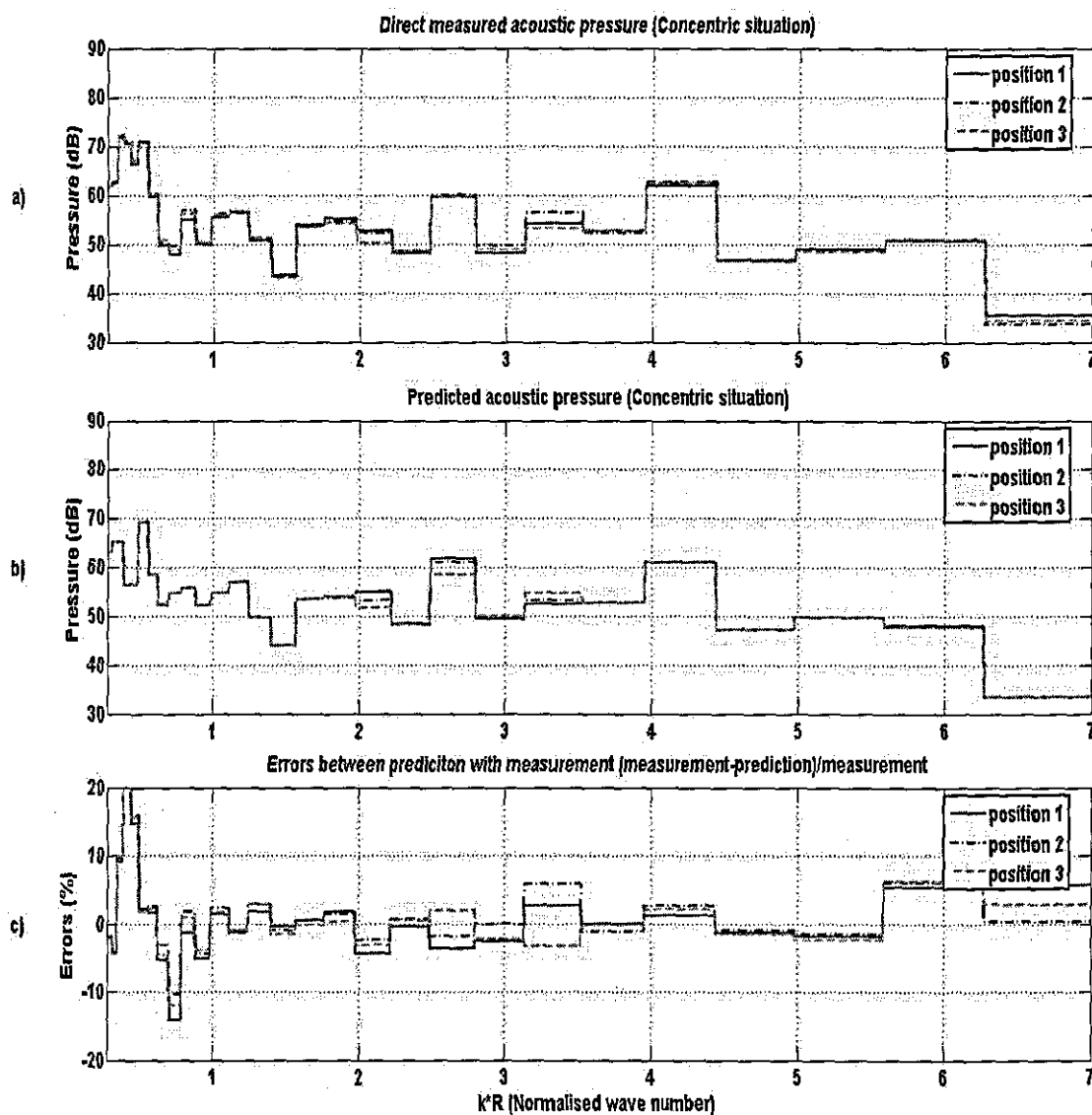


Fig 5.8 Comparison of the errors of different positions along the circumference of the main duct (the point source concentric situation $\delta = 0m$). (a) shows the direct measurements at these three positions; b) shows the predicted results for these three positions; c) shows the errors between the predictions and the direct measurements at these three positions.)

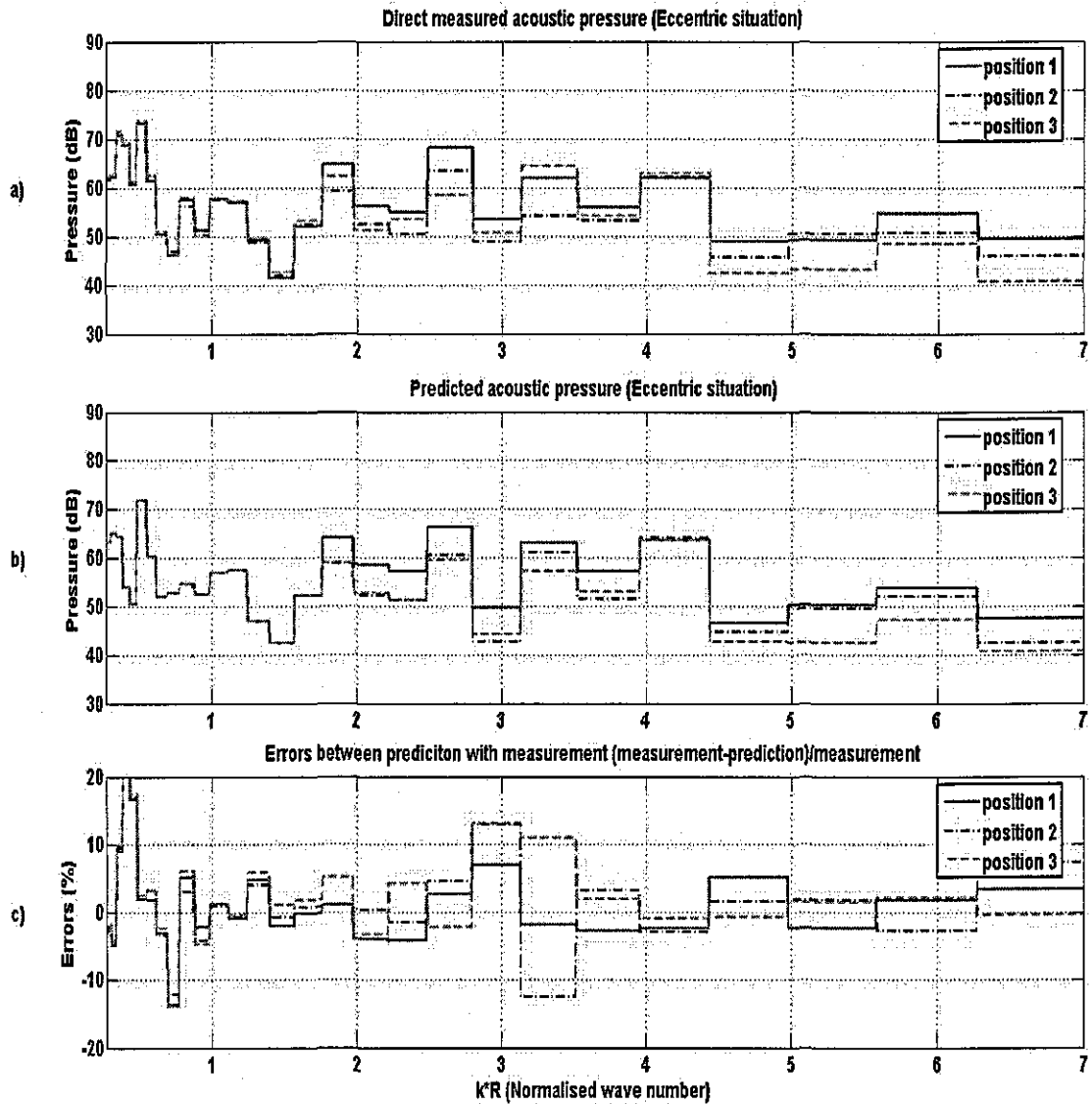


Fig 5.9 Comparison of the errors of different positions along the circumference of the main duct (the point source eccentric situation $\delta = 0.06m(40\%R)$). (a) shows the direct measurements at these three positions; b) shows the predicted results for these three positions; c) shows the errors between the predictions and the direct measurements at these three positions.)

From Fig 5.8 -5.9, it can be seen that

1. For the concentric situation, Fig 5.8 shows that there is nearly no difference between the predictions of these three positions, but for direct measurements, there is a small difference between these three positions, which may be caused by the measurement errors or the source duct location errors (the source duct is not

perfectly concentric to the main duct). Even though the measurements of these three positions are quite similar, and the errors between prediction and direct measurement are similar and considered acceptable. This means that for the concentric situation, the in-duct field is really dominant by those axially-symmetric modes ($m = 0$).

2. For the eccentric situation, other higher-order modes cut on and propagate along the duct. Both predictions and direct measurements for these three positions are very different due to the spiralling higher-order modes. But by comparing errors of these three positions, one can see that the errors for all these three positions are large at normalized wave number range of $k * R \approx 3$, which is just around $(\pm 1, 1)$, $(\pm 2, 1)$ modes cut on. These errors are all different for these three positions, which means prediction along the circumferential position for eccentric situation is dependent on the circumferential angle and frequency range.
3. No matter whether the concentric or the eccentric situation is considered, compared with other parts of the frequency range, the low normalized wave number range ($k * R < 0.8$) prediction has largest errors, which means this model is not applicable to the low normalized wave number range.
4. Through these two figures, one can see that for both the concentric and the eccentric source location, the errors between predictions and direct measurements mainly fall into $\pm 10\%$ of the direct measurements, which is considered acceptable for prediction.

5.5 Discussion

According to the analysis above, it can be seen that this theoretical decomposition approach can be successfully applied in the duct terminated with an infinite flange. The total errors (including the errors caused by the model description, the neglecting of those cut off higher-order modes and measurement errors at reference points and measurement points) inherent in this model are considered acceptable.

Most important of all, it provides an effective and accurate approach for the decomposition of the in-duct field with the point source. It combines the theoretical and experimental approach together. Unlike other time-consuming experimental decomposition approaches, it makes the decomposition of the in-duct field for the circular ducts without simple aperture devices much easier (only two points measurement needed).

In next chapter, another type of sound source (the plane wave source) in circular duct without simple aperture devices will be studied and analysed.

Chapter 6 Sound field produced by a plane wave source propagating in a circular duct without simple aperture devices

6.1 Introduction

Two different types of sound source have been introduced and the acoustic properties of the sound field produced by the point source in circular duct have been discussed. The acoustic field produced by another type of source, the plane wave source, in circular duct will be introduced in this chapter. In Chapter 4, the plane wave source is introduced and its properties and description are presented. Also in Chapter 3, sound radiation from the open end of the circular duct is discussed and the complex reflection coefficients R_{mL} are obtained. Based on the reflection coefficients R_{mL} , one can get the relationships between the incident and the reflected waves in duct. In this chapter, consideration is given to combine these two boundary conditions together and hence the acoustic properties in circular duct without simple aperture devices.

As discussed by C. L. Morfey in Ref [33], it is difficult to decompose the in-duct field experimentally, especially when there are many higher-order modes propagating in circular duct. In order to achieve the effective decomposition, at least $2 * N$ independent different measurements for N higher-order modes propagating in the duct are needed and any inaccurate measurement will introduce errors to the final results. So in this chapter, based on the theoretical descriptions of these two boundary conditions, only two reference measurements (either in source region or main duct region) are required for the decomposition of the in-duct field. Also in this chapter, the effects of the length of the duct and the eccentric locations of the sound source are investigated.

6.2 Theoretical derivation

For the open end of the duct, equation (3.57) is obtained to describe this open-end boundary condition:

$$B_{mn} = \sum_{L=1}^{\infty} R_{mL} A_{mL}. \quad (6.1)$$

Also for the plane wave source boundary condition, equation (4.11) to equation (4.18) are obtained. So from these two groups of the equations, one can get the matrix below,

$$[X]_{D \times D} \begin{bmatrix} SB_{01} \\ \vdots \\ SB_{mn}^- \\ A_{01} \\ \vdots \\ B_{mn}^- \end{bmatrix}_{D \times 1} = \begin{bmatrix} SA_{01} \\ \vdots \\ SA_{mn}^- \\ 0 \\ \vdots \\ 0 \end{bmatrix}_{D \times 1} \quad (6.2)$$

in which X is the coefficient matrix for these amplitudes. Its dimension D is also decided by how many higher-order modes are considered.

However compared equation (6.2) with equation (5.10), it is noticed that one extra item SB_{mn} , which are the amplitudes of the reflected waves in the source duct region, appear in this equation. So if $m = \pm 5$ and $n = 5$, the dimension of the matrix X should be 165×165 $((n + 2 * |m| * n) + (2 * n + 4 * |m| * n))$ rather than 110×110 $(2 * n + 4 * |m| * n)$ for the point source situation. Still one should first try to invert the matrix X to get the solution.

$$\begin{bmatrix} SB_{01} \\ \vdots \\ SB_{mn}^- \\ A_{01} \\ \vdots \\ B_{mn}^- \end{bmatrix}_{D \times 1} = [X]_{D \times D}^{-1} * \begin{bmatrix} SA_{01} \\ \vdots \\ SA_{mn}^- \\ 0 \\ \vdots \\ 0 \end{bmatrix}_{D \times 1} \quad (6.3)$$

During the matrix inversion, it is also noted that the matrix is ill conditioned and approaches singular. Similar to the analysis presented in Chapter 5, the third approach is selected to keep $k_{z,m,n}''$ always real at the source boundary. So for the main duct region, only those modes that can propagate along the main duct are considered in this matrix. Again at different frequencies, there are different higher-order modes propagating in the duct. For the source duct region, because the radius of the duct is $r = 0.024m$, there should be only the plane wave propagating along the source duct in the frequency range from $0 - 2600 Hz$. So only $(0, 1)$ mode is considered for the source duct region.

By considering only those modes that have cut on in both the main duct region and the source duct region, one can rewrite equation (6.3) as follow,

$$\begin{bmatrix} SB_{01} \\ A_{01} \\ \vdots \\ B_{m(n-1)}^- \\ B_{mn}^- \end{bmatrix}_{D \times 1} = [X]_{D \times D}^{-1} * \begin{bmatrix} SA_{01}e^{jkl}R_1/2 \\ SA_{01}e^{jkl}R_1^2 \\ \vdots \\ 0 \\ 0 \end{bmatrix}_{D \times 1} \quad (6.4)$$

From this equation, it can be seen that for the source duct region, only (0, 1) mode is considered. Of course, if the radius of the source duct is larger, other higher-order modes should be cut on at this frequency range, so one should just include those cut on modes in this equation. However in this chapter, it is assumed that the source duct can propagate only the plane wave and this is why it is called the plane wave source.

In this situation, the neglecting of those cut off higher-order modes will bring some errors to the results obtained from equation (6.4). In the following sections, comparison will be made between the actual results (direct measurements) and results obtained from this equation (predictions).

6.3 Experiment measurements and results

In order to get the modal amplitudes, the experimental set-up used is shown in Fig 6.1 and Fig 6.2. A 0.94m long duct with radius 0.024m acts as the source duct. On one end it is connected to a speaker from which a sound wave is produced, on the other end, it is connected to a rigid circular plate. This plate is placed at one end of the main duct, the other end of the main duct is left open and one large wooden plate is used as the rigid baffle.

The detailed experimental set-up is given in Fig 6.2 and the equipment set-up and connections are given in Appendix A. From this figure, it can be seen that there are three measurement points in the source duct region, in which the single one is used as reference measurement and two closely located (20mm) points are used for the microphone pair measurement. For the main duct region, there are two rings of

measurement positions which are located at $z = -0.18m$ and $z = -0.54m$ from the open end of the main duct. Each ring contains six equally circumferential positioned measurement points. At each point, two closely located ($20mm$) holes are drilled on the duct wall, which are used for microphone pair measurement (acoustic pressure and particle velocity). The origin point of the coordinate system is taken at the centre of the open duct end plane. There are also two reference measurement points in the main duct, which are located at $(0.15m, 0, -2.33m)$ and $(0.15m, 3 * \pi / 4, -1.5m)$ respectively.

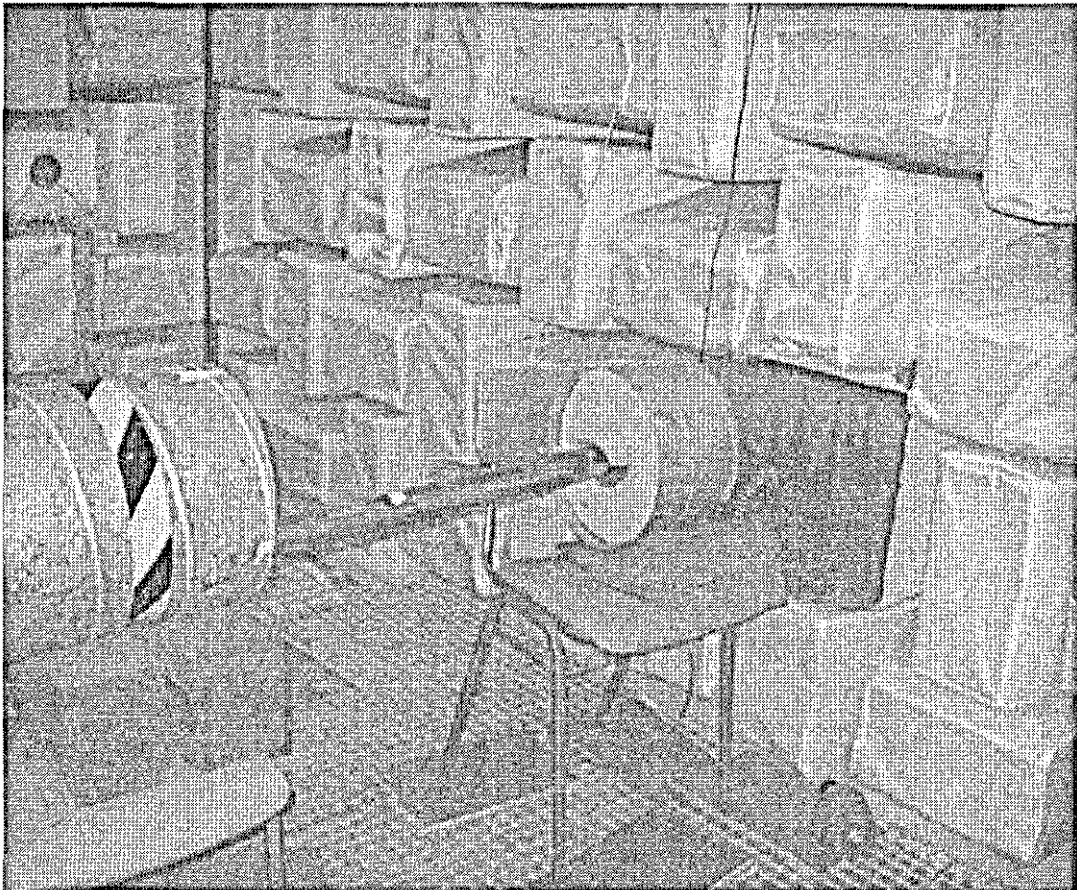


Fig 6.1 The picture of the plane wave source set-up for the measurement

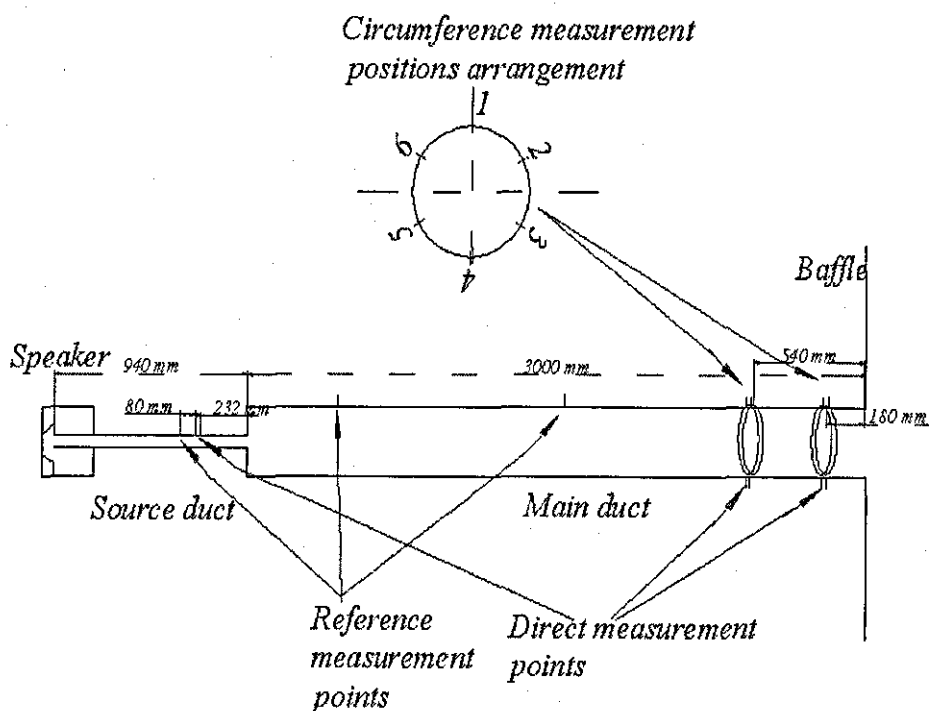


Fig 6.2 Detailed sketch of the plane wave source measurement set-up

Because the sound source is a constant one, the acoustic fields it produces in the source duct and the main duct are also constant. Consequently it does not need many microphones to measure simultaneously to catch those acoustic properties both in the source duct and the main duct. For convenience four microphones are used to measure acoustic pressures and particle velocities at appointed positions. For the measurement in the main duct region, one pair is used to measure acoustic pressure and particle velocity at the appointed positions (direct measurements); the other two microphones are used to measure at those two reference positions in the main duct, which are located at the positions with different z -axis and circumferential angle (reference measurements for prediction). The reasons for using two-reference positions measurement are given in Chapter 5.

For the measurement in the source duct region, only three microphones are used. One pair is used to measure acoustic pressure and particle velocity at appointed positions (direct measurements); the other one microphone is used to measure at the reference position. Because only the plane wave propagate in the source region, so it is assumed one point measurement is sufficient for the prediction.

In order to obtain the amplitudes of those acoustic properties, it is necessary to know the amplitude of the incident wave SA_{01} first. However it is quite difficult to get this value. So two methods are proposed.

The first method (*Method 1*) is proposed as below:

First let the amplitude of the incident wave SA_{01} be 1, then substitute it in equation (6.4), one can get other amplitudes (not the actual values but the relative ones) such as, SB_{01} , A_{01} , B_{01} Then substituting SB_{01} and the coordinate of the reference point $Z = -l$ into equation below,

$$p = SA_{01}e^{jkl} + SB_{01}e^{-jkl} . \quad (6.5)$$

Let this value equal acoustic pressure measured directly at this point, one can get the real values of the amplitudes SA_{01} and SB_{01} . Then substituting these values into equation (6.4) again, one can get those amplitudes A_{01} , B_{01} ... in the main duct.

Substituting these amplitudes and the coordinate of the this point (r, θ, L) into equation below,

$$P = \sum_{m=0}^{\infty} \sum_{n=1}^{\infty} (J_m(k_{r,m,n}^H r)) [(A_{mn}^+ e^{-jm\theta} + A_{mn}^- e^{jm\theta}) e^{jk_{z,m,n}^H L} + (B_{mn}^+ e^{-jm\theta} + B_{mn}^- e^{jm\theta}) e^{-jk_{z,m,n}^H L}] , \quad (6.6)$$

one can predict the acoustic pressure at the measurement point. By comparing this value with the direct measurement, one can see whether or not this method works. If it works, one can also see how large are the errors brought in by neglecting those cut off higher-order modes. This method is named *the source duct region measurement prediction* and is known as *Method 1*.

Sometimes it is difficult to measure at the source region because of the small radius, so a second method (*Method 2*) is proposed. The procedure of the calculation in this method is given in Appendix F. Comparing with the former method (*Method 1*), this method is named *the main duct region measurement prediction* and is known as *Method 2*. Of course, one can also predict the source region with this method.

As discussed in Chapter 5, if the sound source is located at the centre of the duct, it can only produce and propagate axially-symmetric higher-order modes ($m = 0$). However if the sound source is located at other points rather than the centre of the duct, all other higher-order modes begin to propagate along the duct. So three situations, shown in Fig 6.3, are considered in the following sections, one situation is the source duct is concentric to the main duct; the other two situations are the eccentric distance of source duct is $\delta = 0.06m(40\% R_0)$ and $\delta = 0.09m(60\% R_0)$ respectively from the centre of the main duct. Comparison will be made on the effects of eccentric distance on the errors of the prediction.

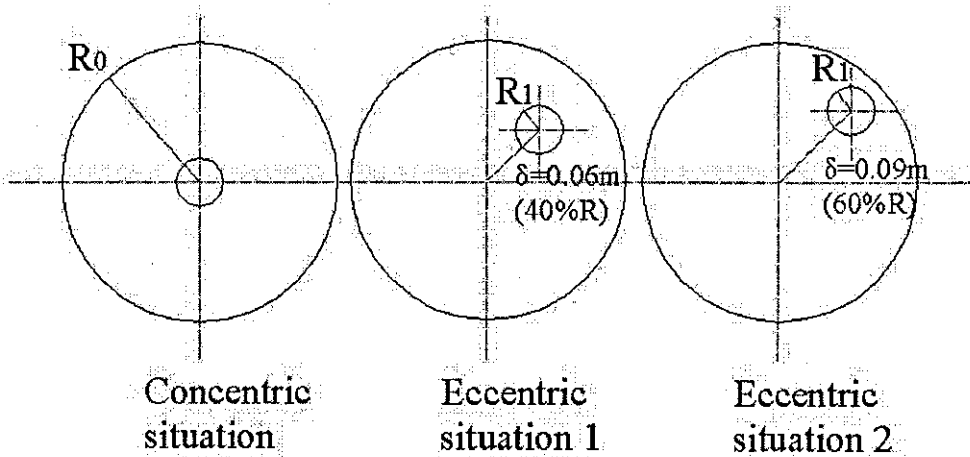


Fig 6.3 The relationship of the source duct with the main duct

In order to show the differences between these two methods, the three source duct – main duct relationships discussed above (concentric, $\delta = 0.06m(40\% R_0)$ and $\delta = 0.09m(60\% R_0)$) are considered. The results for these three situations are similar and the worst one, which is the source duct is located at $\delta = 0.09m(60\% R_0)$, is selected to show the results (results of other two situations are better).

Two figures are plotted to show the results obtained from these two methods for this situation ($\delta = 0.09m(60\% R_0)$). Fig 6.4 shows the comparison of the predictions and the direct measurements using *Method 1*, which is using the reference measurements in the source duct region to do the prediction. Fig 6.5 shows the comparison of the predictions

and the direct measurements using *Method 2*, which is using the reference measurements in the main duct to do the prediction. In each figure, a) shows the comparison of the predicted pressure with the directly measured pressure in the main duct region; b) shows the comparison of the predicted pressure with the directly measured pressure in the source duct region;

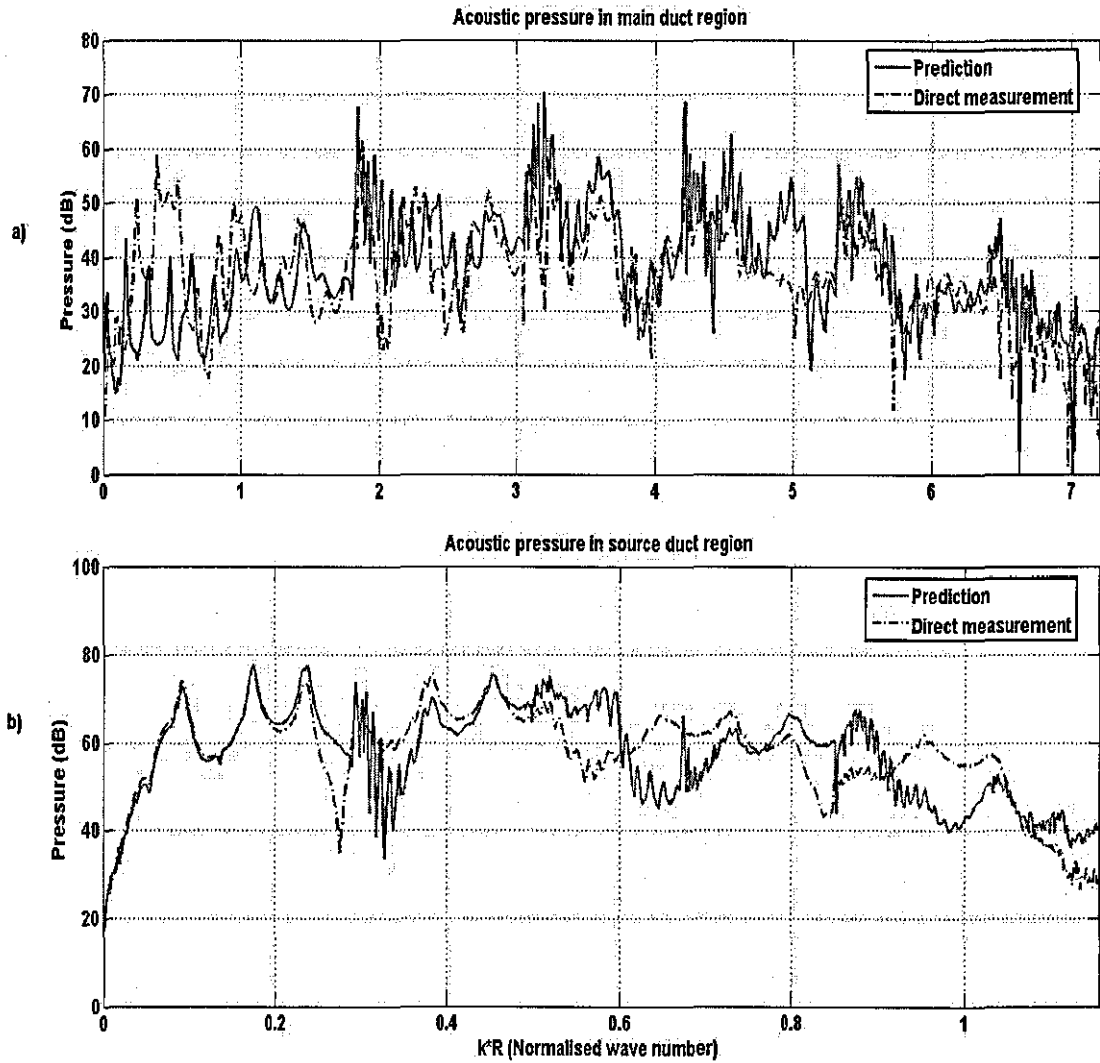


Fig 6.4 Comparison of predictions and direct measurements for *Method 1*

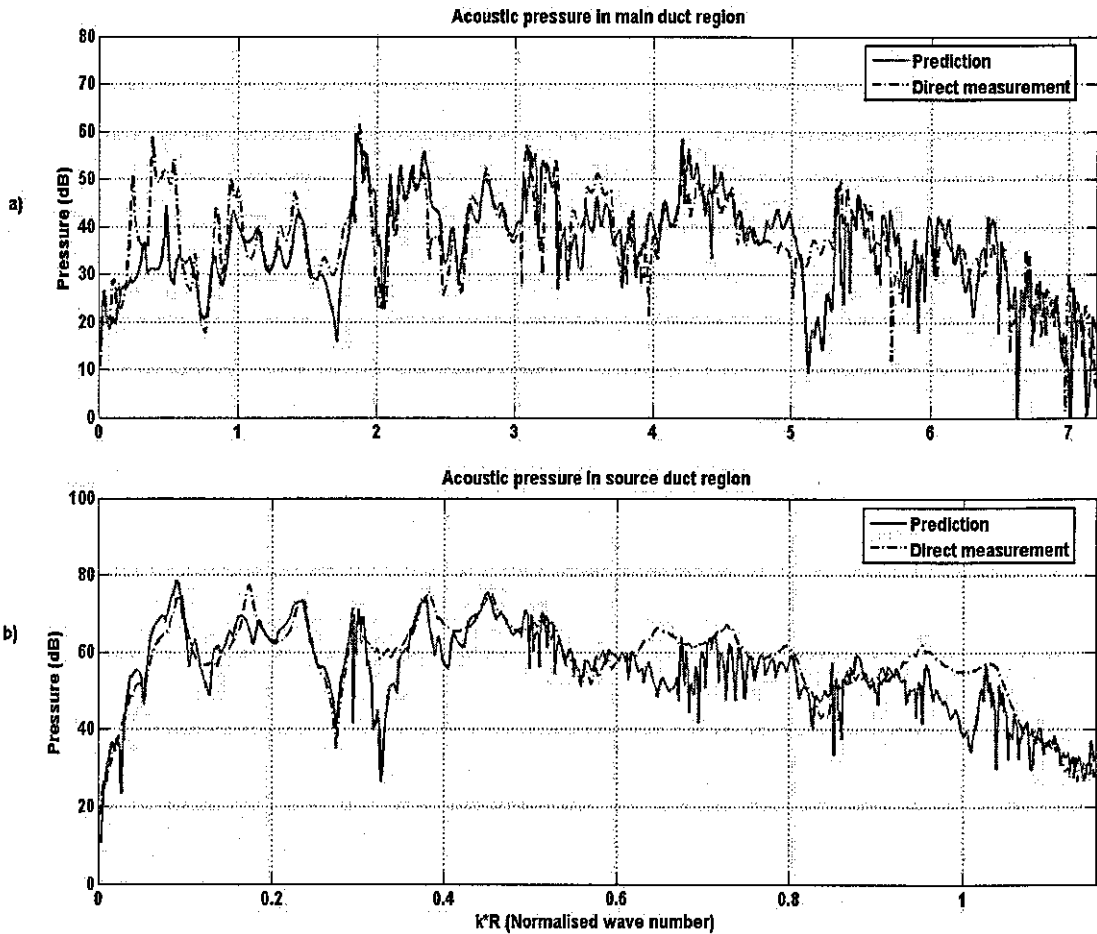


Fig 6.5 Comparison of predictions and direct measurements for *Method 2*

From Fig 6.4 -6.5, it can be seen that:

1. There are some errors between prediction and direct measurement for the main duct region, especially at the very low normalised wave number range ($0 < k \cdot R < 0.8$). Apart from that frequency range, both of methods work well in the prediction of acoustic pressure for the main duct region.
2. The errors between the predictions and direct measurements for *Method 2* are smaller than those for *Method 1* both in the main duct region and in the source duct region. The reason for this is mainly because the measurement in the main duct region can catch the higher-order modes information more accurately. However for the measurement in the source duct region, only the plane wave is considered in this region, although one can see the effects of the higher-order modes from the measurement, but the detailed information of those higher-order modes is difficult to be measured directly in the source duct region.

Using these two methods, through the measurement at only one reference point in the source duct region or two reference points in the main duct region, one can predict the acoustic properties of the whole in-duct field, such as acoustic pressure, particle velocity, etc, at any point both in the source duct region and the main duct region. This makes decomposition of the in-duct field much easier. Then the in-duct field can be decomposed into the different higher-order modes.

In the following sections, comparison will be made between coupled predictions and uncoupled predictions, including the effects of the length of the main duct on the predictions and the effects of the radial location of the sound source on the predictions. The method used in the following sections is *Method 2*, which is to predict in-duct field through the measurement at the reference points in main duct region rather than in source duct region. The reasons to do so are:

1. *Method 2* is more accurate than *Method 1*;
2. it is easier to do the measurement in the main duct. Because the radius of the source region is very small, sometimes it is difficult to measure in that region, especially in Chapter 5, for the point source, the measurement in the point source duct region is impossible;
3. the measurement in the source duct region can bring more errors to the results, because it is more difficult to make ½" microphone flush mounted to the wall of the duct with such small radius, so the intruding part of the microphone will cause disturbance to the measurements in this region.

6.4 Difference between the coupled and uncoupled prediction

For the main duct open end boundary condition, one can get the relationship described in equation (6.1). For this equation, if other modes contributions are considered, it is called the coupled equation. If other modes contributions are neglected, it can be written as,

$$B_{mn} = R_{mnn} A_{mn} , \quad (6.7)$$

which is called the uncoupled equation.

Applying equation (6.1) and equation (6.7) separately into equation (6.2), one can get two groups of results, one is called the coupled prediction and the other is called the

uncoupled prediction. Through the comparison of these two different predictions, one can see the coupling effects between different higher-order modes at the open end of the duct. If the difference is negligible, the coupled equation can be substituted by the uncoupled one, which makes the calculation simpler and easier. Because only the acoustic properties in the main duct are of interest in this investigation, only comparisons in the main duct region are shown below.

All three situations shown in Fig 6.3 are considered and two situations (concentric and $\delta = 0.06m(40\%R_0)$) are chosen and plotted in Fig 6.6. Fig 6.6 a) shows the coupled, uncoupled predicted pressures and directly measured pressures for source duct concentric situation; Fig 6.6 b) shows the coupled, uncoupled predicted pressures and directly measured pressures for source duct located at $\delta = 0.06m(40\%R_0)$ situation;

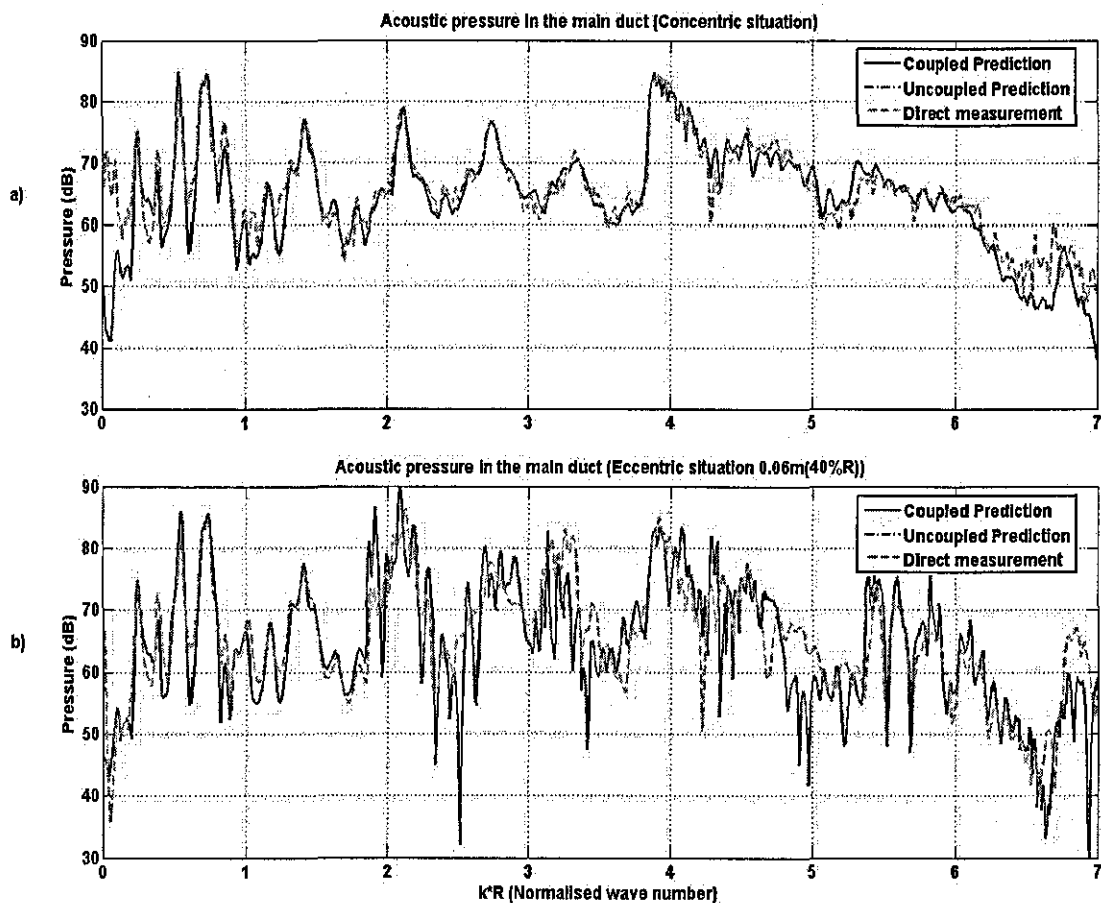


Fig 6.6 Comparison of the coupled and uncoupled predictions with direct measurements in the main duct region for concentric and $\delta = 0.06m(40\%R_0)$ situations

In order to show the results more clearly, the source duct concentric situation is chosen and the results are transferred to 1/6 octave band and shown in Fig 6.7 (errors between predicted and directly measured pressures for other eccentric situations will be shown in Fig 6.10 and 6.11). Fig 6.7 a) shows the coupled, uncoupled predicted pressures and directly measured pressures; Fig 6.7 b) shows the errors between coupled and uncoupled predicted pressures; the errors between coupled predicted and directly measured pressures; the errors between uncoupled predicted and directly measured pressures.

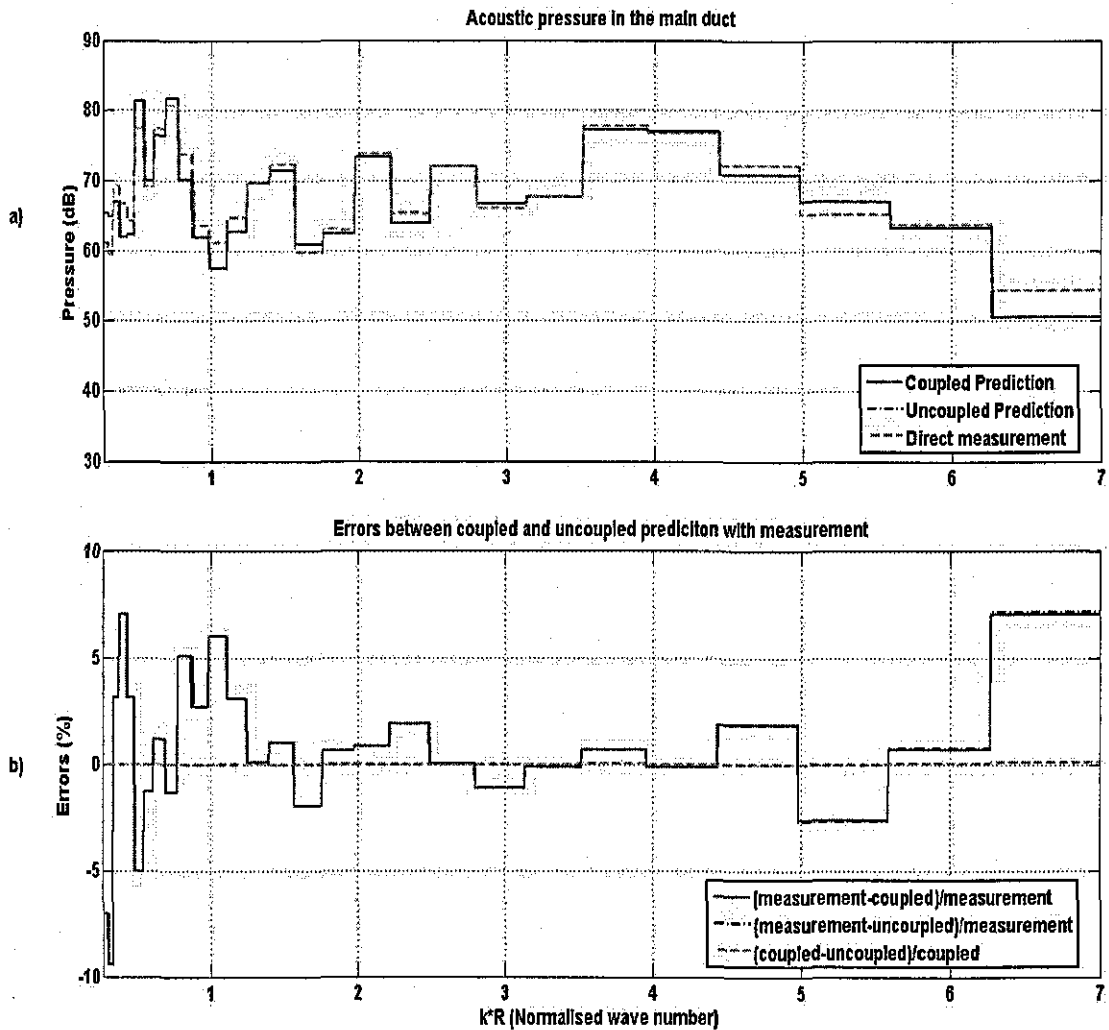


Fig 6.7 Comparison of the difference between uncoupled, uncoupled predictions with direct measurements (source duct is concentric to the main duct)

From Fig 6.6 - 6.7, it can be seen that:

1. There is nearly no difference between coupled and uncoupled predictions, which means the cross coupling effects at the open-end of the main duct between

different higher-order modes are negligible. In this situation, the coupled prediction is not a perfect one because it only considered the cross coupling effects between those cut on modes; actually it should be referred to as the partially coupled prediction.

2. Both coupled and uncoupled predictions agree well with direct measurements for both concentric and eccentric situations. Especially for the concentric situation, from Fig 6.7, it can be seen that apart from the low normalized wave number range, the errors between predictions and direct measurements mainly fall into the range of $\pm 5\%$ of the direct measurements, which is considered acceptable. Similar size errors are found for the two eccentric situations.
3. The errors introduced by the neglecting of those cut off higher-order modes are very small for all three different situations (concentric and eccentric situations). Which means that the approach adopted to eliminate the imaginary exponential items $e^{-jk_{z,m,n}L}$ is acceptable.

6.5 Effects of the length of the duct on prediction

After discussing the difference between coupled and uncoupled predictions, attention is paid to the effects of the length of the duct on the accuracy of the prediction. Because as discussed before, the origin of the coordinates is set at the open end of the duct, the source boundary condition is related to the length of the duct ($e^{-jk_{z,m,n}L}$). So in this section, another 0.53m long duct with the same radius ($R_0 = 0.15m$) is used as the main duct, the plot of the experimental set-up is given in Fig 6.8. The purpose of testing ducts with different lengths is to check that the errors in the prediction are independent of the length of the duct.

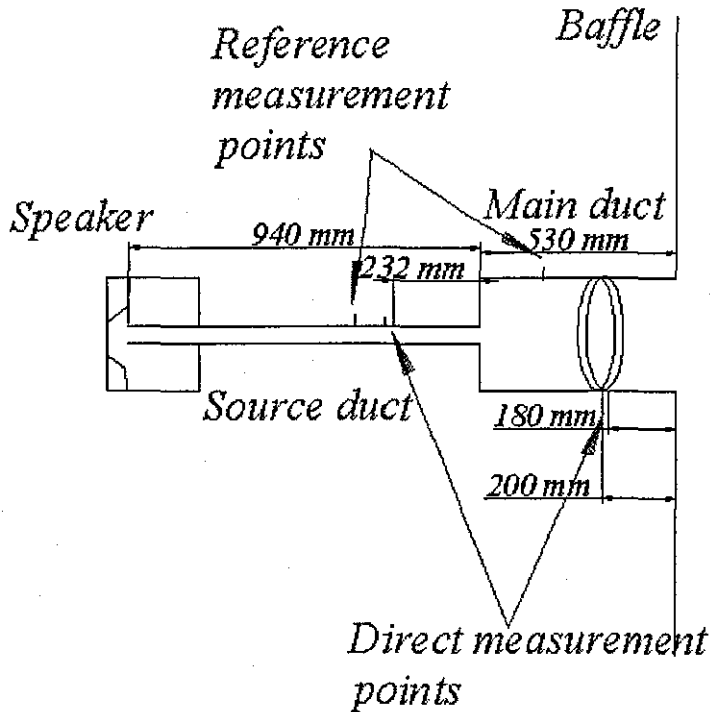


Fig 6.8 The plot of the experimental set-up of the short duct

Two situations, which are source duct concentric to the main duct and source duct eccentric to the main duct ($\delta = 0.06m(40\% R_0)$), are considered. The predictions of acoustic pressures in the main duct region are made for both the long duct and the short duct. The results are shown in Fig 6.9 and Fig 6.10. For clarity, the results are shown in 1/6 octave band rather than linear frequency. Fig 6.9 shows the comparison when the source duct is concentric to the main duct; Fig 6.10 shows the comparison when the source duct is eccentric to the main duct ($\delta = 0.06m(40\% R_0)$). In each figure, *a*) shows the predicted pressures and directly measured pressures in the long duct; *b*) shows the predicted pressures and directly measured pressures in the short duct; *c*) shows the errors between predicted pressures and directly measured pressures for both situations.

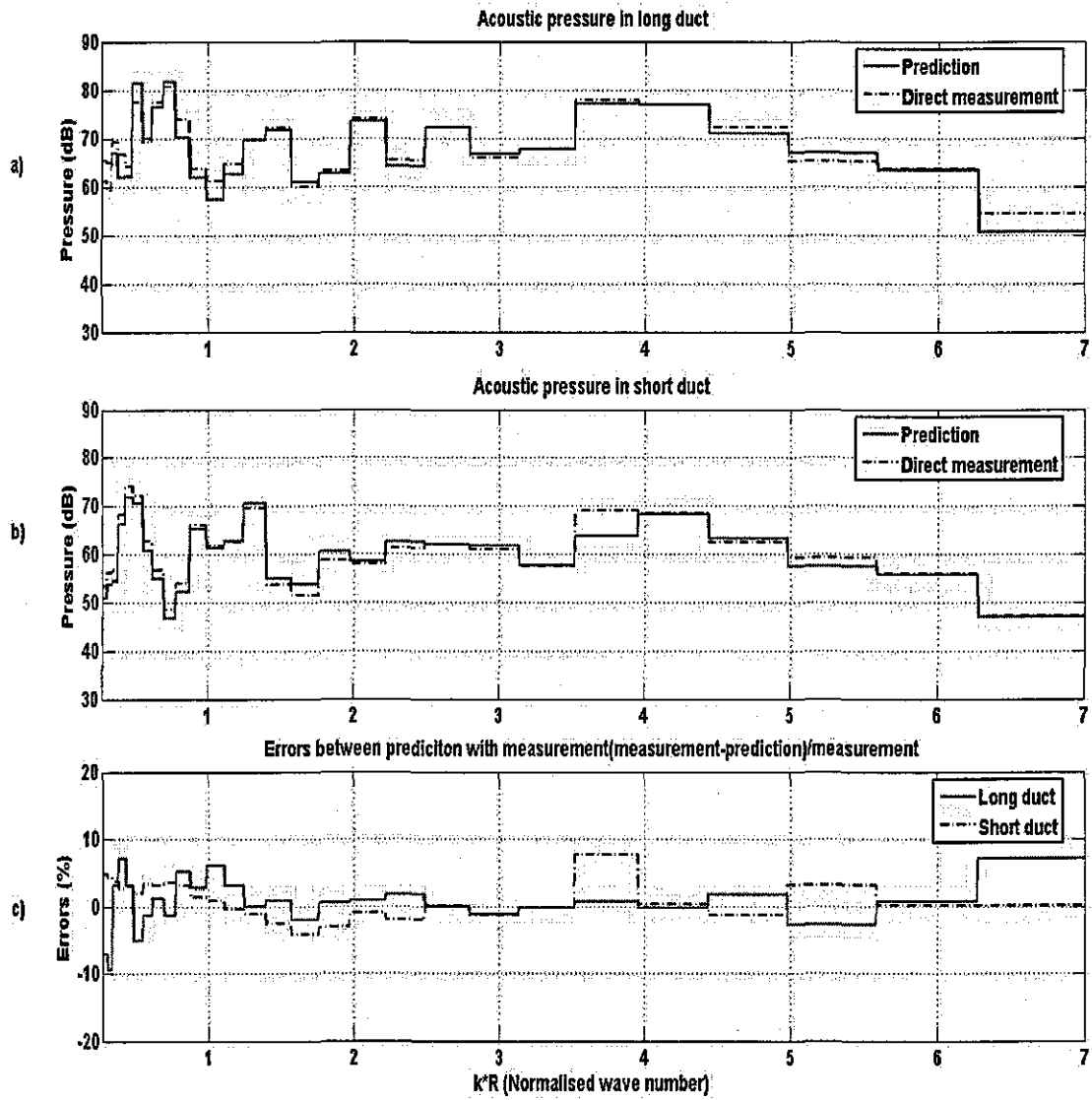


Fig 6.9 Comparison of the predictions with direct measurements for long duct and short duct (source duct is concentric to the main duct)

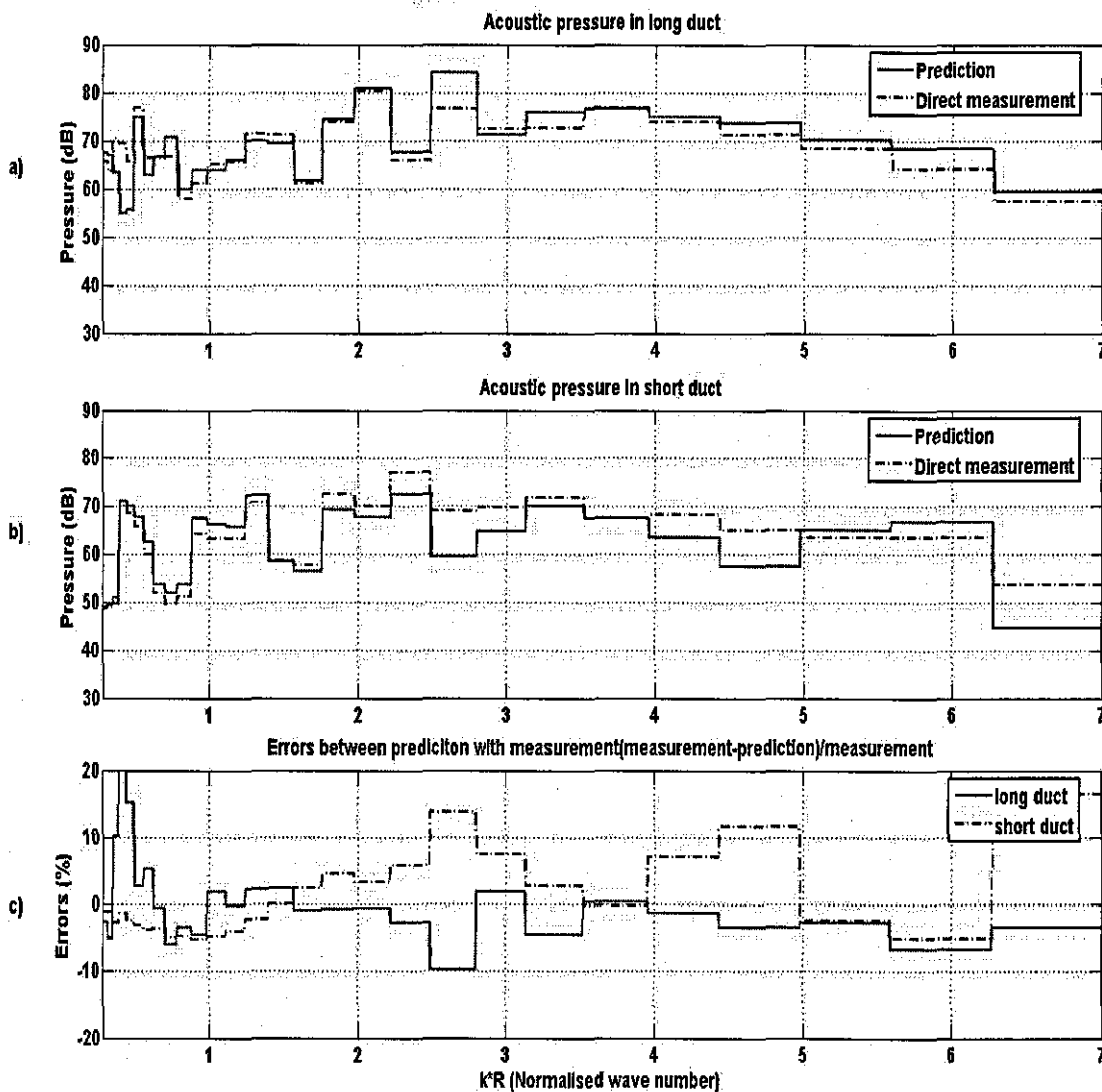


Fig 6.10 Comparison of the predictions with direct measurements for long duct and short duct (source duct is eccentric to the main duct $\delta = 0.06m(40\% R_0)$)

From the comparison shown in Fig 6.9, it can be seen that for the concentric situation the errors for short duct are similar to those for long duct, most of them fall into the range of $\pm 5\%$ of the direct measurements (apart from low frequency range). However for the eccentric situation shown in Fig 6.10, the errors for the short duct are a little bit larger than those for the long duct (most of them fall into the range of $\pm 10\%$ of the direct measurements). The reason for this is if the main duct is too short, the plane wave and some higher-order modes cannot fully develop in the duct, so there should be some errors for the prediction made using the measurement in the main duct. So if the length

of the main duct is not too short, the errors of the prediction are considered acceptable and the effects of the length of the duct on the prediction can be ignored.

6.6 Effects of the radial location of the sound source on the prediction

In this section, the effects of the radial location of the sound source on the predictions are discussed. The three different source duct– main duct relationships shown in Fig 6.3 are tested. Comparison is shown in Fig 6.11.

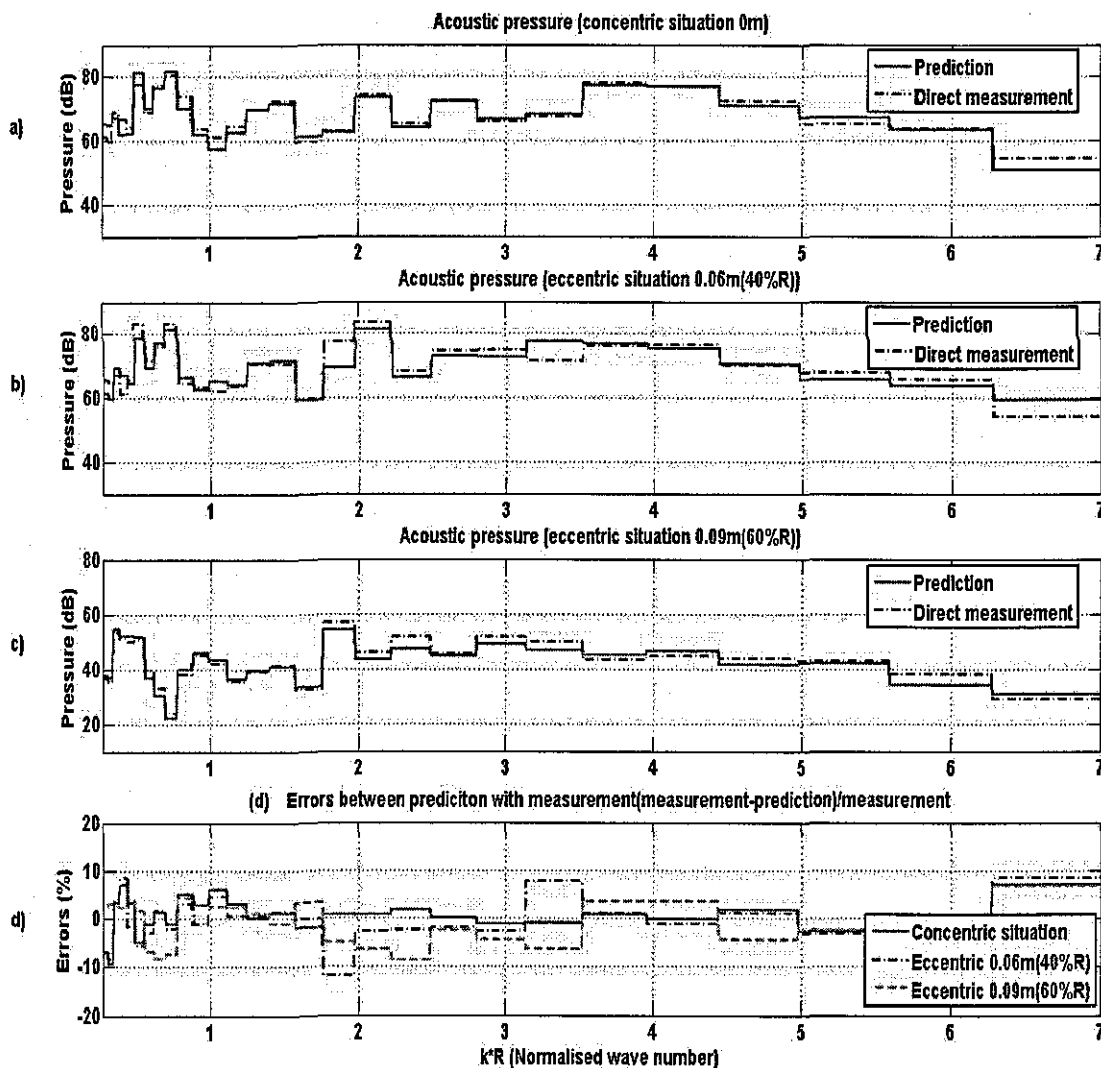


Fig 6.11 Comparison of the errors for the concentric and eccentric source situations
(a) shows concentric situation; b) shows $\delta = 0.06m(40\%R_0)$ situation; c) shows $\delta = 0.09m(60\%R_0)$ situation; d) shows comparison of the errors of these three situations

From this figure, it can be seen that even for the eccentric situations, the predictions agree well with the direct measurements. But the errors for the eccentric situations are larger than those for the concentric situation. This is because, for the concentric situation, only those axially-symmetric higher-order modes, such as (0, 1) mode and (0, 2) mode are dominant in the main duct; on the other hand, for eccentric situations, axially-unsymmetric higher-order modes, such as ($\pm 1, 1$) modes and ($\pm 2, 1$) modes, are dominant in the main duct and there are more of these modes. These spiralling higher-order modes bring some extra errors into the prediction.

Also through the comparison of those two eccentric situations, as expected, one can see that the errors for the $\delta = 0.09m(60\% R_0)$ situation are a little bit larger than those for the $\delta = 0.06m(40\% R_0)$ situation, which means the further the distance of the sound source from the centre of the main duct, the larger errors are produced in predictions.

6.7 Predictions for different circumferential positions

In Chapter 5, comparisons between predictions for different circumferential positions are made and from the analysis one can see that for the point source situation, the model proposed can catch those spiralling higher-order modes accurately. So in this section, for the plane wave source situation, the procedure in Section 5.4.4 is repeated to test the accuracy of the predictions for different circumferential positions.

So predictions for different points along the circumference of the main duct are made. To some extent this highlights the possible errors due to the spiralling wave front of those axially-unsymmetric higher-order modes. As shown in Fig 6.2, at the main duct, there are two rings of measurement points. Take the first ring for example, there are six equally distributed measurement positions. Along that ring, point 1, point 3 and point 5 are taken and named as position 1, position 2 and position 3 respectively in the following two figures.

Fig 6.12 shows the situation when the source duct is concentric to the main duct and Fig 6.13 shows the situation when the source duct is eccentric to the main duct

($\delta = 0.06m(40\% R_0)$). In these two figures, *a*) shows the direct measurements at these three positions; *b*) shows the prediction results for these three positions; *c*) shows the errors between predictions and direct measurements for these three positions.

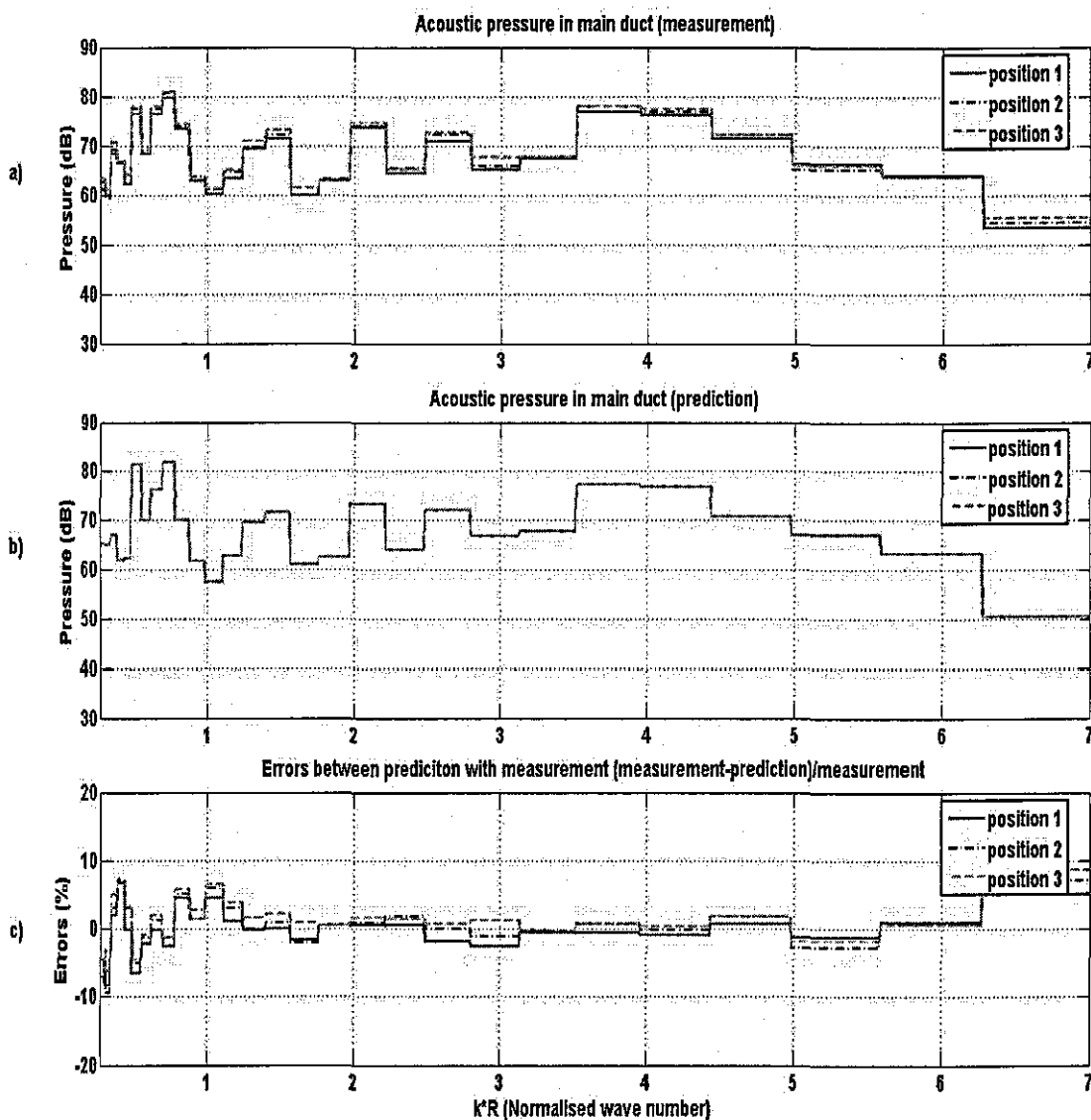


Fig 6.12 Comparison of the errors for three different positions along the circumference of the main duct (concentric situation $\delta = 0m$)

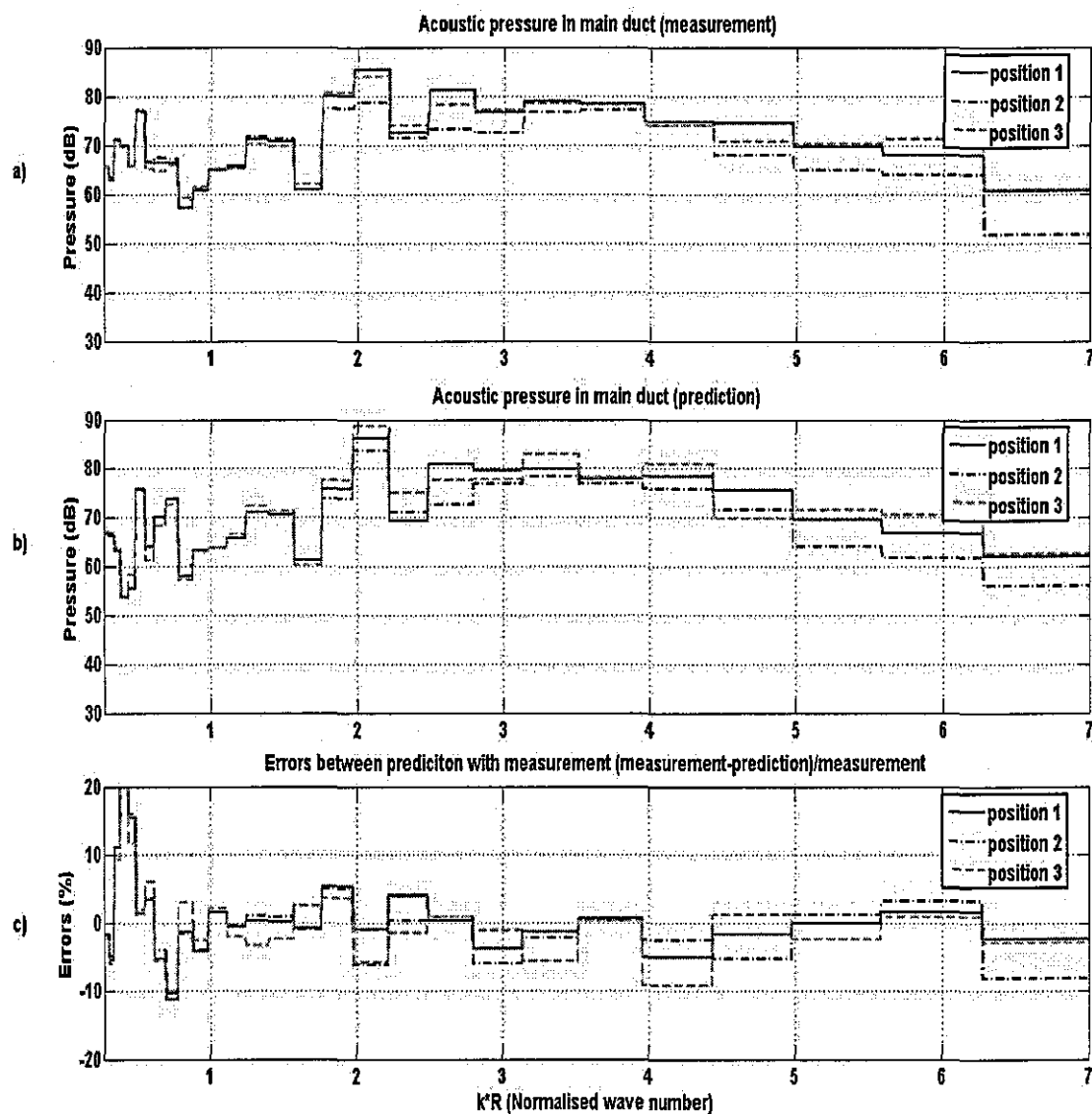


Fig 6.13 Comparison of the errors for three different positions along the circumference of the main duct (eccentric situation $\delta = 0.06m(40\% R_0)$)

From Fig 6.12- 6.13, the similar conclusions as in Chapter 5 are drawn as follow,

1. For the concentric situation, Fig 6.12 shows that there is no difference for the predictions of these three positions, but for direct measurements, there is a small difference between these three positions, which may be caused by the measurement errors or the source duct location errors (the source duct is not perfectly concentric to the main duct). Even though the measurements of these three positions are quite similar, and the errors between predictions and direct measurements are similar and considered acceptable. This means that for the

concentric situation, the in-duct field is really dominant by those axially-symmetric modes ($m = 0$).

2. For the eccentric situation, other higher-order modes cut on and propagate along the duct. Both predictions and direct measurements for these three positions are different, which is caused by the spiralling higher-order modes. But by comparing errors of these three positions, it can be seen that these errors are different at different normalized wave number range. For example, before $(\pm 1,1)$ modes cut on, the errors for these three positions are nearly the same and after $(\pm 1,1)$ mode cuts on ($k * R \approx 2$), the errors for these three positions are different. This means prediction along the circumferential position for the eccentric situation is dependent on the circumferential angle and frequency range. But the errors for these three positions mainly fall into 10% of the direct measurements.
3. For either the concentric or eccentric situation, the low normalized wave number range ($k * R < 0.8$) prediction has the largest errors, which means this model is not applicable for the very low normalized wave number range. The possible reason for this error is given in Chapter 5.

6.8 Discussion

From the analysis presented in this chapter, it can be seen that the model proposed to describe the plane wave source boundary is acceptable. The total errors inherent by this model are acceptable. This model still provides an effective and accurate approach for the decomposition of the in-duct field with the plane wave source. It combines the theoretical and experimental approaches together and makes the decomposition of the in-duct field much easier.

Also by comparing the prediction results for the point source and the plane wave source, it can be seen that the errors for the plane wave source are smaller than those for the point source. This is because the source duct, used to act as a point source in the experiment, is not a perfect one (actually, the smaller the radius of the source duct, the more like it acts as a point source). However the errors are considered small enough to justify the applicability of this model for both source types.

In Chapter 5 and this chapter, two types of sound sources (the point source and the plane wave source) in circular ducts without simple aperture devices are studied and the results obtained from these models are considered acceptable. In the following chapters, simple aperture devices (with one or more circular orifices) will be placed in the circular duct and the effects of these orifices on the in-duct field will be studied.

Chapter 7 Sound field produced by a point source propagating in a circular duct with simple aperture devices

7.1 Introduction

Circular ducts are widely used in many engineering aspects, such as ventilation ducts and mufflers. Usually there are some devices installed in the ducts either for noise control or flow control. So in order to achieve these controls, the effects of these devices on the acoustic fields need to be fully understood. Significant previous works, such as Ref [51] to Ref [53], have been done on different types of devices in circular ducts, but none can provide a generic solution for the effects of the devices on the in-duct field.

The following is based on the study of the acoustic properties of a point source in a circular duct without an aperture device as described in Chapter 5. In this chapter, a simple rigid device with different numbers of circular orifices (single orifice, two orifices and several orifices) is placed in the circular duct and its effects on the acoustic field will be studied. One model is proposed to describe the boundary conditions between the main-duct field and the orifice field. Combining these boundary descriptions with those of the source boundary and open end boundary descriptions, it is possible to get a solution for the amplitudes of the various modes. From the knowledge of these amplitudes, one can study the effects of an aperture device on the acoustic field in detail, especially those effects of the numbers of the orifices; the effects of the comparative cross section positions of different orifices and the effects of comparative cross section position of the point source with those orifices. After getting the theoretical predicted results, measurements of the acoustic field in the duct with same aperture devices are made to compare with those theoretical calculations.

7.2 Aperture device with a single orifice

7.2.1 Theoretical derivation

As shown in Fig 7.1, when there is a simple aperture device (shown in Fig 7.2) placed in the duct, the whole system can be divided into five regions, which are region 1 (radiation

region), region 2 (after orifice region), region 3 (orifice region), region 4 (before orifice region) and region 5 (source region) respectively, separated by four boundaries: boundary 1 (duct end boundary), boundary 2; boundary 3 and boundary 4 (sound source boundary).

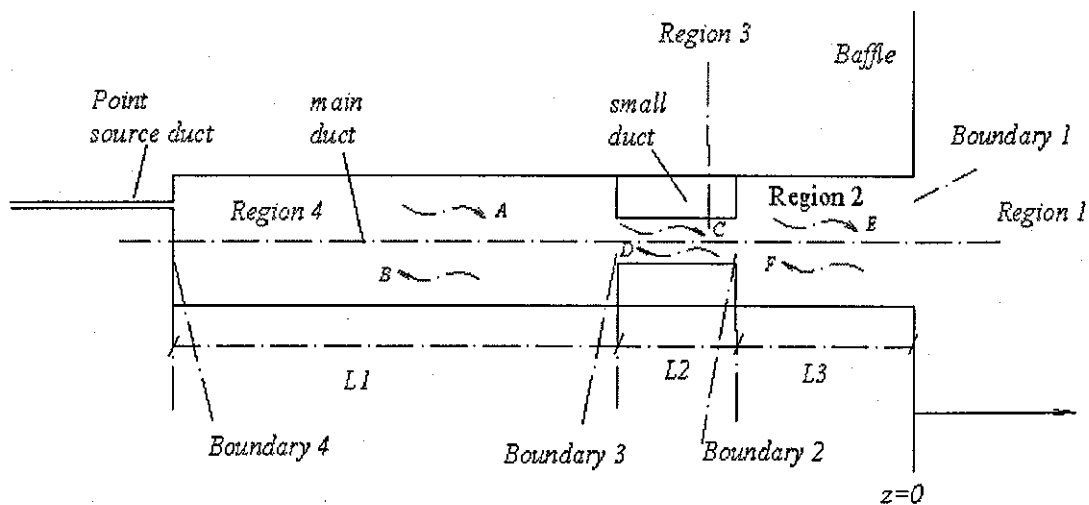


Fig 7.1 Plot of Circular duct with simple aperture device

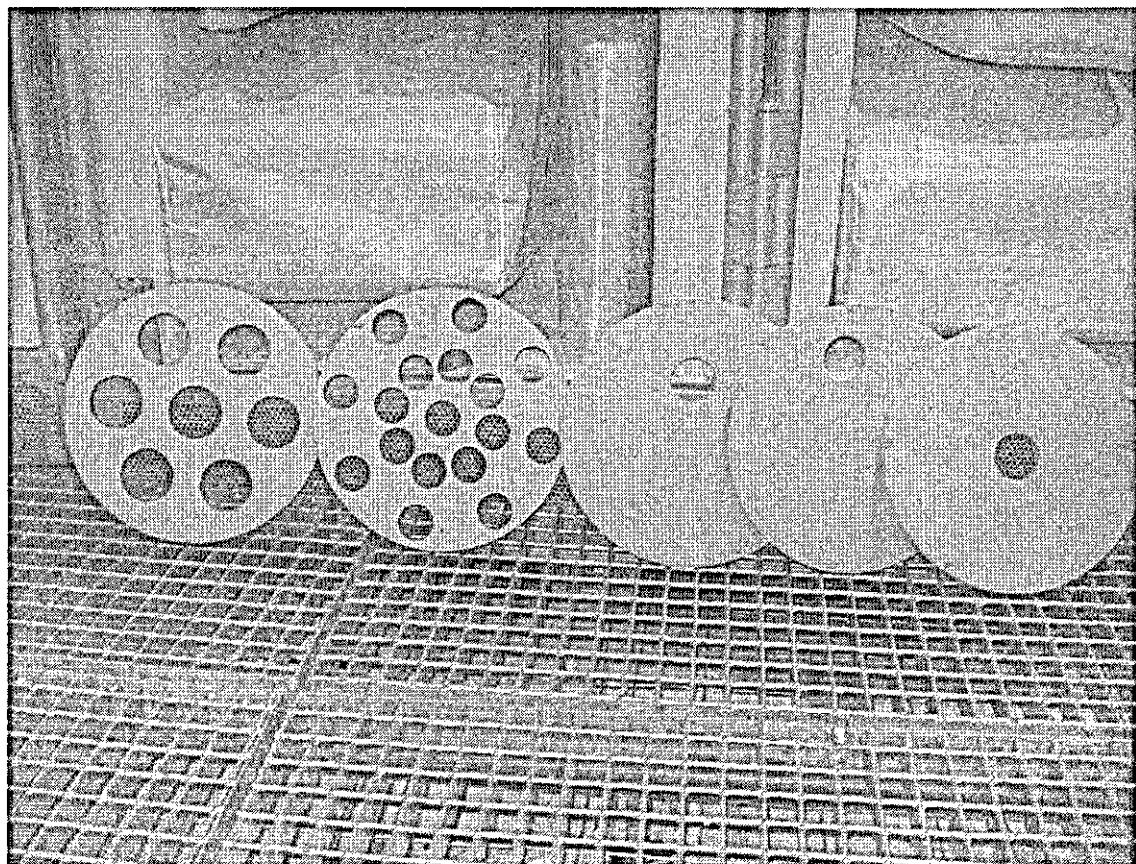


Fig 7.2 Picture of aperture devices used in experimental investigation

According to previous analysis, the acoustic pressure and particle velocity in a circular duct can be written as (for incident wave):

$$P(r, z, \varphi) = \sum_{m=-\infty}^{\infty} \sum_{n=1}^{\infty} J_m(k_{r,m,n} r) e^{jm\varphi} A_{m,n} e^{-jk_{z,m,n} z}, \quad (7.1)$$

$$U_z(r, z, \varphi) = \frac{k_{z,m,n}}{\rho c k} \sum_{m=-\infty}^{\infty} \sum_{n=1}^{\infty} J_m(k_{r,m,n} r) e^{jm\varphi} A_{m,n} e^{-jk_{z,m,n} z}. \quad (7.2)$$

So in Fig 7.1, for region 4, one can write the acoustic pressure as follow, for positive direction travelling wave,

$$P_A = A_{01} e^{-jkz} + \sum_{n=2}^{\infty} A_{0n} J_0(k_{r,0,n} r) e^{-jk_{z,0,n} z} \\ + \sum_{m=1}^{\infty} \sum_{n=1}^{\infty} J_m(k_{r,m,n} r) (A_{mn}^+ e^{-jm\varphi} + A_{mn}^- e^{jm\varphi}) e^{-jk_{z,m,n} z}. \quad (7.3)$$

For negative direction travelling wave,

$$P_B = B_{01} e^{jkz} + \sum_{n=2}^{\infty} B_{0n} J_0(k_{r,0,n} r) e^{jk_{z,0,n} z} \\ + \sum_{m=1}^{\infty} \sum_{n=1}^{\infty} J_m(k_{r,m,n} r) (B_{mn}^+ e^{-jm\varphi} + B_{mn}^- e^{jm\varphi}) e^{jk_{z,m,n} z}. \quad (7.4)$$

For region 3,

$$P_C = C_{01} e^{-jkz} + \sum_{n=2}^{\infty} C_{0n} J_0(k_{r,0,n} r) e^{-jk_{z,0,n} z} \\ + \sum_{m=1}^{\infty} \sum_{n=1}^{\infty} J_m(k_{r,m,n} r) (C_{mn}^+ e^{-jm\varphi} + C_{mn}^- e^{jm\varphi}) e^{-jk_{z,m,n} z}, \quad (7.5)$$

$$P_D = D_{01} e^{jkz} + \sum_{n=2}^{\infty} D_{0n} J_0(k_{r,0,n} r) e^{jk_{z,0,n} z} \\ + \sum_{m=1}^{\infty} \sum_{n=1}^{\infty} J_m(k_{r,m,n} r) (D_{mn}^+ e^{-jm\varphi} + D_{mn}^- e^{jm\varphi}) e^{jk_{z,m,n} z}. \quad (7.6)$$

For region 2,

$$P_E = E_{01} e^{-jkz} + \sum_{n=2}^{\infty} E_{0n} J_0(k_{r,0,n} r) e^{-jk_{z,0,n} z} \\ + \sum_{m=1}^{\infty} \sum_{n=1}^{\infty} J_m(k_{r,m,n} r) (E_{mn}^+ e^{-jm\varphi} + E_{mn}^- e^{jm\varphi}) e^{-jk_{z,m,n} z}, \quad (7.7)$$

$$P_F = F_{01}e^{jkz} + \sum_{n=2}^{\infty} F_{0n} J_0(k_{r,0,n}^{III} r) e^{jk_{z,0,n}^{III} z} + \sum_{m=1}^{\infty} \sum_{n=1}^{\infty} J_m(k_{r,m,n}^{III} r) (F_{mn}^+ e^{-jm\phi} + F_{mn}^- e^{jm\phi}) e^{jk_{z,m,n}^{III} z} \quad (7.8)$$

In which the items with superscript *I* are the values for region 4, the items with superscript *II* are the values for region 3, the items with superscript *III* are the values for region 2.

At boundary 1 (duct end boundary), according to the analysis presented in Chapter 4, from the continuity of the acoustic properties between region 1 and region 2, one can get,

$$F_{mn} = \sum_{L=1}^{\infty} R_{mnL} E_{mL} \quad (7.9)$$

At boundary 2 and boundary 3, the boundary condition continuity can be given as below, At boundary 2, for the continuity of the acoustic pressure, there is:

$$P_C + P_D|_{Z=-L_3} = P_E + P_F|_{Z=-L_3} \quad (\text{over } S_1) \quad (7.10)$$

For the continuity of the particle velocity, there are:

$$U_C + U_D|_{Z=-L_3} = U_E + U_F|_{Z=-L_3} \quad (\text{over } S_1), \quad (7.11)$$

$$U_E + U_F|_{Z=-L_3} = 0 \quad (\text{over } (S-S_1)) \quad (7.12)$$

At boundary 3, for the continuity of the acoustic pressure, there is:

$$P_C + P_D|_{Z=-L_3-L_2} = P_A + P_B|_{Z=-L_3-L_2} \quad (\text{over } S_1) \quad (7.13)$$

For the continuity of the particle velocity, there are:

$$U_C + U_D|_{Z=-L_3-L_2} = U_A + U_B|_{Z=-L_3-L_2} \quad (\text{over } S_1), \quad (7.14)$$

$$U_A + U_B|_{Z=-L_3-L_2} = 0 \quad (\text{over } (S-S_1)) \quad (7.15)$$

In which S_1 is the cross section area of the orifice, S is the cross section area of the main duct, $(S - S_1)$ is the area difference between the main duct and the orifice.

At boundary 2, for the acoustic pressure boundary condition, following the derivation procedure presented in Appendix C, the following equations can be obtained:

For $t = 0, s = 1,$

$$\begin{aligned}
 & (C_{01}e^{jkL_3} + D_{01}e^{-jkL_3})R_1/2 \\
 & = (E_{01}e^{jkL_3} + F_{01}e^{-jkL_3})R_1/2 \\
 & + \sum_{n=2}^{\infty} (E_{0n}e^{jk_{z,0,n}^{III}L_3} + F_{0n}e^{-jk_{z,0,n}^{III}L_3}) \frac{1}{k_{r,0,n}^{III}} J_0(k_{r,0,n}^{III}\delta_1) J_1(k_{r,0,n}^{III}R_1) \\
 & + \sum_{m=1}^{\infty} \sum_{n=1}^{\infty} (((E_{mn}^+ e^{jk_{z,m,n}^{III}L_3} + F_{mn}^+ e^{-jk_{z,m,n}^{III}L_3}) e^{-jm\theta_0} + (E_{mn}^- e^{jk_{z,m,n}^{III}L_3} + F_{mn}^- e^{-jk_{z,m,n}^{III}L_3}) e^{jm\theta_0}) \\
 & \quad \frac{1}{k_{r,m,n}^{III}} J_m(k_{r,m,n}^{III}\delta_1) J_1(k_{r,m,n}^{III}R_1)) .
 \end{aligned} \tag{7.16}$$

For $t = 0, s = 2, 3, \dots, \infty,$

$$\begin{aligned}
 & (C_{0s}e^{jk_{z,0,s}^{II}L_3} + D_{0s}e^{-jk_{z,0,s}^{II}L_3})J_0(k_{r,0,s}^{II}R_1)R_1/2 \\
 & = \sum_{n=2}^{\infty} (E_{0n}e^{jk_{z,0,n}^{III}L_3} + F_{0n}e^{-jk_{z,0,n}^{III}L_3}) \frac{k_{r,0,n}^{III}}{k_{r,0,s}^{II}{}^2 - k_{r,0,n}^{III}{}^2} J_0(k_{r,0,n}^{III}\delta_1) J_0'(k_{r,0,n}^{III}R_1) \\
 & + \sum_{m=1}^{\infty} \sum_{n=1}^{\infty} (((E_{mn}^+ e^{jk_{z,m,n}^{III}L_3} + F_{mn}^+ e^{-jk_{z,m,n}^{III}L_3}) e^{-jm\theta_0} + (E_{mn}^- e^{jk_{z,m,n}^{III}L_3} + F_{mn}^- e^{-jk_{z,m,n}^{III}L_3}) e^{jm\theta_0}) \\
 & \quad \frac{k_{r,m,n}^{III}}{k_{r,0,s}^{II}{}^2 - k_{r,m,n}^{III}{}^2} J_m(k_{r,m,n}^{III}\delta_1) J_0'(k_{r,m,n}^{III}R_1)) .
 \end{aligned} \tag{7.17}$$

For $t = 1, 2, \dots, \infty, s = 1, 2, \dots, \infty,$

$$\begin{aligned}
 & (C_{ts}^- e^{jk_{z,t,s}^{II}L_3} + D_{ts}^- e^{-jk_{z,t,s}^{II}L_3}) \left(1 - \frac{t^2}{k_{r,t,s}^{II}{}^2 R_1^2}\right) J_t(k_{r,t,s}^{II}R_1) R_1/2 \\
 & = \sum_{n=2}^{\infty} (E_{0n}e^{jk_{z,0,n}^{III}L_3} + F_{0n}e^{-jk_{z,0,n}^{III}L_3}) J_t(k_{r,0,n}^{III}\delta_1) \left(\frac{k_{r,0,n}^{III}}{k_{r,t,s}^{II}{}^2 - k_{r,0,n}^{III}{}^2}\right) J_t'(k_{r,0,n}^{III}R_1) \\
 & + \sum_{m=1}^{\infty} \sum_{n=1}^{\infty} ((E_{mn}^+ e^{jk_{z,m,n}^{III}L_3} + F_{mn}^+ e^{-jk_{z,m,n}^{III}L_3}) (-1)^t J_{m-t}(k_{r,m,n}^{III}\delta_1) e^{-jm\theta_0} \\
 & \quad + (E_{mn}^- e^{jk_{z,m,n}^{III}L_3} + F_{mn}^- e^{-jk_{z,m,n}^{III}L_3}) J_{m+t}(k_{r,m,n}^{III}\delta_1) e^{jm\theta_0}) \\
 & \quad \left(\frac{k_{r,m,n}^{III}}{k_{r,t,s}^{II}{}^2 - k_{r,m,n}^{III}{}^2}\right) J_t'(k_{r,m,n}^{III}R_1)) .
 \end{aligned} \tag{7.18}$$

And

$$\begin{aligned}
 & (C_{ts}^+ e^{jk_{z,t,s}^{\text{II}} L_3} + D_{ts}^+ e^{-jk_{z,t,s}^{\text{II}} L_3}) \left(1 - \frac{t^2}{k_{r,t,s}^{\text{II}2} R_1^2}\right) J_t(k_{r,t,s}^{\text{II}} R_1) R_1 / 2 \\
 &= \sum_{n=2}^{\infty} (E_{0n} e^{jk_{z,0,n}^{\text{III}} L_3} + F_{0n} e^{-jk_{z,0,n}^{\text{III}} L_3}) J_t(k_{r,0,n}^{\text{III}} \delta_1) \left(\frac{k_{r,0,n}^{\text{III}}}{k_{r,t,s}^{\text{II}2} - k_{r,0,n}^{\text{III}2}}\right) J_t'(k_{r,0,n}^{\text{III}} R_1) \quad (7.19) \\
 &+ \sum_{m=1}^{\infty} \sum_{n=1}^{\infty} \left[(E_{mn}^+ e^{jk_{z,m,n}^{\text{III}} L_3} + F_{mn}^+ e^{-jk_{z,m,n}^{\text{III}} L_3}) J_{m+t}(k_{r,m,n}^{\text{III}} \delta_1) e^{-jm\theta_0} \right. \\
 &\quad \left. + (E_{mn}^- e^{jk_{z,m,n}^{\text{III}} L_3} + F_{mn}^- e^{-jk_{z,m,n}^{\text{III}} L_3}) (-1)^t J_{m-t}(k_{r,m,n}^{\text{III}} \delta_1) e^{jm\theta_0} \right] \\
 &\quad \left(\frac{k_{r,m,n}^{\text{III}}}{k_{r,t,s}^{\text{II}2} - k_{r,m,n}^{\text{III}2}}\right) J_t'(k_{r,m,n}^{\text{III}} R_1) .
 \end{aligned}$$

For the particle velocity boundary condition, following the derivation procedure presented in Appendix D, the following equations can be obtained:

For $t = 0, s = 1,$

$$(C_{01} e^{jkl_3} - D_{01} e^{-jkl_3}) R_1^2 = (E_{01} e^{jkl_3} - F_{01} e^{-jkl_3}) R_0^2. \quad (7.20)$$

For $t = 0, s = 2, 3, \dots, \infty,$

$$\begin{aligned}
 & (C_{01} e^{jkl_3} - D_{01} e^{-jkl_3}) \frac{R_1}{k_{r,0,s}^{\text{III}}} J_0(k_{r,0,s}^{\text{III}} \delta_1) J_1(k_{r,0,s}^{\text{III}} R_1) \\
 &+ \sum_{n=2}^{\infty} \left(\frac{k_{z,0,n}^{\text{II}}}{k}\right) (C_{0n} e^{jk_{z,0,n}^{\text{II}} L_3} - D_{0n} e^{-jk_{z,0,n}^{\text{II}} L_3}) \frac{R_1 k_{r,0,s}^{\text{III}}}{k_{r,0,n}^{\text{II}2} - k_{r,0,s}^{\text{III}2}} \\
 &\quad J_0(k_{r,0,s}^{\text{III}} \delta_1) J_0(k_{r,0,n}^{\text{II}} R_1) J_0'(k_{r,0,s}^{\text{III}} R_1) \\
 &+ \sum_{m=1}^{\infty} \sum_{n=1}^{\infty} \left(\frac{k_{z,m,n}^{\text{II}}}{k}\right) ((C_{mn}^+ e^{jk_{z,m,n}^{\text{II}} L_3} - D_{mn}^+ e^{-jk_{z,m,n}^{\text{II}} L_3}) + (C_{mn}^- e^{jk_{z,m,n}^{\text{II}} L_3} - D_{mn}^- e^{-jk_{z,m,n}^{\text{II}} L_3})) \\
 &\quad \frac{R_1 k_{r,0,s}^{\text{III}}}{k_{r,m,n}^{\text{II}2} - k_{r,0,s}^{\text{III}2}} J_m(k_{r,0,s}^{\text{III}} \delta_1) J_m(k_{r,m,n}^{\text{II}} R_1) J_m'(k_{r,0,s}^{\text{III}} R_1) \\
 &= \frac{k_{z,0,s}^{\text{III}}}{k} (E_{0s} e^{jk_{z,0,s}^{\text{III}} L_3} - F_{0s} e^{-jk_{z,0,s}^{\text{III}} L_3}) \frac{R_0^2}{2} J_0^2(k_{r,0,s}^{\text{III}} R_0) . \quad (7.21)
 \end{aligned}$$

For $t = 1, 2, \dots, \infty, s = 1, 2, \dots, \infty,$

$$\begin{aligned}
 & (C_{01}e^{jkL_3} - D_{01}e^{-jkL_3})e^{-jt\theta_0} J_t(k_{r,t,s}^{III} \delta_1) \frac{R_1}{k_{r,t,s}^{III}} J_1(k_{r,t,s}^{III} R_1) \\
 & + \sum_{n=2}^{\infty} \left(\frac{k_{z,o,n}^{II}}{k} (C_{0n}e^{jk_{z,o,n}^{II}L_3} - D_{0n}e^{-jk_{z,o,n}^{II}L_3})e^{-jt\theta_0} J_t(k_{r,t,s}^{III} \delta_1) \right. \\
 & \quad \left. \frac{R_1 k_{r,t,s}^{III}}{k_{r,o,n}^{II}{}^2 - k_{r,t,s}^{III}{}^2} J_0'(k_{r,t,s}^{III} R_1) J_0(k_{r,o,n}^{II} R_1) \right) \\
 & + \sum_{m=1}^{\infty} \sum_{n=1}^{\infty} \left([(C_{mn}^+ e^{jk_{z,m,n}^{II}L_3} - D_{mn}^+ e^{-jk_{z,m,n}^{II}L_3}) (-1)^m J_{t-m}(k_{r,t,s}^{III} \delta_1) \right. \\
 & \quad \left. + (C_{mn}^- e^{jk_{z,m,n}^{II}L_3} - D_{mn}^- e^{-jk_{z,m,n}^{II}L_3}) J_{m+t}(k_{r,t,s}^{III} \delta_1)] \right. \\
 & \quad \left. \frac{k_{z,m,n}^{II}}{k} \left(\frac{R_1 k_{r,t,s}^{III}}{k_{r,m,n}^{II}{}^2 - k_{r,t,s}^{III}{}^2} \right) J_m'(k_{r,t,s}^{III} R_1) J_m(k_{r,m,n}^{II} R_1) e^{-jt\theta_0} \right) \quad (7.22) \\
 & = \frac{k_{z,t,s}^{III}}{k} (E_{ts}^- e^{jk_{z,t,s}^{III}L_3} - F_{ts}^- e^{-jk_{z,t,s}^{III}L_3}) \frac{R_0^2}{2} \left(1 - \frac{t^2}{k_{r,t,s}^{III}{}^2 R_0^2} \right) J_t^2(k_{r,t,s}^{III} R_0) .
 \end{aligned}$$

And

$$\begin{aligned}
 & (C_{01}e^{jkL_3} - D_{01}e^{-jkL_3})e^{jt\theta_0} J_t(k_{r,t,s}^{III} \delta_1) \frac{R_1}{k_{r,t,s}^{III}} J_1(k_{r,t,s}^{III} R_1) \\
 & + \sum_{n=2}^{\infty} \left(\frac{k_{z,o,n}^{II}}{k} (C_{0n}e^{jk_{z,o,n}^{II}L_3} - D_{0n}e^{-jk_{z,o,n}^{II}L_3})e^{jt\theta_0} J_t(k_{r,t,s}^{III} \delta_1) \right. \\
 & \quad \left. \frac{R_1 k_{r,t,s}^{III}}{k_{r,o,n}^{II}{}^2 - k_{r,t,s}^{III}{}^2} J_0'(k_{r,t,s}^{III} R_1) J_0(k_{r,o,n}^{II} R_1) \right) \\
 & + \sum_{m=1}^{\infty} \sum_{n=1}^{\infty} \left([(C_{mn}^+ e^{jk_{z,m,n}^{II}L_3} - D_{mn}^+ e^{-jk_{z,m,n}^{II}L_3}) J_{m+t}(k_{r,t,s}^{III} \delta_1) \right. \\
 & \quad \left. + (C_{mn}^- e^{jk_{z,m,n}^{II}L_3} - D_{mn}^- e^{-jk_{z,m,n}^{II}L_3}) (-1)^m J_{t-m}(k_{r,t,s}^{III} \delta_1)] \right. \\
 & \quad \left. \frac{k_{z,m,n}^{II}}{k} \left(\frac{R_1 k_{r,t,s}^{III}}{k_{r,m,n}^{II}{}^2 - k_{r,t,s}^{III}{}^2} \right) J_m'(k_{r,t,s}^{III} R_1) J_m(k_{r,m,n}^{II} R_1) e^{jt\theta_0} \right) \quad (7.23) \\
 & = \frac{k_{z,t,s}^{III}}{k} (E_{ts}^+ e^{jk_{z,t,s}^{III}L_3} - F_{ts}^+ e^{-jk_{z,t,s}^{III}L_3}) \frac{R_0^2}{2} \left(1 - \frac{t^2}{k_{r,t,s}^{III}{}^2 R_0^2} \right) J_t^2(k_{r,t,s}^{III} R_0) .
 \end{aligned}$$

At boundary 3, for the acoustic pressure boundary condition, following the derivation procedure presented in Appendix C, the following equations can be obtained.

For $t = 0, s = 1$,

$$\begin{aligned}
 & (C_{01}e^{jk(L_3+L_2)} + D_{01}e^{-jk(L_3+L_2)})R_1/2 \\
 & = (A_{01}e^{jk(L_3+L_2)} + B_{01}e^{-jk(L_3+L_2)})R_1/2 \\
 & + \sum_{n=2}^{\infty} (A_{0n}e^{jk_{z,0,n}^I(L_3+L_2)} + B_{0n}e^{-jk_{z,0,n}^I(L_3+L_2)}) \frac{1}{k_{r,0,n}^I} J_0(k_{r,0,n}^I \delta_1) J_1(k_{r,0,n}^I R_1) \\
 & + \sum_{m=1}^{\infty} \sum_{n=1}^{\infty} ((A_{mn}^+ e^{jk_{z,m,n}^I L_3} + B_{mn}^+ e^{-jk_{z,m,n}^I L_3}) e^{-jm\theta_0} + (A_{mn}^- e^{jk_{z,m,n}^I L_3} + B_{mn}^- e^{-jk_{z,m,n}^I L_3}) e^{jm\theta_0}) \\
 & \quad \frac{1}{k_{r,m,n}^I} J_m(k_{r,m,n}^I \delta_1) J_1(k_{r,m,n}^I R_1) .
 \end{aligned} \tag{7.24}$$

For $t = 0, s = 2, 3, \dots, \infty$,

$$\begin{aligned}
 & (C_{0s}e^{jk_{z,0,s}^H(L_3+L_2)} + D_{0s}e^{-jk_{z,0,s}^H(L_3+L_2)})J_0(k_{r,0,s}^H R_1)R_1/2 \\
 & = \sum_{n=2}^{\infty} (A_{0n}e^{jk_{z,0,n}^I(L_3+L_2)} + B_{0n}e^{-jk_{z,0,n}^I(L_3+L_2)}) \frac{k_{r,0,n}^I}{k_{r,0,s}^H - k_{r,0,n}^I} J_0(k_{r,0,n}^I \delta_1) J_0'(k_{r,0,n}^I R_1) \\
 & + \sum_{m=1}^{\infty} \sum_{n=1}^{\infty} (((A_{mn}^+ e^{jk_{z,m,n}^I L_3} + B_{mn}^+ e^{-jk_{z,m,n}^I L_3}) e^{-jm\theta_0} + (A_{mn}^- e^{jk_{z,m,n}^I L_3} + B_{mn}^- e^{-jk_{z,m,n}^I L_3}) e^{jm\theta_0}) \\
 & \quad \frac{k_{r,m,n}^I}{k_{r,0,s}^H - k_{r,m,n}^I} J_m(k_{r,m,n}^I \delta_1) J_m'(k_{r,m,n}^I R_1)) .
 \end{aligned} \tag{7.25}$$

For $t = 1, 2, \dots, \infty, s = 1, 2, \dots, \infty$,

$$\begin{aligned}
 & (C_{ts}^- e^{jk_{z,t,s}^H(L_3+L_2)} + D_{ts}^- e^{-jk_{z,t,s}^H(L_3+L_2)}) \left(1 - \frac{t^2}{k_{r,t,s}^H R_1^2}\right) J_t(k_{r,t,s}^H R_1) R_1/2 \\
 & = \sum_{n=2}^{\infty} ((A_{0n}e^{jk_{z,0,n}^I(L_3+L_2)} + B_{0n}e^{-jk_{z,0,n}^I(L_3+L_2)}) \\
 & \quad J_t(k_{r,0,n}^I \delta_1) \left(\frac{k_{r,0,n}^I}{k_{r,t,s}^H - k_{r,0,n}^I}\right) J_t'(k_{r,0,n}^I R_1)) \\
 & + \sum_{m=1}^{\infty} \sum_{n=1}^{\infty} ((A_{mn}^+ e^{jk_{z,m,n}^I(L_3+L_2)} + B_{mn}^+ e^{-jk_{z,m,n}^I(L_3+L_2)}) (-1)^t J_{m-t}(k_{r,m,n}^I \delta_1) e^{-jm\theta_0} \\
 & \quad + (A_{mn}^- e^{jk_{z,m,n}^I(L_3+L_2)} + B_{mn}^- e^{-jk_{z,m,n}^I(L_3+L_2)}) J_{m+t}(k_{r,m,n}^I \delta_1) e^{jm\theta_0}) \\
 & \quad \left(\frac{k_{r,m,n}^I}{k_{r,t,s}^H - k_{r,m,n}^I}\right) J_t'(k_{r,m,n}^I R_1)) .
 \end{aligned} \tag{7.26}$$

And

$$\begin{aligned}
 & (C_{ts}^+ e^{jk_{z,t,s}^H(L_3+L_2)} + D_{ts}^+ e^{-jk_{z,t,s}^H(L_3+L_2)}) \left(1 - \frac{t^2}{k_{r,t,s}^{H^2} R_1^2}\right) J_t(k_{r,t,s}^H R_1) R_1 / 2 \\
 &= \sum_{n=2}^{\infty} ((A_{0n} e^{jk_{z,0,n}^I(L_3+L_2)} + B_{0n} e^{-jk_{z,0,n}^I(L_3+L_2)}) \\
 & \quad J_t(k_{r,0,n}^I \delta_1) \left(\frac{k_{r,0,n}^I}{k_{r,t,s}^{H^2} - k_{r,0,n}^I}\right) J_t'(k_{r,0,n}^I R_1)) \\
 & \quad + \sum_{m=1}^{\infty} \sum_{n=1}^{\infty} ((A_{mn}^+ e^{jk_{z,m,n}^I(L_3+L_2)} + B_{mn}^+ e^{-jk_{z,m,n}^I(L_3+L_2)}) J_{m+1}(k_{r,m,n}^I \delta_1) e^{-jm\theta_0} \\
 & \quad + (A_{mn}^- e^{jk_{z,m,n}^I(L_3+L_2)} + B_{mn}^- e^{-jk_{z,m,n}^I(L_3+L_2)}) (-1)^t J_{m-t}(k_{r,m,n}^I \delta_1) e^{jm\theta_0}] \\
 & \quad \left(\frac{k_{r,m,n}^I}{k_{r,t,s}^{H^2} - k_{r,m,n}^I}\right) J_t'(k_{r,m,n}^I R_1)) .
 \end{aligned} \tag{7.27}$$

For the particle velocity boundary condition, following the derivation procedure presented in Appendix D, the following equations can be obtained:

For $t = 0, s = 1$,

$$(C_{01} e^{jk(L_3+L_2)} - D_{01} e^{-jk(L_3+L_2)}) R_1^2 = (A_{01} e^{jk(L_3+L_2)} - B_{01} e^{-jk(L_3+L_2)}) R_0^2 . \tag{7.28}$$

For $t = 0, s = 2, 3, \dots, \infty$,

$$\begin{aligned}
 & (C_{01} e^{jk(L_3+L_2)} - D_{01} e^{-jk(L_3+L_2)}) \frac{R_1}{k_{r,0,s}^I} J_0(k_{r,0,s}^I \delta_1) J_1(k_{r,0,s}^I R_1) \\
 & + \sum_{n=2}^{\infty} \left(\frac{k_{z,0,n}^{H^2}}{k}\right) (C_{0n} e^{jk_{z,0,n}^{H^2}(L_3+L_2)} - D_{0n} e^{-jk_{z,0,n}^{H^2}(L_3+L_2)}) \\
 & \quad \frac{R_1 k_{r,0,s}^I}{k_{r,0,n}^{H^2} - k_{r,0,s}^I} J_0(k_{r,0,s}^I \delta_1) J_0(k_{r,0,n}^H R_1) J_0'(k_{r,0,s}^I R_1) \\
 & + \sum_{m=1}^{\infty} \sum_{n=1}^{\infty} \left(\frac{k_{z,m,n}^{H^2}}{k}\right) ((C_{mn}^+ e^{jk_{z,m,n}^{H^2}(L_3+L_2)} - D_{mn}^+ e^{-jk_{z,m,n}^{H^2}(L_3+L_2)}) \\
 & \quad + (C_{mn}^- e^{jk_{z,m,n}^{H^2}(L_3+L_2)} - D_{mn}^- e^{-jk_{z,m,n}^{H^2}(L_3+L_2)})) \\
 & \quad \frac{R_1 k_{r,0,s}^I}{k_{r,m,n}^{H^2} - k_{r,0,s}^I} J_m(k_{r,0,s}^I \delta_1) J_m(k_{r,m,n}^H R_1) J_m'(k_{r,0,s}^I R_1)) \\
 & = \frac{k_{z,0,s}^I}{k} (A_{0s} e^{jk_{z,0,s}^I(L_3+L_2)} - B_{0s} e^{-jk_{z,0,s}^I(L_3+L_2)}) \frac{R_0^2}{2} J_0^2(k_{r,0,s}^I R_0) .
 \end{aligned} \tag{7.29}$$

For $t = 1, 2, \dots, \infty, s = 1, 2, \dots, \infty$,

$$\begin{aligned}
 & (C_{01}e^{jk(L_3+L_2)} - D_{01}e^{-jk(L_3+L_2)})e^{-jt\theta_0} J_t(k_{r,t,s}^I \delta_1) \frac{R_1}{k_{r,t,s}^I} J_1(k_{r,t,s}^I R_1) \\
 & + \sum_{n=2}^{\infty} \left(\frac{k_{z,o,n}^{II}}{k} (C_{0n}e^{jk_{z,o,n}^{II}(L_3+L_2)} - D_{0n}e^{-jk_{z,o,n}^{II}(L_3+L_2)}) e^{-jt\theta_0} \right. \\
 & \quad \left. J_t(k_{r,t,s}^I \delta_1) \frac{R_1 k_{r,t,s}^I}{k_{r,o,n}^{II} - k_{r,t,s}^I} J_0'(k_{r,t,s}^I R_1) J_0(k_{r,o,n}^{II} R_1) \right) \\
 & + \sum_{m=1}^{\infty} \sum_{n=1}^{\infty} \left((C_{mn}^+ e^{jk_{z,m,n}^{II}(L_3+L_2)} - D_{mn}^+ e^{-jk_{z,m,n}^{II}(L_3+L_2)}) (-1)^m J_{t-m}(k_{r,t,s}^I \delta_1) \right. \\
 & \quad \left. + (C_{mn}^- e^{jk_{z,m,n}^{II}(L_3+L_2)} - D_{mn}^- e^{-jk_{z,m,n}^{II}(L_3+L_2)}) J_{m+t}(k_{r,t,s}^I \delta_1) \right) \\
 & \quad \frac{k_{z,m,n}^{II}}{k} \left(\frac{R_1 k_{r,t,s}^I}{k_{r,m,n}^{II} - k_{r,t,s}^I} \right) J_m'(k_{r,t,s}^I R_1) J_m(k_{r,m,n}^{II} R_1) e^{-jt\theta_0} \\
 & = \frac{k_{z,t,s}^I}{k} (A_{ts}^+ e^{jk_{z,t,s}^I(L_3+L_2)} - B_{ts}^- e^{-jk_{z,t,s}^I(L_3+L_2)}) \frac{R_0^2}{2} \left(1 - \frac{t^2}{k_{r,t,s}^I{}^2 R_0^2} \right) J_t^2(k_{r,t,s}^I R_0).
 \end{aligned} \tag{7.30}$$

And

$$\begin{aligned}
 & (C_{01}e^{jk(L_3+L_2)} - D_{01}e^{-jk(L_3+L_2)})e^{jt\theta_0} J_t(k_{r,t,s}^I \delta_1) \frac{R_1}{k_{r,t,s}^I} J_1(k_{r,t,s}^I R_1) \\
 & + \sum_{n=2}^{\infty} \left(\frac{k_{z,o,n}^{II}}{k} (C_{0n}e^{jk_{z,o,n}^{II}(L_3+L_2)} - D_{0n}e^{-jk_{z,o,n}^{II}(L_3+L_2)}) e^{jt\theta_0} \right. \\
 & \quad \left. J_t(k_{r,t,s}^I \delta_1) \frac{R_1 k_{r,t,s}^I}{k_{r,o,n}^{II} - k_{r,t,s}^I} J_0'(k_{r,t,s}^I R_1) J_0(k_{r,o,n}^{II} R_1) \right) \\
 & + \sum_{m=1}^{\infty} \sum_{n=1}^{\infty} \left((C_{mn}^+ e^{jk_{z,m,n}^{II}(L_3+L_2)} - D_{mn}^+ e^{-jk_{z,m,n}^{II}(L_3+L_2)}) J_{m+t}(k_{r,t,s}^I \delta_1) \right. \\
 & \quad \left. + (C_{mn}^- e^{jk_{z,m,n}^{II}(L_3+L_2)} - D_{mn}^- e^{-jk_{z,m,n}^{II}(L_3+L_2)}) (-1)^m J_{t-m}(k_{r,t,s}^I \delta_1) \right) \\
 & \quad \frac{k_{z,m,n}^{II}}{k} \left(\frac{R_1 k_{r,t,s}^I}{k_{r,m,n}^{II} - k_{r,t,s}^I} \right) J_m'(k_{r,t,s}^I R_1) J_m(k_{r,m,n}^{II} R_1) e^{jt\theta_0} \\
 & = \frac{k_{z,t,s}^I}{k} (A_{ts}^+ e^{jk_{z,t,s}^I(L_3+L_2)} - B_{ts}^- e^{-jk_{z,t,s}^I(L_3+L_2)}) \frac{R_0^2}{2} \left(1 - \frac{t^2}{k_{r,t,s}^I{}^2 R_0^2} \right) J_t^2(k_{r,t,s}^I R_0).
 \end{aligned} \tag{7.31}$$

Boundary 4 is the boundary between the point source and the main duct, as discussed in Chapter 4, equations (4.28), (4.36), (4.41) and (4.42) have been obtained for this boundary.

So now, a complete description for all these four boundary conditions has been obtained. Combining equation (7.9), equation (7.16) to equation (7.31) with equations (4.28), (4.36), (4.41) and (4.42), an equation group for the solution of the acoustic properties in circular duct with a simple aperture device is given as follow,

$$[X]_{D \times D} \begin{bmatrix} A_{mn} \\ B_{mn} \\ C_{mn} \\ D_{mn} \\ E_{mn} \\ F_{mn} \end{bmatrix}_{D \times 1} = \begin{bmatrix} U \\ 0 \end{bmatrix}_{D \times 1}, \quad (7.32)$$

in which X is the coefficient matrix for these amplitudes. Its dimension D is decided by how many higher-order modes are considered in both the main duct region and the orifice region. For example, in this research project, as discussed before, 17 modes are cut on in the main duct region at the frequency range that of interest. The mode with highest m value is $(\pm 5, 1)$ mode; the mode with highest n value is $(0, 3)$ mode. For the orifice region, the number of the modes cut on is dependent on the radius of the orifice. But the radius of the orifice can only be smaller or equal to the radius of the main duct. So at frequency range $0-2600 \text{ Hz}$, there are at most 17 modes cut on in the orifice region. Thus $m = \pm 5$ and $n = 5$ should be sufficient for the calculation.

If $m = \pm 5$ and $n = 5$, the dimension of the matrix X should be 330×330 ($3 \times (2 \times n + 4 \times |m| \times n)$). That means compared with the matrix appeared in Chapters 5 and 6 for duct without an aperture device, matrix X is a significantly larger one. So in order to keep this matrix well conditioned, the method used in the former two chapters to solve the singularity problem of the matrix will be also adopted here. By only considering those higher-order modes which have been cut on in both the main duct region and the orifice region, one can make sure that the powers of the exponential items $e^{jk_{x,m,n}L}$ appeared in matrix X will be always complex numbers rather than real numbers. So for the matrix X , at this situation its dimension D is not a constant one, it is dependent on the numbers of cut on modes and increases with the increasing frequency.

After treating the matrix X in the manner described above, one can just multiply both sides of the equation (7.32) with the inversion of the matrix X , then the solution for this

equation group is obtained which give the amplitudes, such as A_{mn} , B_{mn} , C_{mn} , D_{mn} , E_{mn} and F_{mn} (the detailed procedure is given in Appendix E).

7.2.2 Experimental set-up and measurement results

According to the theoretical derivation described above, it can be seen that there is no limitation or requirement for the thickness of the aperture devices and the radius of the orifice. However if the thickness of the device is too small, then the descriptions for boundaries 2 and 3 are so similar that the matrix X approaches singularity. Also in engineering situations, the thickness of the aperture device is normally not very large compared to wavelength. So in this investigation, the thickness of the aperture device is taken as $L = 0.025m$ which gives a range of $k * L$ values from 0 to 1.2. As shown in Fig 7.2, two different orifice radii are selected, which are $r = 0.03m$ (open area is 4% of total area) and $r = 0.02m$ (open area is 1.7% of total area) respectively. Through the selection of different numbers of orifices, one can get different open areas.

The experimental set-up is shown in Fig 7.3. It is quite similar to the experimental set-up adopted in Chapter 5. The aperture device is placed in $z = -0.4m$ (-13.3% L). Two rings of measurement points, located at $z = -0.54m$ (-18% L) and $z = -0.18m$ (-6% L) respectively, are taken for appointed position measurements (direct measurements) in the before orifice field and the after orifice field. Two reference measurement positions, located at $(0.15m(100\%R), 0, -2.33m(-74.3\%L))$ and $(0.15m(100\%R), 3 * \pi / 4, -1.5m(-50\%L))$, are taken for the reference measurement in the before orifice field.

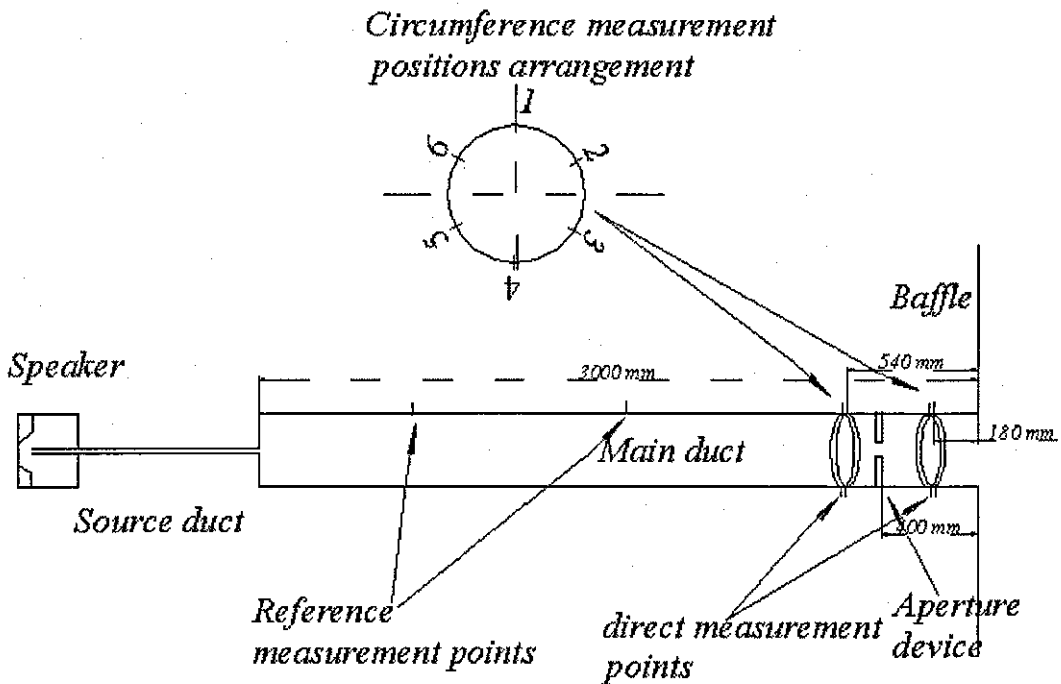


Fig 7.3 Experimental set-up for acoustic properties measurement before and after aperture device

In order to show the effects of the aperture device on the acoustic properties in the circular duct, two situations, which are the sound source is concentric and eccentric to the main duct respectively, are selected and the acoustic pressures measured at positions before and after orifice are shown in Fig 7.4.

Fig7.4 a) and b) show the acoustic pressures when the sound source is concentric to the main duct. In which, 'without aperture device' means there is no aperture device in the duct; 'with aperture device' means there is a device with a single orifice which is also concentric to the main duct (Situation 1 in Fig 7.6) in duct. Fig7.4 c) and d) show the acoustic pressures when the sound source is eccentric to the main duct ($\delta = 0.06m(40\% R_0)$). Again in which, 'without aperture device' means there is no aperture device in the duct; 'with aperture device' means there is a device with a single orifice which is also eccentric to the main duct (Situation 4 in Fig 7.6) in the duct.

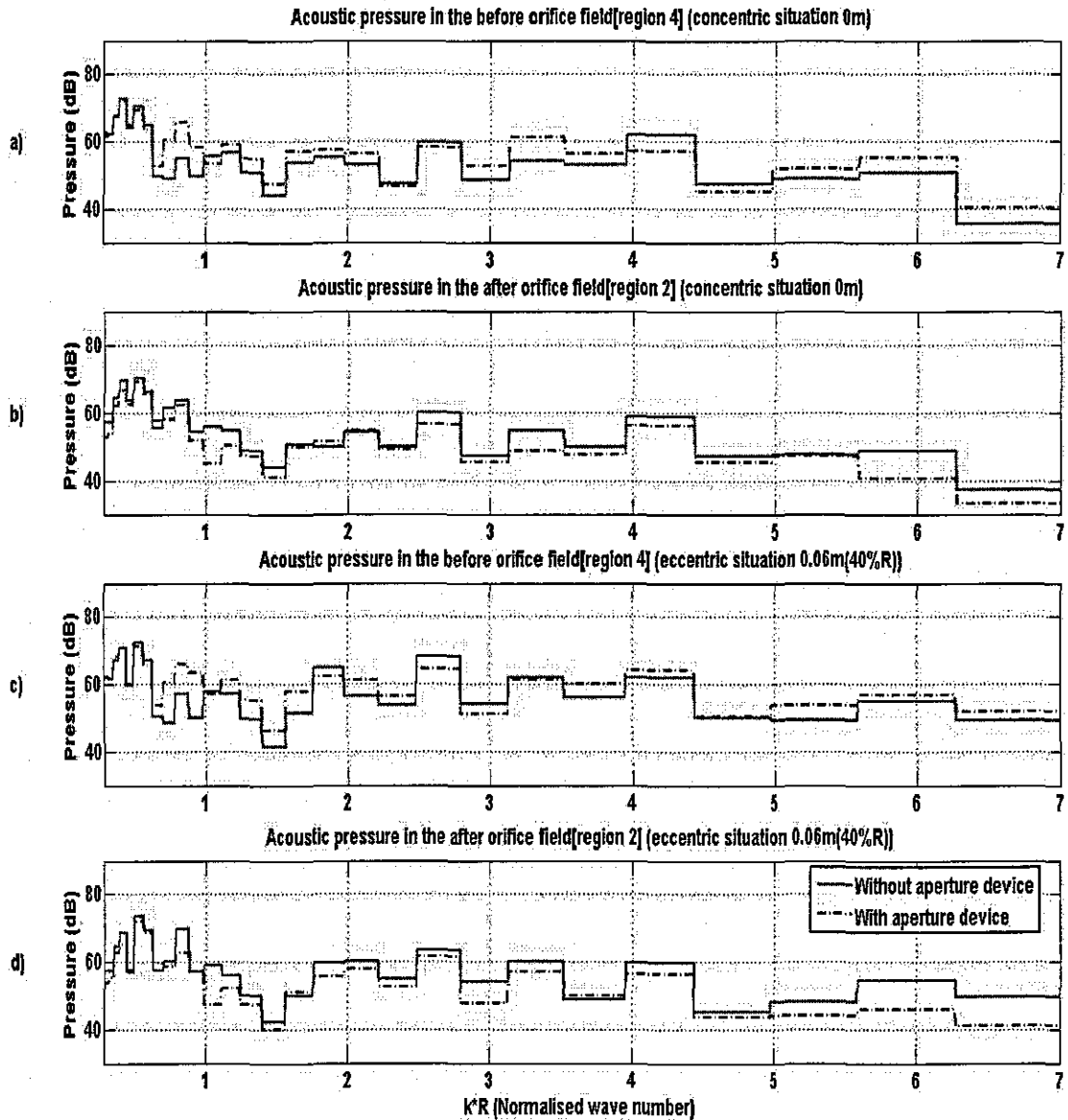


Fig 7.4 Comparison of the acoustic pressures measured at different positions for without aperture device and with aperture device situations

From this figure, it can be seen that at the very low normalized wave number range ($k \cdot R < 0.8$), there is nearly no difference between these two situations. Which means the presence of the aperture device does not affect the acoustic pressures both before and after the aperture device in this normalized wave number range. In this situation, the device thickness is small compared to wavelength. However if the normalised wave number is larger than 0.8, there are some differences between these two situations, which means the presence of the aperture device has an effect on the acoustic properties in the circular duct. Compared with its effects on acoustic field in the region before

aperture device, its effects on acoustic field in the region after the aperture device are larger, especially for higher normalised wave number range ($k * R > 5$).

In following sections, the effects of the aperture device on acoustic field are studied in detail.

7.2.3 Comparison of coupled and uncoupled predictions

In Chapter 5, for a duct without an aperture device, it is concluded that at the open end of the duct, the cross coupling effects between higher-order modes can be neglected. So in this section, these cross coupling effects are reconsidered when there is an aperture device in the duct.

Several combinations of the comparative source-orifice relationships, such as, concentric-concentric, concentric-eccentric, eccentric-concentric and eccentric-eccentric, are considered. The results are similar and only one comparative source-orifice relationship, which is eccentric-eccentric (Situation 5 in Fig 7.6), is chosen and the results are shown in Fig 7.5. Fig 7.5 a) shows coupled prediction, uncoupled prediction and direct measurements for the before orifice field; Fig 7.5 b) shows coupled prediction, uncoupled prediction and direct measurements for the after orifice field; Fig 7.5 c) shows the difference between coupled and uncoupled predictions both for the before orifice field and the after orifice field.

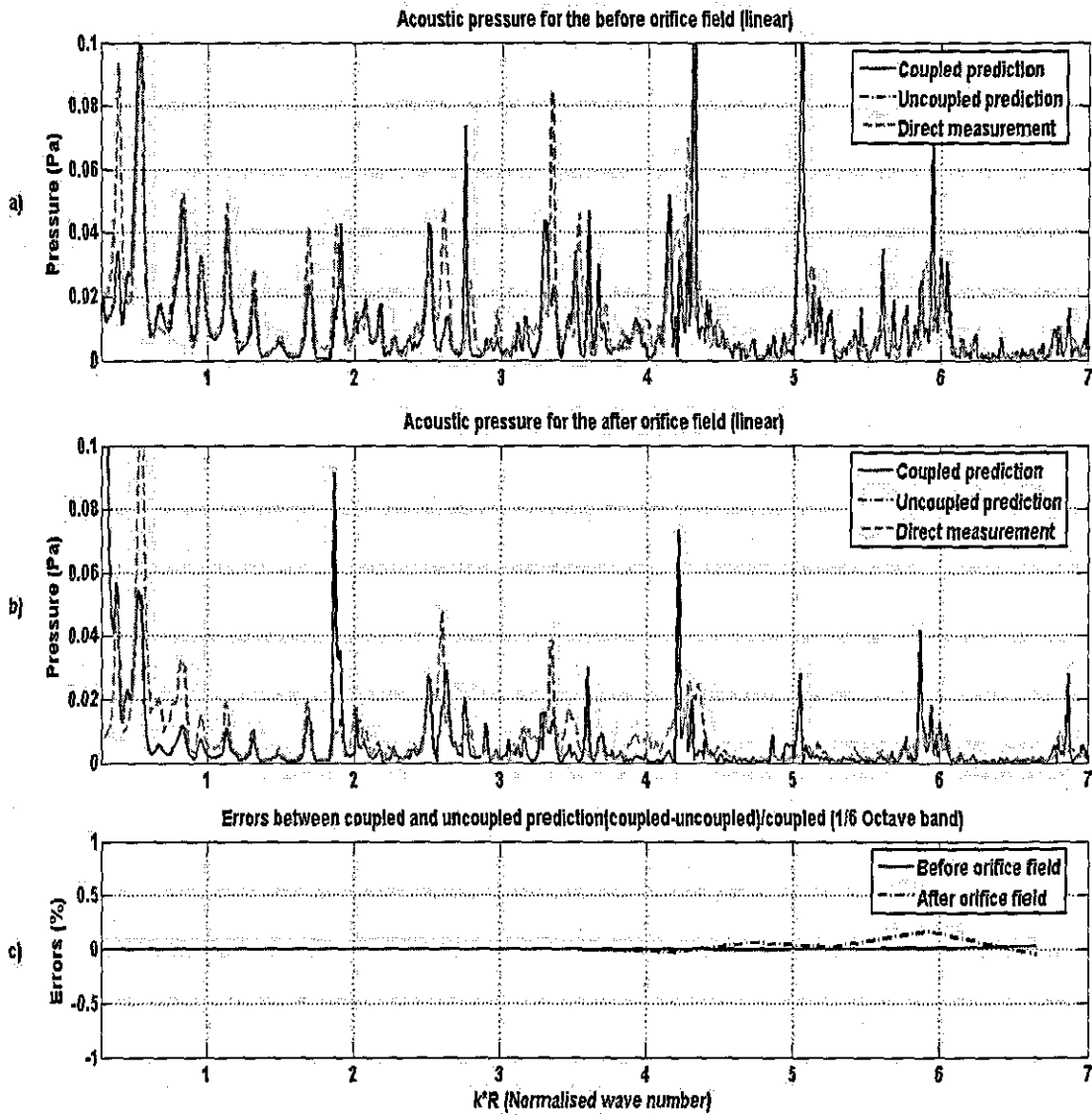


Fig 7.5 Comparison of coupled, uncoupled prediction with direct measurements for the before orifice field and the after orifice field

From this aperture it can be seen that for the after orifice field, there is a little difference between coupled and uncoupled predictions when the normalised wave number is larger than 4. However this difference is so small (less than 0.5%) that it can be neglected. For the before orifice field, there is no difference for coupled and uncoupled predictions, which means that the cross coupling effects shown in equation (3.57) between those higher-order modes at the open end of the duct is negligible. So in following analysis, these cross coupling effects are not considered and it is assumed at the end of the duct, no cross coupling effects occur.

7.2.4 Comparison of predictions with direct measurements for a device with single orifice

For an aperture device with a single orifice, six comparative source-orifice relationships (shown in Fig 7.6), which are concentric-concentric, concentric-eccentric, eccentric-concentric, eccentric-eccentric (three different situations), are considered.

For all situations shown below, the acoustic pressure plotted for the before aperture field is taken at the point with coordinate $(0.15m, \pi/3, -0.54m)$, which is $(100\%R, \pi/3, -18\%L)$ in non-dimensional form; acoustic pressure plotted for the after aperture field is taken at the point with coordinate $(0.15m, \pi/3, -0.18m)$, which is $(100\%R, \pi/3, -6\%L)$ in non-dimensional form.

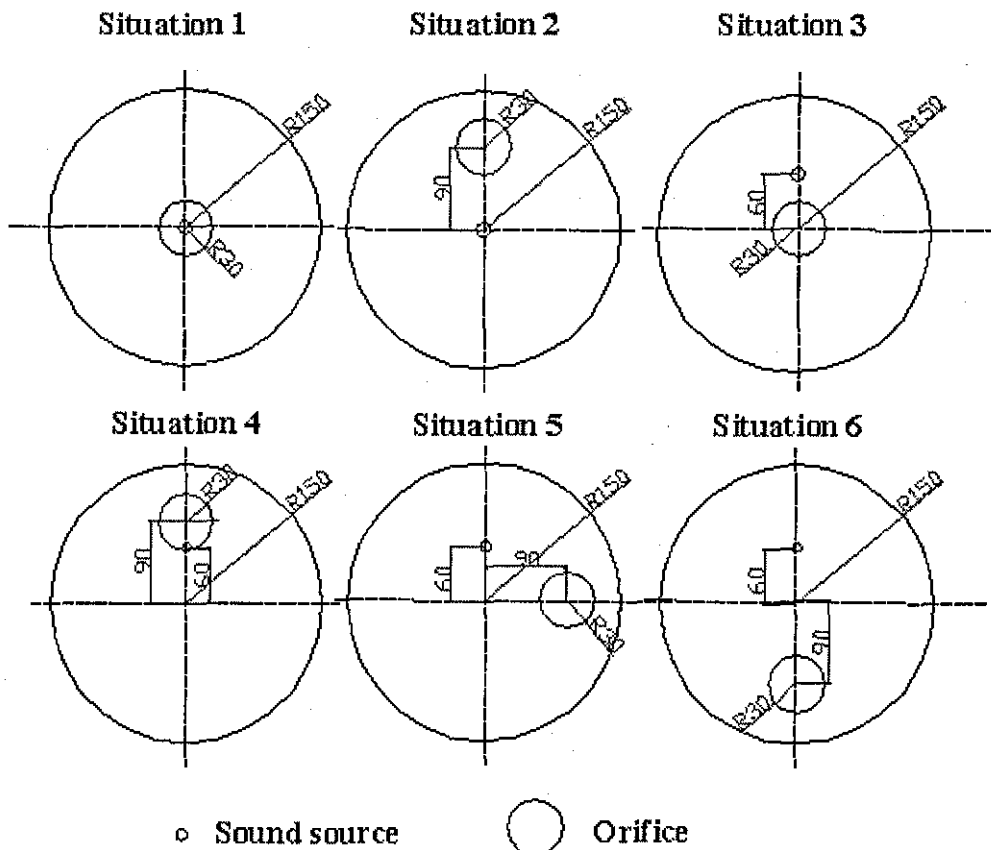


Fig 7.6 Comparative source-orifice relationships for device with single orifice

Not all situations shown in Fig 7.6 are displayed, because the results for some situations are quite similar. So four situations are selected and shown below. In each figure, *a*) shows the acoustic pressure for the before orifice field; *b*) shows the acoustic pressure for the after orifice field; *c*) shows the errors between predictions and direct measurements for both the before orifice field and the after orifice field. In order to show these errors clearly, the results are transferred into 1/6 octave band. Fig 7.7 shows the concentric-concentric situation (Situation 1 in Fig 7.6).

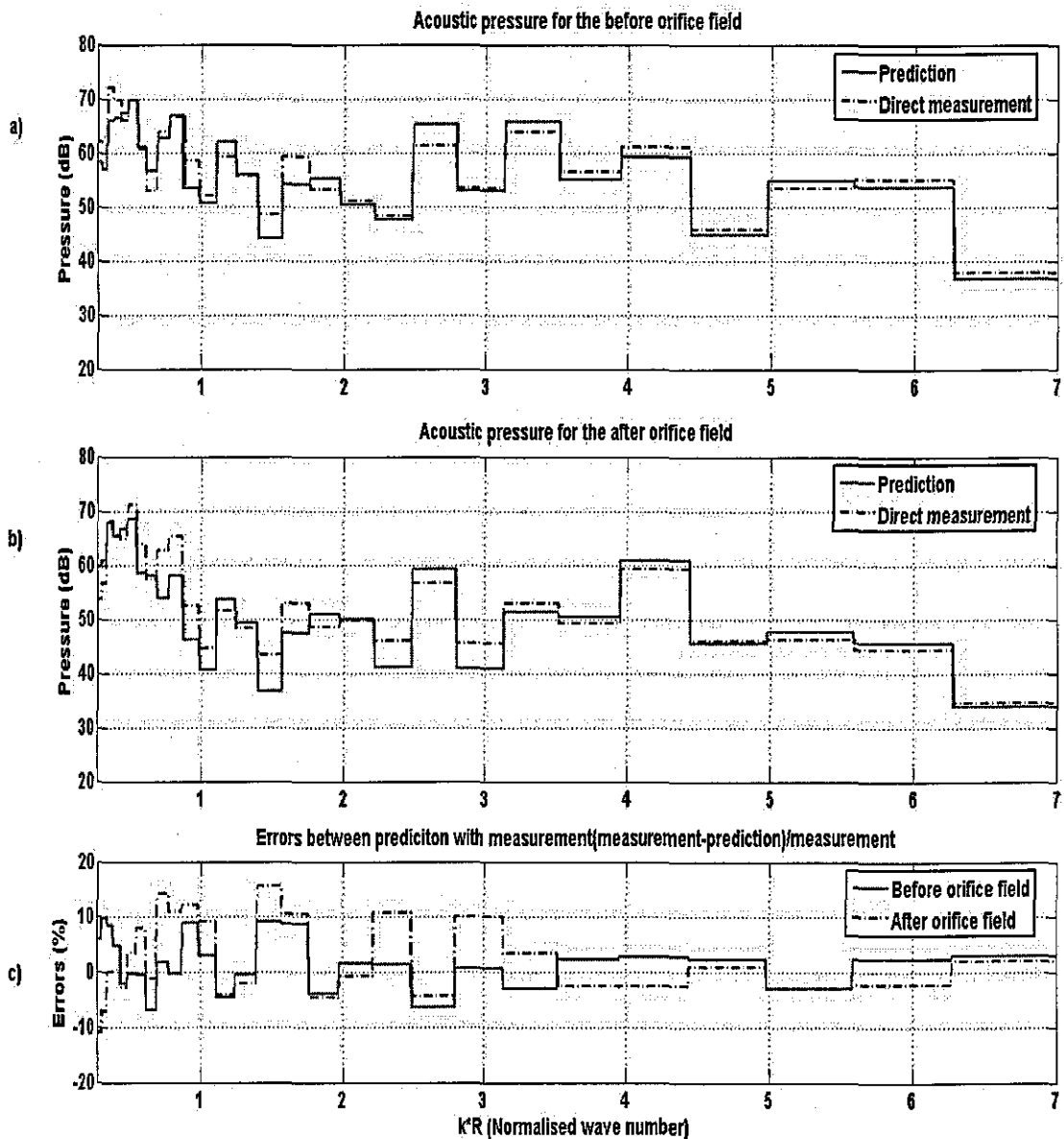


Fig 7.7 Comparison of the acoustic pressure for both the before orifice field and the after orifice field for device with single orifice (Situation 1 in Fig 7.6)

Fig 7.8 shows the concentric–eccentric situation (Situation 2 in Fig 7.6).

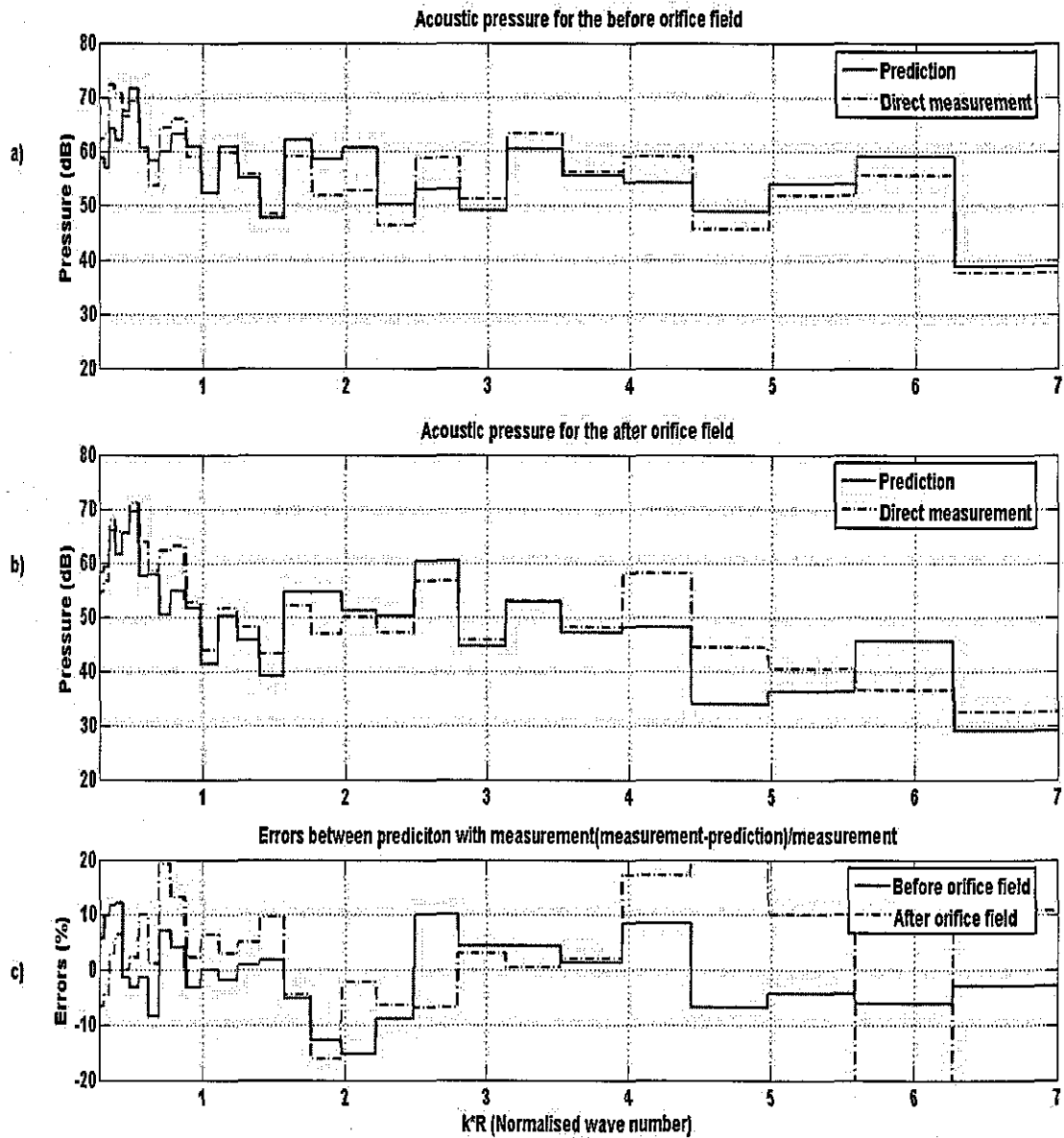


Fig 7.8 Comparison of the acoustic pressure for both the before orifice field and the after orifice field for device with single orifice (Situation 2 in Fig 7.6)

Fig 7.9 shows the eccentric–eccentric situation (Situation 6 in Fig 7.6), for this one it can represent other similar situations, such as Situation 4 and situation 5 in Fig 7.6.

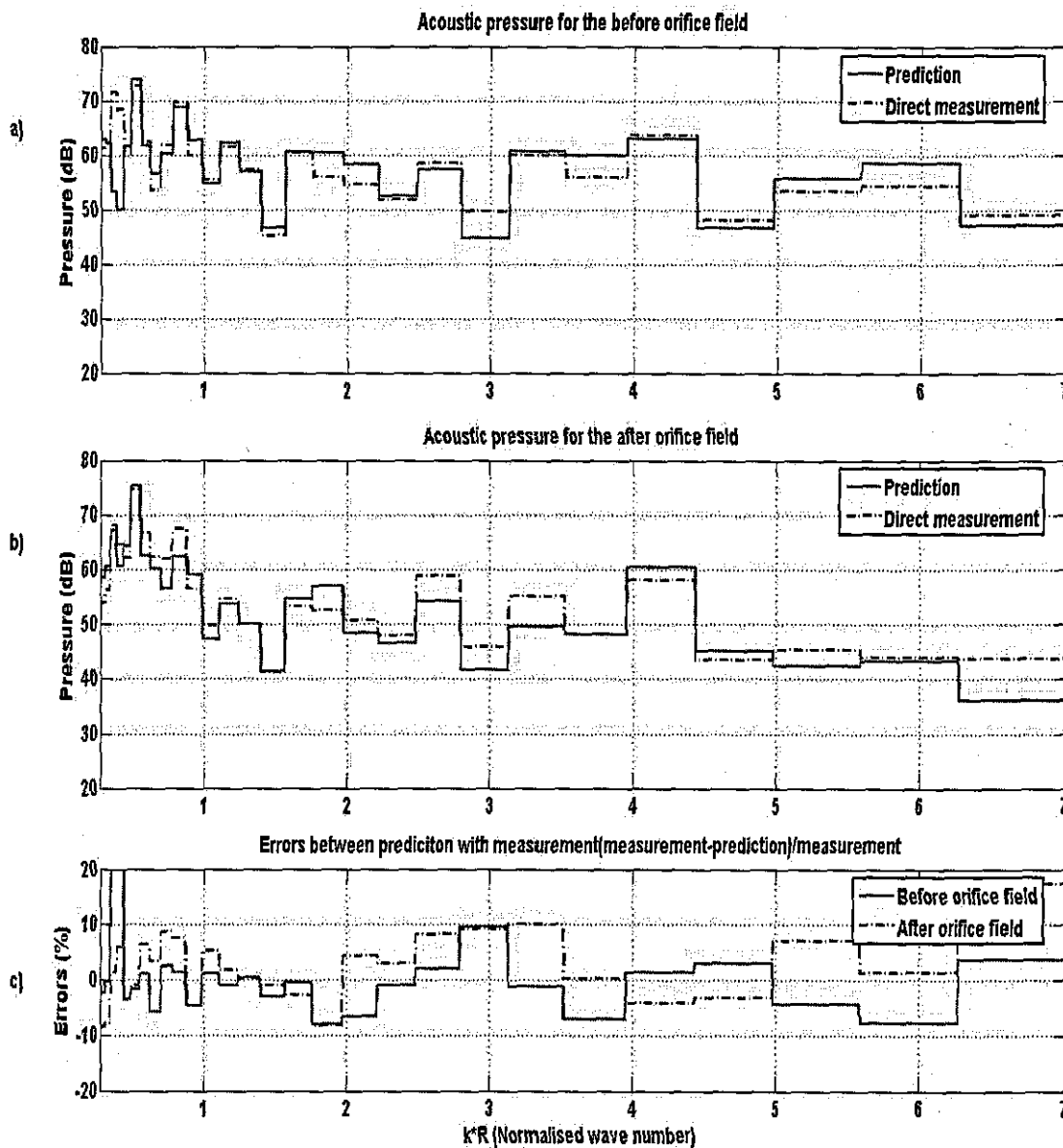


Fig 7.9 Comparison of the acoustic pressure for both the before orifice field and the after orifice field for device with single orifice (Situation 6 in Fig 7.6)

Fig 7.10 shows the eccentric-concentric situation (Situation 3 in Fig 7.6).

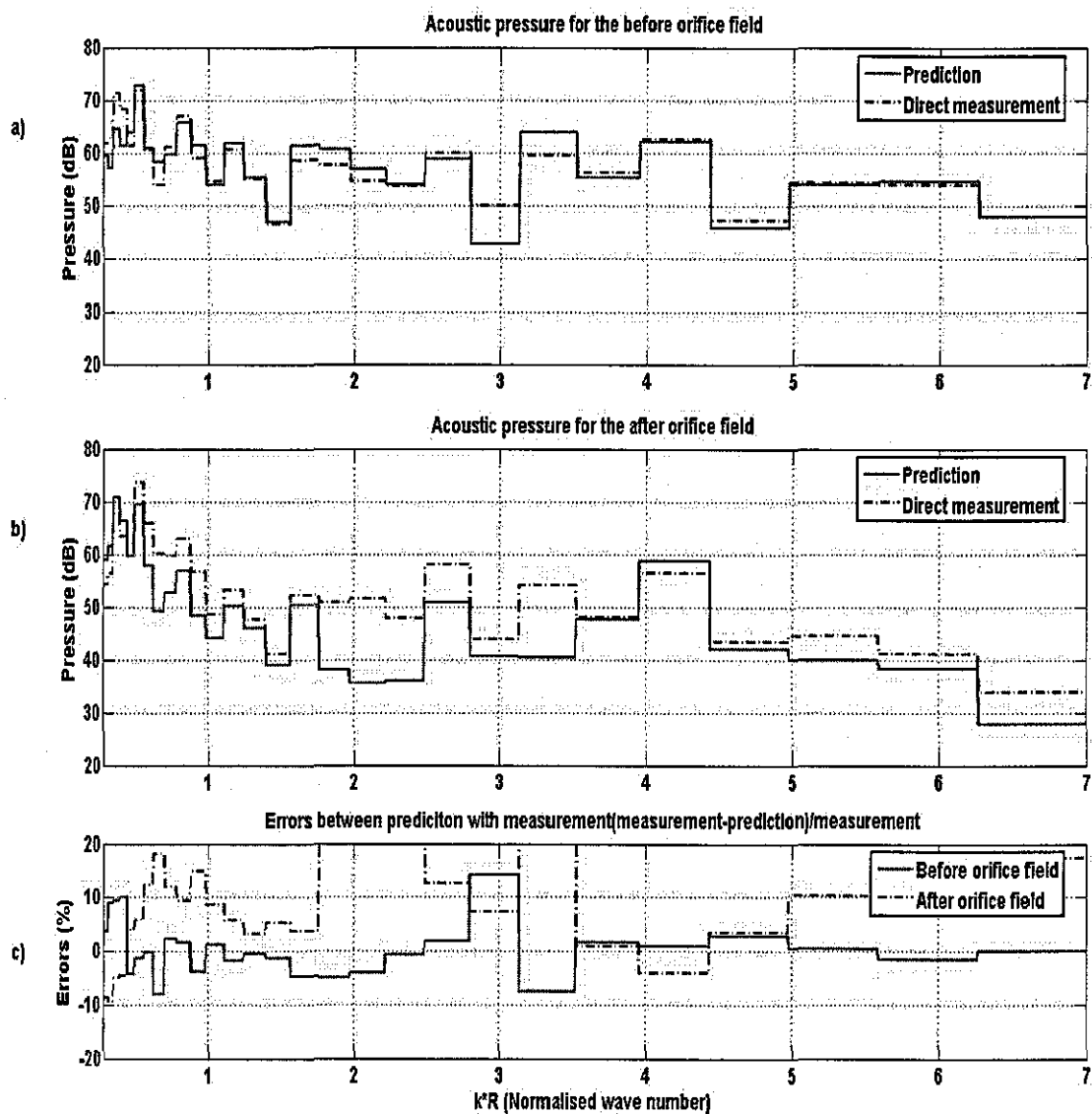


Fig 7.10 Comparison of the acoustic pressure for both the before orifice field and the after orifice field for device with single orifice (Situation 3 in Fig 7.6)

From Fig 7.7 – 7.10, it can be seen that:

1. For the concentric-concentric situation (shown in Fig 7.7), most errors for both the before orifice field and the after orifice field are less than 10% of the direct measurements. At the higher normalized wave number range ($k^*R > 3.5$), these errors are less than 5% of the direct measurements. Also the errors for the after orifice field are a little larger than the before orifice field.

2. For the eccentric-eccentric situation, there are three different configurations for source-orifice relationship. The results are very similar and only one situation is chosen and shown in Fig 7.9. From this one, it can be seen that other than very low normalized wave number range ($k * R < 0.8$), predictions for both the before orifice field and the after orifice field agree well with direct measurements.
3. For the concentric-eccentric situation (shown in Fig 7.8), the predictions for the after orifice field do not agree with the direct measurements. From this figure, it is easy to see that the errors between prediction and direct measurement are largest after the (0, 2) mode cuts on ($k * R = 3.05$). Also the (0, 2) mode dominates in the direct measurement but does not dominate in the prediction. For the after orifice field, it can be treated as one short duct with the plane wave source situation. According to the discussion in Chapter 6, when the plane wave source is eccentric to the main duct, those axially-symmetric higher-order modes, such as (0, 2) mode, should not be dominant in duct. However, for this situation, the (0, 2) mode dominates in the duct, which is in contradiction to the conclusion drawn from Chapter 6. So there is only one explanation for the (0, 2) mode domination in this field, which is that this (0, 2) mode is from the before orifice field. Because the wooden aperture device used is not a perfectly rigid one, so the plate can radiate this (0, 2) mode to the after orifice field; also there are always some gaps between the plate and the wall of the duct, so this (0, 2) mode can also propagate through these gaps to the after orifice field. So this axially-symmetric higher-order mode appears and dominates in the after orifice device. For this situation, *this method cannot be used directly to predict the after orifice field.*
4. For the eccentric-concentric situation (shown in Fig 7.10), the predictions for the after orifice field do not agree with the direct measurements, especially in frequency range $1.8 < k * R < 3.5$. In this frequency range, four axially-unsymmetric higher-order modes, which are ($\pm 1, 1$) modes and ($\pm 2, 1$) modes, cut on in the main duct. For the before orifice field, because the sound source is eccentric to the main duct, so these axially-unsymmetric higher-order modes are dominant and prediction agrees with direct measurement. However for the after orifice field, as discussed in former paragraph, it can be treated as one short duct with the plane wave source (discussed in Chapter 6). If the source is concentric

to the main duct, then the in-duct field should be dominant with those axially-symmetric higher-order modes. However from Fig 7.10, one can see that for the after orifice field, those axially-unsymmetric higher-order modes, $(\pm 1,1)$ modes and $(\pm 2,1)$ modes, dominate in that frequency range, which is contradicted with conclusion drawn in Chapter 6. Again the only explanation for $(\pm 1,1)$ modes and $(\pm 2,1)$ modes domination in this field is $(\pm 1,1)$ modes and $(\pm 2,1)$ modes are from before aperture field. Again it is caused by the non-perfect rigid aperture device and the gaps between the device and the duct wall. So these axially-unsymmetric higher-order modes penetrate the aperture device and appear in after aperture device. For this situation, this method cannot be used directly to predict the after orifice field either.

7.3 Aperture device with two orifices

If there are more than one orifice in the device, as shown in Fig 7.11, it can be divided into two situations: two orifices situation and several orifices situation. The first one to be studied is the two orifices situation.

7.3.1 Theoretical derivation

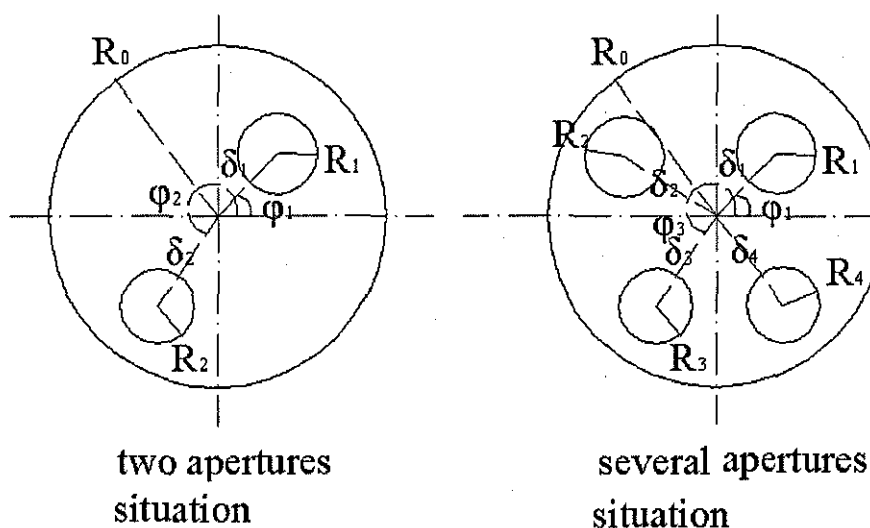


Fig 7. 11 Geometric configurations for orifices in the device

If the aperture device consists of two orifices (as shown in the left one of the Fig 7.11), with radius R_1 and R_2 respectively, the boundary conditions at 2 and 3 are given as below,

At boundary 2, for the acoustic pressure,

$$P_C + P_D|_{Z=-L_3} = P_E + P_F|_{Z=-L_3} \quad (\text{over } S_1 \text{ and } S_2). \quad (7.33)$$

For the velocity,

$$U_C + U_D|_{Z=-L_3} = U_E + U_F|_{Z=-L_3} \quad (\text{over } S_1 \text{ and } S_2), \quad (7.34)$$

$$U_E + U_F|_{Z=-L_3} = 0 \quad (\text{over } (S - S_1 - S_2)). \quad (7.35)$$

At boundary 3, the acoustic pressure,

$$P_C + P_D|_{Z=-L_3-L_2} = P_A + P_B|_{Z=-L_3-L_2} \quad (\text{over } S_1 \text{ and } S_2). \quad (7.36)$$

For the velocity,

$$U_C + U_D|_{Z=-L_3-L_2} = U_A + U_B|_{Z=-L_3-L_2} \quad (\text{over } S_1 \text{ and } S_2), \quad (7.37)$$

$$U_A + U_B|_{Z=-L_3-L_2} = 0 \quad (\text{over } (S - S_1 - S_2)), \quad (7.38)$$

in which S_1 is the area of orifice 1, S_2 is the area of orifice 2, S is the area of the main duct.

Following the derivation procedure of the single orifice situation, at boundary condition 2, for acoustic pressure, one can get, for $t = 0, s = 1$,

$$\begin{aligned} & (C1_{01} e^{jkL_3} + D1_{01} e^{-jkL_3}) R_1 / 2 \\ & = (E_{01} e^{jkL_3} + F_{01} e^{-jkL_3}) R_1 / 2 \\ & + \sum_{n=2}^{\infty} (E_{0n} e^{jk_{z,0,n}^{III} L_3} + F_{0n} e^{-jk_{z,0,n}^{III} L_3}) \frac{1}{k_{r,0,n}^{III}} J_0(k_{r,0,n}^{III} \delta_1) J_1(k_{r,0,n}^{III} R_1) \\ & + \sum_{m=1}^{\infty} \sum_{n=1}^{\infty} (((E_{mn}^+ e^{jk_{z,m,n}^{III} L_3} + F_{mn}^+ e^{-jk_{z,m,n}^{III} L_3}) e^{-jm\theta_1} + (E_{mn}^- e^{jk_{z,m,n}^{III} L_3} + F_{mn}^- e^{-jk_{z,m,n}^{III} L_3}) e^{jm\theta_1}) \\ & \quad \frac{1}{k_{r,m,n}^{III}} J_m(k_{r,m,n}^{III} \delta_1) J_1(k_{r,m,n}^{III} R_1)). \end{aligned} \quad (7.39)$$

$$\begin{aligned}
 & (C2_{01}e^{jkl_3} + D2_{01}e^{-jkl_3})R_2/2 \\
 & = (E_{01}e^{jkl_3} + F_{01}e^{-jkl_3})R_2/2 \\
 & + \sum_{n=2}^{\infty} (E_{0n}e^{jk_{z,0,n}^{III}L_3} + F_{0n}e^{-jk_{z,0,n}^{III}L_3}) \frac{1}{k_{r,0,n}^{III}} J_0(k_{r,0,n}^{III}\delta_2) J_1(k_{r,0,n}^{III}R_2) \quad (7.40) \\
 & + \sum_{m=1}^{\infty} \sum_{n=1}^{\infty} (((E_{mn}^+ e^{jk_{z,m,n}^{III}L_3} + F_{mn}^+ e^{-jk_{z,m,n}^{III}L_3}) e^{-jm\theta_2} + (E_{mn}^- e^{jk_{z,m,n}^{III}L_3} + F_{mn}^- e^{-jk_{z,m,n}^{III}L_3}) e^{jm\theta_2}) \\
 & \quad \frac{1}{k_{r,m,n}^{III}} J_m(k_{r,m,n}^{III}\delta_2) J_1(k_{r,m,n}^{III}R_2)) ,
 \end{aligned}$$

in which $C1_{01}$, $D1_{01}$ are amplitudes in orifice 1 and $C2_{01}$, $D2_{01}$ are amplitudes in orifice 2.

For $t = 0, s = 2, 3, \dots, \infty$,

$$\begin{aligned}
 & (C1_{0s}e^{jk_{z,0,s}^{II}L_3} + D1_{0s}e^{-jk_{z,0,s}^{II}L_3})J_0(k_{1r,0,s}^{II}R_1)R_1/2 \\
 & = \sum_{n=2}^{\infty} (E_{0n}e^{jk_{z,0,n}^{III}L_3} + F_{0n}e^{-jk_{z,0,n}^{III}L_3}) \frac{k_{r,0,n}^{III}}{k_{1r,0,s}^{II}{}^2 - k_{r,0,n}^{III}{}^2} J_0(k_{r,0,n}^{III}\delta_1) J'_0(k_{r,0,n}^{III}R_1) \\
 & + \sum_{m=1}^{\infty} \sum_{n=1}^{\infty} (((E_{mn}^+ e^{jk_{z,m,n}^{III}L_3} + F_{mn}^+ e^{-jk_{z,m,n}^{III}L_3}) e^{-jm\theta_1} + (E_{mn}^- e^{jk_{z,m,n}^{III}L_3} + F_{mn}^- e^{-jk_{z,m,n}^{III}L_3}) e^{jm\theta_1}) \quad (7.41) \\
 & \quad \frac{k_{r,m,n}^{III}}{k_{1r,0,s}^{II}{}^2 - k_{r,m,n}^{III}{}^2} J_m(k_{r,m,n}^{III}\delta_1) J'_0(k_{r,m,n}^{III}R_1)) .
 \end{aligned}$$

$$\begin{aligned}
 & (C2_{0s}e^{jk_{z,0,s}^{II}L_3} + D2_{0s}e^{-jk_{z,0,s}^{II}L_3})J_0(k_{2r,0,s}^{II}R_2)R_2/2 \\
 & = \sum_{n=2}^{\infty} (E_{0n}e^{jk_{z,0,n}^{III}L_3} + F_{0n}e^{-jk_{z,0,n}^{III}L_3}) \frac{k_{r,0,n}^{III}}{k_{2r,0,s}^{II}{}^2 - k_{r,0,n}^{III}{}^2} J_0(k_{r,0,n}^{III}\delta_2) J'_0(k_{r,0,n}^{III}R_2) \\
 & + \sum_{m=1}^{\infty} \sum_{n=1}^{\infty} (((E_{mn}^+ e^{jk_{z,m,n}^{III}L_3} + F_{mn}^+ e^{-jk_{z,m,n}^{III}L_3}) e^{-jm\theta_2} + (E_{mn}^- e^{jk_{z,m,n}^{III}L_3} + F_{mn}^- e^{-jk_{z,m,n}^{III}L_3}) e^{jm\theta_2}) \quad (7.42) \\
 & \quad \frac{k_{r,m,n}^{III}}{k_{2r,0,s}^{II}{}^2 - k_{r,m,n}^{III}{}^2} J_m(k_{r,m,n}^{III}\delta_2) J'_0(k_{r,m,n}^{III}R_2)) .
 \end{aligned}$$

For $t = 1, 2, \dots, \infty, s = 1, 2, \dots, \infty$,

$$\begin{aligned}
 & (C1_{ts}^- e^{jk_{z,t,s}^{II}L_3} + D1_{ts}^- e^{-jk_{z,t,s}^{II}L_3}) (1 - \frac{t^2}{k_{1r,t,s}^{II}{}^2 R_1^2}) J_t(k_{1r,t,s}^{II}R_1) R_1/2 \\
 & = \sum_{n=2}^{\infty} (E_{0n}e^{jk_{z,0,n}^{III}L_3} + F_{0n}e^{-jk_{z,0,n}^{III}L_3}) J_t(k_{r,0,n}^{III}\delta_1) (\frac{k_{r,0,n}^{III}}{k_{1r,t,s}^{II}{}^2 - k_{r,0,n}^{III}{}^2}) J'_t(k_{r,0,n}^{III}R_1) \quad (7.43)
 \end{aligned}$$

$$\begin{aligned}
 & + \sum_{m=1}^{\infty} \sum_{n=1}^{\infty} \left((E_{mn}^+ e^{jk_{z,m,n}^{III} L_3} + F_{mn}^+ e^{-jk_{z,m,n}^{III} L_3}) (-1)^t J_{m-t}(k_{r,m,n}^{III} \delta_1) e^{-jm\theta_1} \right. \\
 & \quad \left. + (E_{mn}^- e^{jk_{z,m,n}^{III} L_3} + F_{mn}^- e^{-jk_{z,m,n}^{III} L_3}) J_{m+t}(k_{r,m,n}^{III} \delta_1) e^{jm\theta_1} \right) \\
 & \quad \left(\frac{k_{r,m,n}^{III}}{k_{1r,t,s}^{II} - k_{r,m,n}^{III}} \right) J_t'(k_{r,m,n}^{III} R_1) \Big) . \\
 & (C1_{1s}^+ e^{jk_{1z,t,s}^{II} L_3} + D1_{1s}^+ e^{-jk_{1z,t,s}^{II} L_3}) \left(1 - \frac{t^2}{k_{1r,t,s}^{II} R_1^2} \right) J_t(k_{1r,t,s}^{II} R_1) R_1 / 2 \\
 & = \sum_{n=2}^{\infty} (E_{0n} e^{jk_{z,0,n}^{III} L_3} + F_{0n} e^{-jk_{z,0,n}^{III} L_3}) J_t(k_{r,0,n}^{III} \delta_1) \left(\frac{k_{r,0,n}^{III}}{k_{1r,t,s}^{II} - k_{r,0,n}^{III}} \right) J_t'(k_{r,0,n}^{III} R_1) \\
 & + \sum_{m=1}^{\infty} \sum_{n=1}^{\infty} \left((E_{mn}^+ e^{jk_{z,m,n}^{III} L_3} + F_{mn}^+ e^{-jk_{z,m,n}^{III} L_3}) J_{m+t}(k_{r,m,n}^{III} \delta_1) e^{-jm\theta_1} \right. \\
 & \quad \left. + (E_{mn}^- e^{jk_{z,m,n}^{III} L_3} + F_{mn}^- e^{-jk_{z,m,n}^{III} L_3}) (-1)^t J_{m-t}(k_{r,m,n}^{III} \delta_1) e^{jm\theta_1} \right) \\
 & \quad \left(\frac{k_{r,m,n}^{III}}{k_{1r,t,s}^{II} - k_{r,m,n}^{III}} \right) J_t'(k_{r,m,n}^{III} R_1) \Big) . \tag{7.44}
 \end{aligned}$$

$$\begin{aligned}
 & (C2_{1s}^- e^{jk_{2z,t,s}^{II} L_3} + D2_{1s}^- e^{-jk_{2z,t,s}^{II} L_3}) \left(1 - \frac{t^2}{k_{2r,t,s}^{II} R_2^2} \right) J_t(k_{2r,t,s}^{II} R_2) R_2 / 2 \\
 & = \sum_{n=2}^{\infty} (E_{0n} e^{jk_{z,0,n}^{III} L_3} + F_{0n} e^{-jk_{z,0,n}^{III} L_3}) J_t(k_{r,0,n}^{III} \delta_2) \left(\frac{k_{r,0,n}^{III}}{k_{2r,t,s}^{II} - k_{r,0,n}^{III}} \right) J_t'(k_{r,0,n}^{III} R_2) \\
 & + \sum_{m=1}^{\infty} \sum_{n=1}^{\infty} \left((E_{mn}^+ e^{jk_{z,m,n}^{III} L_3} + F_{mn}^+ e^{-jk_{z,m,n}^{III} L_3}) (-1)^t J_{m-t}(k_{r,m,n}^{III} \delta_2) e^{-jm\theta_2} \right. \\
 & \quad \left. + (E_{mn}^- e^{jk_{z,m,n}^{III} L_3} + F_{mn}^- e^{-jk_{z,m,n}^{III} L_3}) J_{m+t}(k_{r,m,n}^{III} \delta_2) e^{jm\theta_2} \right) \\
 & \quad \left(\frac{k_{r,m,n}^{III}}{k_{2r,t,s}^{II} - k_{r,m,n}^{III}} \right) J_t'(k_{r,m,n}^{III} R_2) \Big) . \tag{7.45}
 \end{aligned}$$

$$\begin{aligned}
 & (C2_{1s}^+ e^{jk_{2z,t,s}^{II} L_3} + D2_{1s}^+ e^{-jk_{2z,t,s}^{II} L_3}) \left(1 - \frac{t^2}{k_{2r,t,s}^{II} R_2^2} \right) J_t(k_{2r,t,s}^{II} R_2) R_2 / 2 \\
 & = \sum_{n=2}^{\infty} (E_{0n} e^{jk_{z,0,n}^{III} L_3} + F_{0n} e^{-jk_{z,0,n}^{III} L_3}) J_t(k_{r,0,n}^{III} \delta_2) \left(\frac{k_{r,0,n}^{III}}{k_{2r,t,s}^{II} - k_{r,0,n}^{III}} \right) J_t'(k_{r,0,n}^{III} R_2) \\
 & + \sum_{m=1}^{\infty} \sum_{n=1}^{\infty} \left((E_{mn}^+ e^{jk_{z,m,n}^{III} L_3} + F_{mn}^+ e^{-jk_{z,m,n}^{III} L_3}) J_{m+t}(k_{r,m,n}^{III} \delta_2) e^{-jm\theta_2} \right. \\
 & \quad \left. + (E_{mn}^- e^{jk_{z,m,n}^{III} L_3} + F_{mn}^- e^{-jk_{z,m,n}^{III} L_3}) (-1)^t J_{m-t}(k_{r,m,n}^{III} \delta_2) e^{jm\theta_2} \right) \\
 & \quad \left(\frac{k_{r,m,n}^{III}}{k_{2r,t,s}^{II} - k_{r,m,n}^{III}} \right) J_t'(k_{r,m,n}^{III} R_2) \Big) . \tag{7.46}
 \end{aligned}$$

For the velocity boundary condition, multiplying equation (7.34) by $J_1(k_{r,t,s}^{III} r) e^{-jt\theta} dS$ and integrating over orifice S_1 and orifice S_2 respectively; also multiplying equation (7.35) by $J_1(k_{r,t,s}^{III} r) e^{-jt\theta} dS$ and integrating over the region $S - S_1 - S_2$, then adding these three integration together, one can get,

For $t = 0, s = 1$,

$$(C1_{01} e^{jkl_3} - D1_{01} e^{-jkl_3}) R_1^2 + (C2_{01} e^{jkl_3} - D2_{01} e^{-jkl_3}) R_2^2 = (E_{01} e^{jkl_3} - F_{01} e^{-jkl_3}) R_0^2 \quad (7.47)$$

For $t = 0, s = 2, 3, \dots, \infty$,

$$\begin{aligned} & (C1_{01} e^{jkl_3} - D1_{01} e^{-jkl_3}) \frac{R_1}{k_{r,o,s}^{III}} J_0(k_{r,o,s}^{III} \delta_1) J_1(k_{r,o,s}^{III} R_1) \\ & + \sum_{n=2}^{\infty} \left(\frac{k_{1z,0,n}^{II}}{k} (C1_{0n} e^{jk_{1z,0,n}^{II} L_3} - D1_{0n} e^{-jk_{1z,0,n}^{II} L_3}) \right. \\ & \quad \left. \frac{R_1 k_{r,o,s}^{III}}{k_{1r,0,n}^{II}{}^2 - k_{r,o,s}^{III}{}^2} J_0(k_{r,o,s}^{III} \delta_1) J_0(k_{1r,0,n}^{II} R_1) J_0'(k_{r,o,s}^{III} R_1) \right) \\ & + \sum_{m=1}^{\infty} \sum_{n=1}^{\infty} \left(\frac{k_{1z,m,n}^{II}}{k} ((C1_{mn}^+ e^{jk_{1z,m,n}^{II} L_3} - D1_{mn}^+ e^{-jk_{1z,m,n}^{II} L_3}) + (C1_{mn}^- e^{jk_{1z,m,n}^{II} L_3} - D1_{mn}^- e^{-jk_{1z,m,n}^{II} L_3})) \right. \\ & \quad \left. \frac{R_1 k_{r,o,s}^{III}}{k_{1r,m,n}^{II}{}^2 - k_{r,o,s}^{III}{}^2} J_m(k_{r,o,s}^{III} \delta_1) J_m(k_{1r,m,n}^{II} R_1) J_m'(k_{r,o,s}^{III} R_1) \right) \\ & + (C2_{01} e^{jkl_3} - D2_{01} e^{-jkl_3}) \frac{R_2}{k_{r,o,s}^{III}} J_0(k_{r,o,s}^{III} \delta_2) J_1(k_{r,o,s}^{III} R_2) \\ & + \sum_{n=2}^{\infty} \left(\frac{k_{2z,0,n}^{II}}{k} (C2_{0n} e^{jk_{2z,0,n}^{II} L_3} - D2_{0n} e^{-jk_{2z,0,n}^{II} L_3}) \right. \\ & \quad \left. \frac{R_2 k_{r,o,s}^{III}}{k_{2r,0,n}^{II}{}^2 - k_{r,o,s}^{III}{}^2} J_0(k_{r,o,s}^{III} \delta_2) J_0(k_{2r,0,n}^{II} R_2) J_0'(k_{r,o,s}^{III} R_2) \right) \\ & + \sum_{m=1}^{\infty} \sum_{n=1}^{\infty} \left(\frac{k_{2z,m,n}^{II}}{k} ((C2_{mn}^+ e^{jk_{2z,m,n}^{II} L_3} - D2_{mn}^+ e^{-jk_{2z,m,n}^{II} L_3}) + (C2_{mn}^- e^{jk_{2z,m,n}^{II} L_3} - D2_{mn}^- e^{-jk_{2z,m,n}^{II} L_3})) \right. \\ & \quad \left. \frac{R_2 k_{r,o,s}^{III}}{k_{2r,m,n}^{II}{}^2 - k_{r,o,s}^{III}{}^2} J_m(k_{r,o,s}^{III} \delta_2) J_m(k_{2r,m,n}^{II} R_2) J_m'(k_{r,o,s}^{III} R_2) \right) \\ & = \frac{k_{z,o,s}^{III}}{k} (E_{0s} e^{jk_{z,o,s}^{III} L_3} - F_{0s} e^{-jk_{z,o,s}^{III} L_3}) \frac{R_0^2}{2} J_0^2(k_{r,o,s}^{III} R_0) . \end{aligned} \quad (7.48)$$

For $t = 1, 2, \dots, \infty, s = 1, 2, \dots, \infty,$

$$\begin{aligned}
 & (C1_{01} e^{jkL_3} - D1_{01} e^{-jkL_3}) e^{-jt\theta_1} J_t(k_{r,t,s}^{III} \delta_1) \frac{R_1}{k_{r,t,s}^{III}} J_1(k_{r,t,s}^{III} R_1) \\
 & + \sum_{n=2}^{\infty} \left(\frac{k_{1z,0,n}^{II}}{k} (C1_{0n} e^{jk_{1z,0,n}^{II} L_3} - D1_{0n} e^{-jk_{1z,0,n}^{II} L_3}) e^{-jt\theta_1} \right. \\
 & \quad \left. J_t(k_{r,t,s}^{III} \delta_1) \frac{R_1 k_{r,t,s}^{III}}{k_{1r,0,n}^{II}{}^2 - k_{r,t,s}^{III}{}^2} J_0'(k_{r,t,s}^{III} R_1) J_0(k_{1r,0,n}^{II} R_1) \right) \\
 & + \sum_{m=1}^{\infty} \sum_{n=1}^{\infty} [(C1_{mn}^+ e^{jk_{1z,m,n}^{II} L_3} - D1_{mn}^+ e^{-jk_{1z,m,n}^{II} L_3}) (-1)^m J_{t-m}(k_{r,t,s}^{III} \delta_1) \\
 & \quad + (C1_{mn}^- e^{jk_{1z,m,n}^{II} L_3} - D1_{mn}^- e^{-jk_{1z,m,n}^{II} L_3}) J_{m+t}(k_{r,t,s}^{III} \delta_1)] \\
 & \quad \frac{k_{1z,m,n}^{II}}{k} \left(\frac{R_1 k_{r,t,s}^{III}}{k_{1r,m,n}^{II}{}^2 - k_{r,t,s}^{III}{}^2} \right) J_m'(k_{r,t,s}^{III} R_1) J_m(k_{1r,m,n}^{II} R_1) e^{-jt\theta_1} \\
 & + (C2_{01} e^{jkL_3} - D2_{01} e^{-jkL_3}) e^{-jt\theta_2} J_t(k_{r,t,s}^{III} \delta_2) \frac{R_2}{k_{r,t,s}^{III}} J_1(k_{r,t,s}^{III} R_2) \\
 & + \sum_{n=2}^{\infty} \left(\frac{k_{2z,0,n}^{II}}{k} (C2_{0n} e^{jk_{2z,0,n}^{II} L_3} - D2_{0n} e^{-jk_{2z,0,n}^{II} L_3}) e^{-jt\theta_2} \right. \\
 & \quad \left. J_t(k_{r,t,s}^{III} \delta_2) \frac{R_2 k_{r,t,s}^{III}}{k_{2r,0,n}^{II}{}^2 - k_{r,t,s}^{III}{}^2} J_0'(k_{r,t,s}^{III} R_2) J_0(k_{2r,0,n}^{II} R_2) \right) \\
 & + \sum_{m=1}^{\infty} \sum_{n=1}^{\infty} [(C2_{mn}^+ e^{jk_{2z,m,n}^{II} L_3} - D2_{mn}^+ e^{-jk_{2z,m,n}^{II} L_3}) (-1)^m J_{t-m}(k_{r,t,s}^{III} \delta_2) \\
 & \quad + (C2_{mn}^- e^{jk_{2z,m,n}^{II} L_3} - D2_{mn}^- e^{-jk_{2z,m,n}^{II} L_3}) J_{m+t}(k_{r,t,s}^{III} \delta_2)] \\
 & \quad \frac{k_{2z,m,n}^{II}}{k} \left(\frac{R_2 k_{r,t,s}^{III}}{k_{2r,m,n}^{II}{}^2 - k_{r,t,s}^{III}{}^2} \right) J_m'(k_{r,t,s}^{III} R_2) J_m(k_{2r,m,n}^{II} R_2) e^{-jt\theta_2} \\
 & = \frac{k_{z,t,s}^{III}}{k} (E_{ts}^- e^{jk_{z,t,s}^{III} L_3} - F_{ts}^- e^{-jk_{z,t,s}^{III} L_3}) \frac{R_0^2}{2} \left(1 - \frac{t^2}{k_{r,t,s}^{III}{}^2 R_0^2} \right) J_t^2(k_{r,t,s}^{III} R_0).
 \end{aligned} \tag{7.49}$$

And

$$\begin{aligned}
 & (C1_{01} e^{jkL_3} - D1_{01} e^{-jkL_3}) e^{j\theta_1} J_t(k_{r,t,s}^{III} \delta_1) \frac{R_1}{k_{r,t,s}^{III}} J_1(k_{r,t,s}^{III} R_1) \\
 & + \sum_{n=2}^{\infty} \left(\frac{k_{1z,0,n}^{II}}{k} (C1_{0n} e^{jk_{1z,0,n}^{II} L_3} - D1_{0n} e^{-jk_{1z,0,n}^{II} L_3}) e^{j\theta_1} \right. \\
 & \quad \left. J_t(k_{r,t,s}^{III} \delta_1) \frac{R_1 k_{r,t,s}^{III}}{k_{1r,0,n}^{II}{}^2 - k_{r,t,s}^{III}{}^2} J_0'(k_{r,t,s}^{III} R_1) J_0(k_{1r,0,n}^{II} R_1) \right) \\
 & + \sum_{m=1}^{\infty} \sum_{n=1}^{\infty} \left[(C1_{mn}^+ e^{jk_{1z,m,n}^{II} L_3} - D1_{mn}^+ e^{-jk_{1z,m,n}^{II} L_3}) J_{m+t}(k_{r,t,s}^{III} \delta_1) \right. \\
 & \quad \left. + (C1_{mn}^- e^{jk_{1z,m,n}^{II} L_3} - D1_{mn}^- e^{-jk_{1z,m,n}^{II} L_3}) (-1)^m J_{t-m}(k_{r,t,s}^{III} \delta_1) \right] \\
 & \quad \frac{k_{1z,m,n}^{II}}{k} \left(\frac{R_1 k_{r,t,s}^{III}}{k_{1r,m,n}^{II}{}^2 - k_{r,t,s}^{III}{}^2} \right) J_m'(k_{r,t,s}^{III} R_1) J_m(k_{1r,m,n}^{II} R_1) e^{j\theta_1} \\
 & + (C2_{01} e^{jkL_3} - D2_{01} e^{-jkL_3}) e^{j\theta_2} J_t(k_{r,t,s}^{III} \delta_2) \frac{R_2}{k_{r,t,s}^{III}} J_1(k_{r,t,s}^{III} R_2) \\
 & + \sum_{n=2}^{\infty} \left(\frac{k_{2z,0,n}^{II}}{k} (C2_{0n} e^{jk_{2z,0,n}^{II} L_3} - D2_{0n} e^{-jk_{2z,0,n}^{II} L_3}) e^{j\theta_2} \right. \\
 & \quad \left. J_t(k_{r,t,s}^{III} \delta_2) \frac{R_2 k_{r,t,s}^{III}}{k_{2r,0,n}^{II}{}^2 - k_{r,t,s}^{III}{}^2} J_0'(k_{r,t,s}^{III} R_2) J_0(k_{2r,0,n}^{II} R_2) \right) \\
 & + \sum_{m=1}^{\infty} \sum_{n=1}^{\infty} \left[(C2_{mn}^+ e^{jk_{2z,m,n}^{II} L_3} - D2_{mn}^+ e^{-jk_{2z,m,n}^{II} L_3}) J_{m+t}(k_{r,t,s}^{III} \delta_2) \right. \\
 & \quad \left. + (C2_{mn}^- e^{jk_{2z,m,n}^{II} L_3} - D2_{mn}^- e^{-jk_{2z,m,n}^{II} L_3}) (-1)^m J_{t-m}(k_{r,t,s}^{III} \delta_2) \right] \\
 & \quad \frac{k_{2z,m,n}^{II}}{k} \left(\frac{R_2 k_{r,t,s}^{III}}{k_{2r,m,n}^{II}{}^2 - k_{r,t,s}^{III}{}^2} \right) J_m'(k_{r,t,s}^{III} R_2) J_m(k_{2r,m,n}^{II} R_2) e^{j\theta_2} \\
 & = \frac{k_{z,t,s}^{III}}{k} (E_{ts}^+ e^{jk_{z,t,s}^{III} L_3} - F_{ts}^+ e^{-jk_{z,t,s}^{III} L_3}) \frac{R_0^2}{2} \left(1 - \frac{t^2}{k_{r,t,s}^{III}{}^2 R_0^2} \right) J_t^2(k_{r,t,s}^{III} R_0).
 \end{aligned} \tag{7.50}$$

At boundary 3, following the derivation procedure of the boundary 2, one can get these equations for the acoustic pressure as follow.

For $t = 0, s = 1$,

$$\begin{aligned}
 & (C1_{01}e^{jk(L_3+L_2)} + D1_{01}e^{-jk(L_3+L_2)})R_1/2 \\
 & = (A_{01}e^{jk(L_3+L_2)} + B_{01}e^{-jk(L_3+L_2)})R_1/2 \\
 & + \sum_{n=2}^{\infty} (A_{0n}e^{jk_{z,0,n}^I(L_3+L_2)} + B_{0n}e^{-jk_{z,0,n}^I(L_3+L_2)}) \frac{1}{k_{r,0,n}^I} J_0(k_{r,0,n}^I \delta_1) J_1(k_{r,0,n}^I R_1) \\
 & + \sum_{m=1}^{\infty} \sum_{n=1}^{\infty} \left[(A_{mn}^+ e^{jk_{z,m,n}^I(L_3+L_2)} + B_{mn}^+ e^{-jk_{z,m,n}^I(L_3+L_2)}) e^{-jm\theta_1} \right. \\
 & \quad \left. + (A_{mn}^- e^{jk_{z,m,n}^I(L_3+L_2)} + B_{mn}^- e^{-jk_{z,m,n}^I(L_3+L_2)}) e^{jm\theta_1} \right] \\
 & \quad \frac{1}{k_{r,m,n}^I} J_m(k_{r,m,n}^I \delta_1) J_1(k_{r,m,n}^I R_1) .
 \end{aligned} \tag{7.51}$$

$$\begin{aligned}
 & (C2_{01}e^{jk(L_3+L_2)} + D2_{01}e^{-jk(L_3+L_2)})R_2/2 \\
 & = (A_{01}e^{jk(L_3+L_2)} + B_{01}e^{-jk(L_3+L_2)})R_2/2 \\
 & + \sum_{n=2}^{\infty} (A_{0n}e^{jk_{z,0,n}^I(L_3+L_2)} + B_{0n}e^{-jk_{z,0,n}^I(L_3+L_2)}) \frac{1}{k_{r,0,n}^I} J_0(k_{r,0,n}^I \delta_2) J_1(k_{r,0,n}^I R_2) \\
 & + \sum_{m=1}^{\infty} \sum_{n=1}^{\infty} \left[(A_{mn}^+ e^{jk_{z,m,n}^I(L_3+L_2)} + B_{mn}^+ e^{-jk_{z,m,n}^I(L_3+L_2)}) e^{-jm\theta_2} \right. \\
 & \quad \left. + (A_{mn}^- e^{jk_{z,m,n}^I(L_3+L_2)} + B_{mn}^- e^{-jk_{z,m,n}^I(L_3+L_2)}) e^{jm\theta_2} \right] \\
 & \quad \frac{1}{k_{r,m,n}^I} J_m(k_{r,m,n}^I \delta_2) J_1(k_{r,m,n}^I R_2) .
 \end{aligned} \tag{7.52}$$

For $t = 0, s = 2, 3, \dots, \infty$,

$$\begin{aligned}
 & (C1_{0s}e^{jk_{z,0,s}^I(L_3+L_2)} + D1_{0s}e^{-jk_{z,0,s}^I(L_3+L_2)})J_0(k_{1r,0,s}^I R_1)R_1/2 \\
 & = \sum_{n=2}^{\infty} (A_{0n}e^{jk_{z,0,n}^I(L_3+L_2)} + B_{0n}e^{-jk_{z,0,n}^I(L_3+L_2)}) \frac{k_{r,0,n}^I}{k_{1r,0,s}^I - k_{r,0,n}^I} J_0(k_{r,0,n}^I \delta_1) J_0(k_{r,0,n}^I R_1) \\
 & + \sum_{m=1}^{\infty} \sum_{n=1}^{\infty} \left[(A_{mn}^+ e^{jk_{z,m,n}^I(L_3+L_2)} + B_{mn}^+ e^{-jk_{z,m,n}^I(L_3+L_2)}) e^{-jm\theta_1} \right. \\
 & \quad \left. + (A_{mn}^- e^{jk_{z,m,n}^I(L_3+L_2)} + B_{mn}^- e^{-jk_{z,m,n}^I(L_3+L_2)}) e^{jm\theta_1} \right] \\
 & \quad \frac{k_{r,m,n}^I}{k_{1r,0,s}^I - k_{r,m,n}^I} J_m(k_{r,m,n}^I \delta_1) J_0(k_{r,m,n}^I R_1) .
 \end{aligned} \tag{7.53}$$

$$\begin{aligned}
 & (C2_{0s} e^{jk_{2r,0,s}^{\parallel}(L_3+L_2)} + D2_{0s} e^{-jk_{2r,0,s}^{\parallel}(L_3+L_2)}) J_0(k_{2r,0,s}^{\parallel} R_2) R_2 / 2 \\
 &= \sum_{n=2}^{\infty} (A_{0n} e^{jk_{z,0,n}^{\perp}(L_3+L_2)} + B_{0n} e^{-jk_{z,0,n}^{\perp}(L_3+L_2)}) \frac{k_{r,0,n}^{\perp}}{k_{2r,0,s}^{\parallel} - k_{r,0,n}^{\perp}} J_0(k_{r,0,n}^{\perp} \delta_2) J_0'(k_{r,0,n}^{\perp} R_2) \\
 &+ \sum_{m=1}^{\infty} \sum_{n=1}^{\infty} [(A_{mn}^+ e^{jk_{z,m,n}^{\perp}(L_3+L_2)} + B_{mn}^+ e^{-jk_{z,m,n}^{\perp}(L_3+L_2)}) e^{-jm\theta_2} \\
 &\quad + (A_{mn}^- e^{jk_{z,m,n}^{\perp}(L_3+L_2)} + B_{mn}^- e^{-jk_{z,m,n}^{\perp}(L_3+L_2)}) e^{jm\theta_2}] \\
 &\quad \frac{k_{r,m,n}^{\perp}}{k_{2r,0,s}^{\parallel} - k_{r,m,n}^{\perp}} J_m(k_{r,m,n}^{\perp} \delta_2) J_0'(k_{r,m,n}^{\perp} R_2) .
 \end{aligned} \tag{7.54}$$

For $t = 1, 2, \dots, \infty, s = 1, 2, \dots, \infty,$

$$\begin{aligned}
 & (C1_{ts}^- e^{jk_{1r,t,s}^{\parallel}(L_3+L_2)} + D1_{ts}^- e^{-jk_{1r,t,s}^{\parallel}(L_3+L_2)}) (1 - \frac{t^2}{k_{1r,t,s}^{\parallel} R_1^2}) J_t(k_{1r,t,s}^{\parallel} R_1) R_1 / 2 \\
 &= \sum_{n=2}^{\infty} (A_{0n} e^{jk_{z,0,n}^{\perp}(L_3+L_2)} + B_{0n} e^{-jk_{z,0,n}^{\perp}(L_3+L_2)}) J_t(k_{r,0,n}^{\perp} \delta_1) (\frac{k_{r,0,n}^{\perp} J_t'(k_{r,0,n}^{\perp} R_1)}{k_{1r,t,s}^{\parallel} - k_{r,0,n}^{\perp}}) \\
 &+ \sum_{m=1}^{\infty} \sum_{n=1}^{\infty} [(A_{mn}^+ e^{jk_{z,m,n}^{\perp}(L_3+L_2)} + B_{mn}^+ e^{-jk_{z,m,n}^{\perp}(L_3+L_2)}) (-1)^t J_{m-t}(k_{r,m,n}^{\perp} \delta_1) e^{-jm\theta_1} \\
 &\quad + (A_{mn}^- e^{jk_{z,m,n}^{\perp}(L_3+L_2)} + B_{mn}^- e^{-jk_{z,m,n}^{\perp}(L_3+L_2)}) J_{m+t}(k_{r,m,n}^{\perp} \delta_1) e^{jm\theta_1}] \\
 &\quad (\frac{k_{r,m,n}^{\perp}}{k_{1r,t,s}^{\parallel} - k_{r,m,n}^{\perp}}) J_t'(k_{r,m,n}^{\perp} R_1) .
 \end{aligned} \tag{7.55}$$

$$\begin{aligned}
 & (C1_{ts}^+ e^{jk_{1r,t,s}^{\parallel}(L_3+L_2)} + D1_{ts}^+ e^{-jk_{1r,t,s}^{\parallel}(L_3+L_2)}) (1 - \frac{t^2}{k_{1r,t,s}^{\parallel} R_1^2}) J_t(k_{1r,t,s}^{\parallel} R_1) R_1 / 2 \\
 &= \sum_{n=2}^{\infty} (A_{0n} e^{jk_{z,0,n}^{\perp}(L_3+L_2)} + B_{0n} e^{-jk_{z,0,n}^{\perp}(L_3+L_2)}) J_t(k_{r,0,n}^{\perp} \delta_1) (\frac{k_{r,0,n}^{\perp} J_t'(k_{r,0,n}^{\perp} R_1)}{k_{1r,t,s}^{\parallel} - k_{r,0,n}^{\perp}}) \\
 &+ \sum_{m=1}^{\infty} \sum_{n=1}^{\infty} [(A_{mn}^+ e^{jk_{z,m,n}^{\perp}(L_3+L_2)} + B_{mn}^+ e^{-jk_{z,m,n}^{\perp}(L_3+L_2)}) J_{m+t}(k_{r,m,n}^{\perp} \delta_1) e^{-jm\theta_1} \\
 &\quad + (A_{mn}^- e^{jk_{z,m,n}^{\perp}(L_3+L_2)} + B_{mn}^- e^{-jk_{z,m,n}^{\perp}(L_3+L_2)}) (-1)^t J_{m-t}(k_{r,m,n}^{\perp} \delta_1) e^{jm\theta_1}] \\
 &\quad (\frac{k_{r,m,n}^{\perp}}{k_{1r,t,s}^{\parallel} - k_{r,m,n}^{\perp}}) J_t'(k_{r,m,n}^{\perp} R_1) .
 \end{aligned} \tag{7.56}$$

$$\begin{aligned}
 & (C2_{ts}^- e^{jk_{2r,t,s}^H(L_3+L_2)} + D2_{ts}^- e^{-jk_{2r,t,s}^H(L_3+L_2)}) \left(1 - \frac{t^2}{k_{2r,t,s}^H R_2^2}\right) J_t(k_{2r,t,s}^H R_2) R_2 / 2 \\
 &= \sum_{n=2}^{\infty} (A_{0n} e^{jk_{r,0,n}^I(L_3+L_2)} + B_{0n} e^{-jk_{r,0,n}^I(L_3+L_2)}) J_t(k_{r,0,n}^I \delta_2) \left(\frac{k_{r,0,n}^I J_t'(k_{r,0,n}^I R_2)}{k_{2r,t,s}^H R_2^2 - k_{r,0,n}^I R_2^2}\right) \\
 &+ \sum_{m=1}^{\infty} \sum_{n=1}^{\infty} [(A_{mn}^+ e^{jk_{z,m,n}^I(L_3+L_2)} + B_{mn}^+ e^{-jk_{z,m,n}^I(L_3+L_2)}) (-1)^t J_{m-t}(k_{r,m,n}^I \delta_2) e^{-jm\theta_2} \\
 &\quad + (A_{mn}^- e^{jk_{z,m,n}^I(L_3+L_2)} + B_{mn}^- e^{-jk_{z,m,n}^I(L_3+L_2)}) J_{m+t}(k_{r,m,n}^I \delta_2) e^{jm\theta_2}] \\
 &\quad \left(\frac{k_{r,m,n}^I}{k_{2r,t,s}^H R_2^2 - k_{r,m,n}^I R_2^2}\right) J_t'(k_{r,m,n}^I R_2) \cdot
 \end{aligned} \tag{7.57}$$

$$\begin{aligned}
 & (C2_{ts}^+ e^{jk_{2r,t,s}^H(L_3+L_2)} + D2_{ts}^+ e^{-jk_{2r,t,s}^H(L_3+L_2)}) \left(1 - \frac{t^2}{k_{2r,t,s}^H R_2^2}\right) J_t(k_{2r,t,s}^H R_2) R_2 / 2 \\
 &= \sum_{n=2}^{\infty} (E_{0n} e^{jk_{r,0,n}^I(L_3+L_2)} + F_{0n} e^{-jk_{r,0,n}^I(L_3+L_2)}) J_t(k_{r,0,n}^I \delta_2) \left(\frac{k_{r,0,n}^I J_t'(k_{r,0,n}^I R_2)}{k_{2r,t,s}^H R_2^2 - k_{r,0,n}^I R_2^2}\right) \\
 &+ \sum_{m=1}^{\infty} \sum_{n=1}^{\infty} [(E_{mn}^+ e^{jk_{z,m,n}^I(L_3+L_2)} + F_{mn}^+ e^{-jk_{z,m,n}^I(L_3+L_2)}) J_{m+t}(k_{r,m,n}^I \delta_2) e^{-jm\theta_2} \\
 &\quad + (E_{mn}^- e^{jk_{z,m,n}^I(L_3+L_2)} + F_{mn}^- e^{-jk_{z,m,n}^I(L_3+L_2)}) (-1)^t J_{m-t}(k_{r,m,n}^I \delta_2) e^{jm\theta_2}] \\
 &\quad \left(\frac{k_{r,m,n}^I}{k_{2r,t,s}^H R_2^2 - k_{r,m,n}^I R_2^2}\right) J_t'(k_{r,m,n}^I R_2) \cdot
 \end{aligned} \tag{7.58}$$

Also for the particle velocity boundary condition, one can get

For $t = 0, s = 1$,

$$\begin{aligned}
 & (C1_{01} e^{jk(L_3+L_2)} - D1_{01} e^{-jk(L_3+L_2)}) R_1^2 + (C2_{01} e^{jk(L_3+L_2)} - D2_{01} e^{-jk(L_3+L_2)}) R_2^2 \\
 &= (A_{01} e^{jk(L_3+L_2)} - B_{01} e^{-jk(L_3+L_2)}) R_0^2 \cdot
 \end{aligned} \tag{7.59}$$

For $t = 0, s = 2, 3, \dots, \infty$,

$$\begin{aligned}
 & (C1_{01} e^{jk(L_3+L_2)} - D1_{01} e^{-jk(L_3+L_2)}) \frac{R_1}{k_{r,o,s}^I} J_0(k_{r,o,s}^I \delta_1) J_1(k_{r,o,s}^I R_1) \\
 &+ \sum_{n=2}^{\infty} \left(\frac{k_{1z,0,n}^H}{k}\right) (C1_{0n} e^{jk_{1z,0,n}^H(L_3+L_2)} - D1_{0n} e^{-jk_{1z,0,n}^H(L_3+L_2)}) \\
 &\quad \frac{R_1 k_{r,o,s}^I}{k_{1r,0,n}^H R_2^2 - k_{r,o,s}^I R_2^2} J_0(k_{r,o,s}^I \delta_1) J_0(k_{1r,0,n}^H R_1) J_0'(k_{r,o,s}^I R_1)
 \end{aligned}$$

$$\begin{aligned}
 & + \sum_{m=1}^{\infty} \sum_{n=1}^{\infty} \left(\frac{k_{1z,m,n}^{II}}{k} \left((C1_{mn}^+ e^{jk_{1z,m,n}^{II}(L_3+L_2)} - D1_{mn}^+ e^{-jk_{1z,m,n}^{II}(L_3+L_2)}) \right. \right. \\
 & \quad \left. \left. + (C1_{mn}^- e^{jk_{1z,m,n}^{II}(L_3+L_2)} - D1_{mn}^- e^{-jk_{1z,m,n}^{II}(L_3+L_2)}) \right) \right. \\
 & \quad \left. \frac{R_1 k_{r,o,s}^I}{k_{1r,m,n}^{II} - k_{r,o,s}^I} J_m(k_{r,o,s}^I \delta_1) J_m(k_{1r,m,n}^{II} R_1) J_m'(k_{r,o,s}^I R_1) \right) \\
 & + (C2_{01} e^{jk(L_3+L_2)} - D2_{01} e^{-jk(L_3+L_2)}) \frac{R_2}{k_{r,o,s}^I} J_0(k_{r,o,s}^I \delta_2) J_1(k_{r,o,s}^I R_2) \\
 & + \sum_{n=2}^{\infty} \left(\frac{k_{2z,0,n}^{II}}{k} (C2_{0n} e^{jk_{2z,0,n}^{II}(L_3+L_2)} - D2_{0n} e^{-jk_{2z,0,n}^{II}(L_3+L_2)}) \right. \\
 & \quad \left. \frac{R_2 k_{r,o,s}^I}{k_{2r,0,n}^{II} - k_{r,o,s}^I} J_0(k_{r,o,s}^I \delta_2) J_0(k_{2r,0,n}^{II} R_2) J_0'(k_{r,o,s}^I R_2) \right) \quad (7.60) \\
 & + \sum_{m=1}^{\infty} \sum_{n=1}^{\infty} \left(\frac{k_{2z,m,n}^{II}}{k} \left((C2_{mn}^+ e^{jk_{2z,m,n}^{II}(L_3+L_2)} - D2_{mn}^+ e^{-jk_{2z,m,n}^{II}(L_3+L_2)}) \right. \right. \\
 & \quad \left. \left. + (C2_{mn}^- e^{jk_{2z,m,n}^{II}(L_3+L_2)} - D2_{mn}^- e^{-jk_{2z,m,n}^{II}(L_3+L_2)}) \right) \right. \\
 & \quad \left. \frac{R_2 k_{r,o,s}^I}{k_{2r,m,n}^{II} - k_{r,o,s}^I} J_m(k_{r,o,s}^I \delta_2) J_m(k_{2r,m,n}^{II} R_2) J_m'(k_{r,o,s}^I R_2) \right) \\
 & = \frac{k_{z,0,s}^I}{k} (A_{0s} e^{jk_{z,0,s}^I(L_3+L_2)} - B_{0s} e^{-jk_{z,0,s}^I(L_3+L_2)}) \frac{R_0^2}{2} J_0^2(k_{r,0,s}^I R_0) .
 \end{aligned}$$

For $t = 1, 2, \dots, \infty, s = 1, 2, \dots, \infty,$

$$\begin{aligned}
 & (C1_{01} e^{jk(L_3+L_2)} - D1_{01} e^{-jk(L_3+L_2)}) e^{-j\theta_1} J_t(k_{r,t,s}^I \delta_1) \frac{R_1}{k_{r,t,s}^I} J_1(k_{r,t,s}^I R_1) \\
 & + \sum_{n=2}^{\infty} \left(\frac{k_{1z,0,n}^{II}}{k} (C1_{0n} e^{jk_{1z,0,n}^{II}(L_3+L_2)} - D1_{0n} e^{-jk_{1z,0,n}^{II}(L_3+L_2)}) e^{-j\theta_1} \right. \\
 & \quad \left. J_t(k_{r,t,s}^I \delta_1) \frac{R_1 k_{r,t,s}^I}{k_{1r,0,n}^{II} - k_{r,t,s}^I} J_0'(k_{r,t,s}^I R_1) J_0(k_{1r,0,n}^{II} R_1) \right) \\
 & + \sum_{m=1}^{\infty} \sum_{n=1}^{\infty} \left((C1_{mn}^+ e^{jk_{1z,m,n}^{II}(L_3+L_2)} - D1_{mn}^+ e^{-jk_{1z,m,n}^{II}(L_3+L_2)}) (-1)^m J_{t-m}(k_{r,t,s}^I \delta_1) \right. \\
 & \quad \left. + (C1_{mn}^- e^{jk_{1z,m,n}^{II}(L_3+L_2)} - D1_{mn}^- e^{-jk_{1z,m,n}^{II}(L_3+L_2)}) J_{m+t}(k_{r,t,s}^I \delta_1) \right) \\
 & \quad \frac{k_{1z,m,n}^{II}}{k} \left(\frac{R_1 k_{r,t,s}^I}{k_{1r,m,n}^{II} - k_{r,t,s}^I} \right) J_m'(k_{r,t,s}^I R_1) J_m(k_{1r,m,n}^{II} R_1) e^{-j\theta_1} \\
 & + (C2_{01} e^{jk(L_3+L_2)} - D2_{01} e^{-jk(L_3+L_2)}) e^{-j\theta_2} J_t(k_{r,t,s}^I \delta_2) \frac{R_2}{k_{r,t,s}^I} J_1(k_{r,t,s}^I R_2) \quad (7.61)
 \end{aligned}$$

$$\begin{aligned}
 & + \sum_{n=2}^{\infty} \left(\frac{k_{2z,0,n}^H}{k} (C2_{0n} e^{jk_{2z,0,n}^H(L_3+L_2)} - D1_{0n} e^{-jk_{2z,0,n}^H(L_3+L_2)}) e^{-j\theta_2} \right. \\
 & \quad \left. J_t(k_{r,t,s}^I \delta_2) \frac{R_2 k_{r,t,s}^I}{k_{2r,0,n}^H - k_{r,t,s}^I} J_0'(k_{r,t,s}^I R_2) J_0(k_{2r,0,n}^H R_2) \right) \\
 & + \sum_{m=1}^{\infty} \sum_{n=1}^{\infty} \left[(C2_{mn}^+ e^{jk_{2z,m,n}^H(L_3+L_2)} - D2_{mn}^+ e^{-jk_{2z,m,n}^H(L_3+L_2)}) (-1)^m J_{t-m}(k_{r,t,s}^I \delta_2) \right. \\
 & \quad \left. + (C2_{mn}^- e^{jk_{2z,m,n}^H(L_3+L_2)} - D2_{mn}^- e^{-jk_{2z,m,n}^H(L_3+L_2)}) J_{m+t}(k_{r,t,s}^I \delta_2) \right] \\
 & \quad \frac{k_{2z,m,n}^H}{k} \left(\frac{R_2 k_{r,t,s}^I}{k_{2r,m,n}^H - k_{r,t,s}^I} \right) J_m'(k_{r,t,s}^I R_2) J_m(k_{2r,m,n}^H R_2) e^{-j\theta_2} \\
 & = \frac{k_{2z,t,s}^I}{k} (A_{1s}^- e^{jk_{2z,t,s}^I(L_3+L_2)} - B_{1s}^- e^{-jk_{2z,t,s}^I L_3}) \frac{R_0^2}{2} \left(1 - \frac{t^2}{k_{r,t,s}^I R_0^2} \right) J_t^2(k_{r,t,s}^I R_0).
 \end{aligned}$$

And

$$\begin{aligned}
 & (C1_{01} e^{jk(L_3+L_2)} - D1_{01} e^{-jk(L_3+L_2)}) e^{j\theta_1} J_t(k_{r,t,s}^I \delta_1) \frac{R_1}{k_{r,t,s}^I} J_1(k_{r,t,s}^I R_1) \\
 & + \sum_{n=2}^{\infty} \left(\frac{k_{1z,0,n}^H}{k} (C1_{0n} e^{jk_{1z,0,n}^H(L_3+L_2)} - D1_{0n} e^{-jk_{1z,0,n}^H(L_3+L_2)}) e^{j\theta_1} \right. \\
 & \quad \left. J_t(k_{r,t,s}^I \delta_1) \frac{R_1 k_{r,t,s}^I}{k_{1r,0,n}^H - k_{r,t,s}^I} J_0'(k_{r,t,s}^I R_1) J_0(k_{1r,0,n}^H R_1) \right) \\
 & + \sum_{m=1}^{\infty} \sum_{n=1}^{\infty} \left[(C1_{mn}^+ e^{jk_{1z,m,n}^H(L_3+L_2)} - D1_{mn}^+ e^{-jk_{1z,m,n}^H(L_3+L_2)}) J_{m+t}(k_{r,t,s}^I \delta_1) \right. \\
 & \quad \left. + (C1_{mn}^- e^{jk_{1z,m,n}^H(L_3+L_2)} - D1_{mn}^- e^{-jk_{1z,m,n}^H(L_3+L_2)}) (-1)^m J_{t-m}(k_{r,t,s}^I \delta_1) \right] \\
 & \quad \frac{k_{1z,m,n}^H}{k} \left(\frac{R_1 k_{r,t,s}^I}{k_{1r,m,n}^H - k_{r,t,s}^I} \right) J_m'(k_{r,t,s}^I R_1) J_m(k_{1r,m,n}^H R_1) e^{j\theta_1} \tag{7.62} \\
 & + (C2_{01} e^{jk(L_3+L_2)} - D2_{01} e^{-jk(L_3+L_2)}) e^{j\theta_0} J_t(k_{r,t,s}^I \delta_2) \frac{R_2}{k_{r,t,s}^I} J_1(k_{r,t,s}^I R_2) \\
 & + \sum_{n=2}^{\infty} \left(\frac{k_{2z,0,n}^H}{k} (C2_{0n} e^{jk_{2z,0,n}^H(L_3+L_2)} - D2_{0n} e^{-jk_{2z,0,n}^H(L_3+L_2)}) e^{j\theta_2} \right. \\
 & \quad \left. J_t(k_{r,t,s}^I \delta_2) \frac{R_2 k_{r,t,s}^I}{k_{2r,0,n}^H - k_{r,t,s}^I} J_0'(k_{r,t,s}^I R_2) J_0(k_{2r,0,n}^H R_2) \right)
 \end{aligned}$$

$$\begin{aligned}
 & + \sum_{m=1}^{\infty} \sum_{n=1}^{\infty} [(C2_{mn}^+ e^{jk_{2z,m,n}^H(L_3+L_2)} - D2_{mn}^+ e^{-jk_{2z,m,n}^H(L_3+L_2)}) J_{m+t}(k_{r,t,s}^I \delta_2) \\
 & \quad + (C2_{mn}^- e^{jk_{2z,m,n}^H(L_3+L_2)} - D2_{mn}^- e^{-jk_{2z,m,n}^H(L_3+L_2)}) (-1)^m J_{t-m}(k_{r,t,s}^I \delta_2)] \\
 & \quad \frac{k_{2z,m,n}^H}{k} \left(\frac{R_2 k_{r,t,s}^I}{k_{2r,m,n}^H - k_{r,t,s}^I} \right) J_m'(k_{r,t,s}^I R_2) J_m(k_{2r,m,n}^H R_2) e^{j\theta_2} \\
 & = \frac{k_{z,t,s}^I}{k} (A_{ts}^+ e^{jk_{z,t,s}^I(L_3+L_2)} - B_{ts}^+ e^{-jk_{z,t,s}^I(L_3+L_2)}) \frac{R_0^2}{2} \left(1 - \frac{t^2}{k_{r,t,s}^I R_0^2} \right) J_t^2(k_{r,t,s}^I R_0) .
 \end{aligned}$$

7.3.2 Experimental set-up

The experimental set-up for the two orifices situation is the same as that for the single orifice situation. The devices used in measurements are shown in Fig 7.2, with unused orifices being blocked with wooden blocks of the same thickness.

For device with two orifices situation, nine different comparative source-orifice relationship situations (shown in Fig 7.12) are considered. These situations can represent most possible source-orifice relationships for a device with two orifices.

7.3.3 Comparison of predictions with direct measurements for a device with two orifices

The predicted and direct measured acoustic pressures of different situations are shown in the figures below. In each figure, a) shows the predicted and direct measured acoustic pressures for the before orifice field; b) shows the predicted and direct measured acoustic pressures for the after orifice field; c) shows the errors between prediction and direct measurement for both the before orifice field and the after orifice field. In order to show these errors clearly, the results are transferred into 1/6 octave band.

For all situations shown below, the acoustic pressure plotted for the before orifice field is taken at the point with coordinate $(0.15m, \pi/3, -0.54m)$, which is $(100\%R, \pi/3, -18\%L)$ in non-dimensional form; acoustic pressure plotted for the after

aperture field is taken at the point with coordinate $(0.15m, \pi/3, -0.18m)$, which is $(100\%R, \pi/3, -6\%L)$ in non-dimensional form.

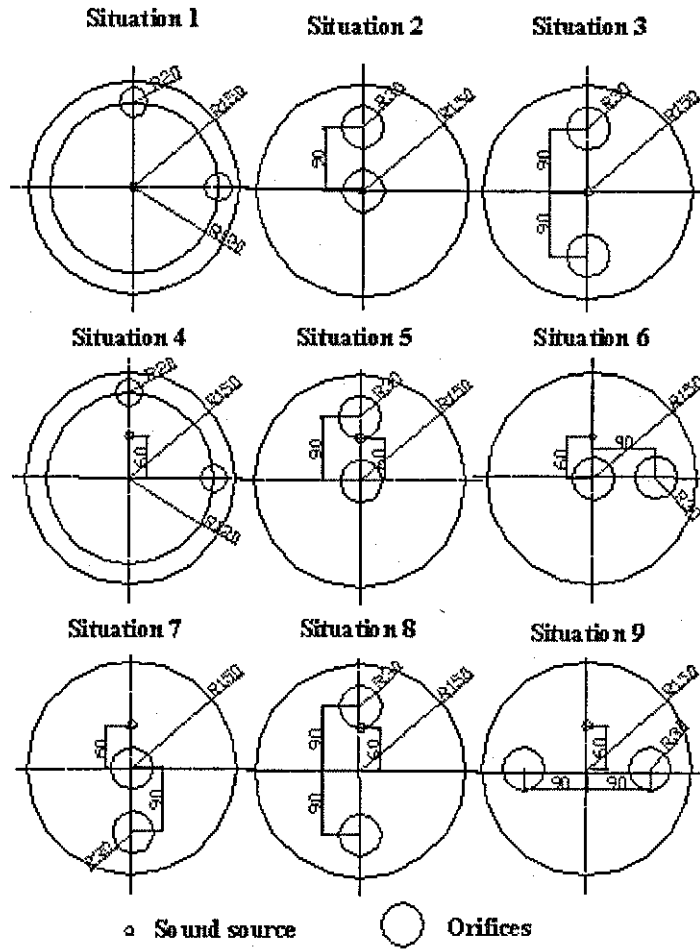


Fig 7.12 Comparative source – orifice relationships for device with two orifices

Because for some situations, the results are similar, so there is no need to shown all. Then only three situations are chosen and shown in the figures below. Two of the situations are source concentric situations and one is source eccentric situation. Fig 7.13 shows the concentric - axially-unsymmetric with concentric orifice situation (Situation 2 in Fig 7.12).

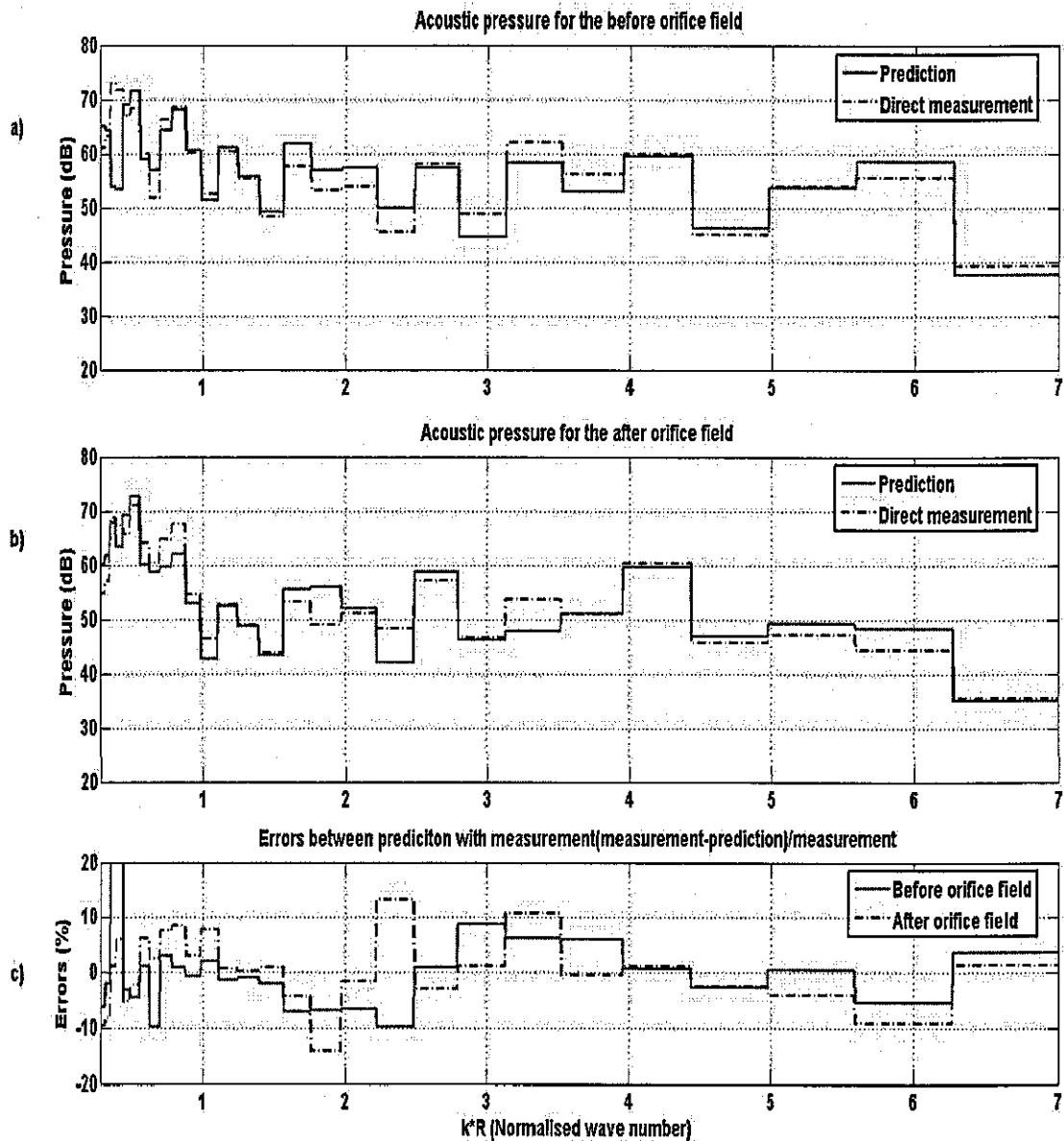


Fig 7.13 Comparison of the acoustic pressure for both the before orifice field and the after orifice field for device with two orifices (Situation 2 in Fig 7.12)

Fig 7.14 shows the concentric - axially-unsymmetric without concentric orifice situation (Situation 3 in Fig 7.12).

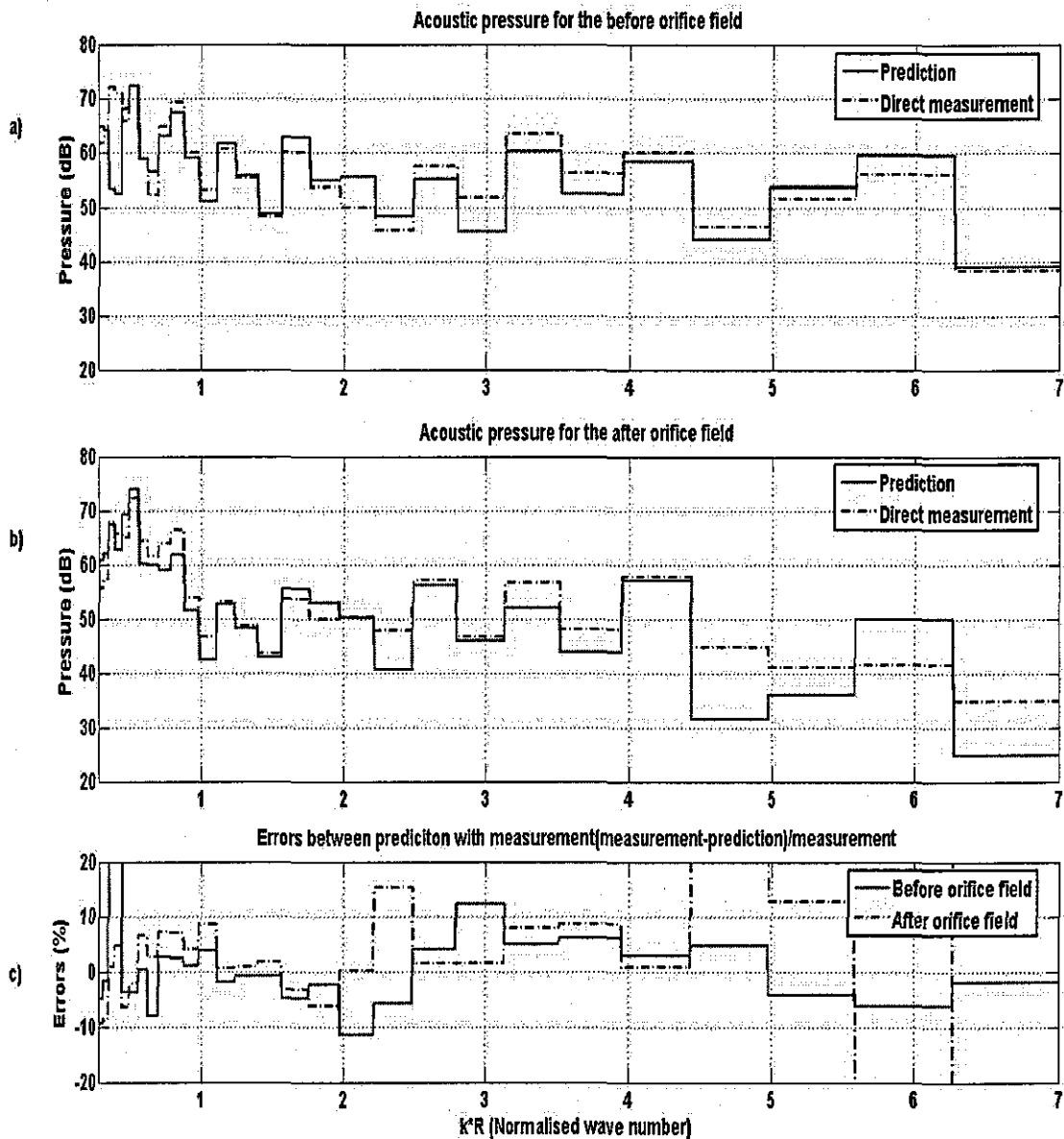


Fig 7.14 Comparison of the acoustic pressure for both the before orifice field and the after orifice field for device with two orifices (Situation 3 in Fig 7.12)

For the source eccentric situation, all six different orifice configurations give similar results. So only one situation (Situation 9 in Fig 7.12) is chosen and the results are shown below.

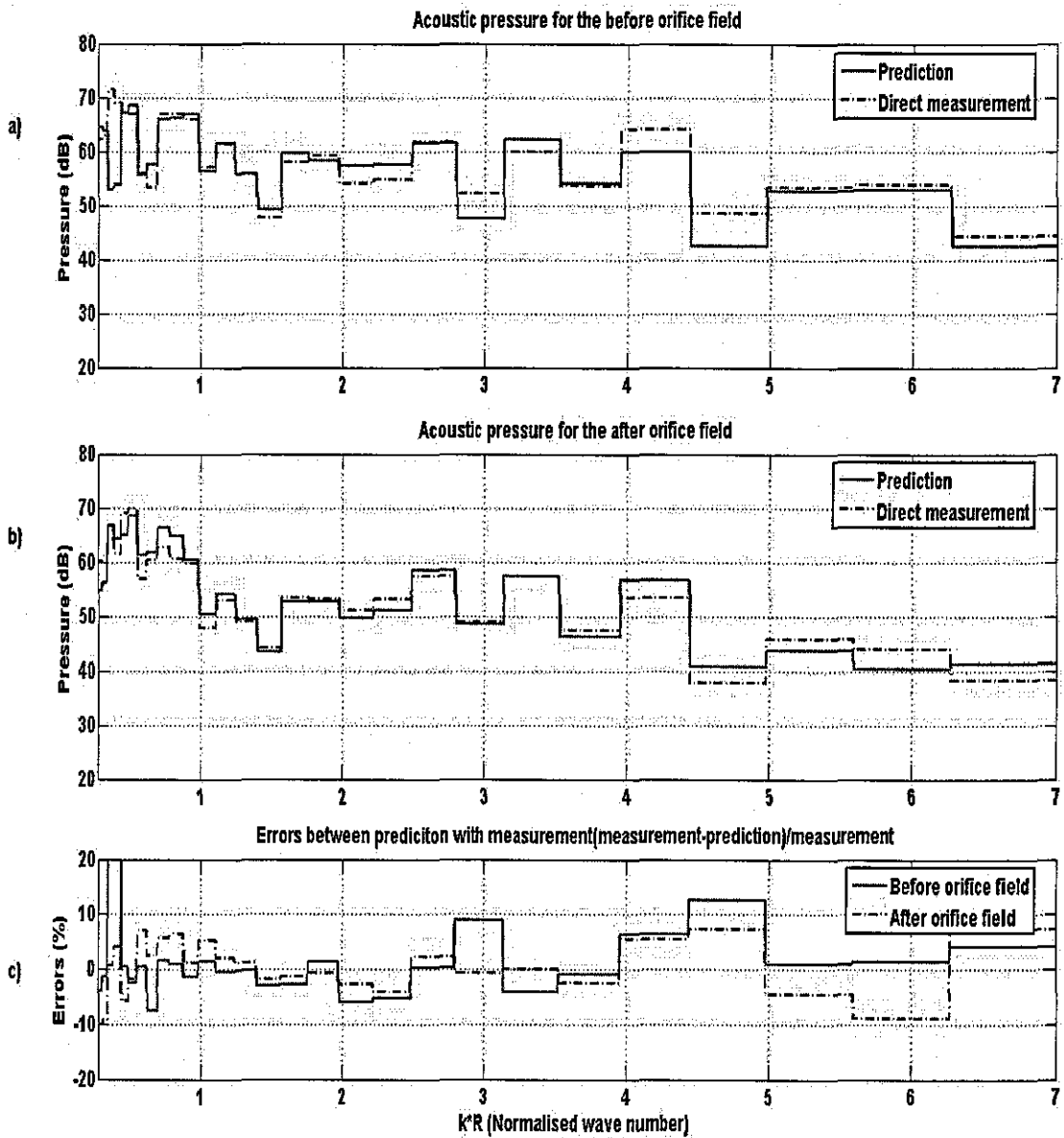


Fig 7.15 Comparison of the acoustic pressure for both the before orifice field and the after orifice field for device with two orifices (Situation 9 in Fig 7.12)

From Fig 7.13 -7.15, it can be seen that

1. For the source concentric situation, if an orifice in the device is concentric to the main duct, predictions for both the before orifice field and the after orifice field agree with the direct measurements (less than $\pm 10\%$ of direct measurements).
2. However if there is no orifice in the device which is concentric to the main duct, such as Situation 1 and Situation 3, predictions do not agree with the direct measurements, especially for the after orifice field. As shown in Fig 7.14, the largest errors appear when (0, 2) mode cuts on ($k * R > 4$). The reason is given in the single orifice situation.
3. For source eccentric situation, six different configurations of the orifices have been considered and from the results shown in Fig 7.15, it can be seen that other than at very low normalized wave number range, the predictions for both the before orifice field and the after orifice field agree with the direct measurements (less than $\pm 10\%$ of direct measurements). Which means for these situations, this model works well in the decomposition of the in-duct field. Because for all these situations, there are always at least one eccentric orifice in the aperture device, so for both the before orifice field and the after orifice field, those axially-unsymmetric higher-order modes are dominant in the in-duct field.

7.4 Device with several orifices

7.4.1 Theoretical derivation

The effects of the device with two orifices situation have been studied in previous section. In this section, the effects of several orifices on the in-duct field will be discussed. If the device consists of more than two orifices (as shown in the right picture of Fig 7.2), with radius $R_1, R_2 \dots R_n$ respectively, the boundary conditions at 2 and 3 are given as below,

At boundary 2, for the acoustic pressure,

$$P_C + P_D|_{Z=-L_3} = P_E + P_F|_{Z=-L_3} \quad (\text{over } S_1, S_2 \dots S_n). \quad (7.63)$$

For the velocity,

$$U_C + U_D|_{Z=-L_3} = U_E + U_F|_{Z=-L_3} \quad (\text{over } S_1, S_2 \dots S_n), \quad (7.64)$$

$$U_E + U_F \Big|_{Z=-L_3} = 0 \quad (\text{over } (S - S_1 - S_2 \dots - S_n)) . \quad (7.65)$$

At boundary 3, the acoustic pressure,

$$P_C + P_D \Big|_{Z=-L_3-L_2} = P_A + P_B \Big|_{Z=-L_3-L_2} \quad (\text{over } S_1, S_2 \dots S_n) . \quad (7.66)$$

For the velocity,

$$U_C + U_D \Big|_{Z=-L_3-L_2} = U_A + U_B \Big|_{Z=-L_3-L_2} \quad (\text{over } S_1, S_2 \dots S_n) , \quad (7.67)$$

$$U_A + U_B \Big|_{Z=-L_3-L_2} = 0 \quad (\text{over } (S - S_1 - S_2 \dots - S_n)) . \quad (7.68)$$

Just following the derivation procedure of the two orifices situation, one can easily get the equations for the device with several orifices situation. These equations are similar to those obtained for the two orifices situation.

7.4.2 Experimental set-up

The experimental set-up for several orifices situation is the same as that for the single orifice situation and the two orifices situation. The devices used in measurements are shown in Fig 7.2, with unused orifices being blocked with wooden blocks of same thickness.

For several orifices situation, ten different comparative source - orifice relationship situations are considered. These situations can represent many possible source - orifice relationships for several orifices situation. From these ten different situations, one can not only test the effects of up to 28% open area in the device on the in-duct field, but also test the effects of different orifice combinations on the in-duct field.

7.4.3 Comparison of predictions with direct measurements for a device with several orifices

In order to keep the results comparable, the predicted and direct measured acoustic pressures of different situations are shown in figures below. In each figure, a) shows the predicted and direct measured acoustic pressures for the before orifice field; b) shows the predicted and direct measured acoustic pressures for the after orifice field; c) shows

the errors between prediction and direct measurement for both the before orifice and the after orifice field. In order to show these errors clearly, the results are transferred into 1/6 octave band.

For all situations shown below, the acoustic pressure plotted for the before aperture field is taken at the point with coordinate $(0.15m, \pi/3, -0.54m)$, which is $(100\%R, \pi/3, -18\%L)$ in non-dimensional form; acoustic pressure plotted for the after aperture field is taken at the point with coordinate $(0.15m, \pi/3, -0.18m)$, which is $(100\%R, \pi/3, -6\%L)$ in non-dimensional form.

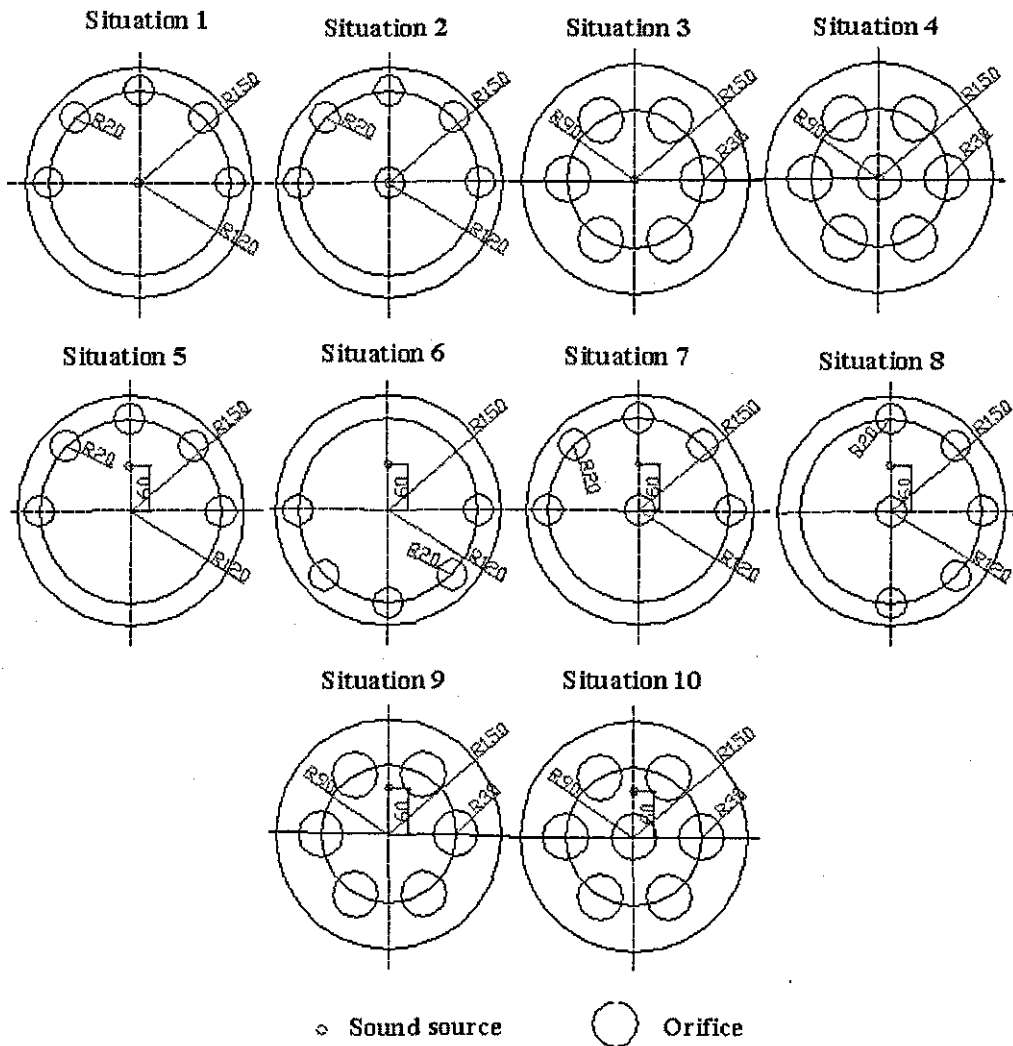


Fig 7.16 Comparative source – orifice relationships for device with several orifices

For all these ten situations, three situations are chosen and shown in Fig 7.17 to Fig 7.19. In which two of them are the source concentric situations and one is the source eccentric situation. Fig 7.17 shows the sound source concentric to the main duct, while the orifices are axially-unsymmetric to the main duct without concentric orifice situation (Situation 1 in Fig 7.16).

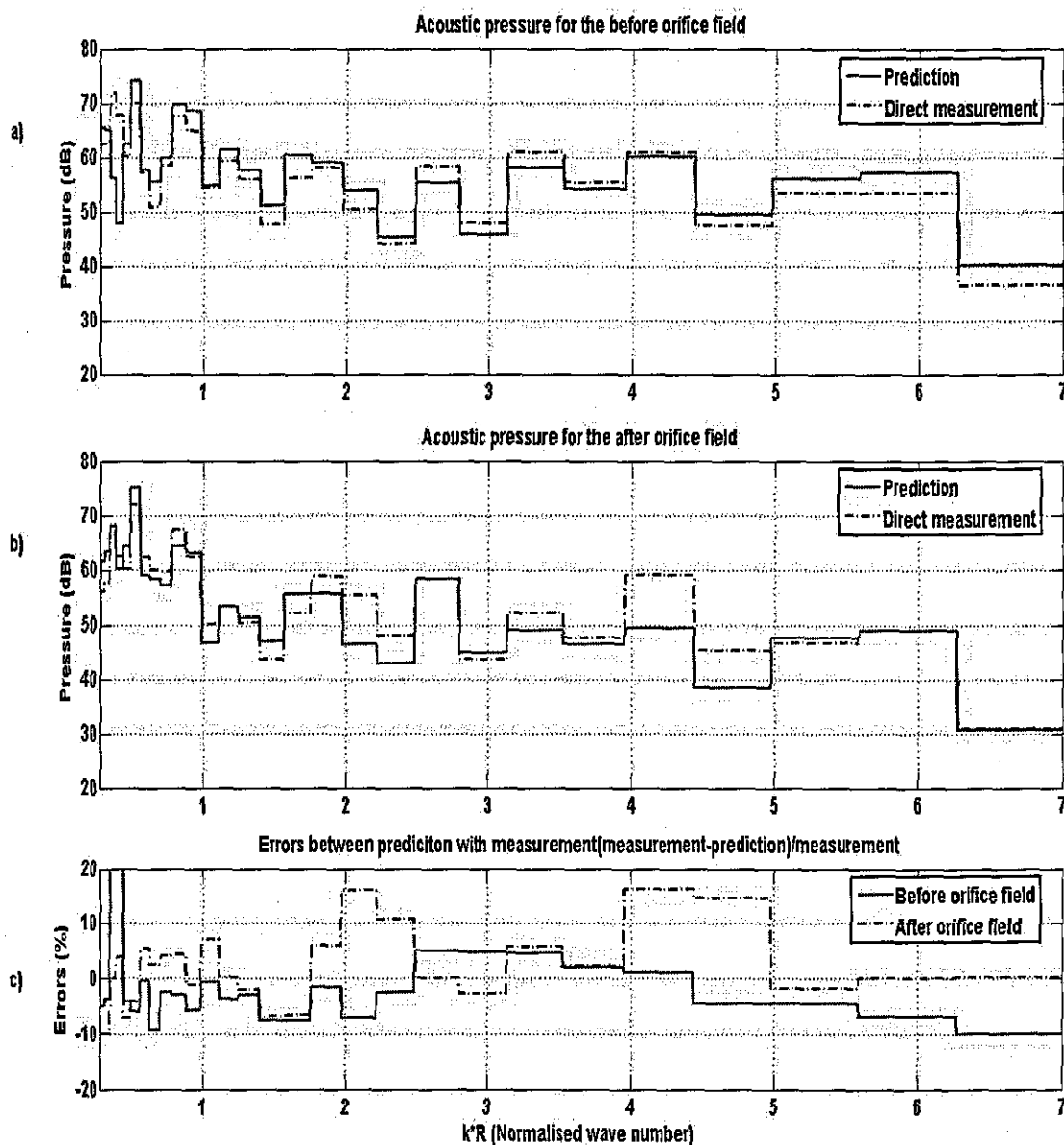


Fig 7.17 Comparison of the acoustic pressure for both the before orifice field and the after orifice field for device with several orifices (Situation 1 in Fig 7.16)

Fig 7.18 shows the sound source is concentric to the main duct, while the orifices are axially-symmetric to the main duct with concentric orifice situation (Situation 4 in Fig 7.16).

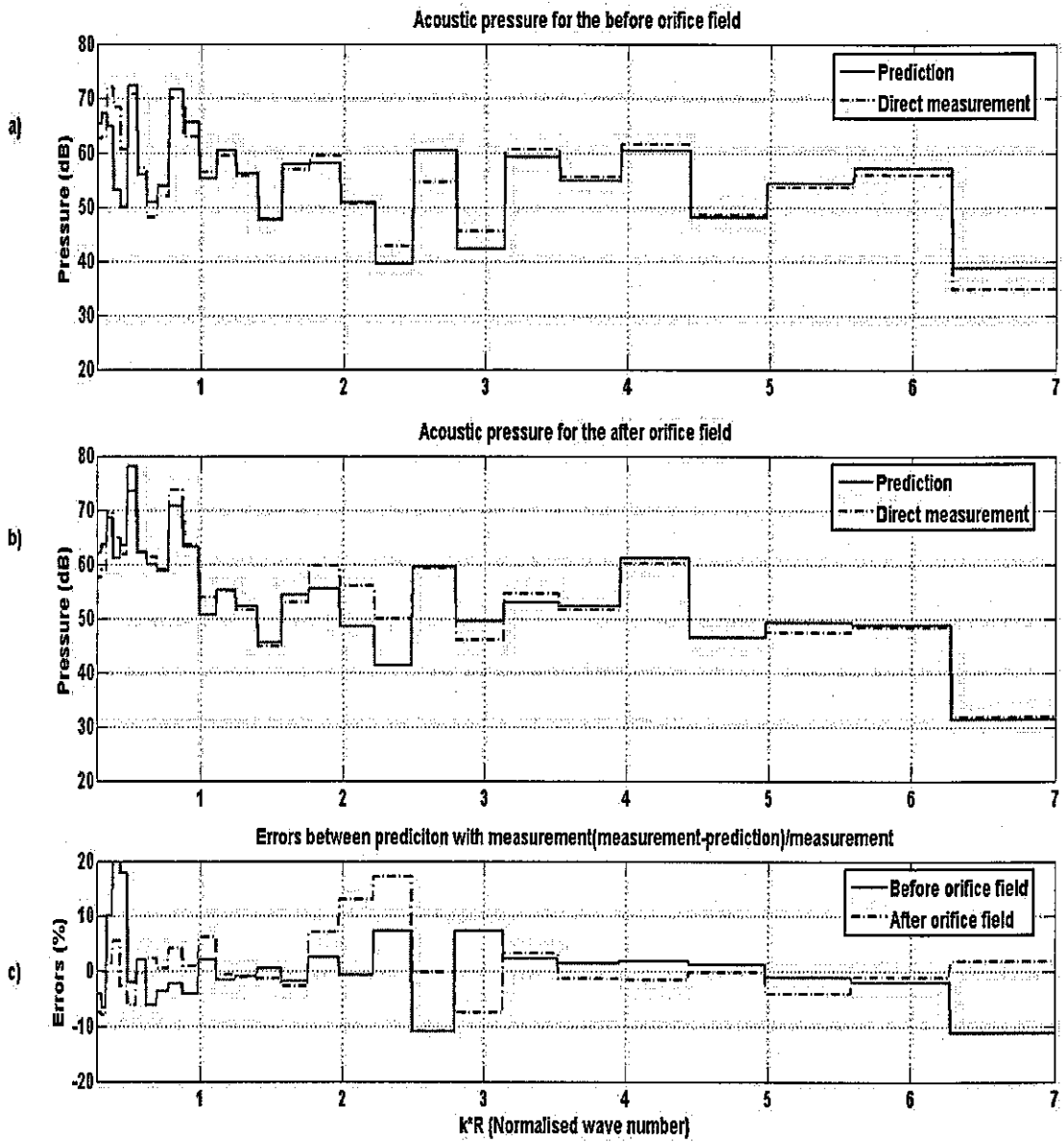


Fig 7.18 Comparison of the acoustic pressure for both the before orifice field and the after orifice field for device with several orifices (Situation 4 in Fig 7.16)

Fig 7.19 shows the sound source eccentric to the main duct, while the orifices are axially-unsymmetric to the main duct with concentric orifice situation (Situation 8 in Fig 7.16).

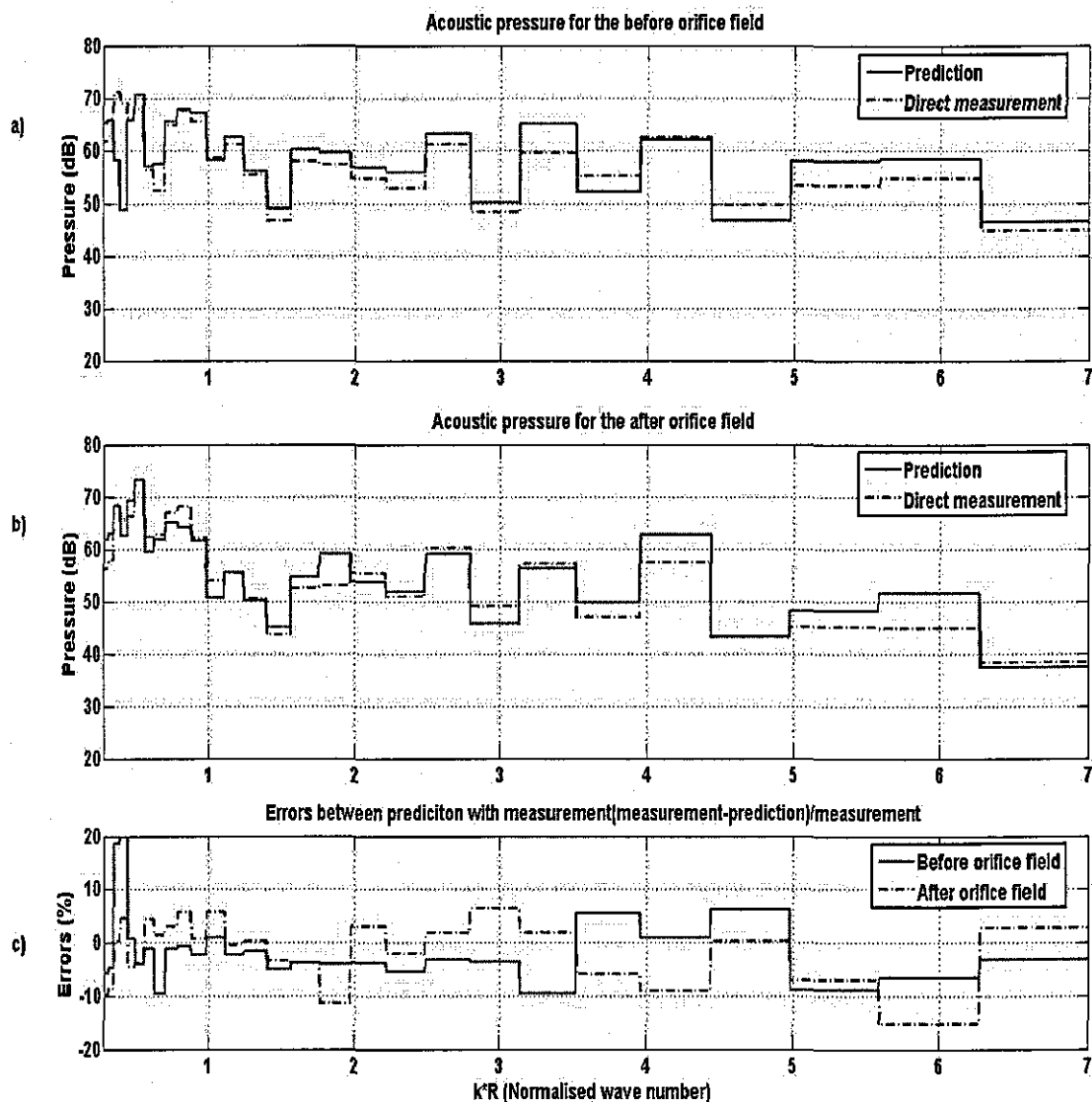


Fig 7.19 Comparison of the acoustic pressure for both the before orifice field and the after orifice field for device with several orifices (Situation 8 in Fig 7.16)

From Fig 7.17-7.19, it can be seen that

1. For source concentric situation, still if an orifice in the device is concentric to the main duct (Situation 2 and Situation 4), predictions for both the before orifice field and the after orifice field agree with the direct measurements (less than $\pm 10\%$ of direct measurements). However if there is no orifice in the device which is concentric to the main duct, such as Situation 1 and Situation 3, no

matter those orifices are axially-symmetric (Situation 3) or axially-unsymmetric (Situation 1), predictions do not agree with the direct measurements, especially for the after orifice field. As shown in Fig 7.17, the largest errors appear when (0, 2) mode cuts on ($k * R > 4$). The reason is given in the single orifice situation.

2. For source eccentric situation, six different configurations of the orifices have been considered and from the results shown in Fig 7.19, one can see that other than at very low normalized wave number range, the predictions for both the before orifice field and the after orifice field agree with the direct measurements (less than $\pm 10\%$ of direct measurements). Which means for these situations, this model works well in the decomposition of the in-duct field.

7.5 Error analysis

From all these figures shown above, it can be seen that for all these situations, predictions for the before orifice field agree with direct measurements. Other than the very low normalized wave number range ($k * R < 0.8$), the errors between predictions and direct measurements are less than 10% of direct measurements, or even smaller. Which means this model is effective in prediction of acoustic properties in the before orifice field, as well as in decomposition of the before orifice field into single higher-order mode.

For most situations, such as concentric-concentric situation and eccentric-eccentric situations, predictions for the after orifice field agree with direct measurements. Still other than the normalized wave number range ($k * R < 0.8$), the errors between predictions and direct measurements in these situations are less than 10% of the direct measurements. Which means for these situations, through measurements in the before orifice field, one can accurately predict those acoustic properties in the after orifice field.

However for some other situations, predictions for the after orifice field do not agree with direct measurements in some normalized wave number range. These situations can be divided into two groups: source concentric group and source eccentric group.

For the source concentric group, if there is no orifice located concentric to the main duct, no matter how many orifices are in the device (Situation 2 in Fig 7.6, Situation 1 and 3 in Fig 7.12, Situation 1 and 3 in Fig 7.16), the predictions for the after orifice field do not agree with the direct measurements. However, through the comparison between Fig 7.8 and Fig 7.13, one can see if there is an extra concentric orifice presented in the device, the predictions agree with the direct measurements. This concentric orifice can produce those axially-symmetric higher-order modes in the after orifice field. So these situations can be described as *source concentric and no concentric orifice* situation.

For the source eccentric group, if there is only a single concentric orifice in the device (Situation 3 in Fig 7.6), the predictions for the after orifice field do not agree with the direct measurements. For all other situations, predictions agree well with the direct measurement. So this situation can be described as *source eccentric and only one concentric orifice* situation.

So other than these two different situations discussed above, one can predict both the before orifice field and the after orifice field with just two reference measurements in the before orifice field. But for these two special situations, in order to get accurate prediction for the after orifice field, another two reference points in the after orifice field, which are located at $(0.15m(100\%R), 0, -0.12m(-4\%L))$ and $(0.15m(100\%R), 2 * \pi / 3, -0.20m(-6.67\%L))$, respectively, are used.

Using these two reference measurements for the predictions in the after orifice field (the procedure is given in Appendix E), for *source concentric and no concentric orifice* situation, take the source-orifice relationship shown as Situation 3 in Fig 7.12 for example, the results are shown in Fig 7.20. For *source eccentric and only one concentric orifice* situation, the results are shown in Fig 7.21 (predictions for the before orifice field are still using those two before orifice field reference measurements and are not shown here).

7. Sound field produced by a point source propagating in a circular duct with simple aperture devices

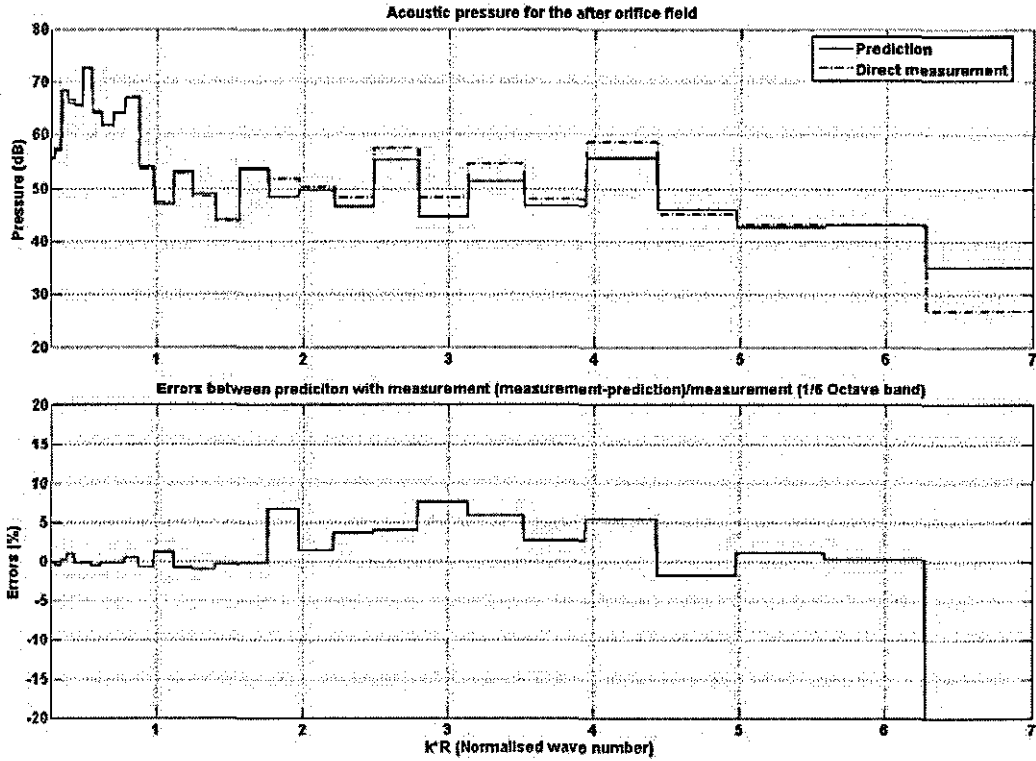


Fig 7.20 Comparison of prediction with direct measurement for the after orifice field (a) shows pressure; b) shows errors between prediction and measurement)

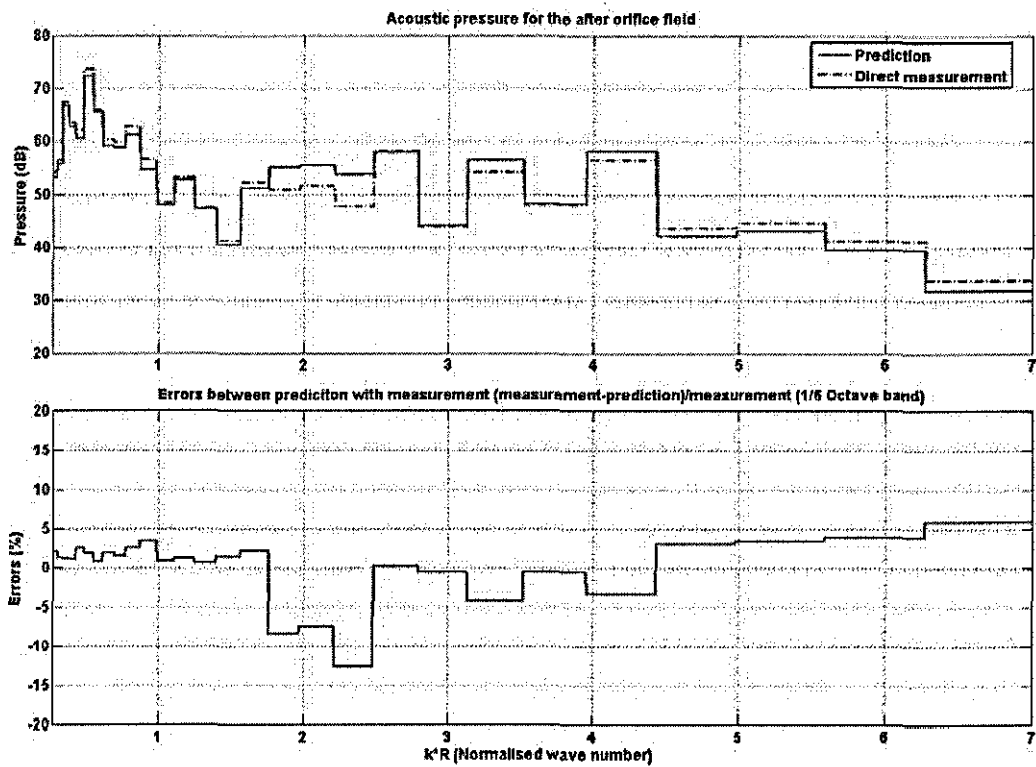


Fig 7.21 Comparison of prediction with direct measurement for the after orifice field (a) shows pressure; b) shows errors between prediction and measurement)

From Fig 7.20 - 7.21, it can be seen that for these two specific situations, predictions for the after orifice field by using reference measurements in the after orifice field agree with direct measurements. Which means through the reference measurements in the after orifice field, one can still decompose the after orifice field effectively for these two specific situations.

7.6 Discussion

In this chapter, a simple aperture device is placed in the duct and twenty five different source-orifice relationships (including one orifice, two orifices and several orifices) are discussed and from the results shown, one can see that the predictions for both the before and the after orifice fields are considered acceptable. This means the model proposed to describe the boundary conditions of the simple aperture device is effective and the combination of the simple aperture device boundary conditions with the point source boundary and open end boundary can give accurate solution for the whole in-duct field. So using this model, one can achieve the decomposition of the in-duct field both before and after aperture device.

By successfully decomposing the in-duct field into different higher-order modes, one can study the effects of different aperture devices on the different higher-order modes. This will be discussed in detail in Chapter 9.

Chapter 8 Sound field produced by a plane wave source propagating in a circular duct with simple aperture devices

8.1 Introduction

Compared with the point source, the plane wave source is more widely adopted in the analysis of engineering utilities, such as ventilation ducts and mufflers. In most situations there are devices installed in duct either for noise reduction or flow control. So in order to analyse the acoustic properties of these systems, the effects of the devices on the acoustic fields need to be fully understood.

In Chapter 7, the sound field produced by a point source in a circular duct with a simple aperture device has been studied and the model which combines those boundary condition descriptions together to decompose the in-duct field is considered to be acceptable for further use. So based on the study made in Chapter 6, the same simple aperture device used in the last chapter is placed in the circular duct and its effects on the acoustic field produced by the plane wave source will be studied. The same model proposed to describe the boundary conditions between the main duct field and the orifice field in Chapter 7 is still applied here. Combining these boundary descriptions with those of the plane wave source boundary and open end boundary descriptions, it is possible to get the solution for the amplitudes of the acoustic field in the duct. By knowing these amplitudes, one can study the effects of the aperture device on the acoustic field in detail.

8.2 Aperture device with a single orifice

8.2.1 Theoretical derivation

Fig 8.1 shows the various regions with an aperture device presented in the duct. It is quite similar to that is shown in Fig 7.1. Compared with Fig 7.1, the only difference lies in the region 5 (source region). In this chapter, the sound field produced by a plane wave source is investigated.

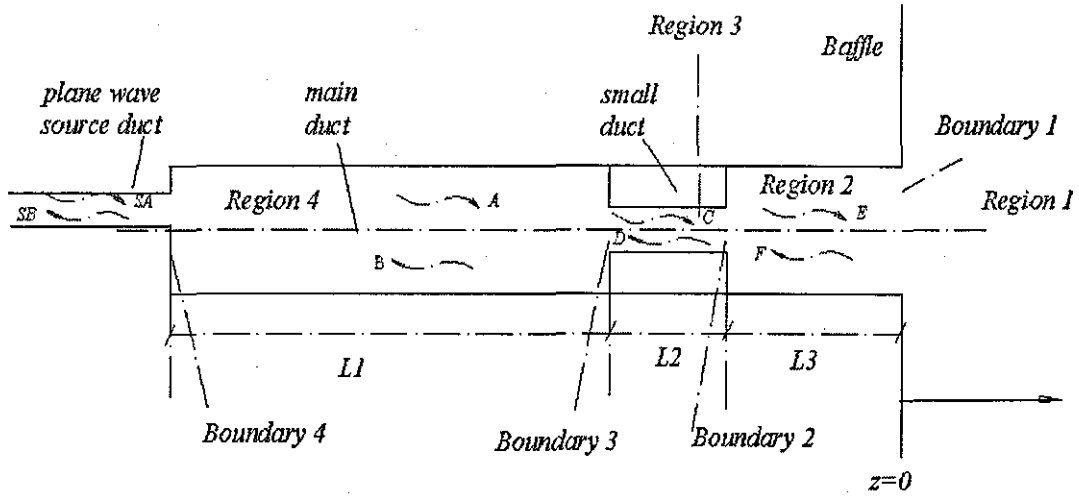


Fig 8.1 Plot of Circular duct with simple aperture device

At boundary 1 (open end boundary), according to the analysis presented in Chapter 4, the following equation can be obtained,

$$F_{mn} = \sum_{L=1}^{\infty} R_{mL} E_{mL} \tag{8.1}$$

At boundary 2 and boundary 3, the boundary conditions continuities can be expressed in the same form as equation (7.10) to equation (7.15). So following the same procedure, one can get the same equations as those from equation (7.16) to equation (7.31).

Boundary 4 is the boundary between the plane wave source and the main duct, As discussed in Chapter 4, one can get eight equations from equation (4.11) to (4.18) for this boundary. So combining equation (8.1), equation (7.16) to equation (7.31) with equation (4.11) to equation (4.18), one can have an equation group for the solution of the acoustic properties in circular duct with a simple aperture device, which is given as

$$[X]_{D \times D} \begin{bmatrix} A_{mn} \\ B_{mn} \\ SB_{01} \\ C_{mn} \\ D_{mn} \\ E_{mn} \\ F_{mn} \end{bmatrix}_{D \times 1} = \begin{bmatrix} SA_{01} \\ 0 \end{bmatrix}_{D \times 1} \tag{8.2}$$

in which X is the coefficient matrix for these amplitudes. Again like the matrix X in Chapter 7, its dimension D is decided by how many higher-order modes are considered in the main duct region, the orifice region and the source duct region.

If $m = \pm 5$ and $n = 5$, the dimension of the matrix X should be 385×385 ($3 \times (2 \times n + 4 \times |m| \times n) + (n + 2 \times |m| \times n)$). This means compared with the matrix X obtained in Chapter 6 for duct without aperture device, matrix X in this chapter is a significantly larger one. So in order to keep this matrix well conditioned, the method used in the former three chapters to solve the singularity of the matrix is also adopted here. By only considering those higher-order modes which have been cut on in the main duct region, the orifice region and the source duct region, one can make sure that the powers of the exponential items $e^{jk_{z,m,n}L}$ appeared in matrix X are always complex numbers rather than real numbers.

After treating the matrix X in the manner as described in Chapter 5, one can multiply both sides of equation (8.2) by the inversion of the matrix X , then the solution for this equation is obtained as well as those amplitudes, such as SB_{01} , A_{mn} , B_{mn} , C_{mn} , D_{mn} , E_{mn} and F_{mn} (The detailed procedure is given in Appendix F).

8.2.2 Experimental set-up and measurement results

According to the theoretical derivation described above, one can see there is no limitation on or requirement for the thickness of the aperture devices and the radius of the orifice. However if the thickness of the device is very small, then the descriptions for boundaries 2 and 3 are so similar that the matrix X approaches singularity. Also in engineering situations, the thickness of the aperture device is normally not very large compared to wavelength. So in this investigation, the thickness of the aperture device is taken as $L = 0.025m$ which gives a range of $k * L$ values from 0 to 1.2. As shown in Fig 7.2, two different orifice radii are selected, which are $r = 0.03m$ (open area is 4% of total area) and $r = 0.02m$ (open area is 1.7% of total area) respectively.

The experimental set-up is shown in Fig 8.2. It is similar to experimental set-up adopted in Chapter 6. The aperture device is still placed in $z = -0.4m$ ($-13.3\%L$). Two rings of measurement points, located at $z = -0.54m$ ($-18\%L$) and $z = -0.18m$ ($-6\%L$) respectively, are taken for appointed position measurements (direct measurements) in the before orifice field and the after orifice field. Two reference measurement positions, located at $(0.15m(100\%R), 0, -2.33m(-74.3\%L))$ and $(0.15m(100\%R), 3 * \pi / 4, -1.5m(-50\%L))$, are taken for the reference measurement in the before orifice field.

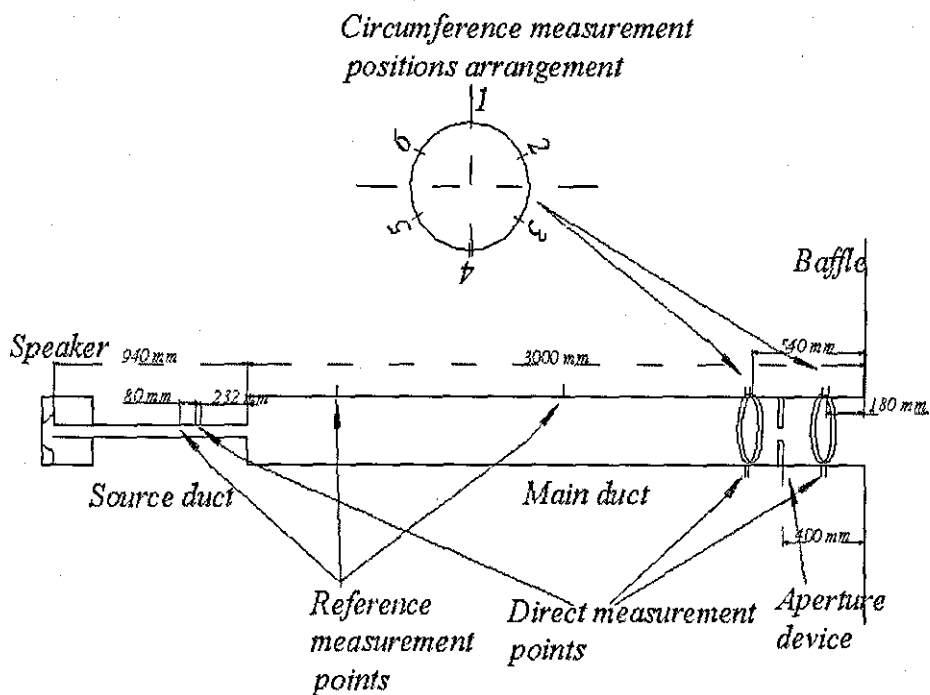


Fig 8.2 Experimental set-up for acoustic properties measurement for both the before orifice field and the after orifice field

In order to show the effects of aperture device on the acoustic properties in the circular duct, two situations, which are the sound source concentric and eccentric to the main duct respectively, are selected. The acoustic pressures measured at positions before the orifice and after the orifice are shown in Fig 8.3. Fig 8.3 a) and Fig 8.3 b) show the acoustic pressure when the sound source is concentric to the main duct. In which, 'without aperture device' means there is no aperture device in duct; 'with aperture device' means there is a device with a single orifice which is also concentric to the main

duct (Situation 1 in Fig 8.5). Fig 8.3 c) and Fig 8.3 d) show the acoustic pressure when the sound source is eccentric to the main duct. Again in which, 'without aperture device' means there is no aperture device in duct; 'with aperture device' means there is a device with a single orifice which is also eccentric to the main duct (Situation 5 in Fig 8.5).

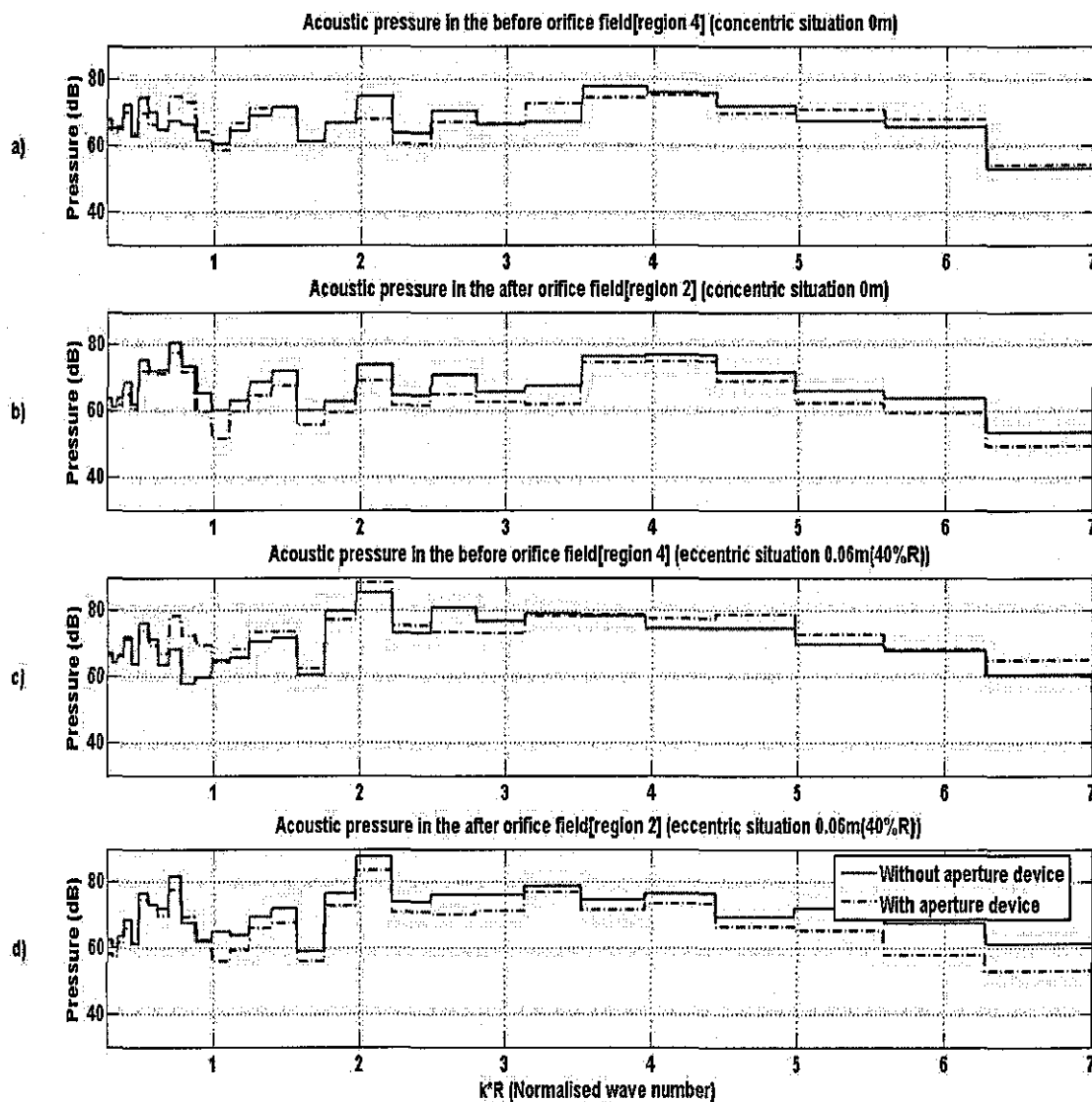


Fig 8.3 Comparison of the acoustic pressures measured at different positions for without aperture device and with aperture device situations

This figure is similar to Fig 7.4, so it can also be seen from this figure that

1. For very low normalized wave number range ($k \cdot R < 0.8$), the presence of the aperture device has very little effect on the acoustic pressures in both the before orifice field and the after orifice field at very low frequency range.

2. However other than that normalized wave number range ($k * R > 0.8$), the effects of the aperture device on the acoustic properties in circular duct are apparent. However the effects on the before orifice field are not very significant.
3. For the before orifice field, in the normalized wave number region $k * R > 3.5$, there is an increased pressure when the device is installed. However for the after orifice field, there is a decreased pressure when the device is installed. So the installation of the device reduces the pressure in the after orifice field at higher wave numbers.
4. Compared with the effects on the before orifice field, the effects on the after orifice field are larger, especially for higher normalized wave number range ($k * R > 5$).

8.2.3 Comparison of coupled and uncoupled predictions

In Chapter 6 for duct without an aperture device, it was concluded that at the open end of the duct, the cross coupling effects between higher-order modes could be neglected. So in this section, these cross coupling effects are reconsidered when there is an aperture device placed in the duct.

Consider the plane wave source located at $r = 0.06m(40\%R)$ and the aperture device located at $z = -0.4m(-13.3\%L)$ for example. The results from this configuration are shown in Fig 8.4. Fig 8.4 a) shows the coupled, uncoupled predictions and direct measurements for the before orifice field; Fig 8.4 b) shows coupled, uncoupled predictions and direct measurements for the after orifice field; Fig 8.4 c) shows the difference between coupled and uncoupled predictions for both the before orifice field and the after orifice field.

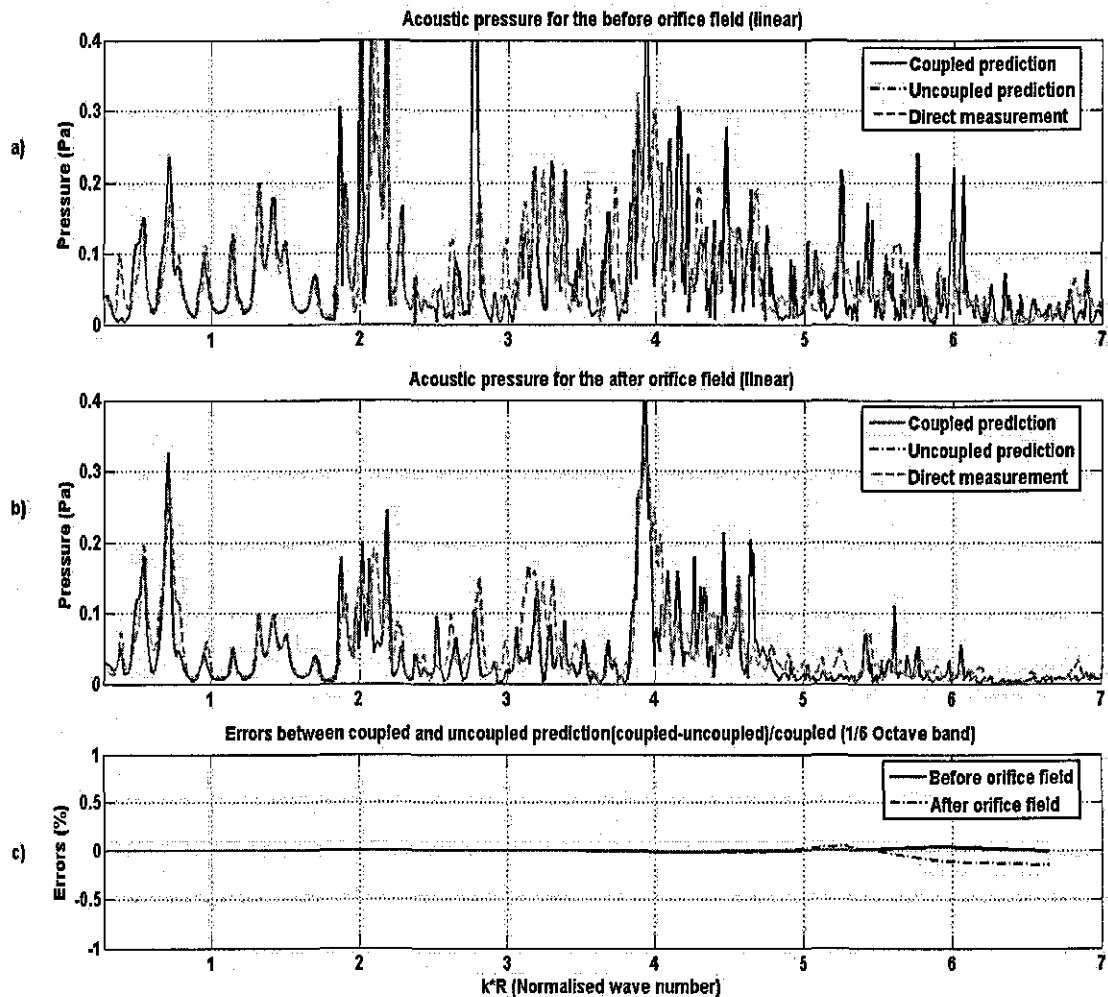


Fig 8.4 Comparison of coupled, uncoupled predictions with direct measurements in the before orifice and the after orifice field

From this figure it can be seen that for the after orifice field, there is a small difference between the coupled and uncoupled predictions when the normalised wave number is larger than 5. However this difference is so small (less than 0.5%) that it can be neglected. For the before orifice field, there is nearly no difference between the coupled and uncoupled predictions, which means that the cross coupling effects shown in equation (3.57) between the higher-order modes at the open end of the duct are negligible. So in following analysis, the cross coupling effects are not considered and it is assumed that no cross coupling effects happen at the end of the duct.

This conclusion is the same as those obtained in Chapter 5 and Chapter 7. Which means for both types of the sound source, no matter there is an simple aperture device in the

duct or not, the self coupling effects (coupling between (m,n) mode and (m,n) mode) are the dominate one and the cross coupling effects (coupling between (m,n) mode and (m,N) modes) are very small. From these conclusions, it can also be seen that the coupling effects at the open end of the duct are independent on the type of the sound source, as well as the aperture device. So the cross coupling effects can be considered negligible for both types of source in the situations under consideration.

8.2.4 Comparison of predictions with direct measurements for a device with single orifice

For a device with a single orifice, six source-orifice relationships (shown in Fig 8.5), which are concentric-concentric, concentric-eccentric, eccentric-concentric, eccentric-eccentric (three situations), are considered. Again for all situations shown below, the acoustic pressure plotted for the before aperture field is taken at the point with coordinate $(0.15m, \pi/3, -0.54m)$, which is $(100\%R, \pi/3, -18\%L)$ in non-dimensional form; pressure plotted for the after aperture field is taken at the point with coordinate $(0.15m, \pi/3, -0.18m)$, which is $(100\%R, \pi/3, -6\%L)$ in non-dimensional form.

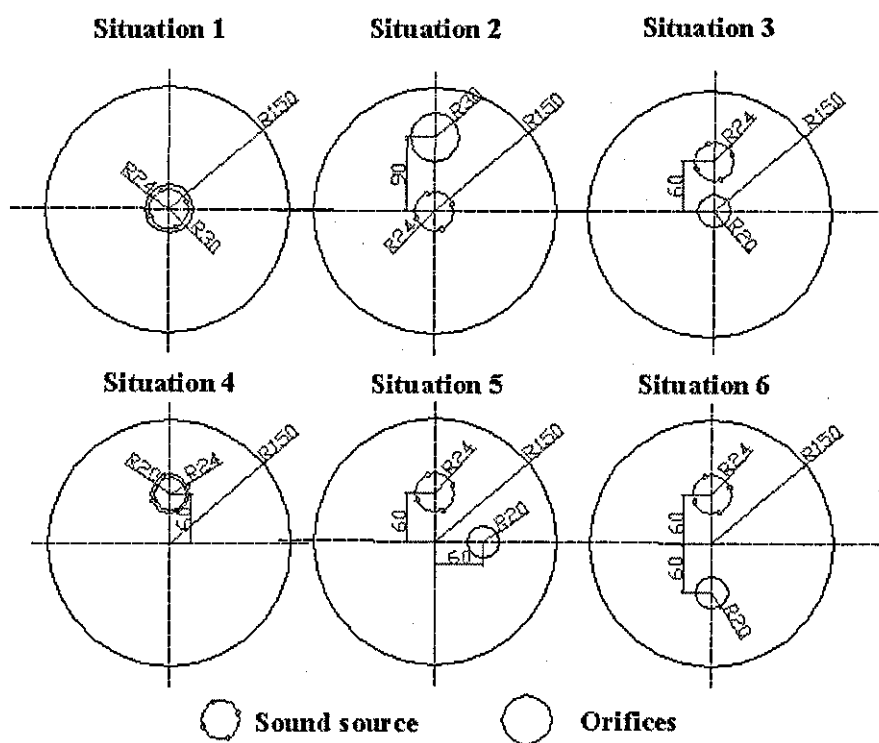


Fig 8.5 Comparative source – orifice relationships for device with single orifice

Because the results for some situations are similar, so not all situations shown in Fig 8.5 are displayed, only four situations are selected and shown below. In each figure, *a*) shows the acoustic pressure for the before orifice field; *b*) shows the acoustic pressure for the after orifice field; *c*) shows the errors between predictions and direct measurements for both the before orifice field and the after orifice field. In order to show these errors clearly, the results are transferred into 1/6 octave band.

Fig 8.6 shows the concentric-concentric situation (Situation 1 in Fig 8.5).

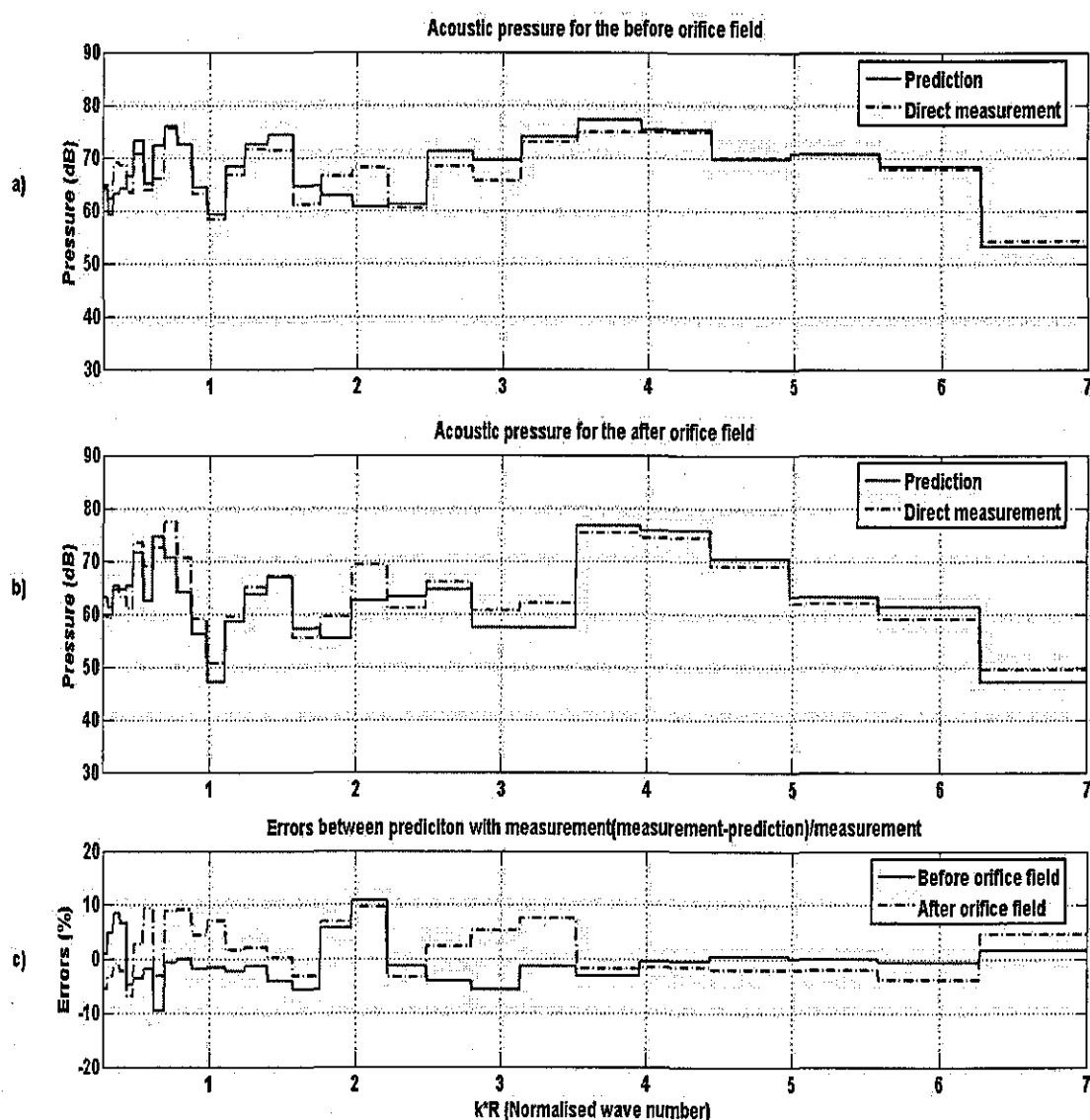


Fig 8.6 Comparison of the acoustic pressure for both the before orifice field and the after orifice field for device with single orifice (Situation 1 in Fig 8.5)

Fig 8.7 is for the concentric-eccentric situation (situation 2 in Fig 8.5).

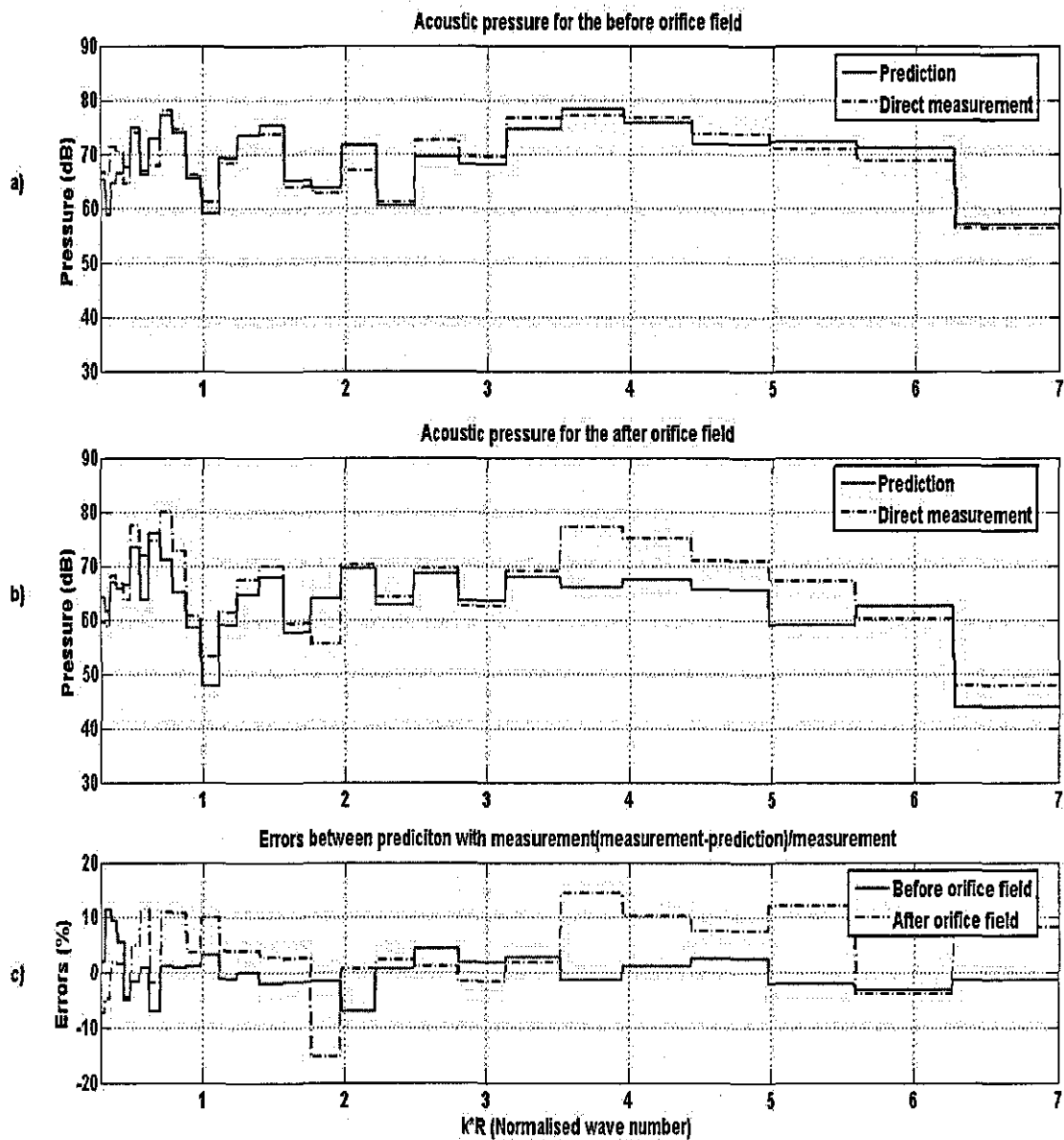


Fig 8.7 Comparison of the acoustic pressure for both the before orifice field and the after orifice field for device with single orifice (Situation 2 in Fig 8.5)

Fig 8.8 is for the eccentric-eccentric situation (situation 5 in Fig 8.5). Altogether three different comparative relationships (Situation 4, 5 and 6 in Fig 8.5) are considered and the results for these three different situations are similar, so situation 5 is chosen to show below.

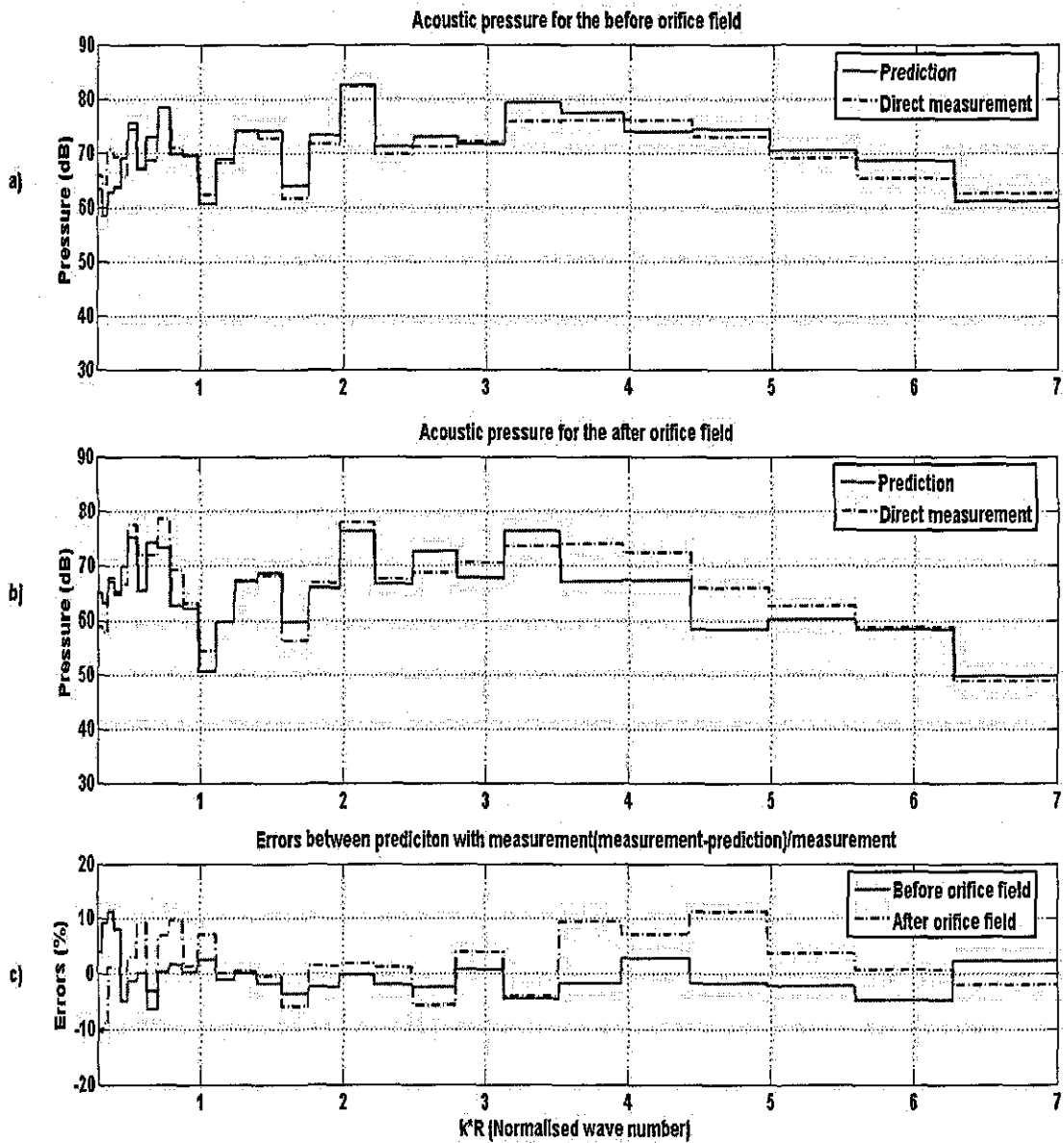


Fig 8.8 Comparison of the acoustic pressure for both the before orifice field and the after orifice field for device with single orifice (Situation 5 in Fig 8.5)

Finally, Fig 8.9 is for the eccentric-concentric situation (Situation 3 in Fig 8.5).

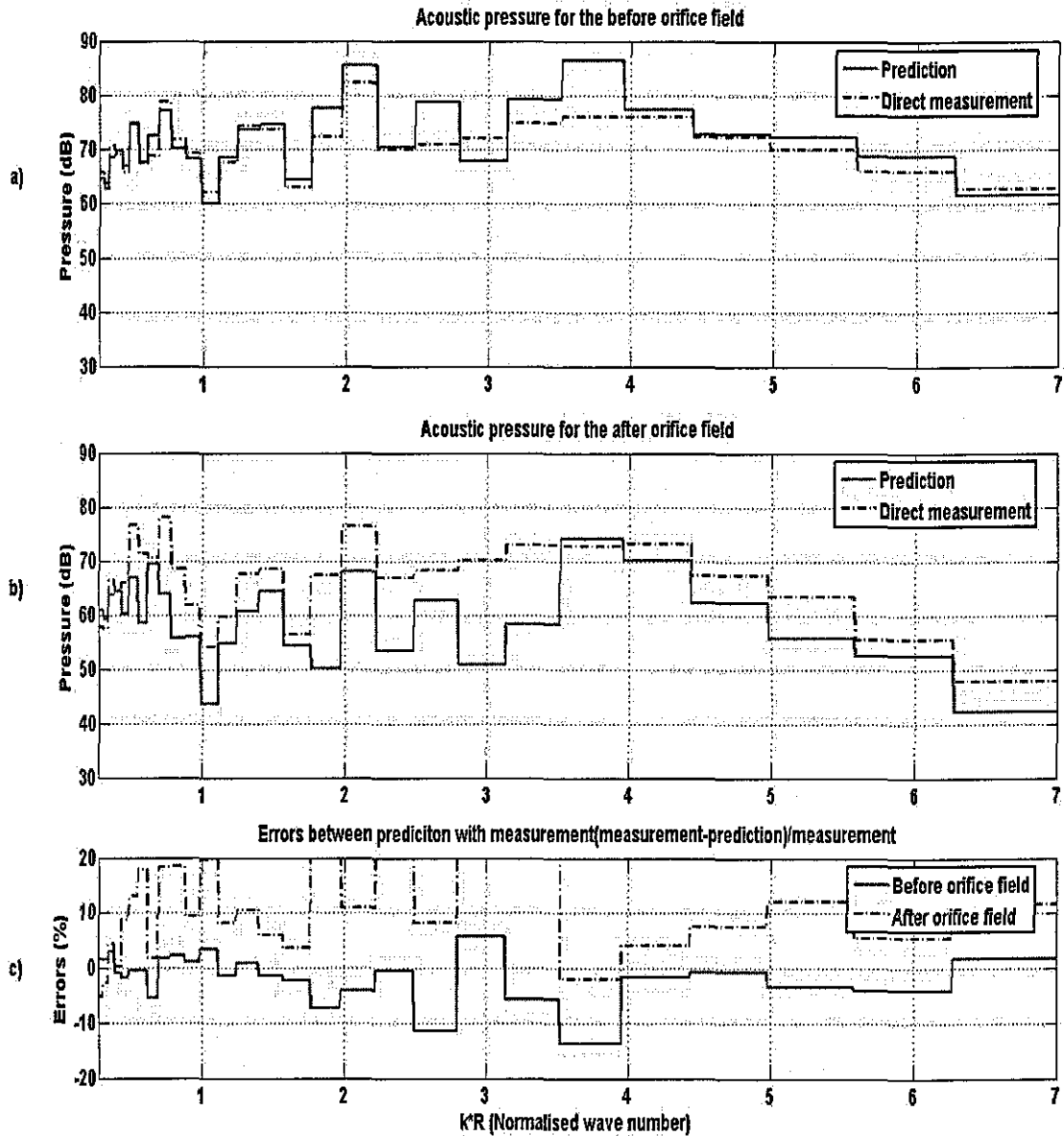


Fig 8.9 Comparison of the acoustic pressure for both the before orifice field and the after orifice field for device with single orifice (Situation 3 in Fig 8.5)

From Fig 8.6 - 8.9, it can be seen that

1. For the concentric-concentric situation (shown in Fig 8.6), all errors for both the before orifice field and the after orifice field are less than 10% of the direct

measurements, at higher normalized wave number range ($k * R > 3.5$), the errors are less than 5% of the direct measurements.

2. For the eccentric-eccentric situation, there are three different configurations for the source-orifice relationship. From Fig 8.8, it can be seen that other than very low normalized wave number range ($k * R < 0.8$), predictions for both the before orifice field and the after orifice field agree well with the direct measurements.
3. For the concentric-eccentric situation (shown in Fig 8.7), the predictions for the after orifice field do not agree with the direct measurements. From this figure, it is easy to see that the errors between predictions and direct measurements for the after orifice field are largest just after the (0, 2) mode cuts on. This is the same as the point source situation, so the explanation given in the previous chapter is also applicable here. For this situation, this method cannot be used directly to predict the after orifice field.
4. For the eccentric-concentric situation (shown in Fig 8.9), the predictions for the after orifice field do not agree with the direct measurements, especially in the normalized wave number range $1.8 < k * R < 3.5$. Also the same explanation given in the previous chapter is suitable for this situation. For this situation, this method cannot be used directly to predict the after orifice field.

8.3 Aperture device with two orifices

If there are more than one orifice in the device, as shown in Fig 7.12, it can be divided into two situations: two orifices situation and several orifices situation. The first one to be studied is the two orifices situation.

8.3.1 Theoretical derivation

If the device consists of two orifices (as shown in the left one of the Fig 7.12), with the radius R_1 and R_2 respectively, following the same procedure, one still can get the same equations as those from equation (7.39) to equation (7.62). So combining these equations with those for the plane wave source and the open end of the duct, one can

have an equation group for the solution of the acoustic properties in circular duct with simple aperture device (two orifices), which is similar to equation (8.2).

8.3.2 Experimental set-up

The experimental set-up for two orifices situation is the same as that for the single orifice situation. The aperture devices used are shown in Fig 7.2, with unused orifices being blocked with wooden blocks of same thickness.

For a device with two orifices situation, ten different comparative source-orifice relationships (shown in Fig 8.11) are considered. These situations can represent most possible source-orifice relationships for a device with two orifices.

8.3.3 Comparison of predictions with direct measurements for a device with two orifices

The predicted and direct measured acoustic pressures of different situations are shown in figures below. Still in each figure, *a*) shows the predicted and direct measured acoustic pressures for the before orifice field; *b*) shows the predicted and direct measured acoustic pressures for the after orifice field; *c*) shows the errors between predictions and direct measurements for both the before orifice and the after orifice field. In order to show these errors clearly, the results are transferred into 1/6 octave band.

For all situations shown below, the acoustic pressures plotted for the before orifice field and the after orifice field are taken at the same points used for the device with a single orifice situation.

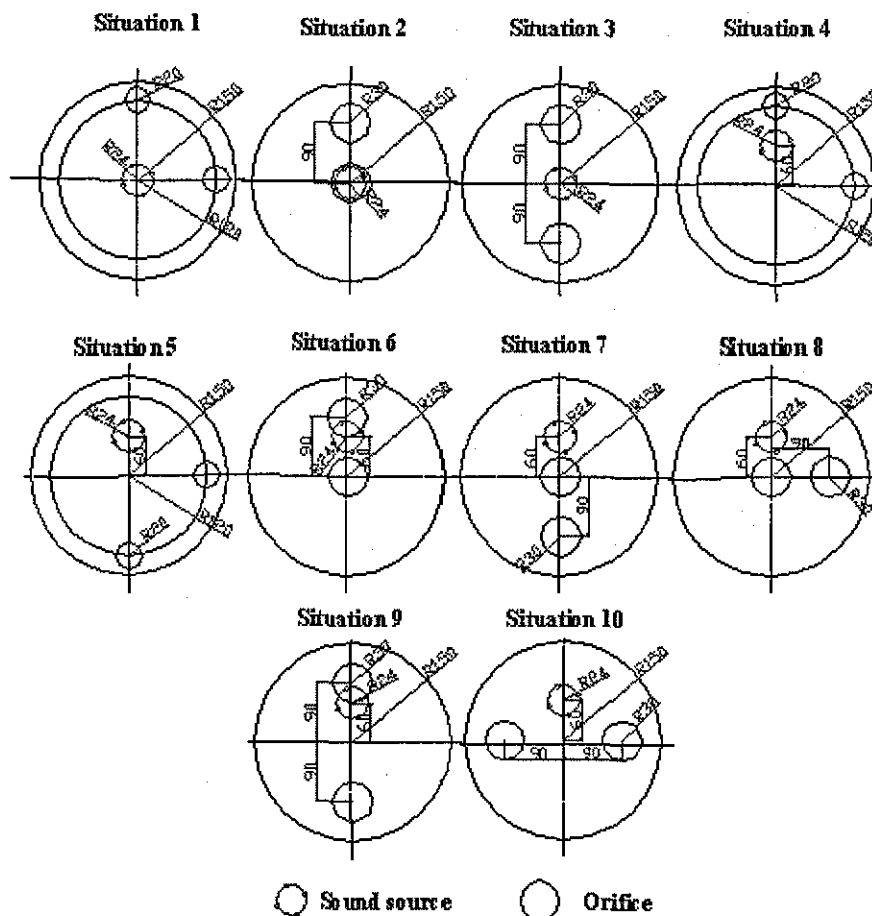


Fig 8.11 Comparative source – orifice relationships for a device with two orifices

For some situations, the results are similar, so there is no need to shown them all. Only three situations are chosen and shown in the figures below. Two of them are for the source concentric situation and one is for the source eccentric situation. Fig 8.12 is for the axially-unsymmetric to the main duct with a concentric orifice situation (Situation 2 in Fig 8.11).

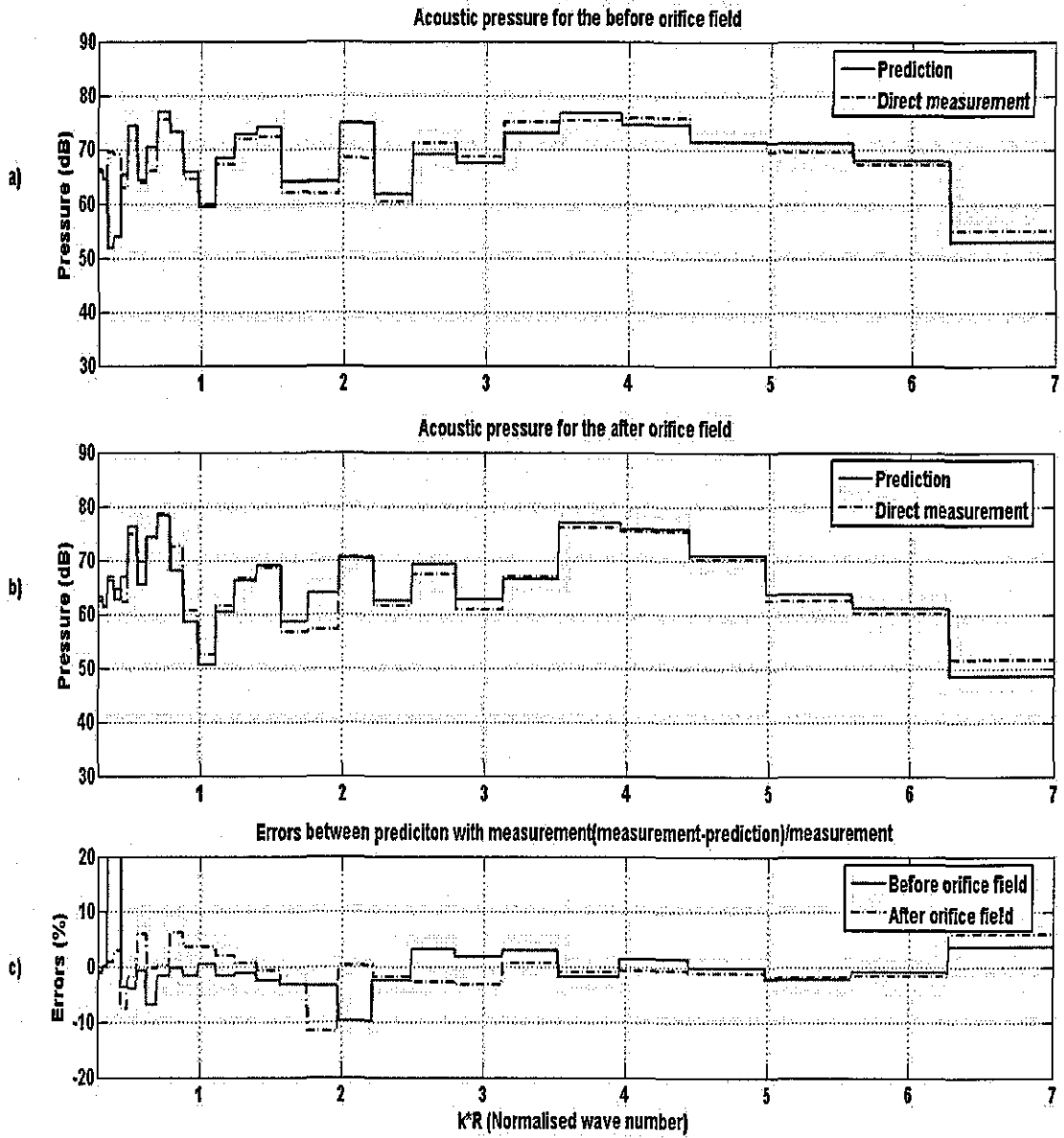


Fig 8.12 Comparison of the acoustic pressure for both the before orifice field and the after orifice field for device with two orifices (Situation 2 in Fig 8.11)

Fig 8.13 is for the concentric - axially-unsymmetric to the main duct without concentric orifice situation (Situation 1 in Fig 8.11).

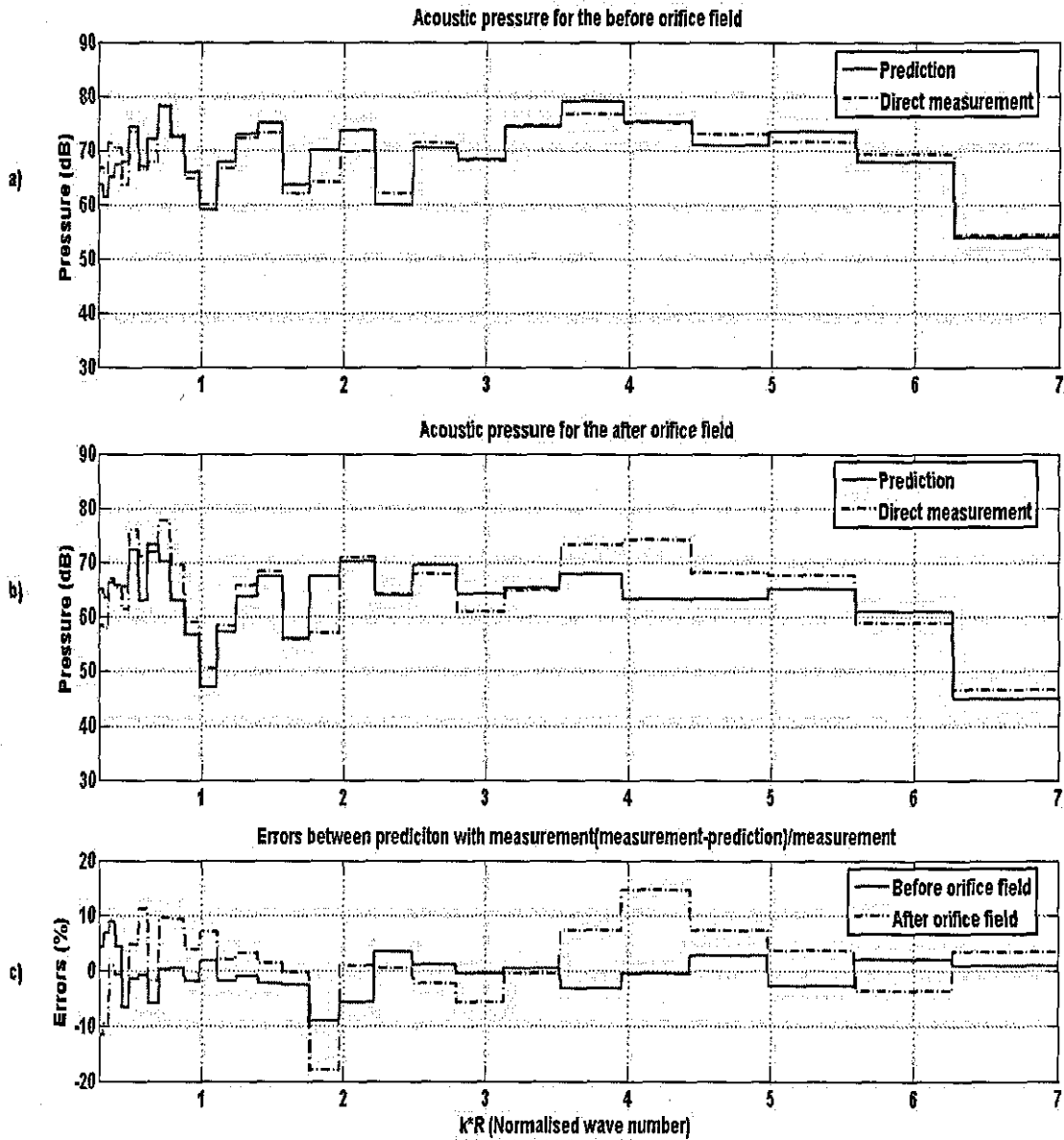


Fig 8.13 Comparison of the acoustic pressure for both the before orifice field and the after orifice field for device with two orifices (Situation 1 in Fig 8.11)

Because for the source eccentric situation, all seven different orifice configurations give similar results, so only one situation (Situation 10 in Fig 8.11) is chosen and the results are shown in Fig 8.14.

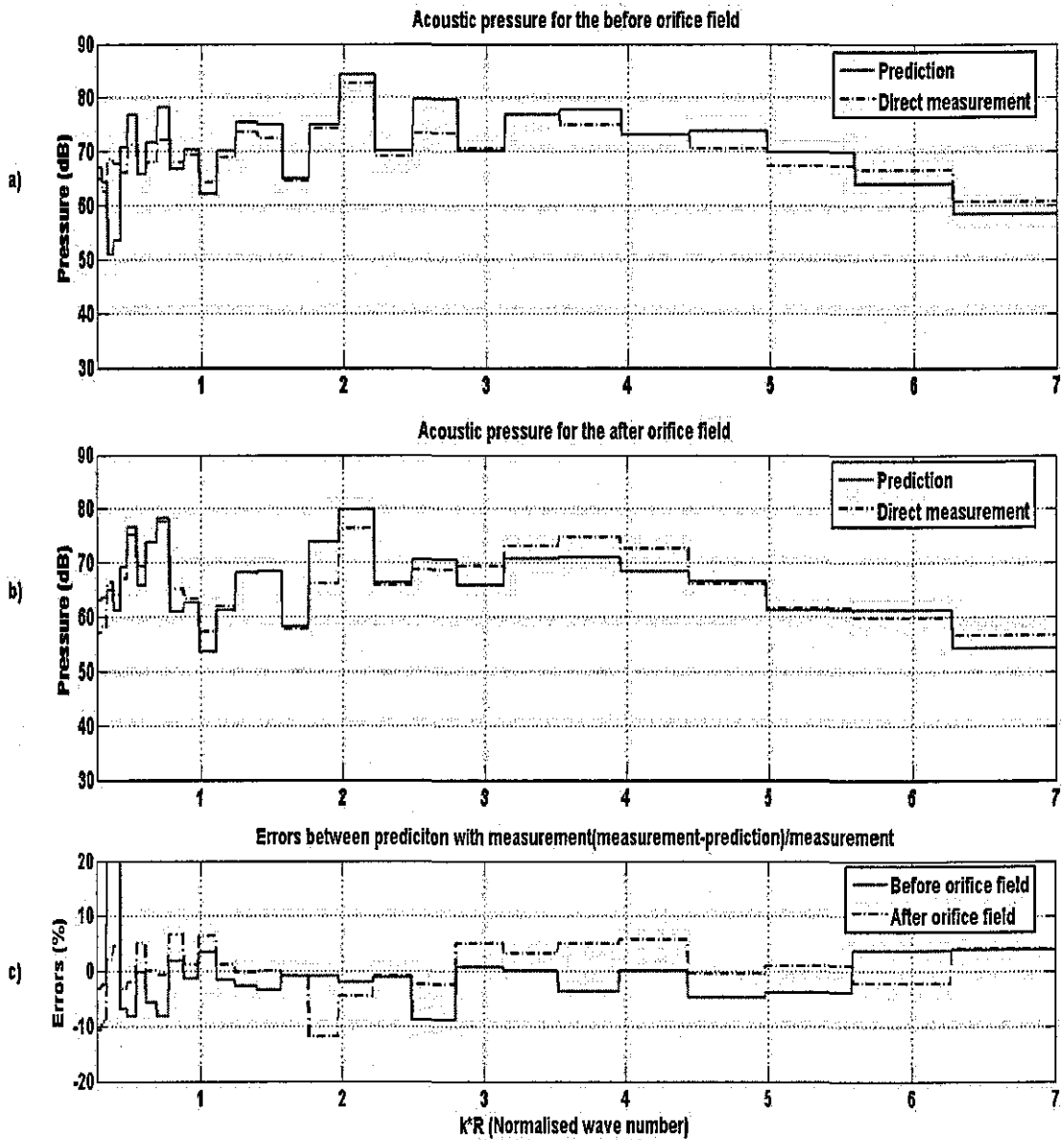


Fig 8.14 Comparison of the acoustic pressure for both the before orifice field and the after orifice field for device with two orifices (Situation 10 in Fig 8.11)

From Fig 8.12 – Fig 8.14, it can be seen that

1. For the source concentric situation, if an orifice in the device is concentric to the main duct, predictions for both the before orifice field and the after orifice field agree well with the direct measurements (less than $\pm 5\%$ of direct measurements).
2. However if there is no orifice in the device which is concentric to the main duct, such as Situation 1 and Situation 3, predictions do not agree with the direct measurements, especially for the after orifice field. As shown in Fig 8.13, the largest errors appear when $(0, 2)$ mode cuts on ($k * R \approx 4$). The reason is given in the previous chapter.
3. For the source eccentric situation, seven different configurations of the orifices have been considered and from the representative results shown in Fig 8.14, it can be seen that other than at very low normalized wave number range, the predictions for both the before orifice field and the after orifice field agree with the direct measurements (less than $\pm 5\%$ of direct measurements). Thus for these situations, this model works quite well for the in-duct field.

8.4 Aperture device with several orifices

8.4.1 Theoretical derivation

If the device consists of n orifices ($n > 2$), with the radius $R_1, R_2 \dots R_n$ respectively, the boundary conditions at 2 and 3 are the same as those from equation (7.63) to equation (7.68). Just following the derivation procedure of the two orifices situation, one can get the equations for the several orifices situation, which are similar with those obtained for the two orifices situation.

8.4.2 Experimental set-up

The experimental set-up for the several orifices situation is same as the single orifice situation, as well as the two orifices situation. The devices used in the measurements are shown in Fig 7.2, with unused orifices being blocked with wooden blocks of same thickness.

For several orifices situation, ten different comparative source - orifice relationships are considered. These situations can represent many possible source - orifice relationships for several orifices situation. From these ten different situations, one can not only test the effects of up to 28% open area in the device on the in-duct field, but also test the effects of different orifice combinations on the in-duct field.

8.4.3 Comparison of predictions with direct measurements for a device with several orifices

In order to keep the results to be shown in the same style, still the predicted and direct measured acoustic pressures of different situations are shown in figures below. And for all situations shown below, the acoustic pressures plotted for the before orifice field and the after orifice field are taken at the same points used in device with single orifice situation.

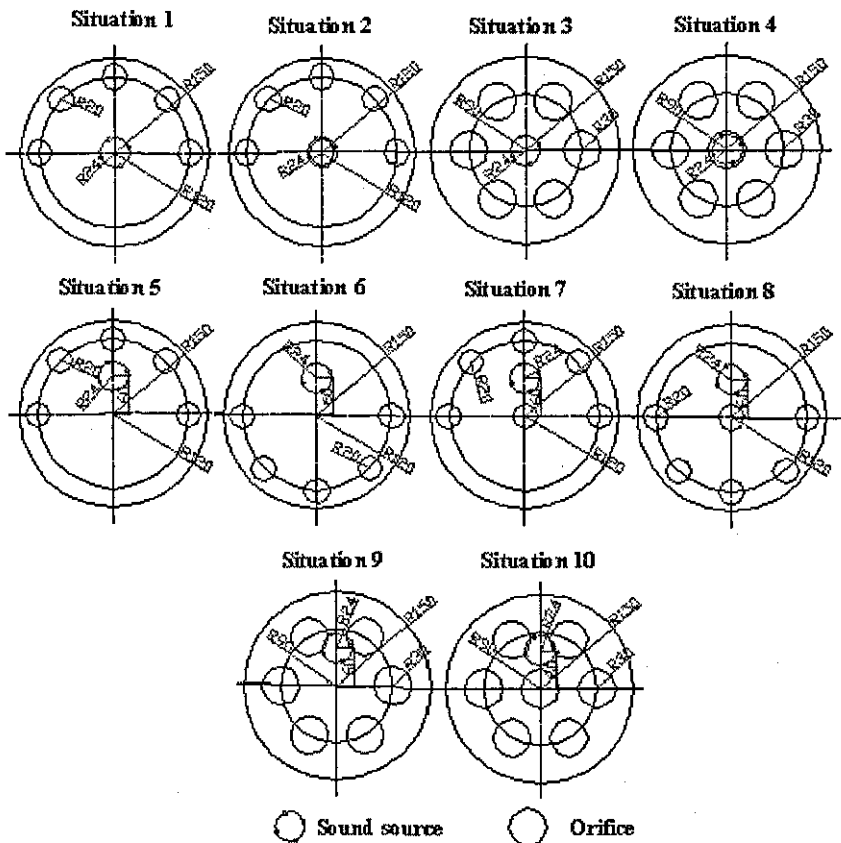


Fig 8.15 Comparative source - orifice relationships for a device with several orifices

8. Sound field produced by a plane wave source propagating in a circular duct with aperture devices

For the ten situations, three situations are chosen as representative and the results are shown in Fig 8.16 to Fig 8.18. Two of them are for the source concentric situation; one is for the source eccentric situation. Fig 8.16 is for the sound source concentric to the main duct, while the orifices are axially-symmetric to the main duct with a concentric orifice (Situation 1 in Fig 8.15).

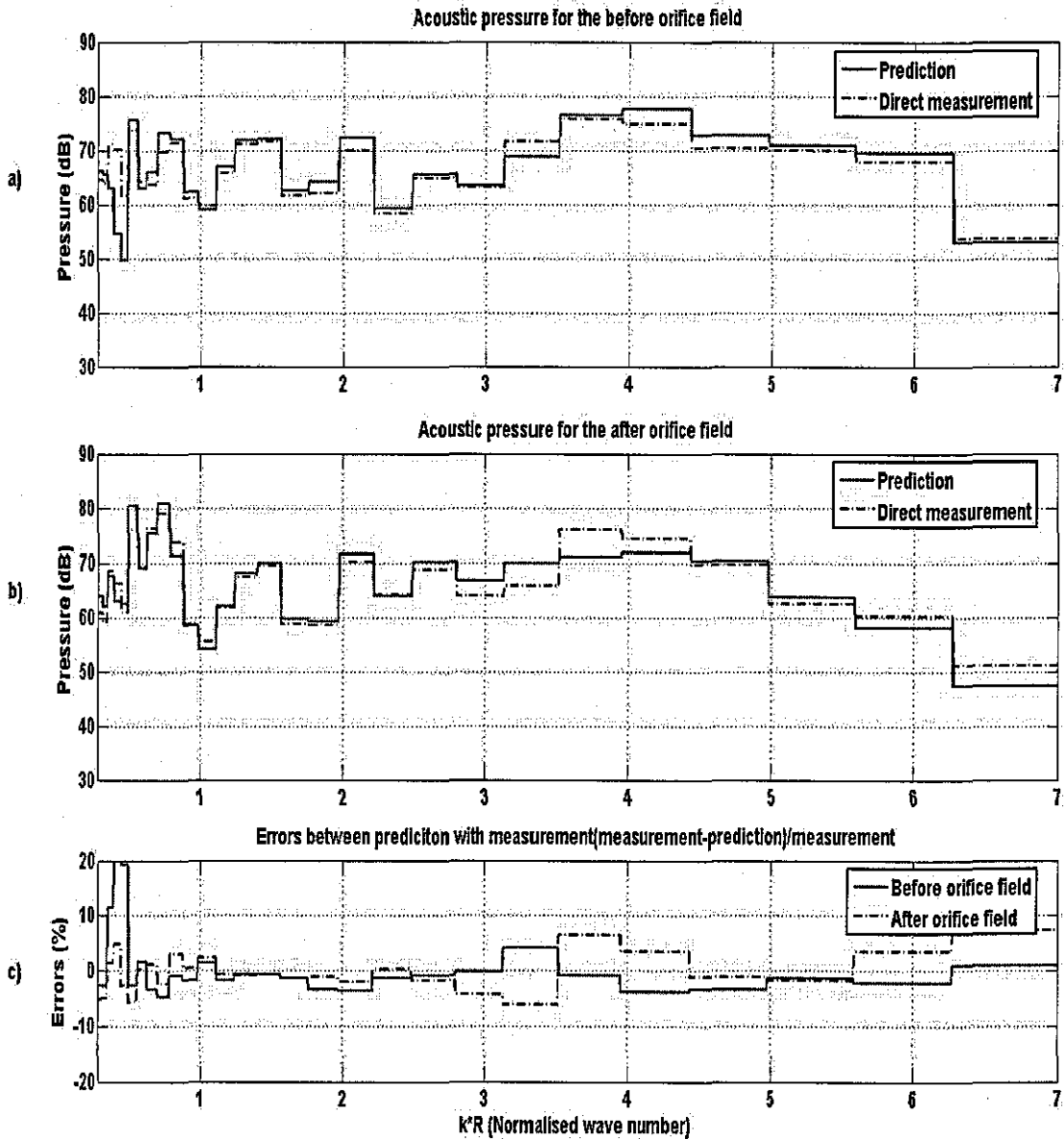


Fig 8.16 Comparison of the acoustic pressure for both the before orifice field and the after orifice field for device with several orifices (Situation 1 in Fig 8.15)

Fig 8.17 is for the sound source concentric to the main duct, while the orifices are axially-unsymmetric to the main duct without a concentric orifice (Situation 4 in Fig 8.15).

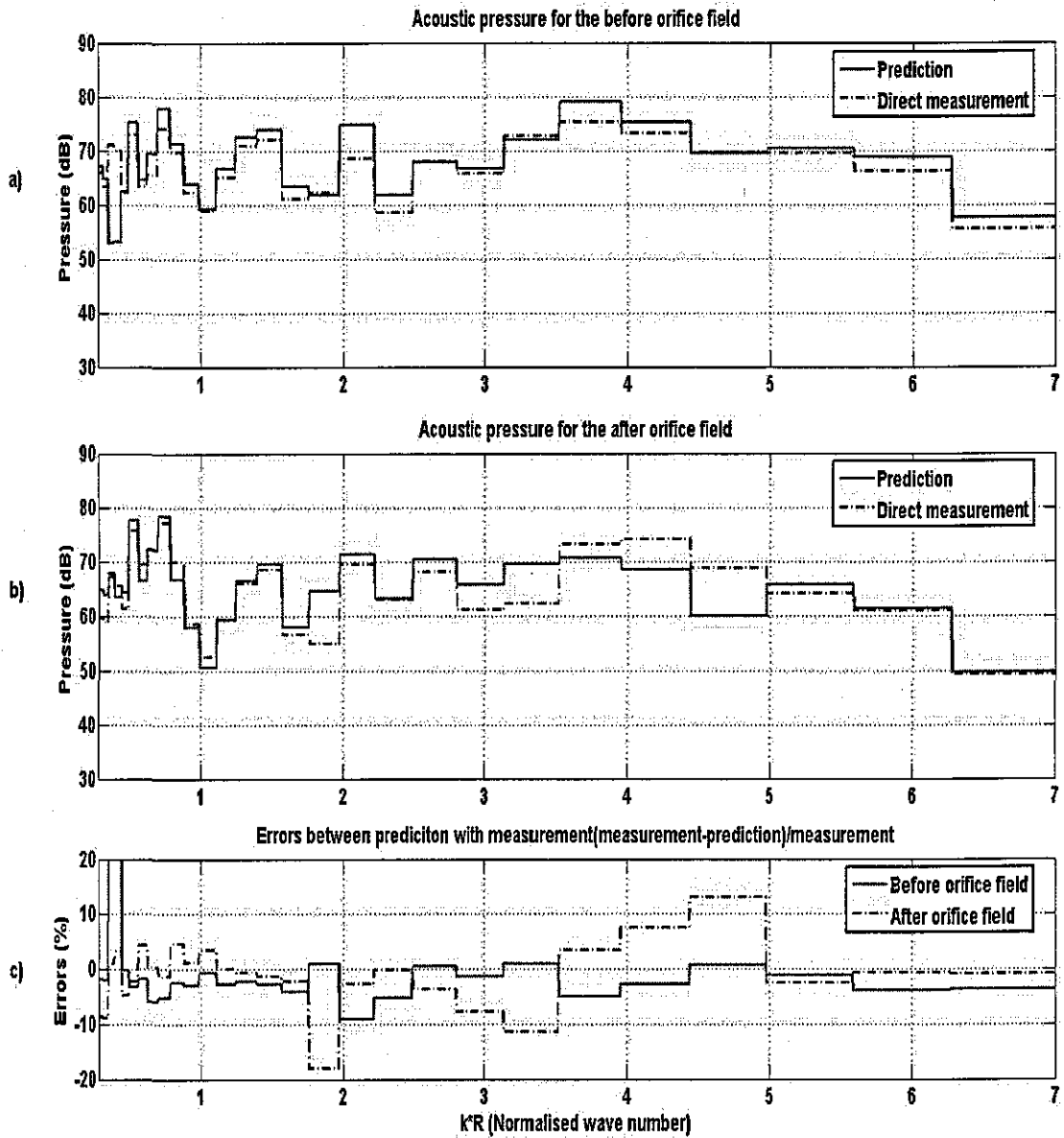


Fig 8.17 Comparison of the acoustic pressure for both the before orifice field and the after orifice field for device with several orifices (Situation 4 in Fig 8.15)

Fig 8.18 is for the sound source eccentric to the main duct, while the orifices are axially-unsymmetric to the main duct without a concentric orifice (Situation 6 in Fig 8.15).

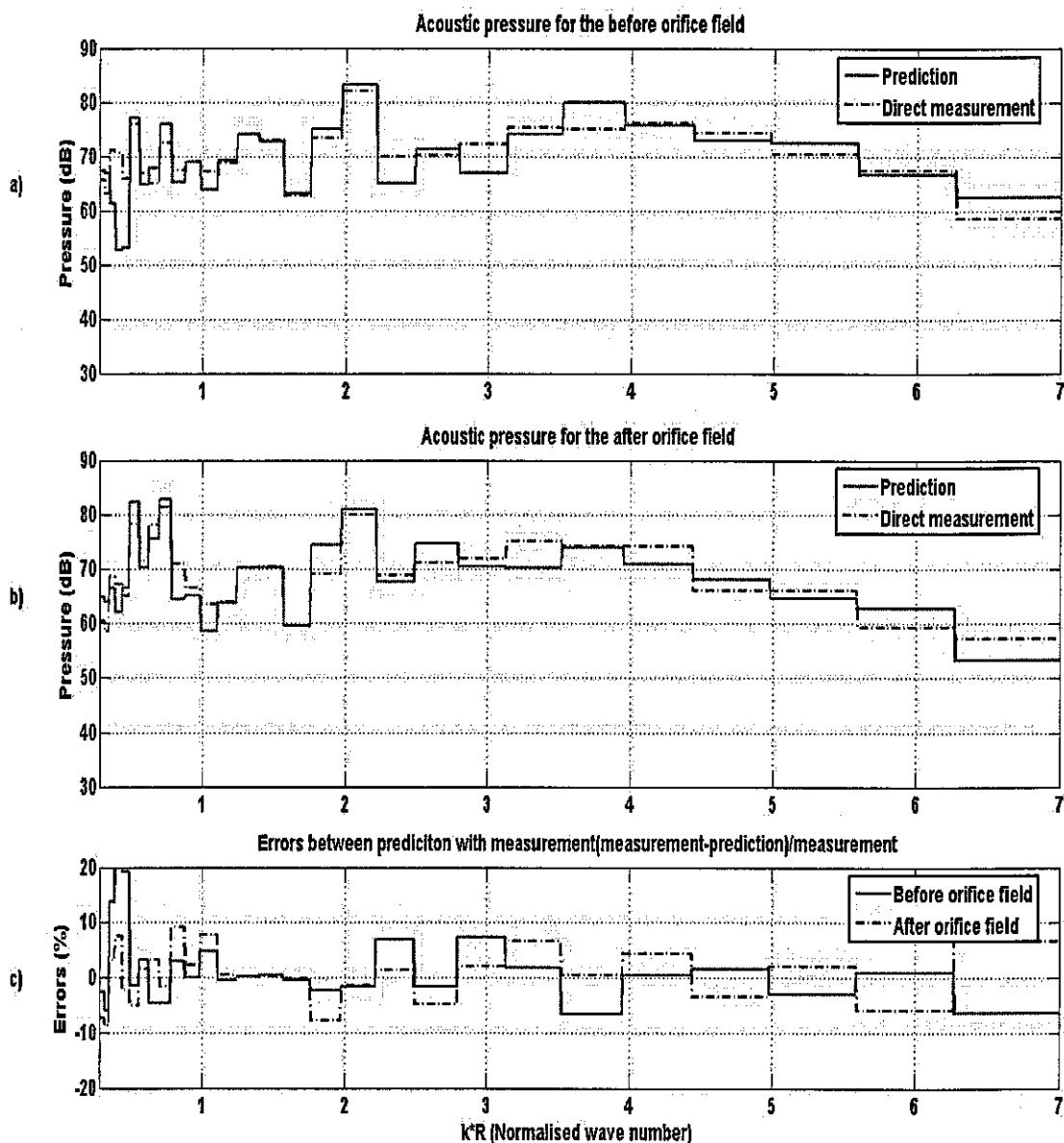


Fig 8.18 Comparison of the acoustic pressure for both the before orifice field and the after orifice field for device with several orifices (Situation 6 in Fig 8.15)

From Fig 8.16- 8.18, one can get the same conclusions as those obtained for two orifices situation. Which means the effects of the number of the orifices on the predictions of the in-duct field is not significant. On the contrary, it is the configuration of the orifices and the comparative source – orifice relationships that affect the predicted results.

8.5 Error analysis

From all twenty-six different source – orifice situations shown above, it can be seen that for all these situations, predictions for the before orifice field agree with the direct measurements. Other than very low normalized wave number range ($k * R < 0.5$), most errors between predictions and direct measurements are less than 5% of the direct measurements, or even smaller. Which means this model is effective in prediction of acoustic properties in the before orifice field, as well as in decomposition of the before orifice field into single higher-order mode.

For most situations (twenty out of twenty-six situations), predictions for the after orifice field agree with the direct measurements. Still other than very low normalized wave number range ($k * R < 0.5$), the errors between predictions and direct measurements are less than 5% of the direct measurements. Which means for these situations, through measurements in the before orifice field, one can accurately predict those acoustic properties in the after orifice field.

For other six situations, predictions for the after orifice field do not agree with direct measurements in some specific frequency range. Still these six situations can be divided into two groups: source concentric group and source eccentric group.

For source concentric group, it can be seen that if there is no orifice located concentric to the main duct, no matter how many orifices are in the device (Situation 2 in Fig 8.5, Situation 1 and 3 in Fig 8.11, Situation 1 and 3 in Fig 8.15), the predictions for the after orifice field do not agree with the direct measurements. However, through the comparison between Fig 8.7 and Fig 8.12, one can see if there is an extra concentric orifice in the device, the predictions agree with the direct measurements. Because this concentric orifice can produce those axially-symmetric higher-order modes in the after orifice field, so these situations can also be named as *source concentric and no concentric orifice* situation. For this situation, this method cannot be used directly to predict the after orifice field.

For source eccentric group, only when there is a single concentric orifice in the device (Situation 3 in Fig 8.5), the predictions for the after orifice field do not agree with the direct measurement. For all other situations, the predictions agree well with the direct measurements. So this situation can also be named as *source eccentric and only one concentric orifice* situation.

For all other situations, one can just predict both the before orifice field and the after orifice field with two reference measurements in the before orifice field. But for those two specific situations mentioned above, in order to get accurate prediction for the after orifice field, another two reference points in the after orifice field, which are located at $(0.15m(100\%R), 0, -0.12m(-4\%L))$ and $(0.15m(100\%R), 2 * \pi / 3, -0.20m(-6.67\%L))$ respectively, are taken. Using these two reference measurements for prediction in the after orifice field (the procedure is given in Appendix F), for *source concentric and no concentric aperture* situation, take Situation 1 in Fig 8.11 for example, the results are shown in Fig 8.19. For *source eccentric and only one concentric orifice* situation (Situation 3 in Fig 8.5), the results are shown in Fig 8.20.

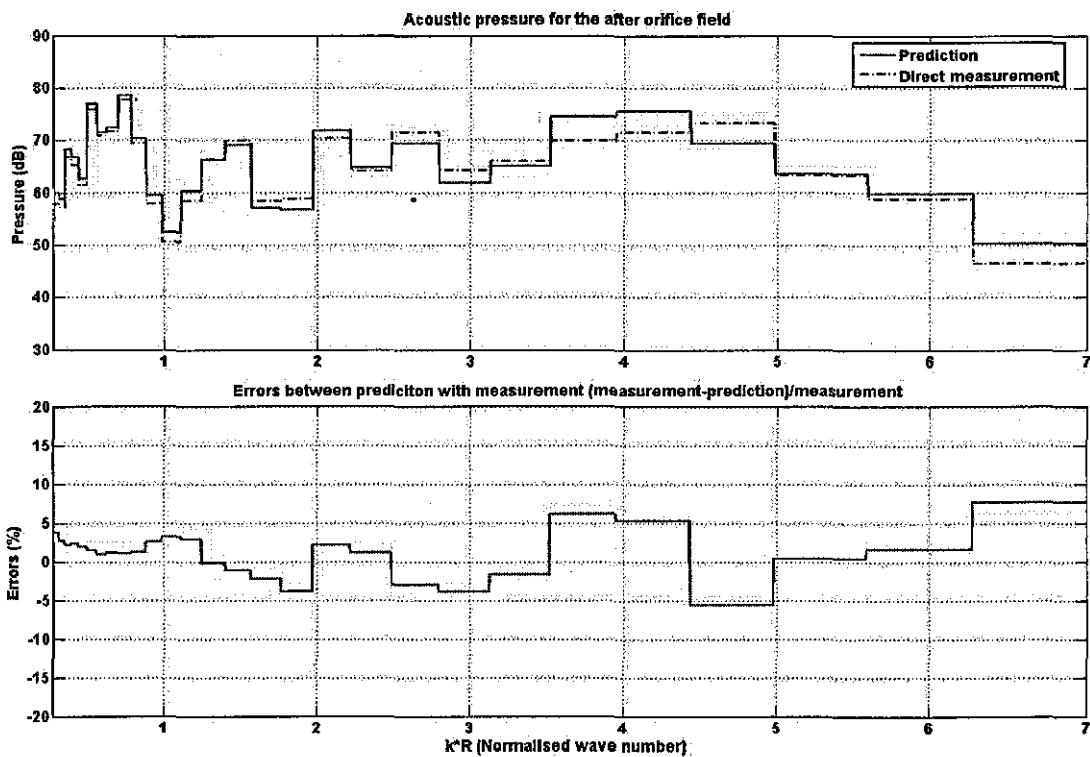


Fig 8.19 Comparison of direct measurements with predictions for the after orifice field (Situation 1 in Fig 8.1)

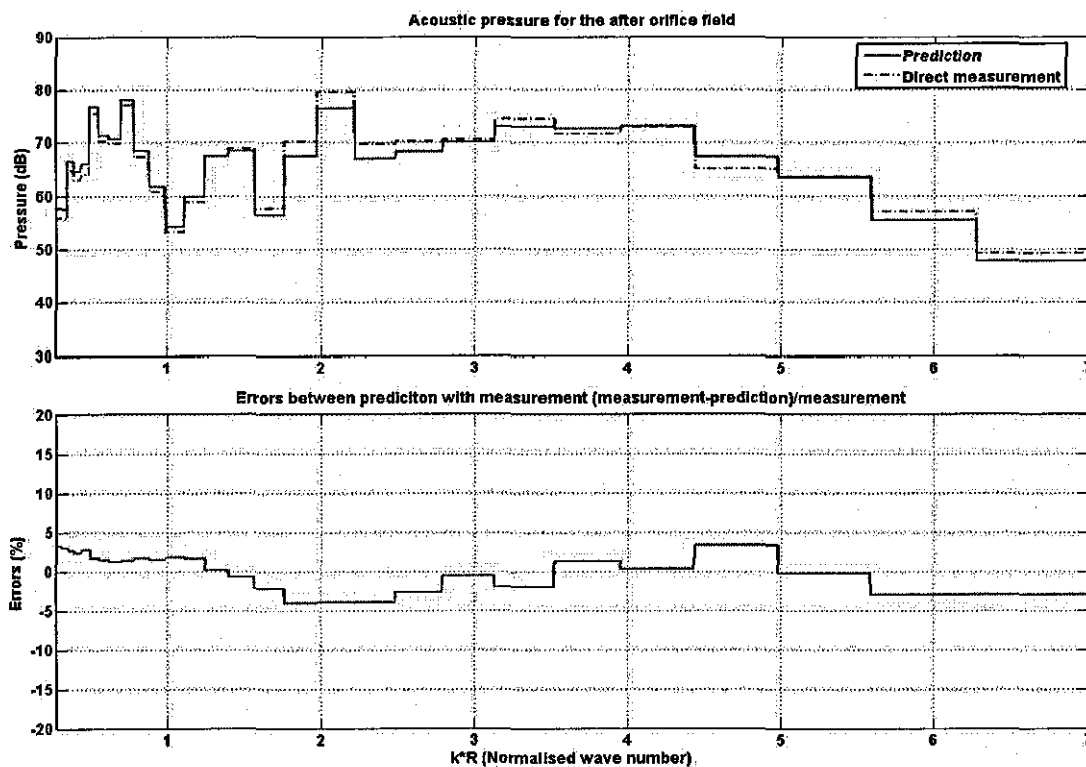


Fig 8.20 Comparison of direct measurements with predictions for the after orifice field (Situation 3 in Fig 8.5)

From Fig 8.19 -8.20, it can be seen that for these two specific situations, predictions for the after orifice field by using reference measurements in the after orifice field agree with the direct measurements. Which means through measurements in the after orifice field, one can still decompose the after orifice field effectively for these two specific situations. So for these two specific situations, the after orifice field is decomposed by this method rather than former one.

8.6 Predictions for different circumferential positions both before and after aperture device

In order to test whether or not this model can detect the spiralling higher-order modes both for the before orifice field and the after orifice field, predictions for different points along the circumference of the main duct are made in this section. To some extent this highlights the possible errors due to the spiralling wave front of the axially-unsymmetric higher-order modes. As shown in Fig 8.2, for the main duct region, there are two rings of

measurement points, which are located at $Z = -0.54m (-18\%L)$ and $Z = -0.18m (-6\%L)$ respectively. The first ring is for the measurement in the before orifice field and the second ring is for the measurement in the after orifice field. For both rings, there are six equally distributed measurement points along the circumference of the duct. Along each ring, point 1, point 3 and point 5 are taken and named as position 1, position 2 and position 3 respectively in the following figures.

Take two different source-orifice situations for example, the first situation is source concentric and single orifice concentric situation (Situation 1 in Fig 8.5), which represents the concentric situation; the second situation is source eccentric and five orifices eccentric situation (Situation 6 in Fig 8.15), which represents the eccentric situation. The results are shown below. Fig 8.21 shows the comparison for the before orifice field of the first situation and Fig 8.22 shows the comparison for the after orifice field of the first situation. Fig 8.23 shows the comparison for the before orifice field of the second situation and Fig 8.24 shows the comparison for the after orifice field of the second situation. In each figure, a) shows the direct measurement at these three positions and b) shows the predicted results for these three positions and c) shows the errors between predictions and direct measurements for these three positions.

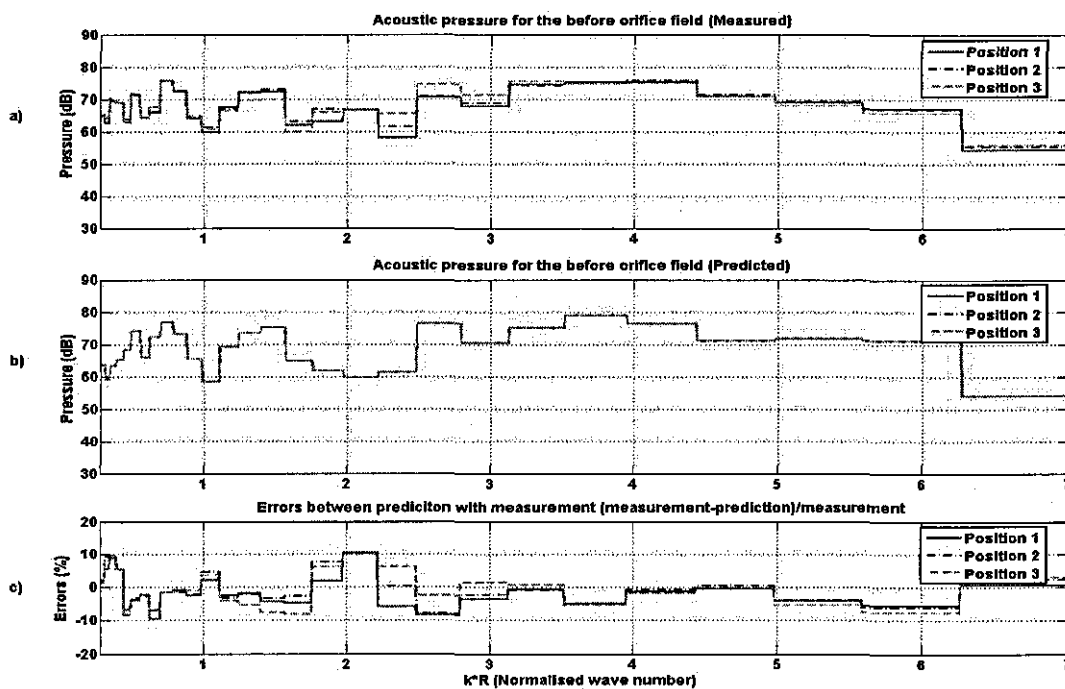


Fig 8.21 Comparison of the errors of different positions along the circumference for the before orifice field (Situation 1 in Fig 8.5)

8. Sound field produced by a plane wave source propagating in a circular duct with aperture devices

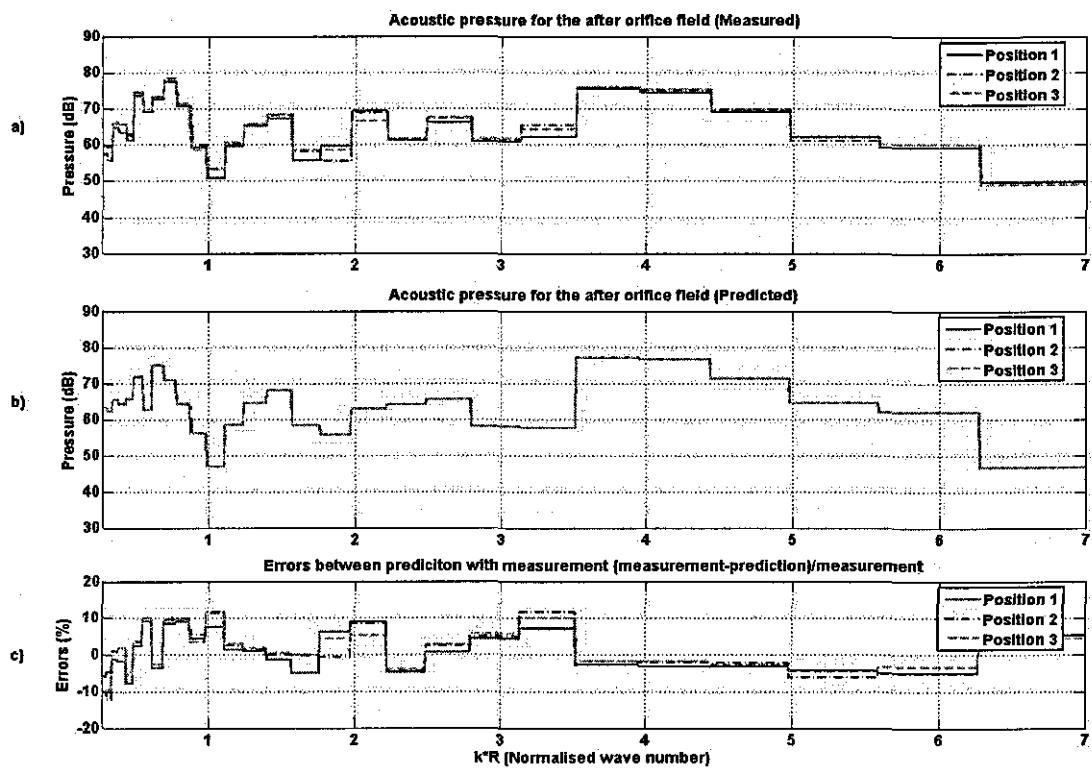


Fig 8.22 Comparison of the errors of different positions along the circumference for the after orifice field (Situation 1 in Fig 8.5)

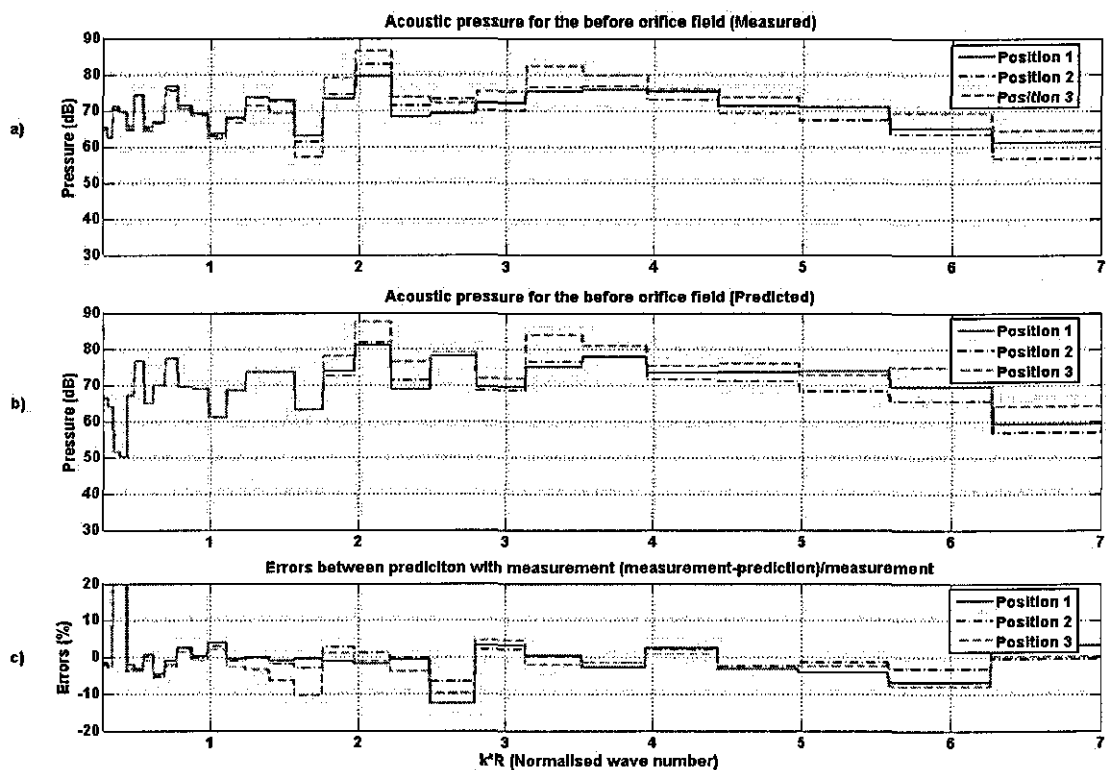


Fig 8.23 Comparison of the errors of different positions along the circumference for the before orifice field (Situation 6 in Fig 8.15)

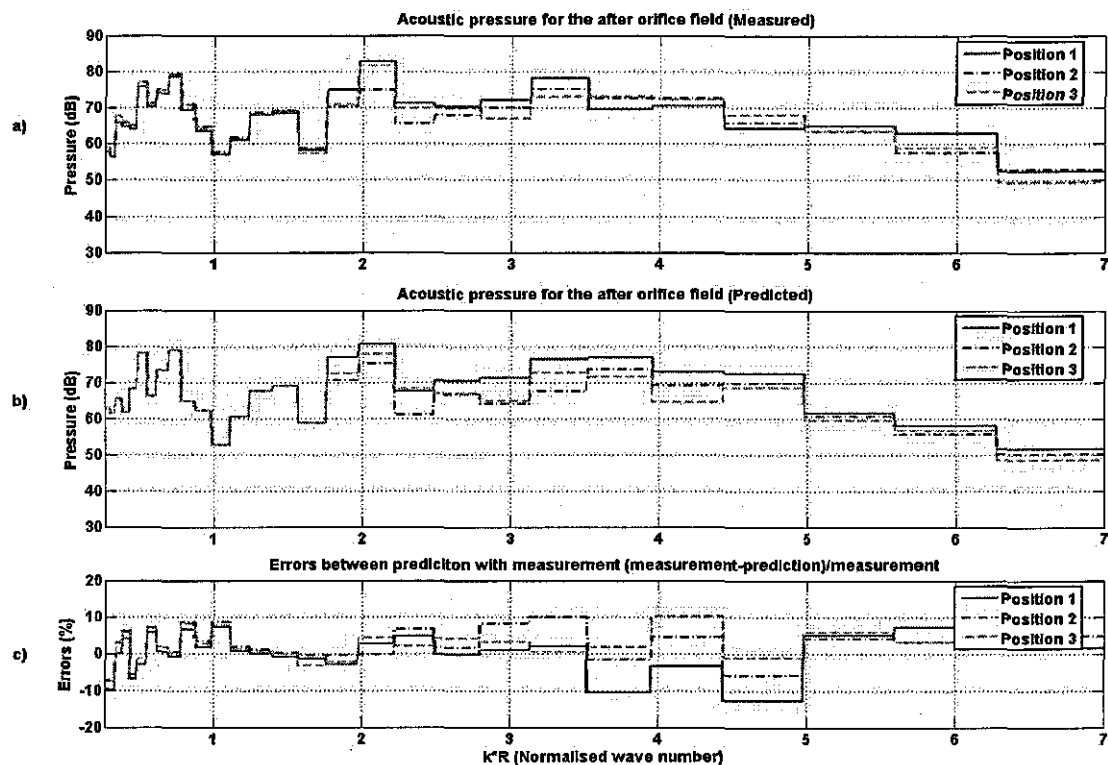


Fig 8.24 Comparison of the errors of different positions along the circumference for the after orifice field (Situation 6 in Fig 8.15)

From Fig 8.21 – 8.24, it can be seen that

1. For the source concentric situation, Fig 8.21 and Fig 8.22 show that there is no difference along the circumference for the predictions of both the before orifice field and the after orifice field. But for the direct measurements, there is a small difference between these three positions both in the before orifice field and in the after orifice field, which may be caused by the measurement errors or the source duct location or the orifice location errors (the source duct and the orifice are not perfectly concentric to the main duct). Even though the measurements of these three positions are quite similar, and the errors between predictions and direct measurements are similar and considered acceptable. These two figures show that when the sound source and orifice are concentric to the main duct, the acoustic properties for both the before and the after orifice field are axially-symmetric (At this situation, the acoustic field is dominated by axially-symmetric higher-order modes).

2. For the source eccentric situation, before the first higher-order mode ($(\pm 1,1)$ mode) cuts on, only the plane wave propagates in the duct. The acoustic pressures for three positions in the before orifice field are nearly equal and the acoustic pressures for three positions in the after orifice field are also equal, which agrees with the plane wave theory.
3. For the source eccentric situation, after the first higher-order mode ($(\pm 1,1)$ mode) cuts on, other higher-order modes cut on and propagate along the duct. Both the predictions and the direct measurements for these three positions are different, which is caused by those spiralling higher-order modes. By comparing errors for these three positions in both the before and the after orifice field, it can be seen that these errors for the before orifice field are nearly the same but these errors for the after orifice field are different at normalized wave number range $2 < k * R < 5$, which should be caused by the spiralling $(\pm 1,1)$ modes and $(\pm 2,1)$ modes. This means the predictions along the circumferential positions for source eccentric situation depend on the circumferential angle and frequency range. Even though, the errors for all six positions in both fields mainly fall into the range $\pm 5\%$ of the direct measurements, which is considered acceptable.
4. So through these four figures, it can be seen that no matter what the comparative relationships between source and the aperture device are (in the plane transverse to z -axis), this model can accurately predict the acoustic properties along the circumference of the duct. Which means those amplitudes, such as A_{mn} , B_{mn} , C_{mn} , D_{mn} , E_{mn} and F_{mn} , obtained from this model are considered to be acceptable.

8.7 Discussion

In this chapter, a simple aperture device is placed in the duct and twenty six different source-orifice relationships (including one orifice, two orifices and several orifices) are discussed and from the results plotted, it can be seen that the prediction for both the before orifice field and the after orifice field are considered acceptable. This means the model proposed to describe the boundary conditions of the orifices are effective and the combination of the orifice boundary conditions with the plane wave source boundary

and open duct end boundary can give accurate solution for the whole in-duct field. So using this model, one can achieve the decomposition of the in-duct field in both the before and after orifice regions.

Comparing the analysis in this chapter with that for the point source in Chapter 7, it can be seen that all conditions are the same except the type of the sound source. From the results shown in these two chapters, it can also be seen that the predictions for these two sound source types are quite similar: The predictions for both the before orifice field and the after orifice field agree with the direct measurements. The errors for both types of sound source are considered acceptable. Normally the errors between the predictions and direct measurements for the plane wave source situation are less than those for the point source situation. Because of the similarity shared by these two types of the sound sources, in next chapter, only the plane wave source is selected to be studied.

From the analysis made in Chapter 7 and this chapter, it can also be seen that it is not the type of the sound source which determines the after orifice field. Actually it is the configuration of the aperture device and the comparative cross sectional source-orifice relationships which determines the after orifice field.

By successfully decomposing the in-duct field into different higher-order modes, one can study the effects of different configurations of the aperture device and cross sectional source-orifice relationships on different higher-order modes. So in next chapter, the power radiated out of the duct for each single higher-order mode will be studied, as well as the insertion loss (IL) for each configuration. By analysing the power and the insertion loss (IL) for each situation, one can have a full understanding of the overall effects of different orifice configurations on the whole in-duct field.

Chapter 9 Radiated power and the insertion loss for different aperture devices

9.1 Introduction

There are many parameters that can be used to describe the effects of the aperture device on the in-duct field, such as the acoustic impedance, acoustic pressure, volume velocity, transmission loss (TL), insertion loss (IL) and level difference (LD), etc. If there is only the plane wave propagating in ducts, these parameters can all be used for the analyses of the effects of different aperture devices. As discussed in Chapter 2, acoustic pressure and volume velocity are treated as two lumped parameters and the acoustic impedance is chosen to show the effects of different aperture devices. However, if higher-order modes begin to propagate along the duct, many of these parameters cannot give the overall effects of the device because the parameters, such as the acoustic pressure, volume velocity and the acoustic impedance, are values which are dependent on not only the z -axis coordinate but also the (r, φ) coordinates in the plane transverse to z -axis. In this situation these parameters are not suitable for the analysis of the higher-order modes in the duct.

Transmission loss (TL) is defined as the difference between the power incident and that transmitted downstream. Level difference (LD) is defined as the difference in sound pressure level at two selected points along the duct. When there are higher-order modes propagating along the duct, the pressure is different in the plane transverse to z -axis, so this parameter can also only be applied to the plane wave propagation situation. So many common parameters are excluded for the analysis in the higher normalized wave number range.

The power radiated out of the duct is an aggregate value, because it is independent of the coordinates (z, r, φ) . Also if the sound produced by the sound source is time invariant, then the power radiated out of the main duct should be also time invariant. So the power radiated out of the duct is taken as a lumped parameter in this chapter and together with

the acoustic pressure, the approximate lumped-parameter model is constructed. The applicability of this approximate model will be discussed.

Also after determining the powers radiated out of the duct for different situations, the insertion loss (IL) is chosen to show the effects of the aperture devices in circular duct at higher normalized wave number range.

As presented in Ref [3] (Chapter II), the insertion loss (IL) is defined as the difference between the acoustic powers radiated without any filter and those with the filter. For the study of the effects of the aperture devices in this investigation, one can treat the aperture device as a filter, so the insertion loss can be written as,

$$IL = L_{wI} - L_{wII} = 10 * \log(W_I / W_{II}), \quad (9.1)$$

in which W_I is the power radiated out of the duct without any aperture device, W_{II} is the power radiated out of the duct with aperture device.

In order to obtain the insertion loss of the aperture device, first one has to get the powers radiated for a duct without an aperture device and a duct with an aperture device respectively.

9.2 Power radiated into and out of the main duct

Equation (9.1) is widely adopted for the study of the effects of filters in an exhaust system, because for most situations in an exhaust system, only the plane wave is considered and it is easier to get the power radiated from the end of the exhaust system through measurement. But if there are higher-order modes cut on in the system, the acoustic pressure and particle velocity are different at any two points, so it is difficult to get the radiated powers only through measurement.

One possible experimental approach to measure the radiated power is to subdivide the area into a mesh outside of the duct, then measure the acoustic pressure and particle velocity at each point in the mesh to get the power transmitted through each point,

finally add them together to get the total power radiated out of the duct. In order to get more accurate results, one should keep the area of each mesh as small as possible. However the smaller the area of each mesh is, the more measurement points are needed. So it requires quite a lot of measurement work to make the result sensible and any measurement errors will be brought into the final results. Thus this time and labour consuming experimental approach is not an ideal way for the study of radiated power, as well as the insertion loss (IL), for the higher-order modes situation.

As discussed in previous chapters, the in-duct field has been decomposed into a combination of single higher-order modes and the amplitude of each higher-order mode has been obtained. If one can calculate the radiated power through these amplitudes, it will provide a theoretical approach for the analysis of radiated power, as well as the insertion loss (IL). The derivation of the power radiated from the end of the duct is given below.

9.2.1 Derivation of the power radiated from the open end of the duct

The acoustic pressure at any point in-duct can be written as,

$$\begin{aligned}
 P(r, z, \varphi) = & (A_{01}e^{-jkz} + B_{01}e^{jkz}) + \sum_{n=2}^{\infty} (A_{0n}e^{-jk_{z,0,n}z} + B_{0n}e^{jk_{z,0,n}z})J_0(k_{r,0,n}r) \\
 & + \sum_{m=1}^{\infty} \sum_{n=1}^{\infty} (J_m(k_{r,m,n}r) [(A_{mn}^+ e^{-jk_{z,m,n}z} + B_{mn}^+ e^{jk_{z,m,n}z}) e^{-jm\varphi} \\
 & + (A_{mn}^- e^{-jk_{z,m,n}z} + B_{mn}^- e^{jk_{z,m,n}z}) e^{jm\varphi}]) , \quad (9.2)
 \end{aligned}$$

and the particle velocity along z -axis can be written as,

$$\begin{aligned}
 v_z(r, z, \varphi) = & \frac{1}{\rho c} ((A_{01}e^{-jkz} - B_{01}e^{jkz}) \\
 & + \sum_{n=2}^{\infty} \frac{k_{z,0,n}}{k} (A_{0n}e^{-jk_{z,0,n}z} - B_{0n}e^{jk_{z,0,n}z})J_0(k_{r,0,n}r) \\
 & + \sum_{m=1}^{\infty} \sum_{n=1}^{\infty} (\frac{k_{z,m,n}}{k} J_m(k_{r,m,n}r) [(A_{mn}^+ e^{-jk_{z,m,n}z} - B_{mn}^+ e^{jk_{z,m,n}z}) e^{-jm\varphi} \\
 & + (A_{mn}^- e^{-jk_{z,m,n}z} - B_{mn}^- e^{jk_{z,m,n}z}) e^{jm\varphi}]) . \quad (9.3)
 \end{aligned}$$

So one can write the sound intensity at any point as,

$$I = P^* v_z^* . \quad (9.4)$$

Then integrate this sound intensity over the whole circular duct region; one can get the power as,

$$W = \int_0^{2\pi R} \int_0^{2\pi R} I^* r dr d\varphi = \int_0^{2\pi R} \int_0^{2\pi R} P^* v_z^* r dr d\varphi \quad (9.5)$$

As discussed in Chapter 3, the origin point of the coordinate system is taken at the plane of the open end of the duct, so at this point

$$z = 0 . \quad (9.6)$$

Substitute $z = 0$ into equation (9.2) and equation (9.3), one can get the acoustic pressure and particle velocity at the open end of the duct as,

$$P(r, z, \varphi) = (A_{01} + B_{01}) + \sum_{n=2}^{\infty} (A_{0n} + B_{0n}) J_0(k_{r,0,n} r) + \sum_{m=1}^{\infty} \sum_{n=1}^{\infty} J_m(k_{r,m,n} r) [(A_{mn}^+ + B_{mn}^+) e^{-jm\varphi} + (A_{mn}^- + B_{mn}^-) e^{jm\varphi}] , \quad (9.7)$$

$$v_z(r, z, \varphi) = \frac{1}{\rho c} ((A_{01} - B_{01}) + \sum_{n=2}^{\infty} \frac{k_{z,0,n}}{k} (A_{0n} - B_{0n}) J_0(k_{r,0,n} r) + \sum_{m=1}^{\infty} \sum_{n=1}^{\infty} \frac{k_{z,m,n}}{k} J_m(k_{r,m,n} r) [(A_{mn}^+ - B_{mn}^+) e^{-jm\varphi} + (A_{mn}^- - B_{mn}^-) e^{jm\varphi}]) . \quad (9.8)$$

Substitute these two equations into equation (9.5), one can get the power at the open end of the duct.

$$W = \int_0^{2\pi R} \int_0^{2\pi R} P^* v_z^* r dr d\varphi = \int_0^{2\pi R} \int_0^{2\pi R} \frac{1}{\rho c} ((A_{01} + B_{01}) + \sum_{n=2}^{\infty} (A_{0n} + B_{0n}) J_0(k_{r,0,n} r) + \sum_{m=1}^{\infty} \sum_{n=1}^{\infty} J_m(k_{r,m,n} r) [(A_{mn}^+ + B_{mn}^+) e^{-jm\varphi} + (A_{mn}^- + B_{mn}^-) e^{jm\varphi}]) * ((A_{01} - B_{01}) + \sum_{n=2}^{\infty} \frac{k_{z,0,n}}{k} (A_{0n} - B_{0n}) J_0(k_{r,0,n} r) + \sum_{m=1}^{\infty} \sum_{n=1}^{\infty} \frac{k_{z,m,n}}{k} J_m(k_{r,m,n} r) [(A_{mn}^+ - B_{mn}^+) e^{-jm\varphi} + (A_{mn}^- - B_{mn}^-) e^{jm\varphi}]) r dr d\varphi . \quad (9.9)$$

For convenience, this equation can be written as the aggregation of following equations.

$$W = W_1 + W_2 + \dots + W_8 + W_9. \quad (9.10)$$

In which $W_1, W_2 \dots W_9$ are given as follow,

$$\begin{aligned} W_1 &= \int_0^{2\pi R} \int_0^{\rho c} \frac{1}{\rho c} (A_{01} + B_{01})(A_{01} - B_{01})^* r dr d\varphi \\ &= \frac{\pi R^2}{\rho c} (A_{01} + B_{01})(A_{01} - B_{01})^*. \end{aligned} \quad (9.11)$$

$$\begin{aligned} W_2 &= \int_0^{2\pi R} \int_0^{\rho c} \frac{1}{\rho c} (A_{01} + B_{01}) \sum_{n=2}^{\infty} \left[\frac{k_{z0n}}{k} J_0(k_{r0n}r) (A_{0n} - B_{0n}) \right]^* r dr d\varphi \\ &= \frac{2\pi}{\rho c k} (A_{01} + B_{01}) \sum_{n=2}^{\infty} [k_{z0n} (A_{0n} - B_{0n})]^* \int_0^R r J_0(k_{r0n}r) dr. \end{aligned} \quad (9.12)$$

Applying equation below into equation (9.12)

$$\int_0^R r J_0(kr) dr = \frac{R}{k} J_1(kR). \quad (9.13)$$

One can get

$$W_2 = \frac{2\pi R}{\rho c k} (A_{01} + B_{01}) \sum_{n=2}^{\infty} [k_{z0n} (A_{0n} - B_{0n})]^* J_1(k_{r0n}R) = 0. \quad (9.14)$$

$$\begin{aligned} W_3 &= \int_0^{2\pi R} \int_0^{\rho c} \frac{1}{\rho c} (A_{01} + B_{01}) \sum_{m=1}^{\infty} \sum_{n=1}^{\infty} \left(\frac{k_{z,m,n}}{k} J_m(k_{r,m,n}r) [(A_{mn}^+ - B_{mn}^+)^* + (A_{mn}^- - B_{mn}^-)^* e^{jm\varphi}] \right) e^{-jm\varphi} r dr d\varphi \\ &= \frac{1}{\rho c k} (A_{01} + B_{01}) \int_0^R J_m(k_{r,m,n}r) r dr \int_0^{2\pi} \sum_{m=1}^{\infty} \sum_{n=1}^{\infty} (k_{z,m,n} [(A_{mn}^+ - B_{mn}^+)^* e^{-jm\varphi} + (A_{mn}^- - B_{mn}^-)^* e^{jm\varphi}]) d\varphi. \end{aligned} \quad (9.15)$$

Applying equation below into this equation

$$\int_0^{2\pi} e^{jm\varphi} d\varphi = \begin{cases} 0 & (m \neq 0) \\ 2\pi & (m = 0) \end{cases}. \quad (9.16)$$

One can get

$$W_3 = 0. \quad (9.17)$$

$$\begin{aligned}
 W_4 &= \int_0^{2\pi} \int_0^R \frac{1}{\rho c} \sum_{n=2} J_0(k_{r0n}r)(A_{0n} + B_{0n})(A_{01} - B_{01})^* r dr d\varphi \\
 &= \frac{2\pi}{\rho c} (A_{01} - B_{01})^* \sum_{n=2} (A_{0n} + B_{0n}) \int_0^R J_0(k_{r0n}r) dr.
 \end{aligned} \tag{9.18}$$

Applying equation (9.13) into this equation, one can get

$$W_4 = \frac{2\pi}{\rho c} (A_{01} - B_{01})^* \sum_{n=2} (A_{0n} + B_{0n}) J_1(k_{r0n}R) = 0. \tag{9.19}$$

$$\begin{aligned}
 W_5 &= \int_0^{2\pi} \int_0^R \frac{1}{\rho c} \sum_{N=2} J_0(k_{r0N}r)(A_{0N} + B_{0N}) \\
 &\quad * \sum_{n=2} \left[\frac{k_{z0n}}{k} J_0(k_{r0n}r)(A_{0n} - B_{0n}) \right]^* r dr d\varphi.
 \end{aligned} \tag{9.20}$$

Applying integral relations of Bessel function (9.21) into this equation

$$\int_0^R r J_m(\lambda r) J_m(\mu r) dr = \begin{cases} \frac{R}{\lambda^2 - \mu^2} [\mu J_m(\lambda R) J'_m(\mu R) - \lambda J_m(\mu R) J'_m(\lambda R)] & (\lambda \neq \mu) \\ \frac{R^2}{2} \left\{ (J'_m(\lambda R))^2 + \left(1 - \frac{m^2}{\lambda^2 R^2}\right) (J_m(\lambda R))^2 \right\} & (\lambda = \mu). \end{cases} \tag{9.21}$$

If $k_{z0N} \neq k_{z0n}$ ($N \neq n$), one can get

$$\int_0^R r J_0(k_{z0N}r) J_0(k_{z0n}r) dr = 0. \tag{9.22}$$

So equation (9.20) can be written as

$$\begin{aligned}
 W_5 &= \frac{1}{\rho c k} \int_0^{2\pi} \int_0^R \sum_{n=2} J_0^2(k_{r0n}r)(A_{0n} + B_{0n}) [k_{z0n}(A_{0n} - B_{0n})]^* r dr d\varphi \\
 &= \frac{2\pi}{\rho c k} \int_0^R \sum_{n=2} (A_{0n} + B_{0n}) [k_{z0n}(A_{0n} - B_{0n})]^* J_0^2(k_{r0n}r) r dr \\
 &= \frac{\pi R^2}{\rho c k} \sum_{n=2} (A_{0n} + B_{0n}) [k_{z0n}(A_{0n} - B_{0n})]^* J_0^2(k_{r0n}R).
 \end{aligned} \tag{9.23}$$

$$\begin{aligned}
 W_6 &= \int_0^{2\pi} \int_0^R \frac{1}{\rho c} \sum_{n=2} J_0(k_{r0n}r)(A_{0n} + B_{0n}) \\
 &\quad * \sum_{m=1}^{\infty} \sum_{n=1}^{\infty} \left(\frac{k_{z,m,n}}{k} J_m(k_{r,m,n}r) [(A_{mn}^+ - B_{mn}^+) e^{-jm\varphi} + (A_{mn}^- - B_{mn}^-) e^{jm\varphi}] \right)^* r dr d\varphi.
 \end{aligned} \tag{9.24}$$

Applying equation (9.16) into this equation, because in this equation, there is $m \neq 0$, so one can get

$$W_6 = 0. \quad (9.25)$$

$$W_7 = \frac{1}{\rho c} \int_0^{2\pi R} \int_0^{\infty} \sum_{m=1}^{\infty} \sum_{n=1}^{\infty} J_m(k_{r,m,n}r) [(A_{mn}^+ + B_{mn}^+)e^{-jm\varphi} + (A_{mn}^- + B_{mn}^-)e^{jm\varphi}]^* (A_{01} - B_{01})^* r dr d\varphi. \quad (9.26)$$

Applying equation (9.16) into this equation, one can get

$$W_7 = 0. \quad (9.27)$$

$$W_8 = \frac{1}{\rho c} \int_0^{2\pi R} \int_0^{\infty} \sum_{m=1}^{\infty} \sum_{n=1}^{\infty} (J_m(k_{r,m,n}r) [(A_{mn}^+ + B_{mn}^+)e^{-jm\varphi} + (A_{mn}^- + B_{mn}^-)e^{jm\varphi}]) \\ * \sum_{n=2}^{\infty} \left[\frac{k_{z0n}}{k} (A_{0n} - B_{0n}) \right]^* r dr d\varphi. \quad (9.28)$$

Still one can apply equation (9.16) into this equation, then there is

$$W_8 = 0. \quad (9.29)$$

$$W_9 = \frac{1}{\rho c} \int_0^{2\pi R} \int_0^{\infty} \sum_{M=1}^{\infty} \sum_{N=1}^{\infty} (J_M(k_{r,M,N}r) [(A_{MN}^+ + B_{MN}^+)e^{-jM\varphi} + (A_{MN}^- + B_{MN}^-)e^{jM\varphi}]) \\ * \sum_{m=1}^{\infty} \sum_{n=1}^{\infty} \left(\frac{k_{z,m,n}}{k} J_m(k_{r,m,n}r) [(A_{mn}^+ - B_{mn}^+)e^{-jm\varphi} + (A_{mn}^- - B_{mn}^-)e^{jm\varphi}] \right)^* r dr d\varphi. \quad (9.30)$$

According to the relationship between the complex conjugates

$$(A^* B)^* = A^* * B^*, \quad (9.31)$$

$$W_9 = \frac{1}{\rho c} \int_0^{2\pi R} \int_0^{\infty} \sum_{M=1}^{\infty} \sum_{N=1}^{\infty} (J_M(k_{r,M,N}r) [(A_{MN}^+ + B_{MN}^+)e^{-jM\varphi} + (A_{MN}^- + B_{MN}^-)e^{jM\varphi}]) \\ * \sum_{m=1}^{\infty} \sum_{n=1}^{\infty} \left(\frac{k_{z,m,n}^*}{k} J_m(k_{r,m,n}r) [(A_{mn}^+ - B_{mn}^+)^* e^{jm\varphi} + (A_{mn}^- - B_{mn}^-)^* e^{-jm\varphi}] \right) r dr d\varphi. \quad (9.32)$$

Applying equation (9.16) into equation (9.32), one can see if $M \neq m$, the integration should be equal zero, so equation (9.32) can be written as,

$$\begin{aligned}
 W_9 = \frac{2\pi}{\rho c} * \int_0^R \left(\sum_{m=1}^{\infty} \sum_{N=1}^{\infty} \left((J_m(k_{r,m,N}r)(A_{mN}^+ + B_{mN}^+))^* \sum_{n=1}^{\infty} \frac{k_{z,m,n}^*}{k} J_m(k_{r,m,n}r)(A_{mn}^+ - B_{mn}^+)^* \right. \right. \\
 \left. \left. + J_m(k_{r,m,N}r)(A_{mN}^- + B_{mN}^-) * \sum_{n=1}^{\infty} \frac{k_{z,m,n}^*}{k} J_m(k_{r,m,n}r)(A_{mn}^- - B_{mn}^-)^* \right) \right) r dr . \quad (9.33)
 \end{aligned}$$

Then according to integral relations of Bessel function (9.21), only those items that agree $N = n$ are not equal to zero. So the equation can be written as,

$$\begin{aligned}
 W_9 = \frac{\pi R^2}{\rho c k} \sum_{m=1}^{\infty} \sum_{n=1}^{\infty} \left(\left(1 - \frac{m^2}{k_{r,m,n}^2 R^2} \right) J_m^2(k_{r,m,n}R) k_{z,m,n}^* [(A_{mn}^+ + B_{mn}^+)(A_{mn}^+ - B_{mn}^+)^* \right. \\
 \left. + (A_{mn}^- + B_{mn}^-)(A_{mn}^- - B_{mn}^-)^*] \right) . \quad (9.34)
 \end{aligned}$$

So From equation (9.11) to equation (9.34), one can get the values of W_1 to W_9 . Also from these equations, one can see that only W_1 , W_5 and W_9 are not zero. So equation (9.10) can be written as,

$$\begin{aligned}
 W &= W_1 + W_2 + \dots + W_8 + W_9 \\
 &= W_1 + W_5 + W_9 \\
 &= \frac{\pi R^2}{\rho c k} \{ k(A_{01} + B_{01})(A_{01} - B_{01})^* + \\
 &\quad \sum_{n=2}^{\infty} k_{z,0,n}^* J_0^2(k_{r0n}R)(A_{0n} + B_{0n})(A_{0n} - B_{0n})^* + \\
 &\quad \sum_{m=1}^{\infty} \sum_{n=1}^{\infty} \left(k_{z,m,n}^* \left(1 - \frac{m^2}{k_{r,m,n}^2 R^2} \right) J_m^2(k_{r,m,n}R) [(A_{mn}^+ + B_{mn}^+)(A_{mn}^+ - B_{mn}^+)^* \right. \\
 &\quad \left. + (A_{mn}^- + B_{mn}^-)(A_{mn}^- - B_{mn}^-)^*] \right) \} . \quad (9.35)
 \end{aligned}$$

From equation (9.35), it can be seen that the power at the open end of the duct is a function of the amplitudes of different higher-order modes, such as A_{01} , B_{01} ... A_{mn}^- and B_{mn}^- . Which means if these amplitudes are obtained, one can get this power easily from equation (9.35). In previous chapters, the amplitudes of those higher-order modes have been obtained. So just substitute these amplitudes into the equation above to get the power theoretically.

The power W obtained from equation (9.35) is a 'complex power', the real part of W is the mean (active) power which is radiated from the end of the duct along z -axis. The imaginary part of W is the reactive power which only exists in the plane transverse to z -

axis and cannot be radiated out of the duct. So the power radiated from the end of duct should be written as

$$\begin{aligned}
 W_r &= \text{real}(W) \\
 &= \text{real} \left(\frac{\pi R^2}{\rho c k} \left\{ k(A_{01} + B_{01})(A_{01} - B_{01})^* + \right. \right. \\
 &\quad \left. \sum_{n=2} k_{z,0,n}^* J_0^2(k_{r,0n} R)(A_{0n} + B_{0n})(A_{0n} - B_{0n})^* + \right. \\
 &\quad \left. \left. \sum_{m=1}^{\infty} \sum_{n=1}^{\infty} \left(k_{z,m,n}^* \left(1 - \frac{m^2}{k_{r,m,n}^2 R^2} \right) J_m^2(k_{r,m,n} R) [(A_{mn}^+ + B_{mn}^+)(A_{mn}^+ - B_{mn}^+)^* \right. \right. \right. \\
 &\quad \left. \left. \left. + (A_{mn}^- + B_{mn}^-)(A_{mn}^- - B_{mn}^-)^* \right] \right) \right\} \right). \tag{9.36}
 \end{aligned}$$

From equation (9.36), it can be seen that the power radiated from the duct end is the sum of the powers radiated in different modes. There is no cross coupling effects appearing in this equation. Which means for the radiated power, the acoustic pressure of one single mode p_{mn} can only drive the particle velocity v_{MN} of same mode ($M = m$ and $N = n$). The cross coupling items, such as $p_{mn}^* v_{MN}$ ($m \neq M$ or $n \neq N$), are all equal to zero.

In equation (9.36), the amplitudes of the higher-order modes, such as A_{01} , $B_{01} \dots A_{mn}^-$ and B_{mn}^- , are complex numbers. Take A_{mn}^+ and B_{mn}^+ for example, one can write them as,

$$\begin{aligned}
 A_{mn}^+ &= x_1 + iy_1, \\
 B_{mn}^+ &= x_2 + iy_2. \tag{9.37}
 \end{aligned}$$

In which, x_1 , y_1 , x_2 and y_2 are all real numbers.

So the item $\text{real}\{(A_{mn}^+ + B_{mn}^+)(A_{mn}^+ - B_{mn}^+)^*\}$ in equation (9.36) can be given as,

$$\begin{aligned}
 &\text{real}((A_{mn}^+ + B_{mn}^+)(A_{mn}^+ - B_{mn}^+)^*) \\
 &= \text{real}\{((x_1 + x_2) + i(y_1 + y_2))^* ((x_1 - x_2) + i(y_2 - y_1))\} \\
 &= (x_1^2 + y_1^2) - (x_2^2 + y_2^2). \tag{9.38}
 \end{aligned}$$

From this equation, it can be seen that the first item is the square of the amplitude of the incident wave A_{mn}^+ and the second item is the square of the amplitude of the reflected

wave B_{mn}^+ . Also from the complex reflections coefficients R_{mnl} shown in Chapter 3, which defines the relationships between A_{mn}^+ and B_{mn}^+ , there is

$$\text{Amplitude}(R_{mnl}) \leq 1. \quad (9.39)$$

So one can have the following relationship

$$(x_1^2 + y_1^2) \geq (x_2^2 + y_2^2). \quad (9.40)$$

Which means the item $\text{real}\{(A_{mn}^+ + B_{mn}^+)(A_{mn}^+ - B_{mn}^+)^*\}$ is always larger than zero, the same is for items such as, $\text{real}\{(A_{mn}^- + B_{mn}^-)(A_{mn}^- - B_{mn}^-)^*\}$ and $\text{real}\{(A_{0n} + B_{0n})(A_{0n} - B_{0n})^*\}$. So every item in equation (9.36) is not a negative value and the total value of the power radiated W_r from the end of the duct is always positive, which agrees with the real situation - the net power is always radiated out of the duct rather than in the duct along the z-axis at the open end.

9.2.2 Approximate lumped-parameter model

For the source duct end, only the plane wave is considered and the amplitudes of the incident and reflected wave, SA_{01} and SB_{01} , are also obtained, substitute these amplitudes and the coordinate of the source plane into equation (9.5), one can also get the power radiated from the source duct end (i.e. the power transmitted into the main duct) as follow,

$$\begin{aligned} W_{s_r} &= \text{real}(W_s) \\ &= \text{real}\left\{\frac{\pi R_s^2}{\rho c} (SA_{01}e^{-jkz} + SB_{01}e^{jkz})(SA_{01}e^{-jkz} - SB_{01}e^{jkz})^*\right\}. \end{aligned} \quad (9.41)$$

From equation (9.41), the power radiated into the main duct can be obtained. From equation (9.36), not only the total powers radiated out of the duct, but also the powers of different modes radiated out of the main duct can be obtained. Then one can take acoustic pressure and power as two parameters and construct the approximate acoustical two-port system as shown in Fig 9.1. Assume that the duct and aperture device consist of a black box, when one apply specific acoustic pressure and power from the input end, accordingly one can get the corresponding acoustic pressure and power pattern from the output end.

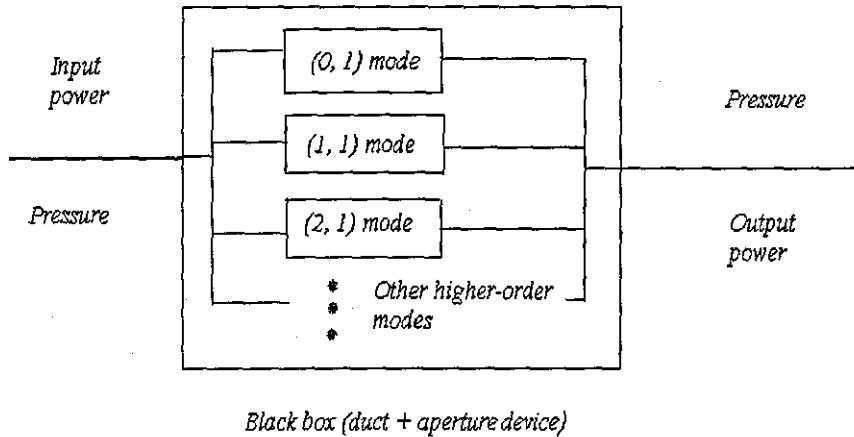


Fig 9.1 The plot of the approximate two-port system model

Compared with the two-ports system model shown in Chapter 2, for the sound source end, there is only the plane wave propagating along the duct, so the acoustic pressure in the plane transverse to z -axis is equal everywhere and the power radiated out is all in the plane wave form.

However, at the open end, the power radiated out in the form of the combination of different higher-order modes, so the powers radiated in different modes rather than the total power can be taken as the lumped parameters. Also at the open end of the duct, the acoustic pressure is dependent on the coordinate (r, φ) in the plane transverse to z -axis. So this model can only be called an approximate lumped-parameter model. This investigation is focused on the distribution of the powers radiated out of the duct rather than the acoustic pressure at the open end.

So one can analyze the performances of different aperture devices in two aspects.

1. Analysis of the radiated power, especially the power of every single mode. Through the comparison of these powers at different normalized wave number ranges, one can get the relationships between the powers of different higher-order modes, as well as the relationship between the power of a single mode with total power radiated out of the duct. Through these relationships one can tell the

effects of the aperture devices on the whole in-duct field, as well as the applicability of this approximate model.

2. Analysis of the insertion loss (IL) of different aperture devices. Through the comparison of the IL for different aperture devices, one can also study the effects of different aperture devices on the in-duct acoustic field. From equation (9.1), it can be seen that the insertion loss is a relative value between the radiated powers for the duct with an aperture device situation and the duct without an aperture device situation. So through the study of the insertion loss, one can separate the performance of the aperture device from the performance of the main duct.

9.2.3 Energy loss along Z-axis in the main duct

From equation (9.36) and equation (9.41), one can get the power radiated from the end of the duct and the source end respectively. Taking several different situations for example, comparison is made between the power radiated from the end of duct W_r and the power radiated from the source duct end W_{s_r} . The results are shown in Fig 9.2 (I) and the comparative relationships between source duct and orifices are shown in Fig 9.2 (II). These different situations include (a) source duct located eccentric and no aperture device in the main duct; (b) source duct located eccentric and a simple aperture device is placed in duct; (c) source duct located concentric and no aperture device in the main duct; (d) source duct located concentric and a simple aperture device is placed in the duct.

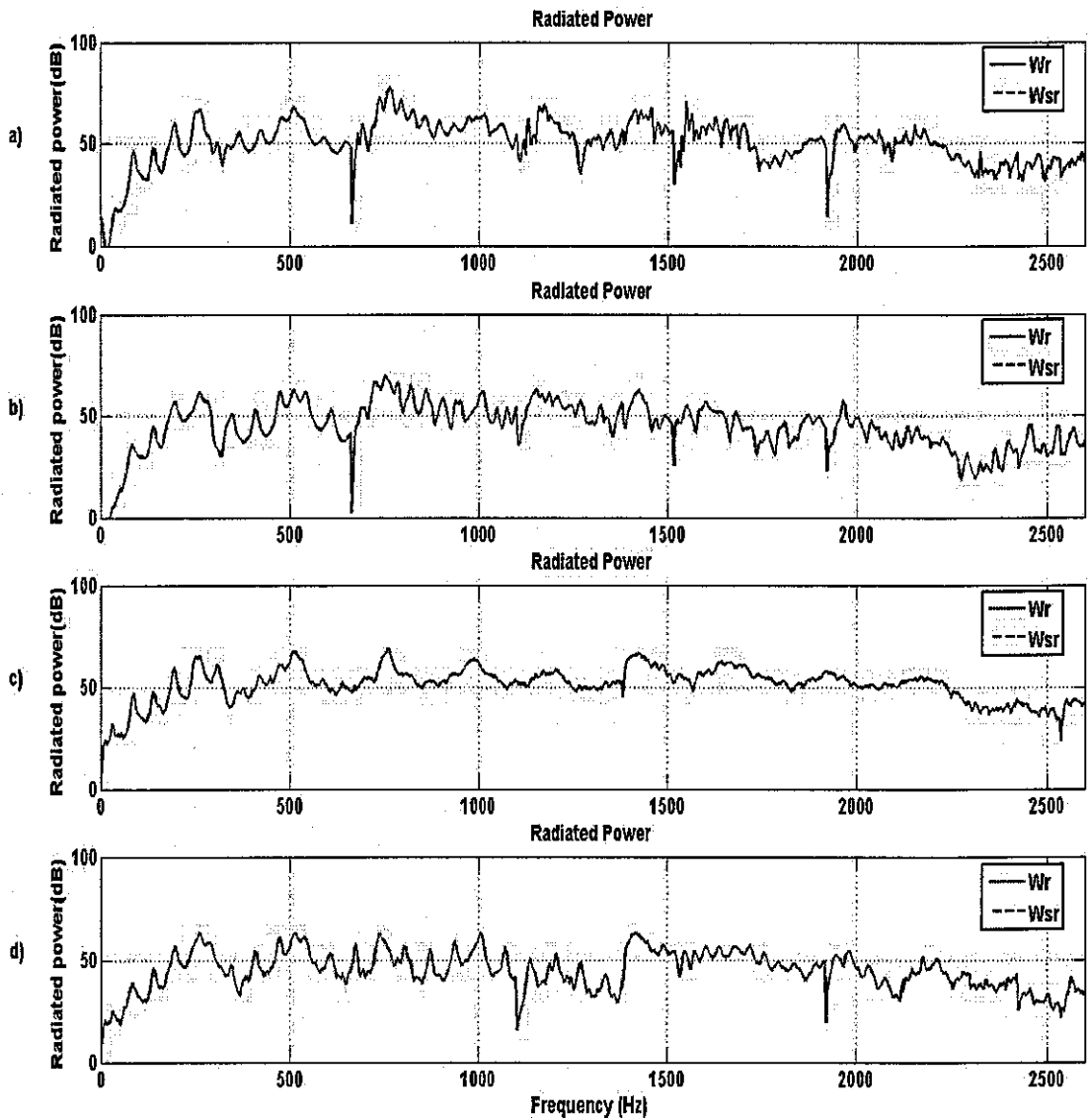


Fig 9.2 (I) Comparison of power radiated from duct end and source duct end for different situations

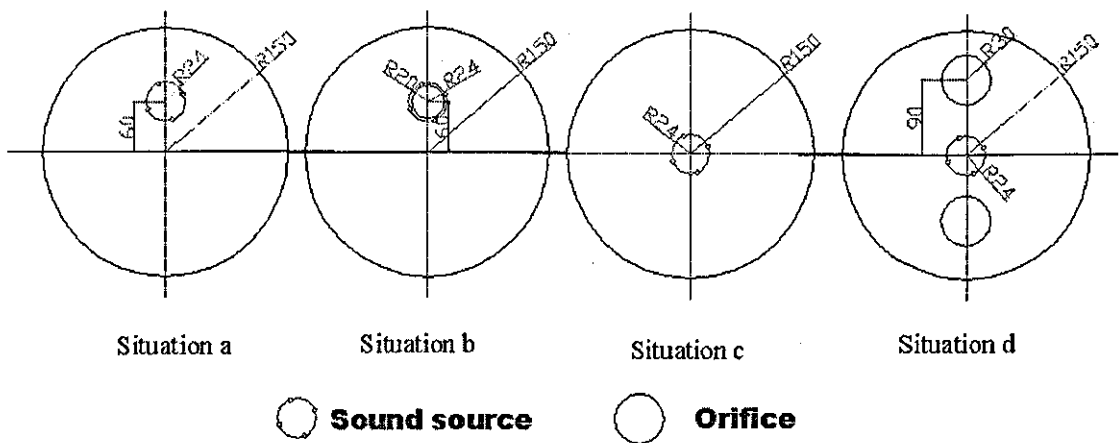


Fig 9.2 (II) Configurations of four source-orifices relationship situations

It can be seen that theoretically for all situations shown in Fig 9.2 (II), the power radiated from the duct end equals to the power radiated from the source duct end. Which means all energies transmitted into the main duct are radiated out from the end of the duct and there is no energy loss along z -axis in duct. This is considered to be reasonable, because first there is no energy absorbing materials applied in the main duct; secondly, the wall of the main duct is considered perfect rigid. So theoretically there is no energy loss mechanism in this situation.

So from this figure it can be seen that the simple aperture device used in the investigation cannot cause any energy loss. Instead it changes the impedance of the acoustic system and then change the amplitudes of different higher-order modes, finally it can change the power radiated from the sound source duct at different parts of the frequency range.

9.2.4 Effects of the source location on the radiated power

First of all, take the duct without an aperture device for example, when the source duct is located at $\partial = 40\%R$ ($0.06m$) (eccentric situation, Situation a in Fig 9.2(II)) and $\partial = 0\%R$ ($0.00m$) (concentric situation, Situation c in Fig 9.2(II)) respectively, the powers radiated from end of the duct are plotted in Fig 9.3. Fig 9.3 a) is plotted in linear frequency range; Fig 9.3 b) is plotted in 1/6 octave band; Fig 9.3 c) shows the difference between these two situations: Powers radiated at eccentric situation - Powers radiated at concentric situation.

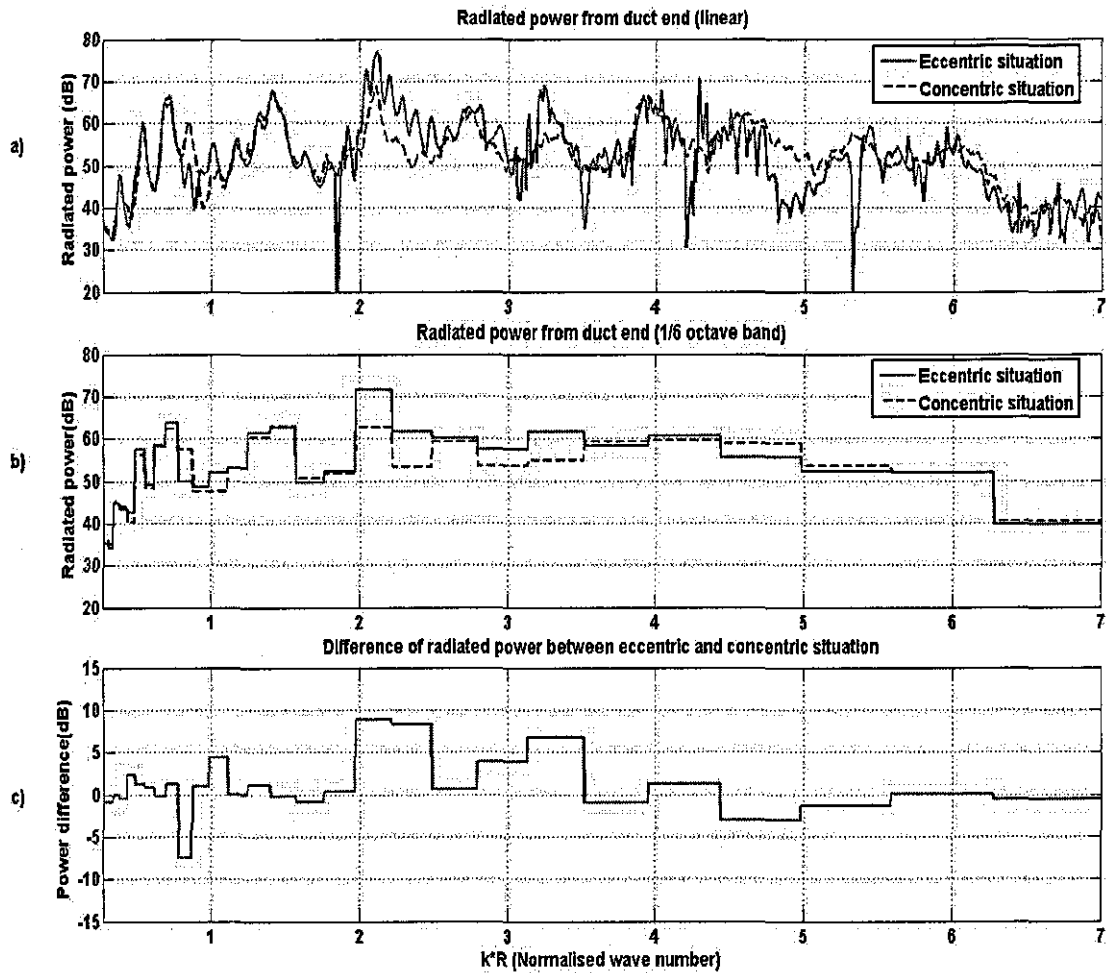


Fig 9.3 Difference of powers radiated from duct end between source eccentric situation and source concentric situation

From this figure, it can be seen that when there is no aperture device in duct, the powers radiated from the duct end for these two situations are different. The biggest difference appears at the normalized wave number range of $1.84 < k^*R < 3.5$. In which four axially-unsymmetric higher-order modes $(\pm 1,1)$ and $(\pm 2,1)$ begin to propagate along the duct. So the powers radiated out of the duct at this normalized wave number range for the source eccentric situation are larger than those for the source concentric situation, because for the source concentric situation, these four axially-unsymmetric higher-order modes do not propagate along the duct at this normalized wave number range. After the symmetric higher-order mode, $(0,2)$ mode cuts on; the power radiated from the duct end for concentric situation is larger than that for the eccentric situation. Because at this frequency range, the axially-symmetric higher-order modes are the dominate ones.

From this figure, one can see the effects of the sound source location in the plane transverse to the z-axis. For the plane wave range and even higher normalized wave number range ($k * R > 6$), this effect is very small, because the radiated powers for these two situations are nearly equal. In the normalized wave number range ($1.8 < k * R < 6$), the powers radiated from duct end for these two situations are quite different from each other. In this normalized wave number range, there are mainly (0, 1) mode, ($\pm 1, 1$) modes, ($\pm 2, 1$) modes, (0, 2) mode and ($\pm 3, 1$) modes propagation in main duct. So discussion in the following sections will be focused on the radiated powers of those modes and the totally radiated power in this normalized wave number range.

9.3 Analysis of the radiated power of different single higher-order mode

From equation (9.36), it is easy to obtain the total power radiated from the end of the duct, as well as the power radiated in the form of each mode. So in this section, the relationships between them are studied. Still according to the relationship between the sound source and the main duct, there are source concentric situation and source eccentric situation. The first one to be studied is the source concentric situation.

9.3.1 Source concentric situation

One can get the power radiated from the end of the duct for each mode from equation (9.36). In order to show the relationships between different modes for different source-orifice situations, some source-orifice situations are chosen and plotted in the figures below. In these figures, *a*) shows power radiated for the each mode from the end of the duct (for clarity, not all propagating modes are plotted, only (0, 1) mode, ($\pm 1, 1$) modes, ($\pm 2, 1$) modes, (0, 2) mode and ($\pm 3, 1$) modes are plotted). *b*) shows the percentages of the power of each mode over the total power radiated from the end of the duct.

Fig 9.4 shows the situation when there is no aperture device in duct; Fig 9.5 shows the situation when there is a single concentric orifice (Situation 1 in Fig 8.5); Fig 9.6 shows the situation when there is a single eccentric orifice (Situation 2 in Fig 8.5).

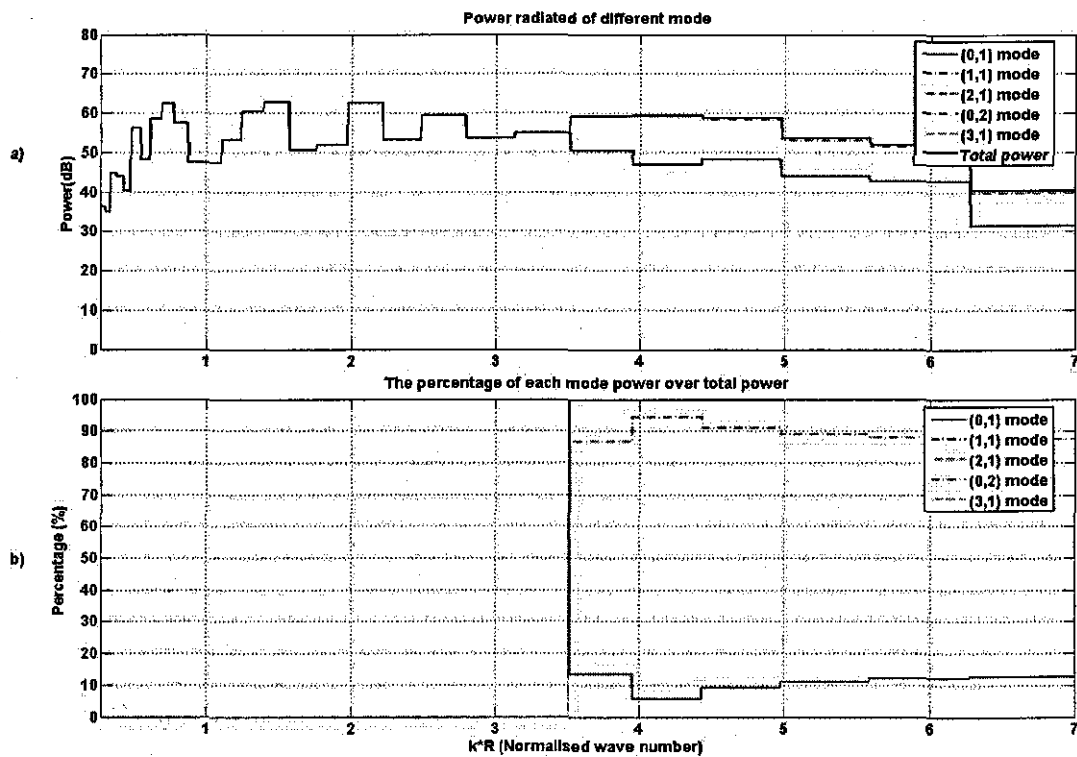


Fig 9.4 Powers radiated from the end of the duct for different modes and their relationships with total power (without aperture device situation)

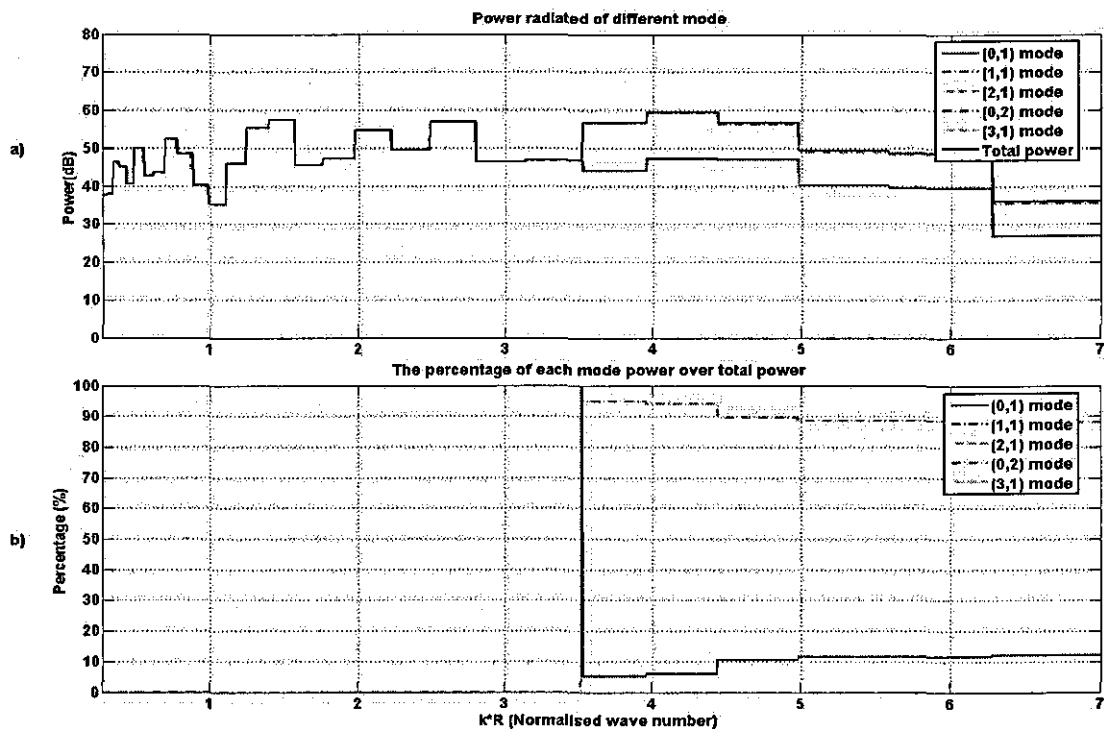


Fig 9.5 Powers radiated from the end of the duct for different modes and their relationships with total power (Situation 1 in Fig 8.5)

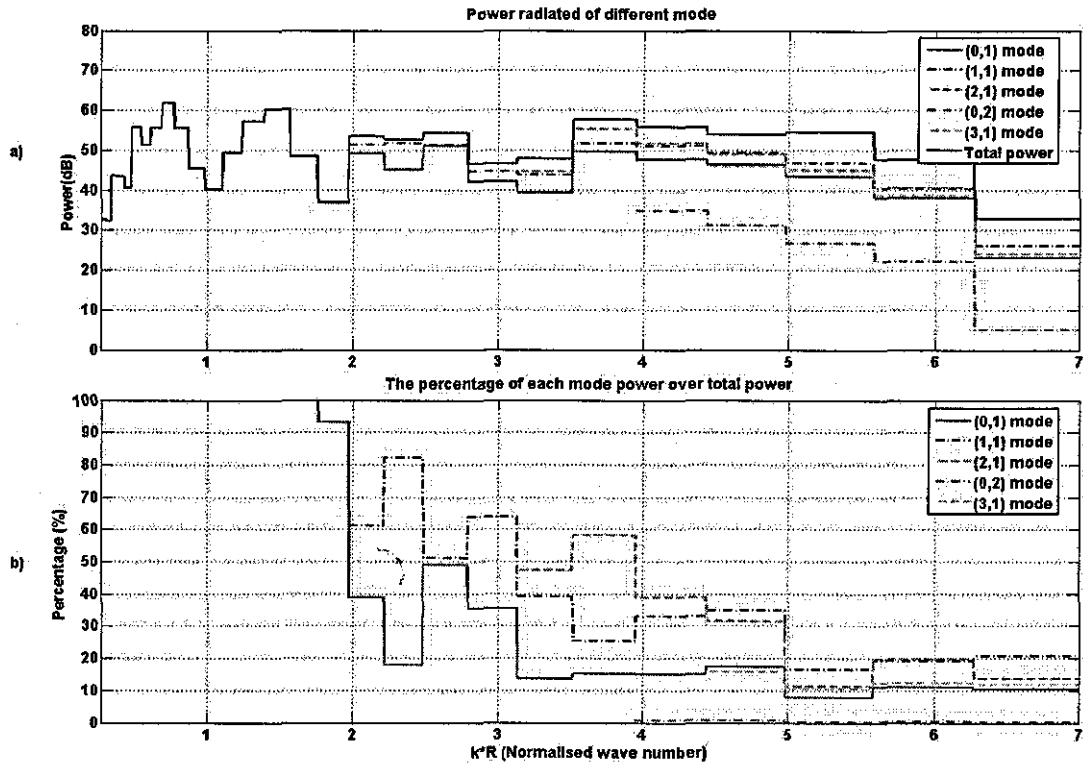


Fig 9.6 Powers radiated from the end of the duct for different modes and their relationships with total power (Situation 2 in Fig 8.5)

From Fig 9.4-9.6, it can be seen that,

1. Without an aperture device in the duct, only axially-symmetric modes radiate energy from the end of the duct. Before (0, 2) mode cuts on, all energy radiated out of the duct is in the form of (0, 1) mode; after (0, 2) mode cuts on, most energy (90% of total energy) radiates in the form of (0, 2) mode.
2. For the device with a single concentric orifice situation, still only axially-symmetric modes radiate energy from the end of the duct. Through the comparison of Fig 9.4 and Fig 9.5, it is easy to find that they are quite similar. Which means the presence of such an aperture device in the duct does not change the pattern of the energy radiated out of the duct.
3. For the device with a single eccentric orifice situation, with such an orifice presence, other higher-order modes begin to radiate some energy out of the duct. After the first higher-order mode cuts on, most energy is radiated in the form of the axially-unsymmetric higher-order modes (the contributions of the axially-symmetric modes only account 10%-20%). Which means the presence

of such an aperture device in the duct changes the pattern of the energy radiated out of the duct dramatically.

All other configurations of the orifices are considered and the configurations fall into four categories, which are the axially-symmetric without concentric orifice situation; the axially-symmetric with concentric orifice situation; the axially-unsymmetric without concentric orifice situation and the axially-unsymmetric with concentric orifice situation. So taking one example from each category and the results are shown below.

Fig 9.7 is for the axially-symmetric with concentric orifice situation (Situation 4 in Fig 8.15); Fig 9.8 is for the axially-symmetric without concentric orifice situation (Situation 3 in Fig 8.15). Fig 9.9 is for the axially-unsymmetric with concentric orifice situation (Situation 2 in Fig 8.11); Fig 9.10 is for the axially-unsymmetric without concentric orifice situation (Situation 3 in Fig 8.11).

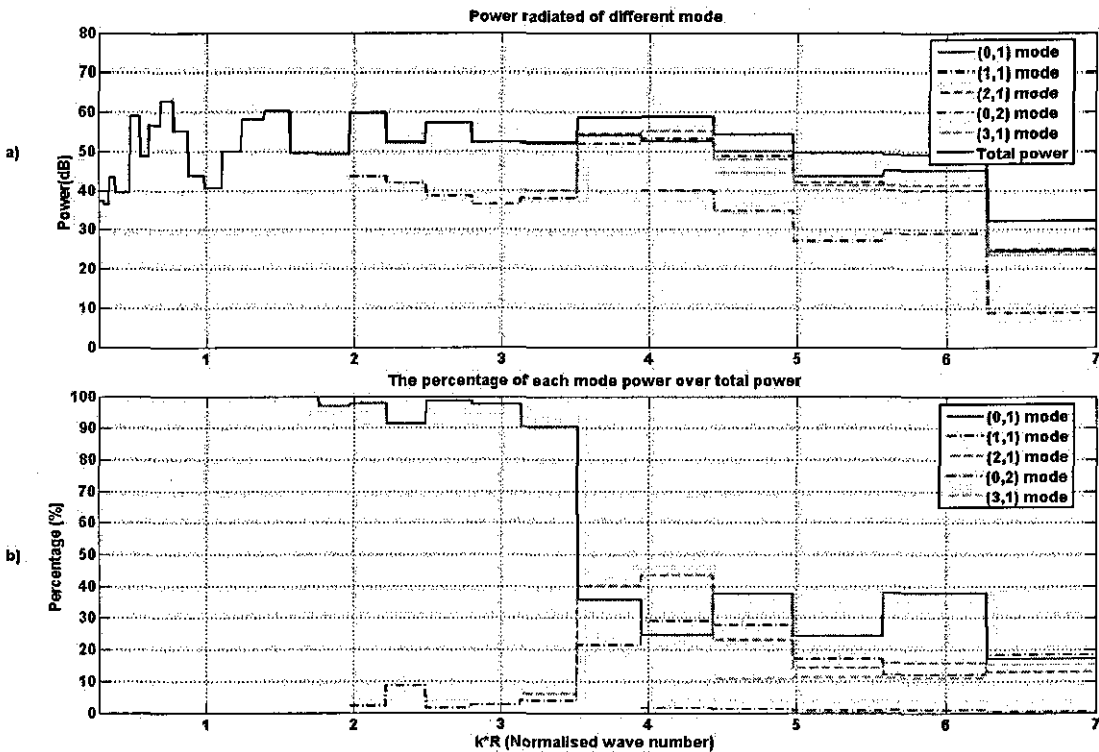


Fig 9.7 Powers radiated from the end of the duct for different modes and the relationships with total power (Situation 4 in Fig 8.15)

9. Radiated power and the insertion loss for different aperture devices

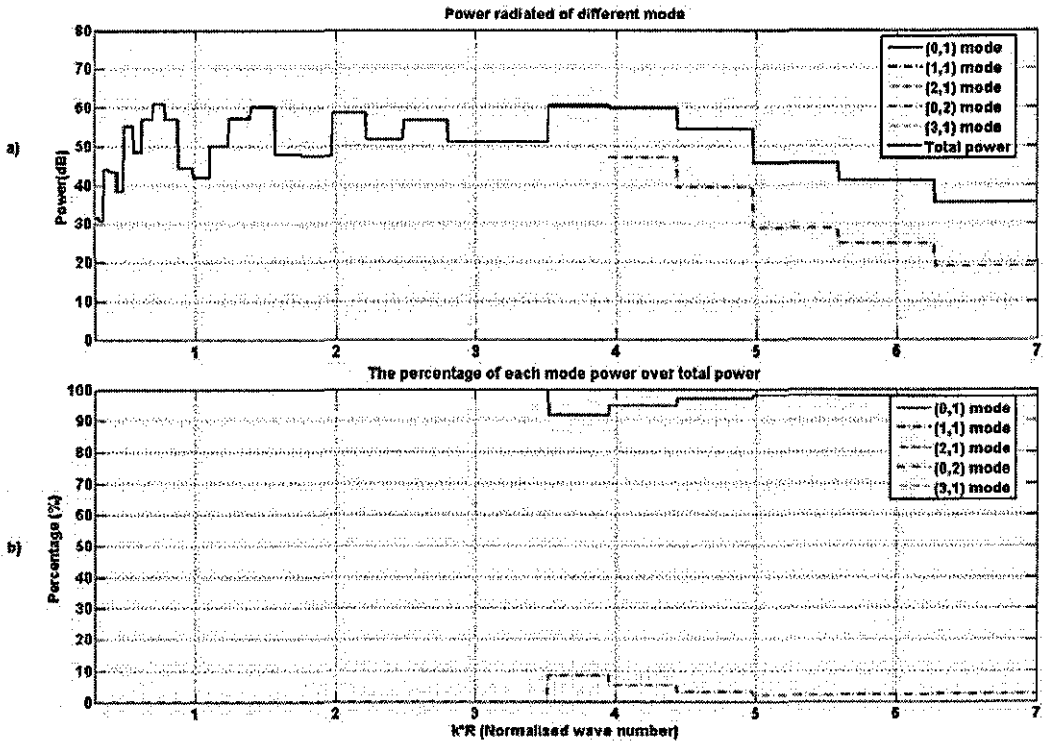


Fig 9.8 Powers radiated from the end of the duct for different modes and the relationships with total power (Situation 3 in Fig 8.15)

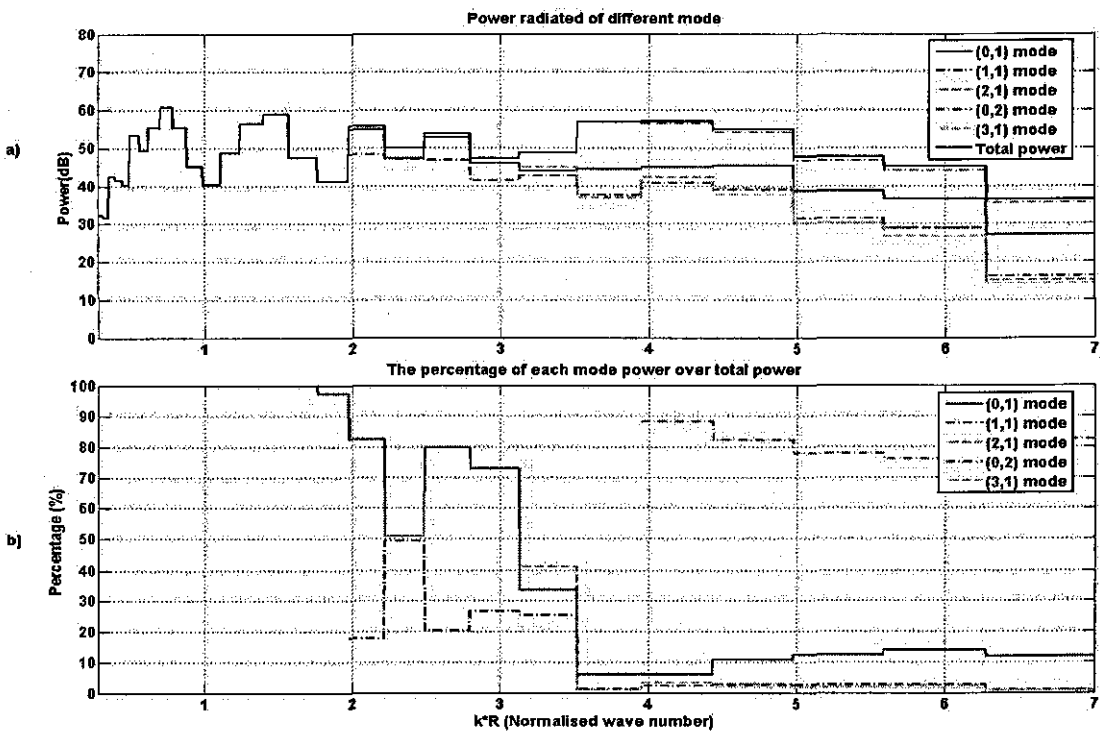


Fig 9.9 Powers radiated from the end of the duct for different modes and the relationships with total power (Situation 2 in Fig 8.11)

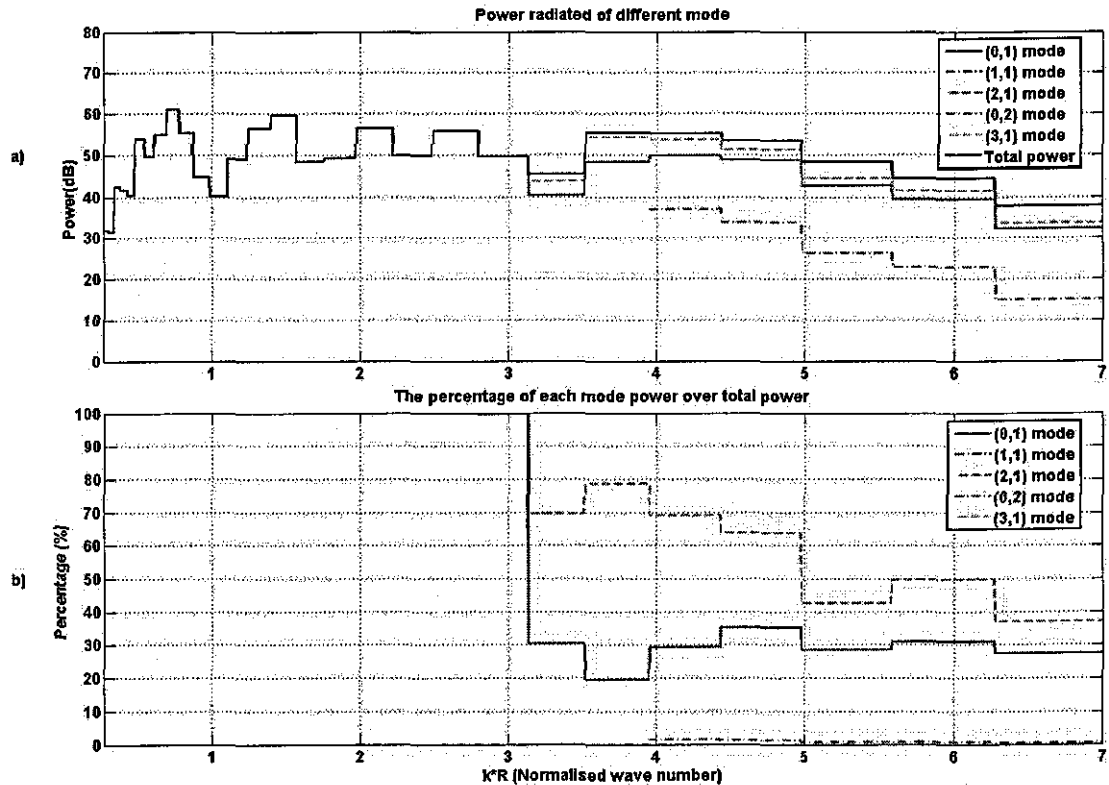


Fig 9.10 Powers radiated from the end of the duct for different modes and the relationships with total power (Situation 3 in Fig 8.11)

From Fig 9.7-9.10, it can be seen that

1. For the axially-symmetric with concentric orifice situation (shown in Fig 9.7), all higher-order modes appear in the after orifice field after these modes cut on. At most of the wave number range, the plane wave contributes most to the total energy. Even with the concentric orifice, after the (0, 2) mode cuts on, this mode contributes only about 2% of total energy, which means although this axially-symmetric higher-order mode appears in the after orifice field, compared with other modes, it is nearly negligible.
2. For the axially-symmetric without concentric orifice situation (shown in Fig 9.8), only axially-symmetric higher-order modes appear in the after orifice field. Which is contrary to what is expected. At this situation, it is expected that those axially-unsymmetric higher-order modes appear or even dominate in the after orifice field after these modes cut on. The only reason for this phenomenon is that those axially-unsymmetric higher-order modes produced by those axially-symmetric orifices counteract with each other and only

axially-symmetric higher-order modes are left in the after orifice field. From this figure, it is also observed there is nearly only the plane wave is left in the after orifice field. Although after (0, 2) mode cuts on, this mode contributes 2%-8% of total energy, compared with the contribution of the plane wave (more than 90% of total energy), this higher-order mode contribution is very small.

3. For the axially-unsymmetric with concentric orifice situation (shown in Fig 9.9), all those modes appear in the after orifice field and the contributions of those axially-symmetric higher-order modes are significant. Before (0, 2) mode cuts on, the plane wave contributes most to the total energy and after (0, 2) mode cuts on, (0, 2) mode contributes more than 70% of total energy.
4. For the axially-unsymmetric without concentric orifice situation (shown in Fig 9.10), it is noticed that only the plane wave, $(\pm 2, 1)$ modes and (0,2) mode appear in the after orifice field; $(\pm 1, 1)$ modes and $(\pm 3, 1)$ modes disappears. This is also contrary to what is expected to be. It is expected these four axially-unsymmetric higher-order modes should appear after those modes cut on. Still the only reason for this phenomenon is those four higher-order modes produced by those two orifices counteract with each other. Also the contribution of (0, 2) mode is negligible, which agrees with the expectation.
5. Through the comparison of Fig 9.7 with Fig 9.8 and Fig 9.9 with Fig 9.10, one can see that for the source concentric situation, the concentric orifice in the device plays a very important role in the distribution of the energies between the higher-order modes. For axially-symmetric placed orifices, the concentric orifice can increase the percentage of the power radiated out of the duct by the axially-unsymmetric higher-order modes. For axially-unsymmetric placed orifices, the concentric orifice can increase the percentage of the power radiated out of the duct by the axially-symmetric higher-order modes.
6. Through the comparison between Fig 9.7 and Fig 9.10, it can be seen that the arrangement of the eccentric orifices also have a significant effect on the distribution of the power radiated out of the duct between higher-order modes. By arranging different numbers of the orifices or the positions of the orifices, one can eliminate some higher-order modes from the after orifice field, as well

as one can increase or decrease the contributions of some specific higher-order modes.

From the analysis above, it can be seen that the arrangement of the orifices in the device do have a decisive effect on the higher-order modes distribution in the after orifice field for the sound source concentric situation. In next section, the effects of those orifices on the after orifice field when the sound source located eccentric to the main duct are discussed.

9.3.2 Source eccentric situation

In this section, the source duct located eccentric to the main duct situation is studied. In order to show the relationships between different source-orifice situations, certain source-orifice situations are chosen and plotted in the figures below. In these figures, a) shows power radiated for the each mode from the end of the duct (for clarity, not all propagating modes are plotted, only $(0, 1)$ mode, $(\pm 1, 1)$ modes, $(\pm 2, 1)$ modes, $(0, 2)$ mode and $(\pm 3, 1)$ modes are plotted); b) shows the percentages of the power of each mode over the total power radiated from the end of the duct.

Fig 9.11 shows the situation when there is no aperture device in the duct; Fig 9.12 shows the situation when there is a single concentric orifice in the duct (Situation 3 in Fig 8.5); Fig 9.13 shows the situation when there is a single eccentric orifice in the duct (Situation 4 in Fig 8.5).

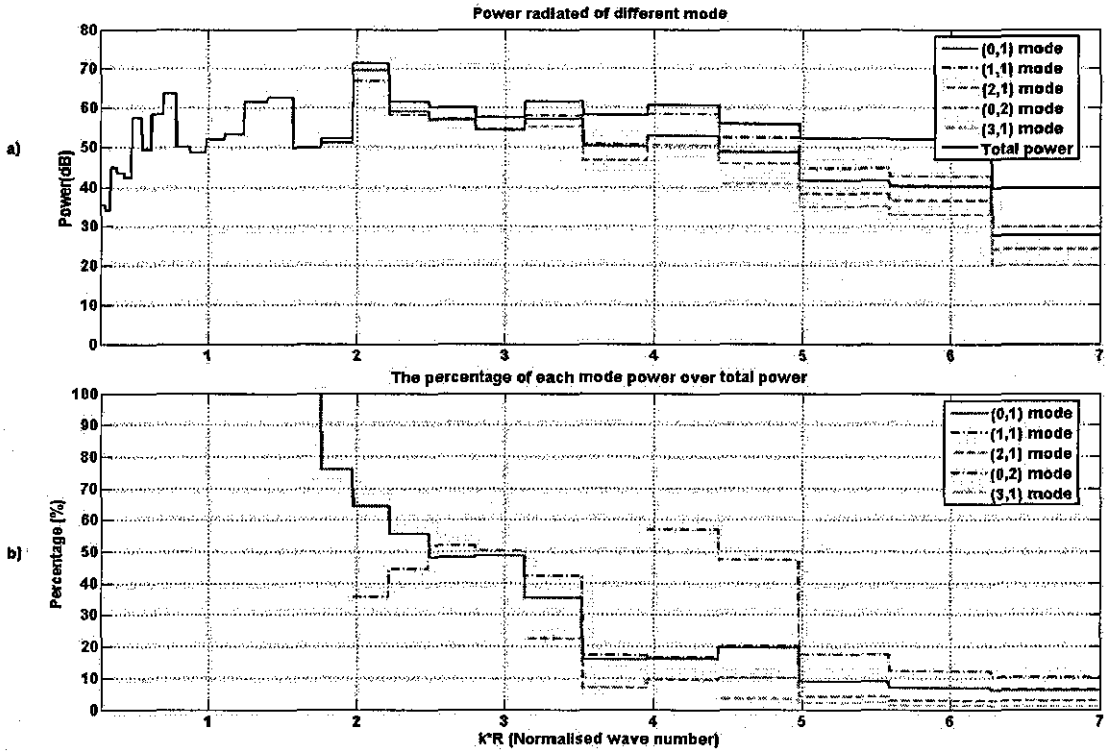


Fig 9.11 Powers radiated from the end of the duct for different modes and the relationships with total power (without aperture device situation)

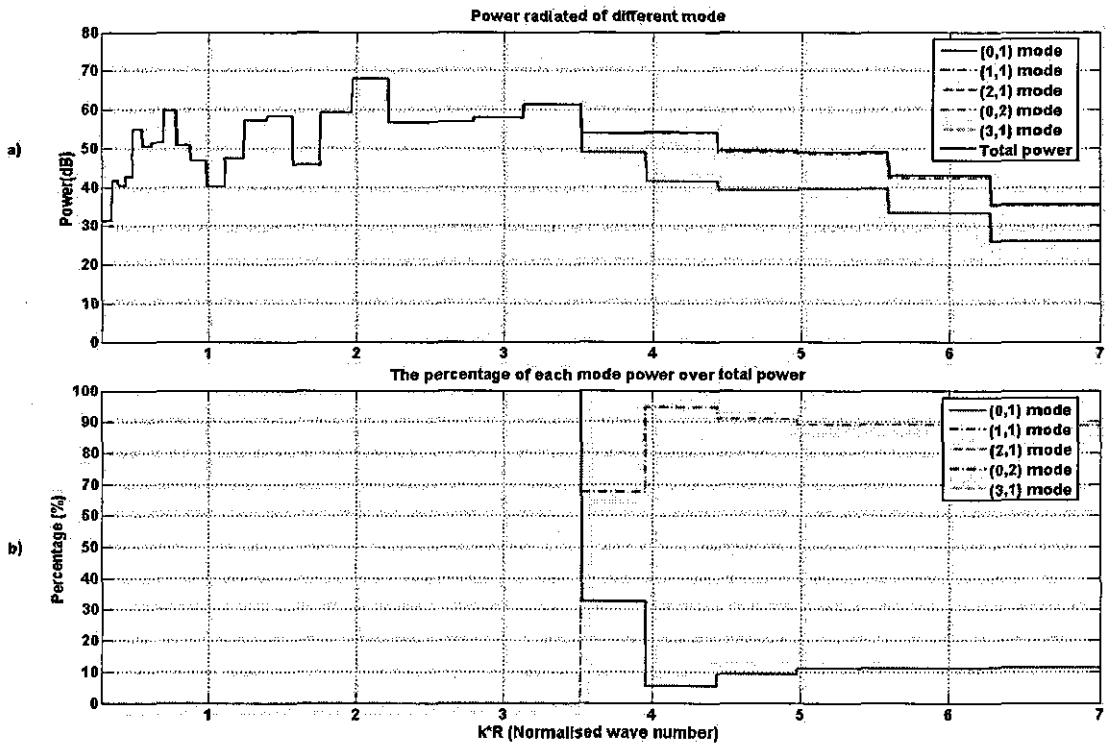


Fig 9.12 Powers radiated from the end of the duct for different modes and the relationships with total power (situation 3 in Fig 8.5)

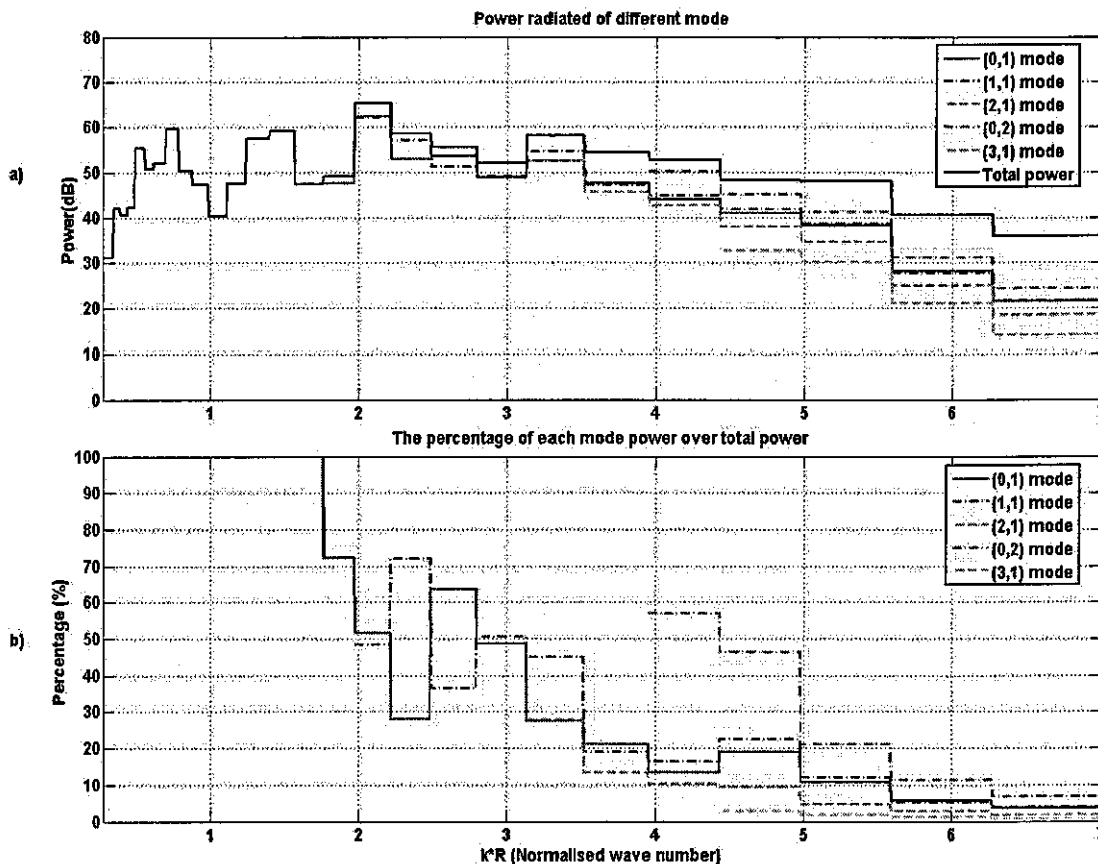


Fig 9.13 Powers radiated from the end of the duct for different modes and the relationships with total power (situation 4 in Fig 8.5)

From Fig 9.11-9.13, it can be seen that

1. Normally, the contribution of each mode to the total power is largest just around that mode cuts on and it decays to a nearly constant lower level with the increasing of the frequency.
2. For the without aperture device situation, all cut on higher-order modes radiate energy from the end of the duct. From Fig 9.11 it can be seen that the plane wave plays a very important role in the power radiation even after $(\pm 1,1)$ modes and $(\pm 2,1)$ modes cut on (when $(\pm 1,1)$ modes cut on, the plane wave contributes 60% of all power and $(\pm 2,1)$ cuts on, the plane wave still contributes nearly 40% of all power). Also when $(\pm 2,1)$ modes cut on, $(\pm 2,1)$ modes contribute only 20% of all power.
3. For the device with single concentric orifice situation, only axially-symmetric modes radiate energy from the end of the duct. Before the $(0, 2)$ mode cuts on,

all energy radiated out of the duct is in the form of (0, 1) mode; after (0, 2) mode cuts on, most energy (90% of total energy) radiates in the form of (0, 2) mode. This is similar to that source concentric situation.

4. For the device with single eccentric orifice situation, still all cut on higher-order modes radiate energy from the end of the duct. Through the comparison of Fig 9.11 and Fig 9.13, it is noticed that the situations are quite similar. Which means the presence of such an eccentric aperture device in the duct does not have a significant effect on the pattern of the energy radiated out of the duct.

Other than these three situations, all source eccentric situations discussed in Chapter 8 have been considered. Still four different configurations of those orifices, which are the axially-symmetric without concentric orifice situation, the axially-symmetric with concentric orifice situation, the axially-unsymmetric without concentric orifice situation and the axially-unsymmetric with concentric orifice situation, are selected and the results are shown below.

Fig 9.14 is for the axially-symmetric with concentric orifice situation (Situation 10 in Fig 8.15); Fig 9.15 is for the axially-symmetric without concentric orifice situation (Situation 9 in Fig 8.15); Fig 9.16 is for the axially-unsymmetric with concentric orifice situation (Situation 5 in Fig 8.15); Fig 9.17 is for the axially-unsymmetric without concentric orifice situation (Situation 7 in Fig 8.15).

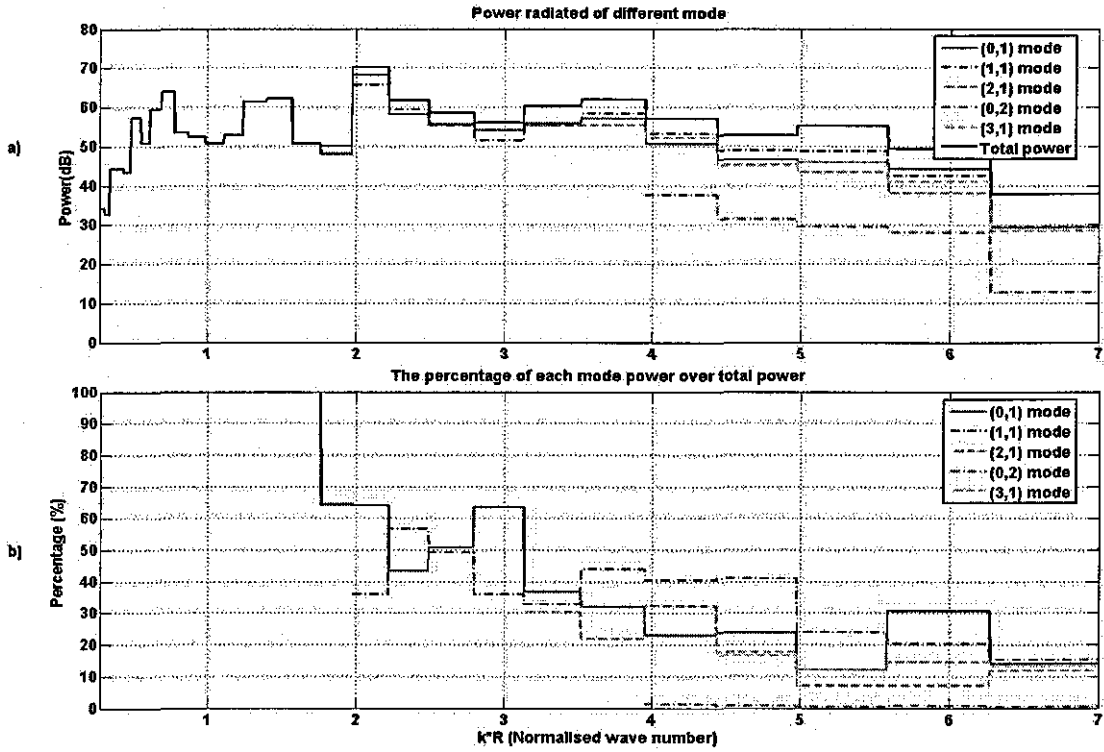


Fig 9.14 Powers radiated from the end of the duct for different modes and the relationships with total power (situation 10 in Fig 8.15)

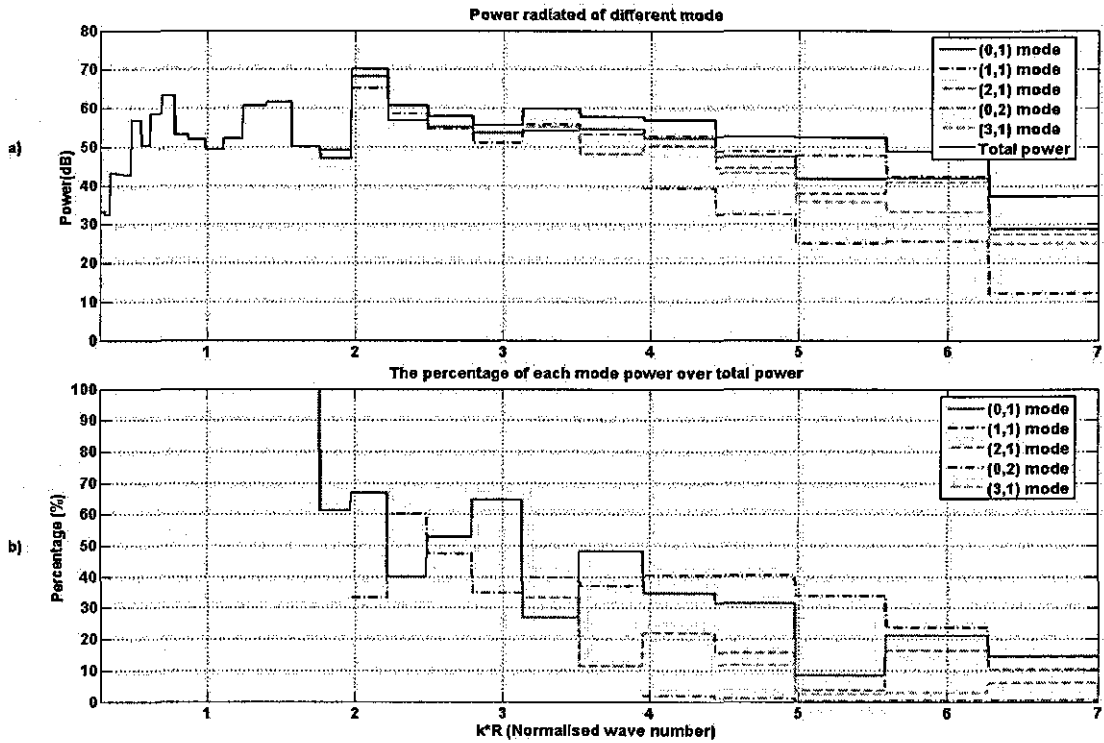


Fig 9.15 Powers radiated from the end of the duct for different modes and the relationships with total power (situation 9 in Fig 8.15)

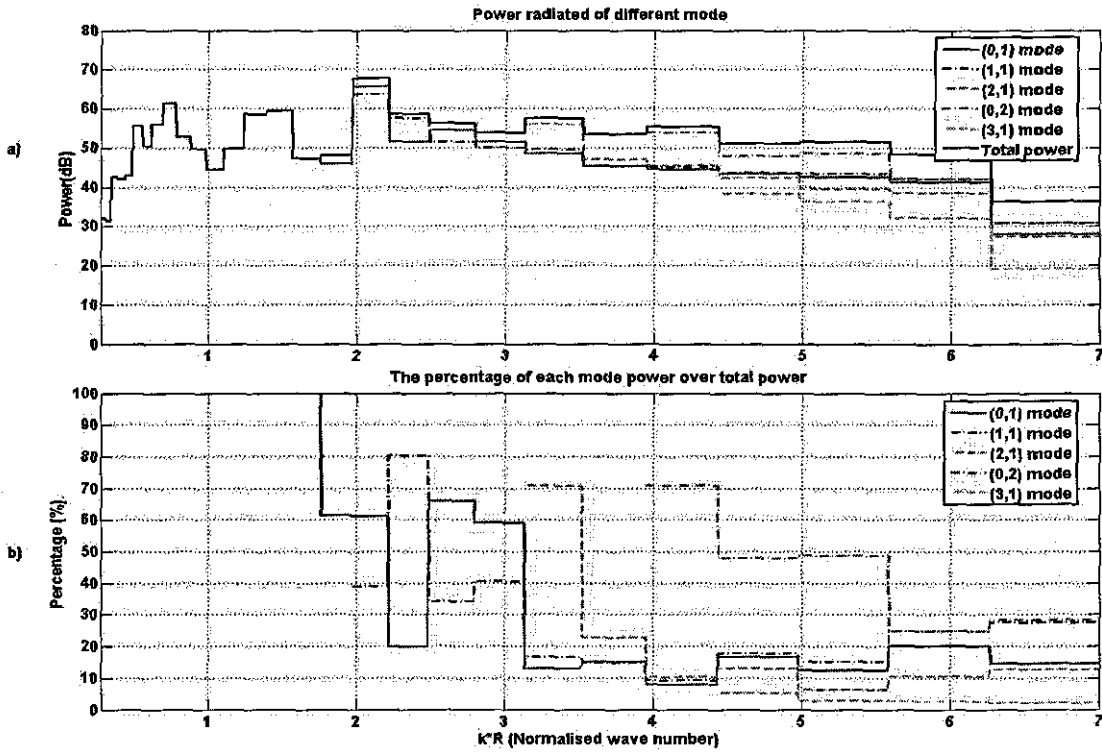


Fig 9.16 Powers radiated from the end of the duct for different modes and the relationships with total power (situation 5 in Fig 8.15)

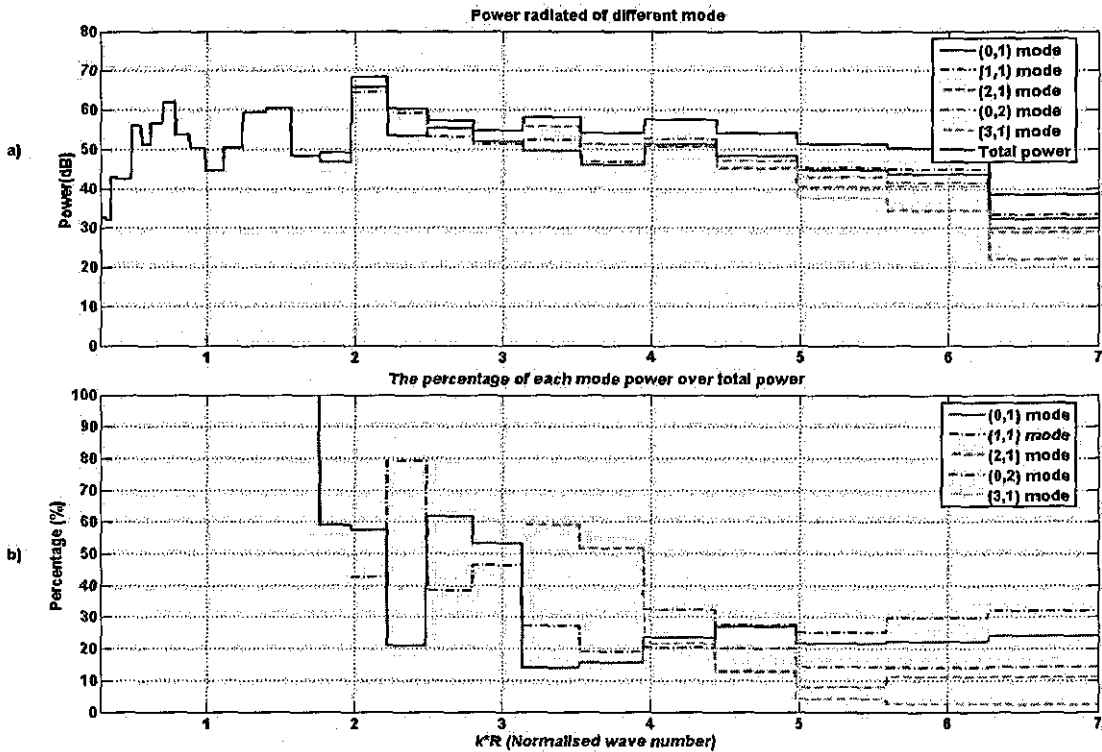


Fig 9.17 Powers radiated from the end of the duct for different modes and the relationships with total power (situation 7 in Fig 8.15)

From Fig 9.13-9.17, it can be seen that

1. Unlike the source concentric situation, every cut on higher-order mode appears in the after orifice field for these four different situations, although the contributions of each mode to the total energy are different from each other.
2. Through the comparison of Fig 9.14 and Fig 9.15, it can be seen they are very similar, which means the extra concentric orifice has little effect on the distribution of the power between those higher-order modes in the after orifice field. At most of the wave number range, the powers mainly radiate in the form of the plane wave, $(\pm 1,1)$ modes and $(\pm 2,1)$ modes, the contributions of other higher-order modes are very small.
3. For the axially-unsymmetric orifices configuration, it can be seen that the presence of the concentric orifice in the device has a significant effect on the distribution of the power radiated out of the duct. For with the concentric orifice situation, after $(0, 2)$ mode cuts on, it contributes 30%-70% of total power and dominate in the after orifice field. However for without the concentric orifice situation (shown in Fig 9.17), after $(0, 2)$ mode cuts on, it contributes only 10%-30% of total power.
4. For the source eccentric situation, the arrangement of the orifices does have some effects on the distribution of the power between higher-order modes. However these effects are not so significant as those for source concentric situation. Even though one can still through the arrangement of those orifices in the device to adjust the relationships between different higher-order modes in the after orifice field. For example, if it is required that the $(0, 2)$ mode to be dominated in the after orifice field, one can make those orifices axially-unsymmetric arranged and add a concentric orifice. If it is required $(0, 2)$ mode to be cancelled in the after orifice field, one can make those orifices axially-symmetric arranged.

9.3.3 Applicability of the approximate lumped-parameter model

In Fig 9.4 -9.17, the total power radiated out of the duct and the powers in the form of some modes (from $(0, 1)$ mode to $(3, 1)$ mode) are plotted. As discussed before, the

power radiated out of the duct is equal to the power radiated into the main duct from the source region. So the relationships between the input power (total power) and the output powers (powers in different single modes) can also be seen from these figures. By successfully separating the total power into the sum of the powers of different modes, one can study the detailed effects of different aperture devices on the distribution of higher-order modes in circular duct. For example, one can eliminate some specific higher-order modes by arranging the configuration of the orifices in the aperture device. These relationships are important for this approximate lumped-parameter model, because the powers are chosen as approximate lumped parameters in this model.

So through the study of the powers distribution, it can be seen that this approximate model is applicable for the study of the higher-order modes propagation in circular duct with a simple aperture device present.

From the discussion made above, it can be seen that not only the configuration of the orifices in the device affects the after orifice field, but also the location of the sound source in the plane transverse to z -axis. So in order to get a clear view on the description of the effects of those devices, one should combine them together. Which is named as *source-orifice relationships* in former discussions. After the study of the powers radiated from the end of the duct, the insertion losses (IL) for different situations are studied below.

9.4 Effects of different configurations of the orifices on the insertion loss

From equation (9.36), one can get the power radiated from the end of the duct for different situations, substituted these powers into equation (9.1), the insertion loss (IL) for these situations can be obtained. During the study of the insertion loss (IL) for those different situations, one phenomenon (also observed and analyzed by August Sauter and Walter in Ref [54]), which is the insertion losses in some frequency ranges for some specific situations are negative values, is observed. However the insertion loss is expected to be a positive value rather than a negative one. In next section, this phenomenon is discussed and also the possible reason is given.

9.4.1 Negative insertion loss (*IL*)

Take the source eccentric and axially-symmetric with concentric orifice situation for example (Situation 2 in Fig 9.20 (*II*)), the results are shown in Fig 9.18 and Fig 9.19. Fig 9.18 *a*) shows the insertion loss (*IL*) for this situation; Fig 9.18 *b*) shows the power radiated out of the duct for this situation and the power radiated out of the duct for without aperture device situation. Fig 9.19 *a*) shows the directed measured acoustic pressure and the predicted acoustic pressure for the after orifice field; In order to show them clearly, Fig 9.19 *b*) shows the directed measured acoustic pressure and predicted pressure in 1/6 octave band.

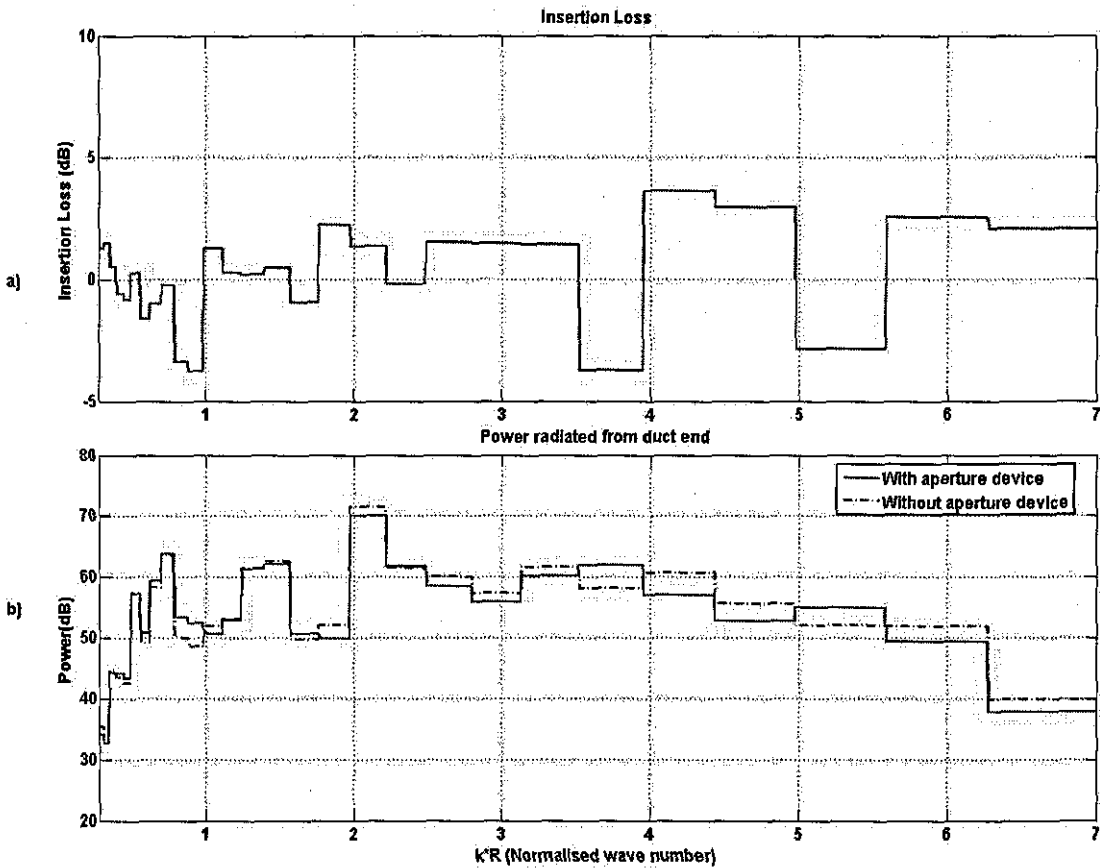


Fig9.18 The insertion loss (*IL*) and power radiated out of the duct (Situation 2 in Fig 9.20 (*II*))

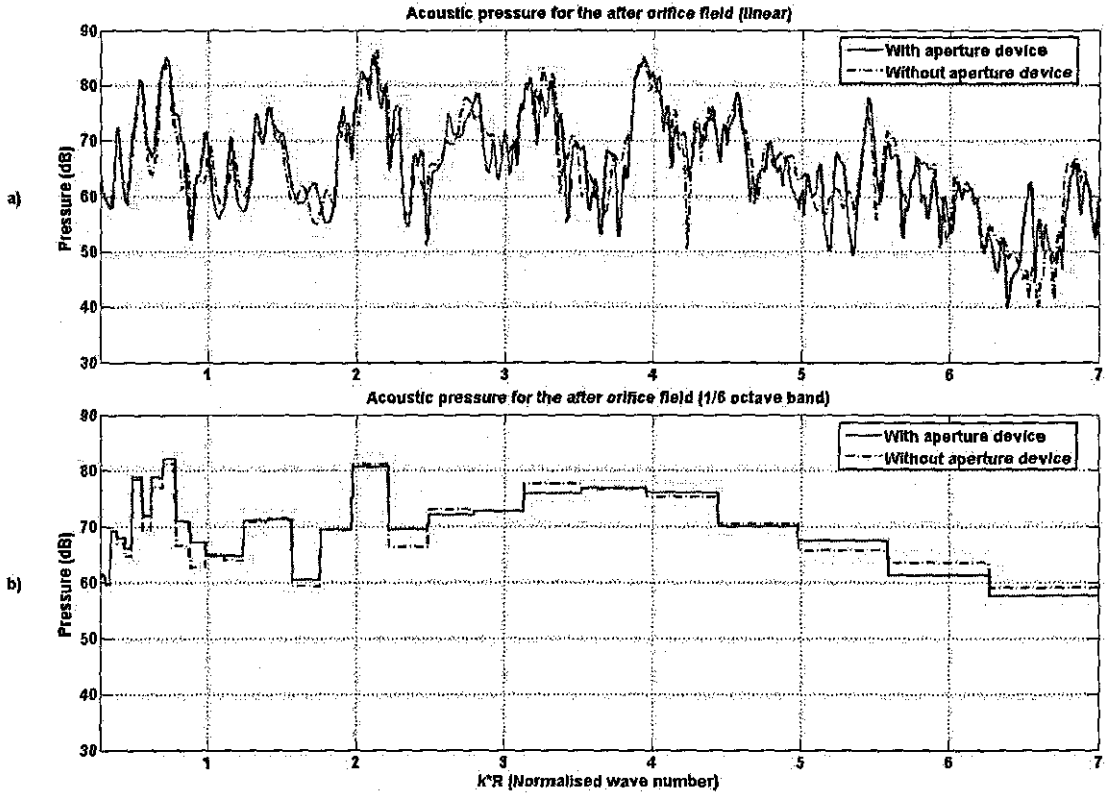


Fig 9.19 Comparison of the direct measured acoustic pressure in the after orifice field for without and with aperture device situations (Situation 2 in Fig 9.20 (II))

For this situation, at some normalized wave number ranges, such as $K^*R \approx 1$, $K^*R \approx 4$ and $K^*R \approx 5$, the insertion loss (IL) are negative values. Which means at these normalized wave number ranges, the powers radiated from the duct end for with aperture device situation is larger than those for without situation. Normally, the insertion loss (IL) should be a positive value. The comparison of the acoustic pressure measured directly at the after aperture device reference point shown in Fig 9.19 shows that at these normalized wave number ranges, acoustic pressures for duct with aperture device are larger than those for duct without aperture device. From the source duct end view point, the presence of the aperture device reduces the radiated impedance rather than increase it, so more energies are radiated into the main duct at these normalized wave number ranges than the duct without aperture device situation, and as discussed above, there are no energy losses, so all these energies are radiated out from the duct

end. This is why the insertion loss (IL) takes negative values at these normalized wave number ranges.

After explaining the reason which causes the negative value for the insertion loss, the insertion losses for different situations are compared and through this, one can see the effects of the configuration of those orifices in the device. Still according to the location of the sound source, the analysis is divided into two groups: source eccentric situation and source concentric situation. The first one to be discussed is the source eccentric situation.

9.4.2 Source eccentric situation

For the source eccentric situation, at first, four different configurations are shown in figure below. Fig 9.20 (I) shows the comparisons of the insertion loss for different situations; Fig 9.20 (II) shows the configurations of the source-orifices for these different situations. In Fig 9.20 (I), there are four sub figures which are labeled as *a*), *b*), *c*) and *d*). *a*) shows the comparison of the IL for situation 1 and situation 2 in Fig 9.20 (II); *b*) shows the comparison of the IL for situation 3 and situation 4 in Fig 9.20 (II); *c*) shows the comparison of the IL for situation 1 and situation 3 in Fig 9.20 (II); *d*) shows the powers radiated out of the duct for these four different situations and the power radiated out of the duct for without aperture device situation.

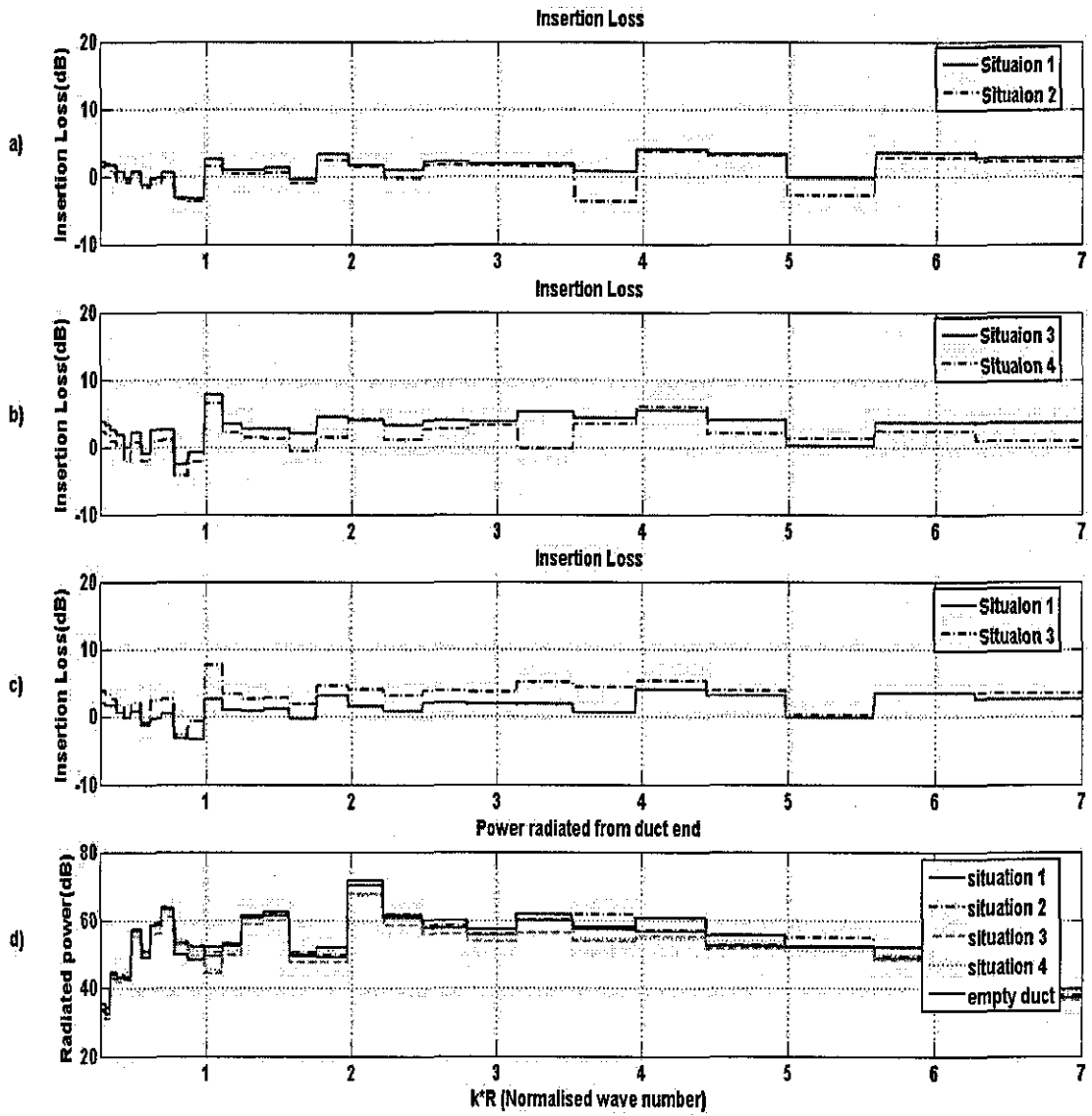


Fig 9.20 (I) Comparison of the insertion loss (IL) of four different situations

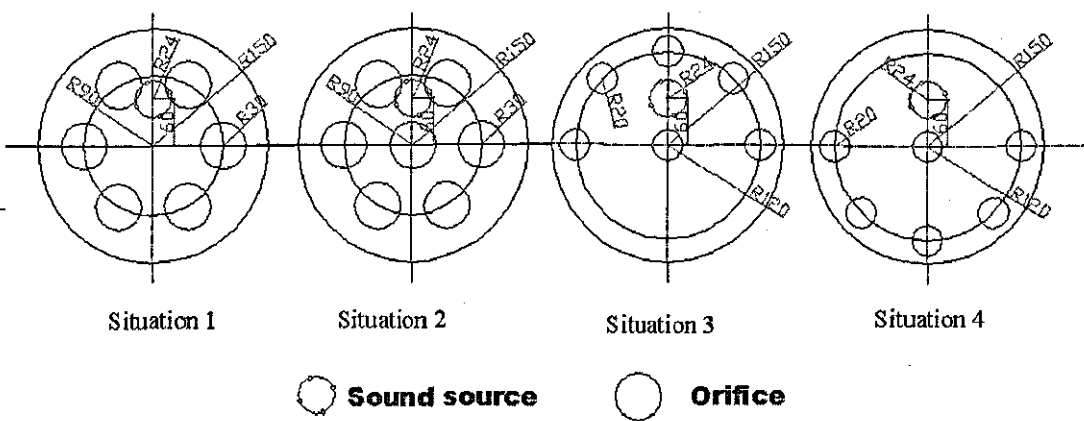


Fig 9.20 (II) Configurations of four source-orifices relationship situations

From this figure, it can be seen that

1. The two configurations of the orifices shown in *a*) are both axially-symmetric, the only difference between these two situations is there is an extra concentric orifice for situation 2. The results show that the insertion losses for these two situations are quite similar; only at some part of the normalized wave number range, the *IL* for situation 1 is larger than that for situation 2. This means the effects of the extra concentric orifice on the *IL* for this situation are very small. Which is also observed from the power radiated in Fig 9.14 and Fig 9.15.
2. The two configurations of the orifices shown in *b*) are both axially-unsymmetric. The results show that the insertion losses for these two situations are also quite similar. This means the changing of the comparative relationship between the source and orifices has an effect on the insertion loss, however this effect is not very large.
3. Comparison between axially-symmetric and axially-unsymmetric situations is shown in *c*). The results show that when $k * R < 5$, the *IL* for unsymmetric situation is larger than that for symmetric situation. But when $k * R > 5$, they are nearly the same. Which means at even higher normalized wave number range, for the insertion loss (*IL*) there is nearly no difference for these two types of configurations of the orifices.
4. It is also noticed that most of the insertion losses resulting from these devices are less than 5 dB or even smaller. Which means the insertion losses incurred by these types of configurations are not very significant.

Comparisons of other four situations with the same open area ratio (8% open area) but different configurations are shown in figure below. Fig 9.21 (*I*) shows the comparisons of the insertion loss for different situations; Fig 9.21 (*II*) shows the configurations of the source-orifices for these different situations. In Fig 9.21 (*I*), there are four sub figures which are labeled as *a*), *b*), *c*) and *d*). *a*) shows the comparison of the *IL* for situation 1 and situation 2 in Fig 9.21 (*II*); *b*) shows the comparison of the *IL* for situation 3 and situation 4 in Fig 9.21 (*II*); *c*) shows the comparison of the *IL* for situation 1 and situation 3 in Fig 9.21 (*II*); *d*) shows the powers radiated out of the duct for these four

different situations and the power radiated out of the duct for without aperture device situation.

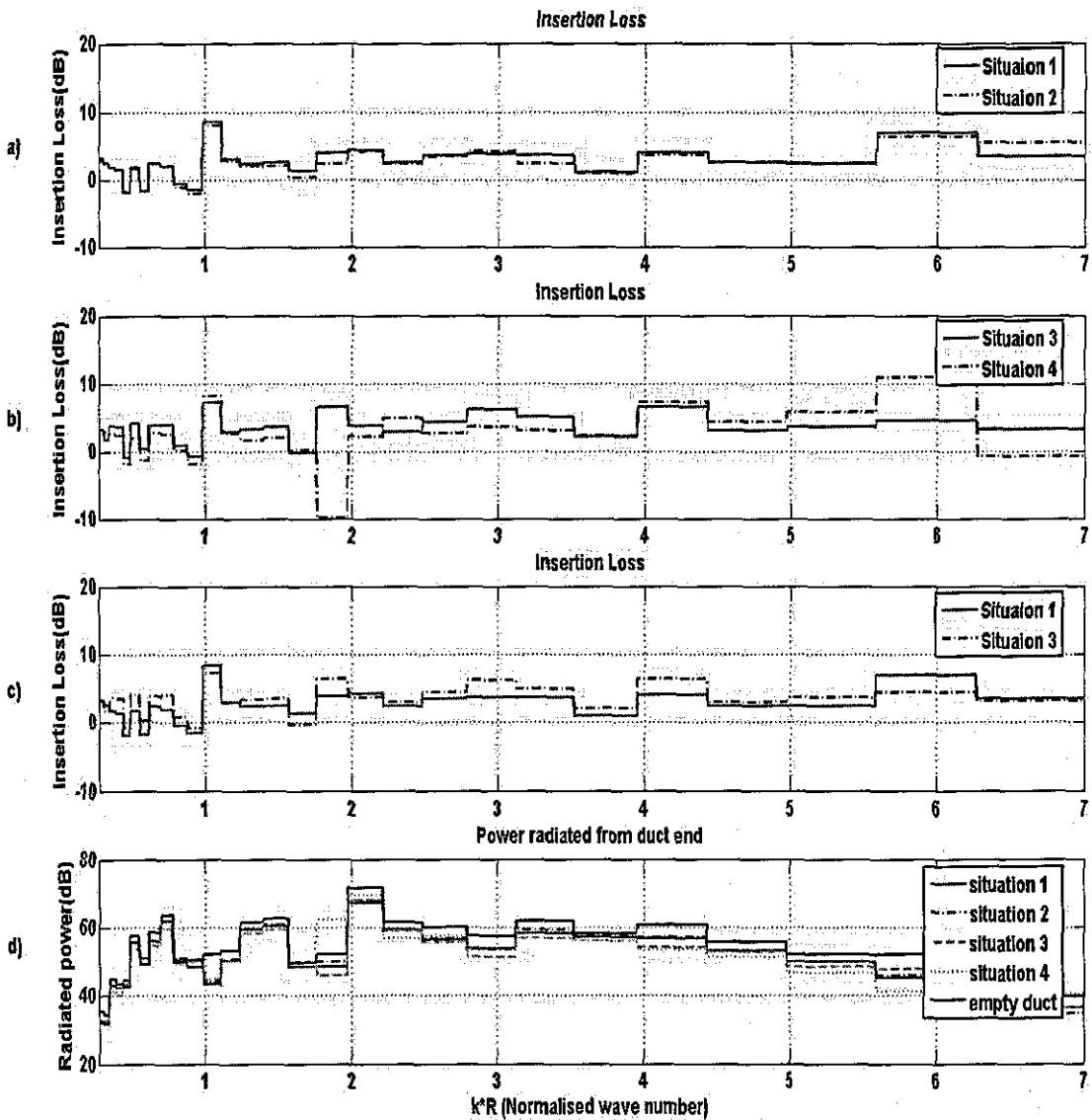


Fig 9.21 (I) Comparison of the insertion loss (IL) of four different situations

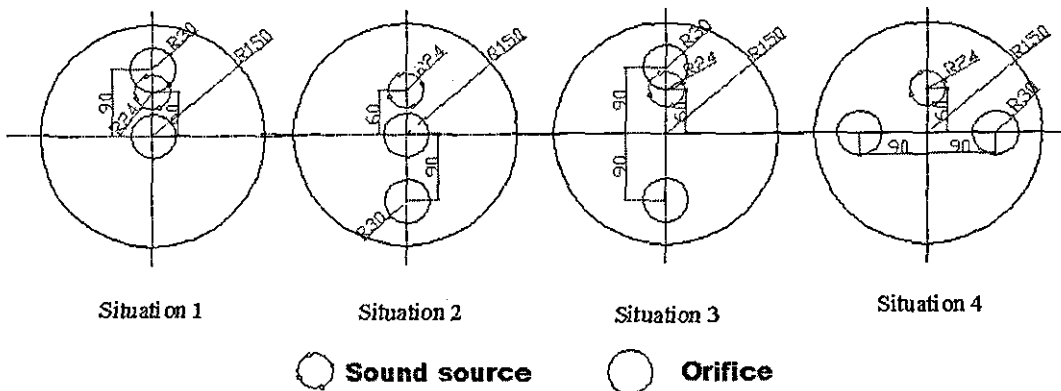


Fig 9.21 (II) Configurations of four source-orifices relationship situations

From results shown in this figure, it can be seen that

1. All of these four situations have the same open area ratios (8% open area), however the insertion losses caused by these situations are different from each other. This means not only the ratio of the open area affects the insertion loss, but also the comparative configuration of the open areas decides the value of the insertion loss.
2. Fig 9.21 (I) *a*) shows that the insertion loss for the first two situations are nearly equal for most of the normalized wave number range, which means for configurations with concentric orifice, the circumferential positions of other orifices have very little effect on the insertion loss.
3. For those situations without the concentric orifice, Fig 9.21 (I) *b*) shows that although the configurations of those two orifices are the same, the insertion losses are quite different from each other. Which means the comparative source-orifices relationships do have a significant effect on the insertion loss. Especially when $k * R \approx 6$, the insertion losses for situation 4 are quite significant (larger than 10 dB).
4. Through the comparison of situation 1 and situation 3, Fig 9.21 (I) *c*) shows that at most part of the normalized wave number range, the insertion losses for situation 3 are larger than those for situation 1. However the difference between them is not very significant (about 1-2 dB).

Comparisons of other four single orifice situations also with the same open area ratio (1.8% open area) but different configurations are shown in Fig 9.22. Fig 9.22 (I) shows the comparisons of the insertion loss for different situation; Fig 9.22 (II) shows the configurations of the source-orifices for these different situations. In Fig 9.22 (I), there are three sub figures which are labeled as *a*), *b*), *c*) and *d*). *a*) shows the comparison of the *IL* for situation 1 and situation 2 in Fig 9.22 (II); *b*) shows the comparison of the *IL* for situation 2, situation 3 and situation 4 in Fig 9.22 (II); *c*) shows the powers radiated out of the duct for these four different situations and the power radiated out of the duct for without aperture device situation.

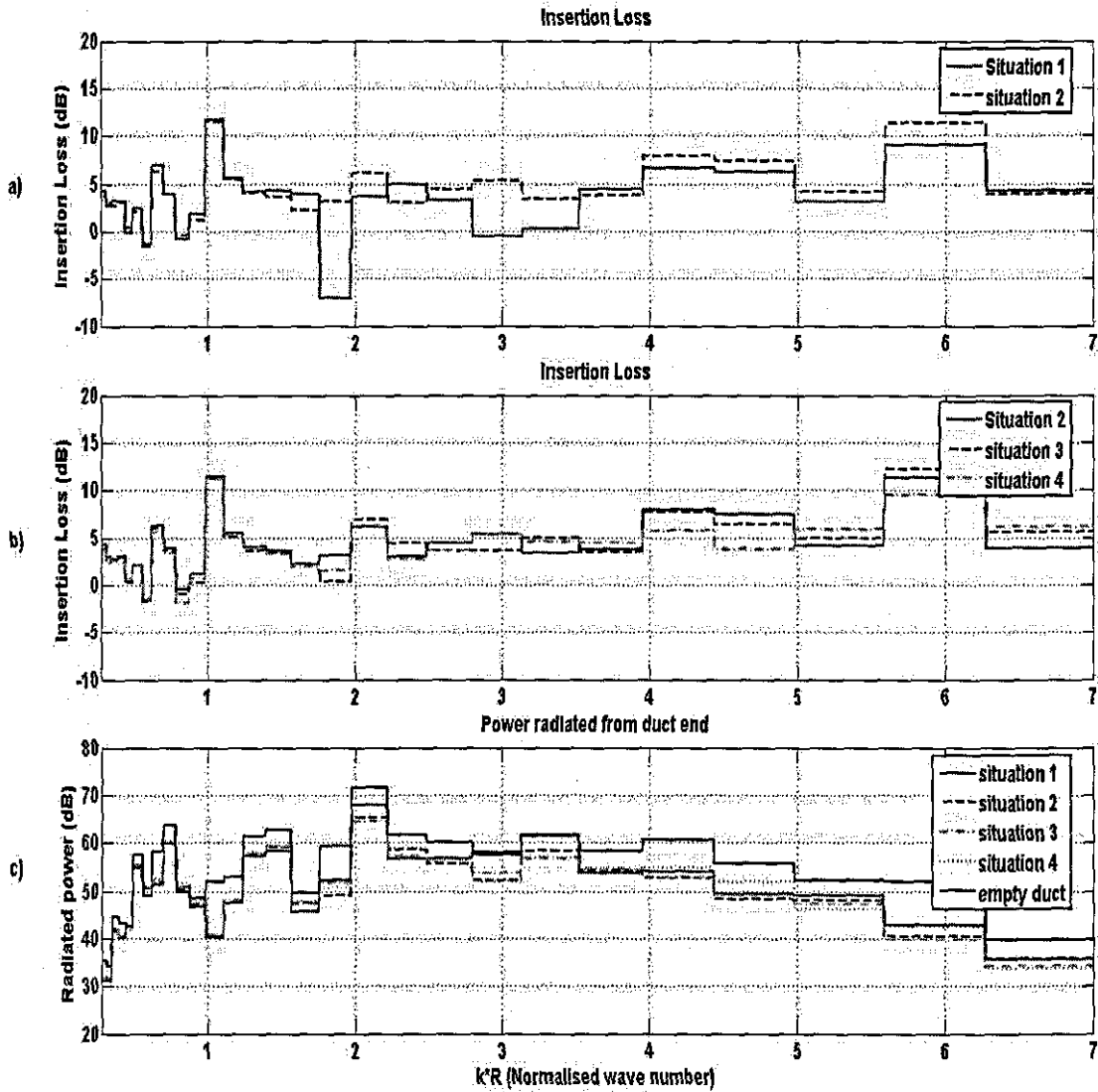


Fig 9.22 (I) Comparison of the insertion loss (*IL*) of four different situations

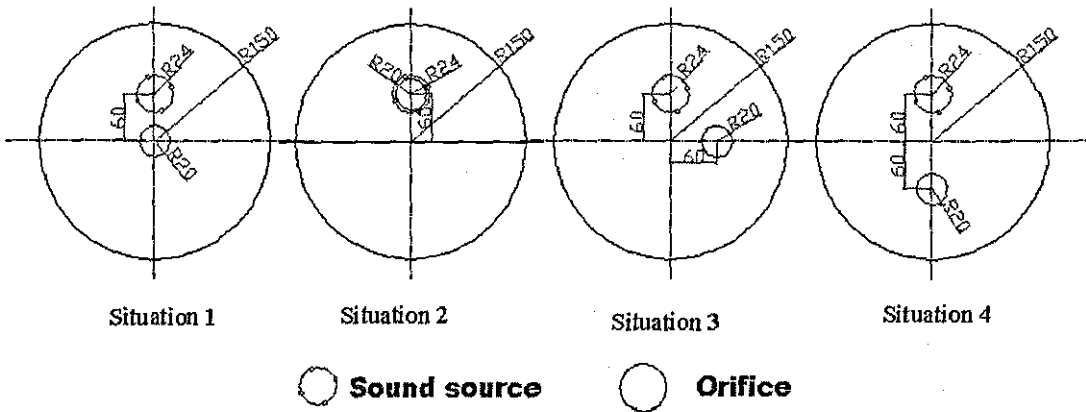


Fig 9.22 (II) Configurations of four source-orifice relationship situations

From this figure, it can be seen that

1. For the plane wave region, the insertion losses for these four different situations are nearly the same. Which means for the single orifice situation, the insertion losses are independent on the location of the orifice in the plane wave range.
2. The insertion losses for these situations are around 5 dB, or even larger 10 dB at some specific part of the normalized wave number range, which is larger than those shown for the several orifices situation.
3. Fig 9.22 (I) a) shows that at most normalized wave number range, the insertion losses for eccentric orifice situation are larger than those for the concentric orifice situation. The largest difference appears in the range of $1.8 < k * R < 3.5$, in which four axially-unsymmetric higher-order modes cut on in the duct.
4. Fig 9.22 (I) b) shows that for those three different eccentric orifice situations, there is no specific trend for the insertion losses. At different normalized wave number range, these three situations give different values.

In order to see the effects of the numbers of the orifices on the insertion losses, i.e. the effects of the open area of the orifices on the IL , several situations are chosen and two figures are plotted below.

In Fig 9.23, four different configurations of the orifices are chosen, which are, one single eccentric orifice situation (1.8% open area); two eccentric orifices situation (8% open area); five eccentric orifices situation (9% open area) and six symmetric eccentric orifices situation (24% open area). In Fig 9.23 (I), a) shows the IL for these four different situations; b) shows the powers radiated out of the duct for these four situations and the power radiated out of the duct for without aperture device situation.

In Fig 9.24, four different configurations of the orifices are chosen, which are, one single concentric orifice situation (1.8% open area); one concentric orifice and one eccentric orifice situation (8% open area); five eccentric orifices plus one concentric orifice situation (11% open area) and six symmetric eccentric orifices plus one concentric orifice situation (28% open area). In Fig 9.24 (I), a) shows the IL for these four different situations; b) shows the powers radiated out of the duct for these four situations and the power radiated out of the duct for without aperture device situation.

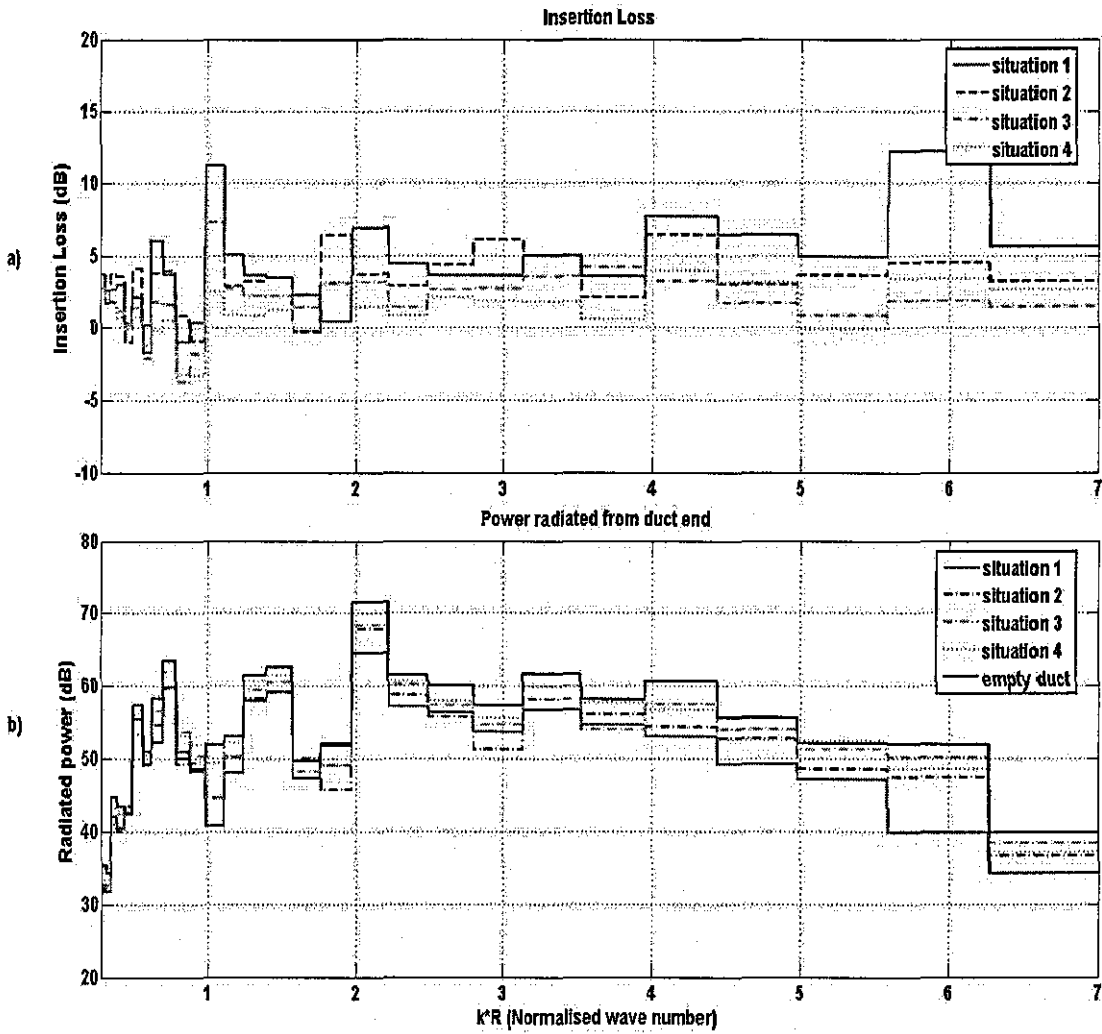


Fig 9.23 (I) Comparison of the insertion loss (IL) for four different situations

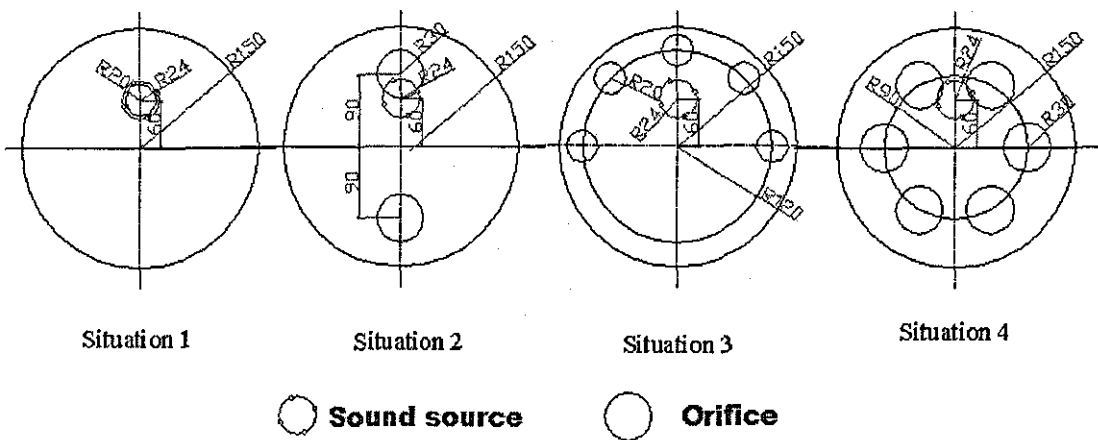


Fig 9.23 (II) Configurations of four source-orifices relationship situations

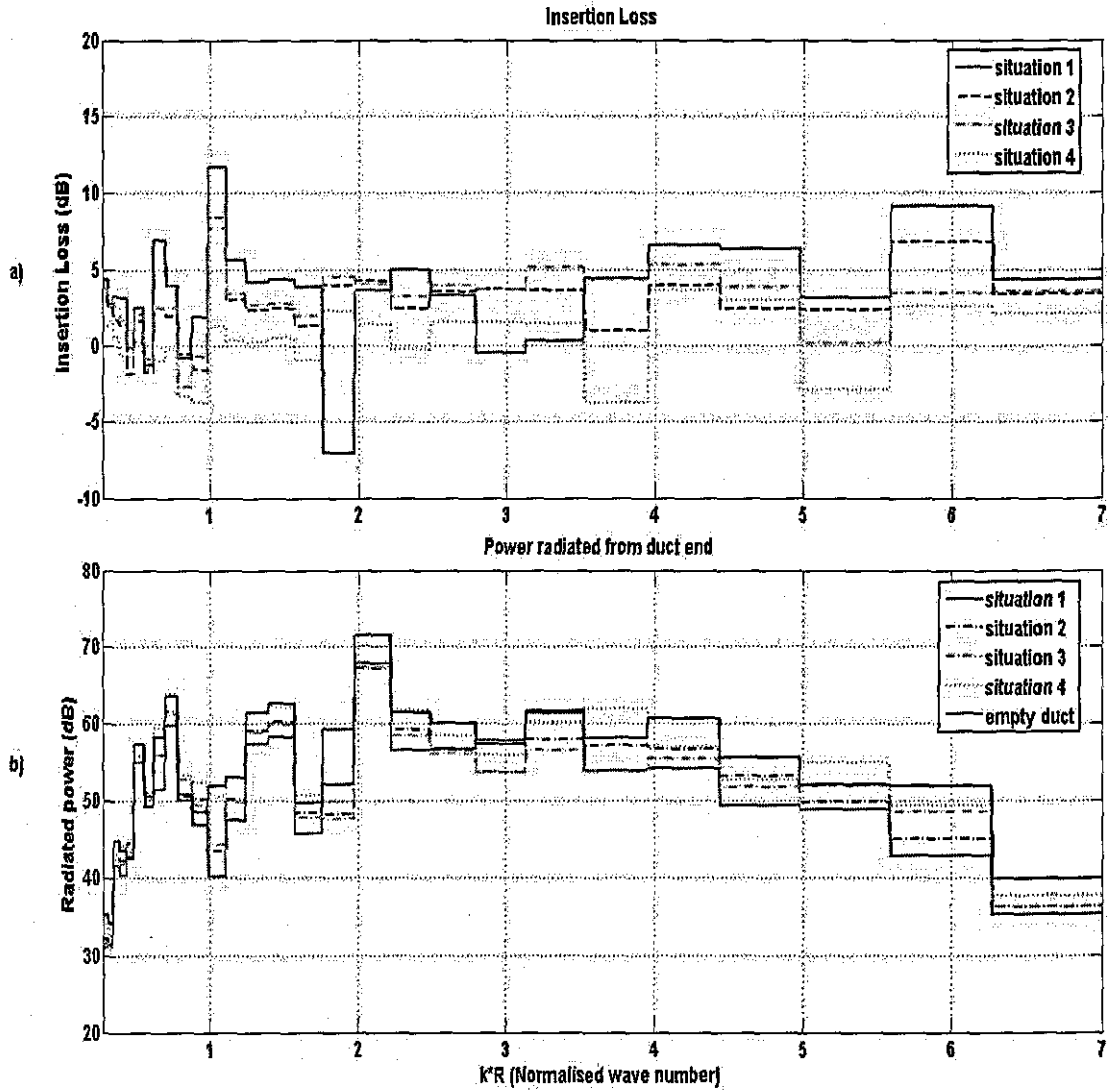


Fig 9.24 (I) Comparison of the insertion loss (IL) of four different situations

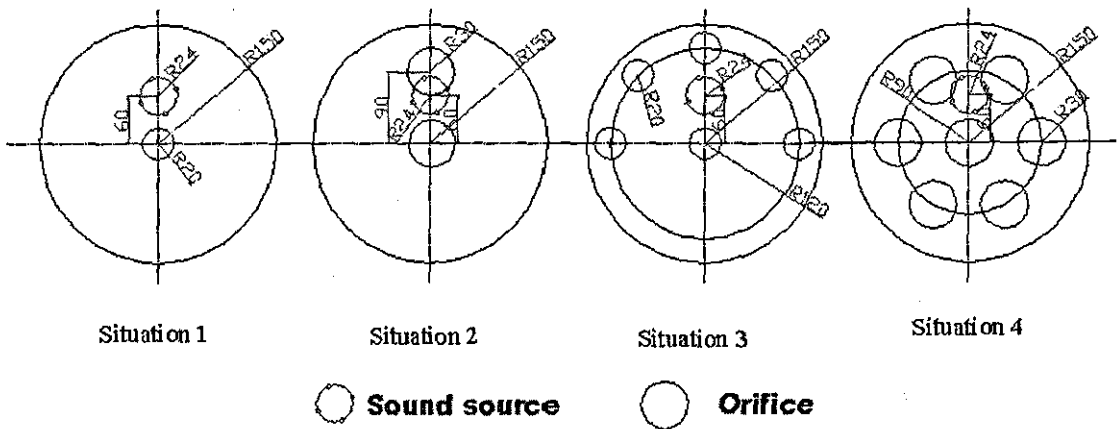


Fig 9.24 (II) Configurations of four source-orifices relationship situations

From Fig 9.23 -9.24, it can be seen that

1. It is hard to find some direct relationships between these insertion losses with the open area ratios, because there are many other items which can affect the insertion losses. However for most part of the normalized wave number range, the open area ratio does have a significant effect on the insertion losses. Normally the larger this ratio is, the less the insertion losses are.
2. For most part of the normalized wave number range, the insertion losses for situations with the concentric orifice are less than those without the concentric orifice. This phenomenon shows the role of such a concentric orifice in the effects on the insertion losses.

In this section, when the sound source located eccentric to the main duct, the effects of the open area ratios, the effects of the configurations of the orifices and the effects of the comparative source-orifices relationships on the insertion losses have been discussed. The source concentric situation is studied in next section.

9.4.3 Source concentric situation

For the source concentric situation, at first, still four different configurations are shown in figure below. Fig 9.25 (I) shows the comparisons of the insertion loss for different situations; Fig 9.25 (II) shows the configurations of the source-orifices for these different situations. In Fig 9.25 (I), there are four sub figures which are labeled as *a*), *b*), *c*) and *d*). *a*) shows the comparison of the *IL* for situation 1 and situation 2 in Fig 9.25 (II); *b*) shows the comparison of the *IL* for situation 3 and situation 4 in Fig 9.25 (II); *c*) shows the comparison of the *IL* for situation 2 and situation 4 in Fig 9.25 (II); *d*) shows the powers radiated out of the duct for these four different situations and the power radiated out of the duct for without aperture device situation.

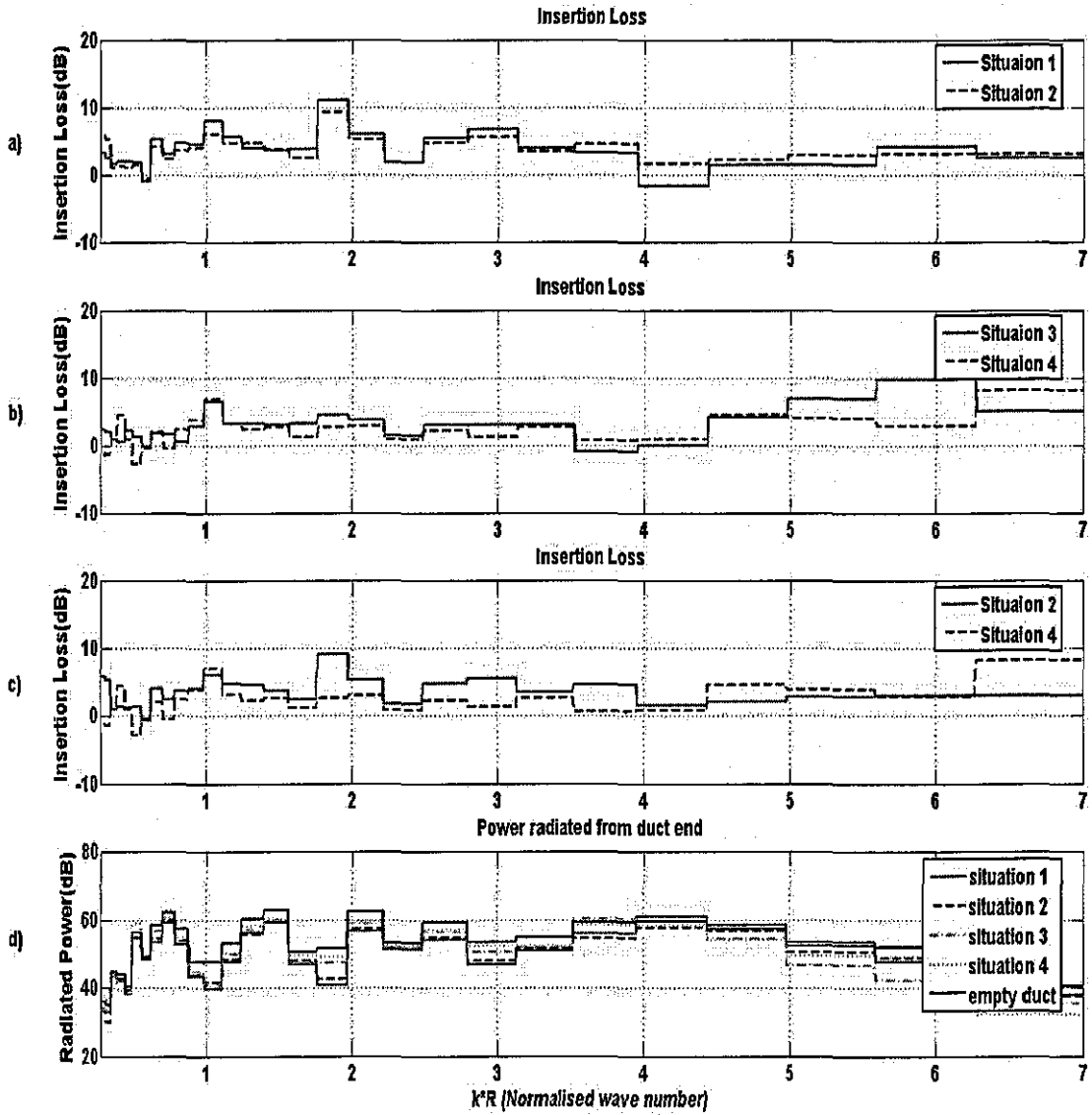


Fig 9.25 (I) Comparison of the insertion loss (IL) of four different situations

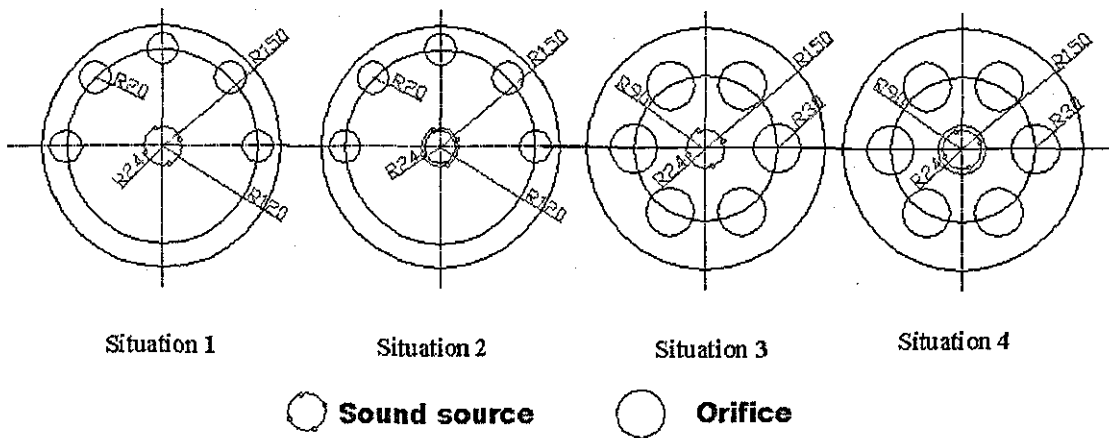


Fig 9.25 (II) Configurations of four source-orifices relationship situations

From this figure, it can be seen that,

1. The two configurations of the orifices shown in Fig 9.25 (I) a) are both axially-unsymmetric, the only difference between these two situations is there is an extra concentric orifice for situation 2. The results show that the insertion losses for these two situations are quite similar, only at some part of normalized wave number range, the IL for situation 1 is larger than that for situation 2. This means the effects of that extra concentric orifice on the IL for this situation are very small.
2. The two configurations of the orifices shown in Fig 9.25 (I) b) are both axially-symmetric. The results show that the insertion losses for these two situations are also quite similar. There is a significant difference when $k * R > 5$, this means the effects of that extra concentric orifice on the IL are obvious only at higher normalized wave number range.
3. Comparison between axially-symmetric and axially-unsymmetric situations is shown in Fig 9.25 (I) c). The results show that when $k * R < 4.5$, the IL for unsymmetric situation is larger than that for symmetric situation. But when $k * R > 4.5$, the IL for symmetric situation is larger than that for unsymmetric situation.
4. It is noticed that most of the insertion losses caused by these devices are less than 5 dB or even smaller. Which means the insertion losses incurred by these types of configurations are not very significant.

Comparisons of three two-orifices situations, which are one concentric orifice plus one eccentric orifice situation (8% open area); two symmetric placed eccentric orifices situation (8% open area) and two asymmetric placed eccentric orifices situation (3.6% open area), are shown in Fig 9.26. Fig 9.26 (I) shows the comparisons of the insertion loss for these three situations; Fig 9.26 (II) shows the configurations of the source-orifices for these three situations. In Fig 9.26 (I), there are two sub figures that are labeled as a), b). a) shows the comparison of the IL ; b) shows the powers radiated out of the duct for these three situations and the power radiated out of the duct for without aperture device situation.

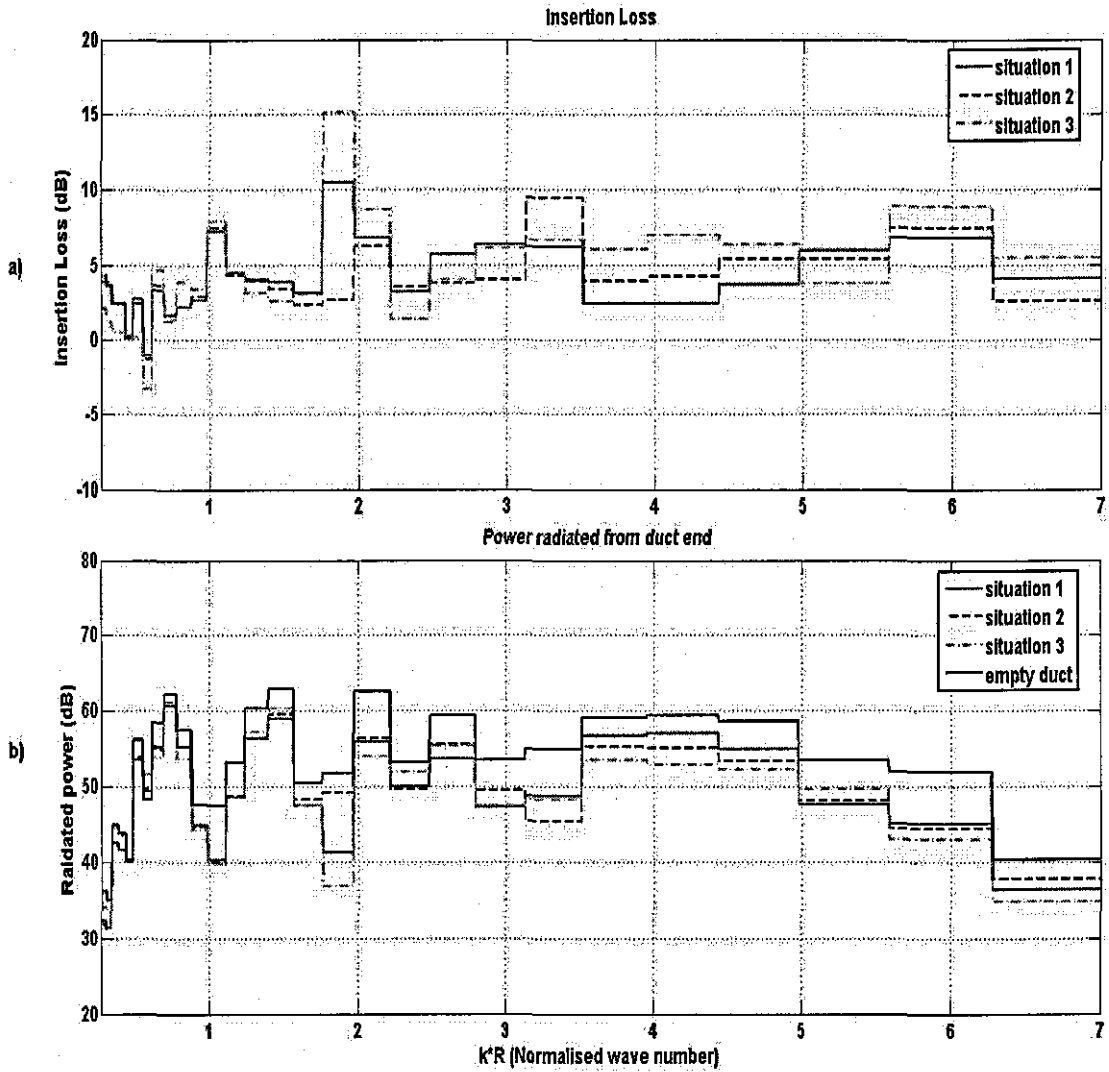


Fig 9.26 (I) Comparison of the insertion loss (*IL*) of three different situations

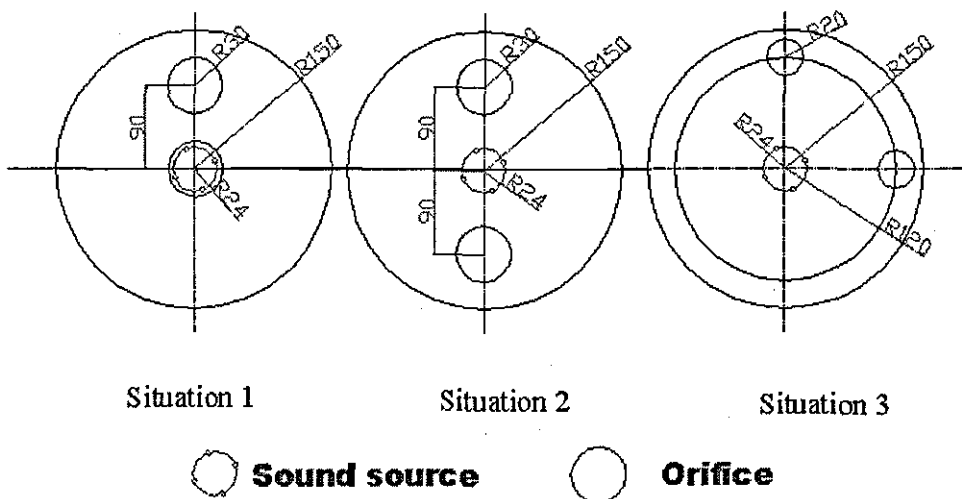


Fig 9.26 (II) Configurations of three source-orifices relationship situations

From this figure, it can be seen that

1. The insertion losses for these three situations are around 5 dB, or even larger 10 dB at some specific normalized wave number range, which is larger than those shown for the several orifices situation.
2. At most part of the normalized wave number range, the insertion losses for two asymmetric placed eccentric orifices situation are larger than those for two symmetric placed eccentric orifices situation, which is caused both by the difference open area and the configuration of the orifices.
3. When $k * R < 3$, the insertion losses caused by situation 1 are larger than those of situation 2; after $k * R > 3$, the insertion losses caused by situation 1 are smaller than those of situation 2. Because these two situations are of the same open area ratio, so this comparison shows that the effects of the concentric orifice on the insertion losses: when axially-symmetric (0, 2) mode cuts on it causes reduced insertion losses; while when those axially-unsymmetric modes cut on, it causes increased insertion losses.

Still in order to see the effects of the numbers of the orifices on the insertion losses, i.e. the effects of the open area of the orifices on the IL . Several situations are chosen and plotted below.

In Fig 9.27, four different configurations of the orifices are chosen, which are, one single concentric orifice situation (4% open area); one concentric orifice and one eccentric orifice situation (8% open area); five eccentric orifices plus one concentric orifice situation (11% open area) and six symmetric eccentric orifices plus one concentric orifice situation (28% open area). In Fig 9.27 (I), a) shows the IL for these four different situations; b) shows the powers radiated out of the duct for these four situations and the power radiated out of the duct for without aperture device situation.

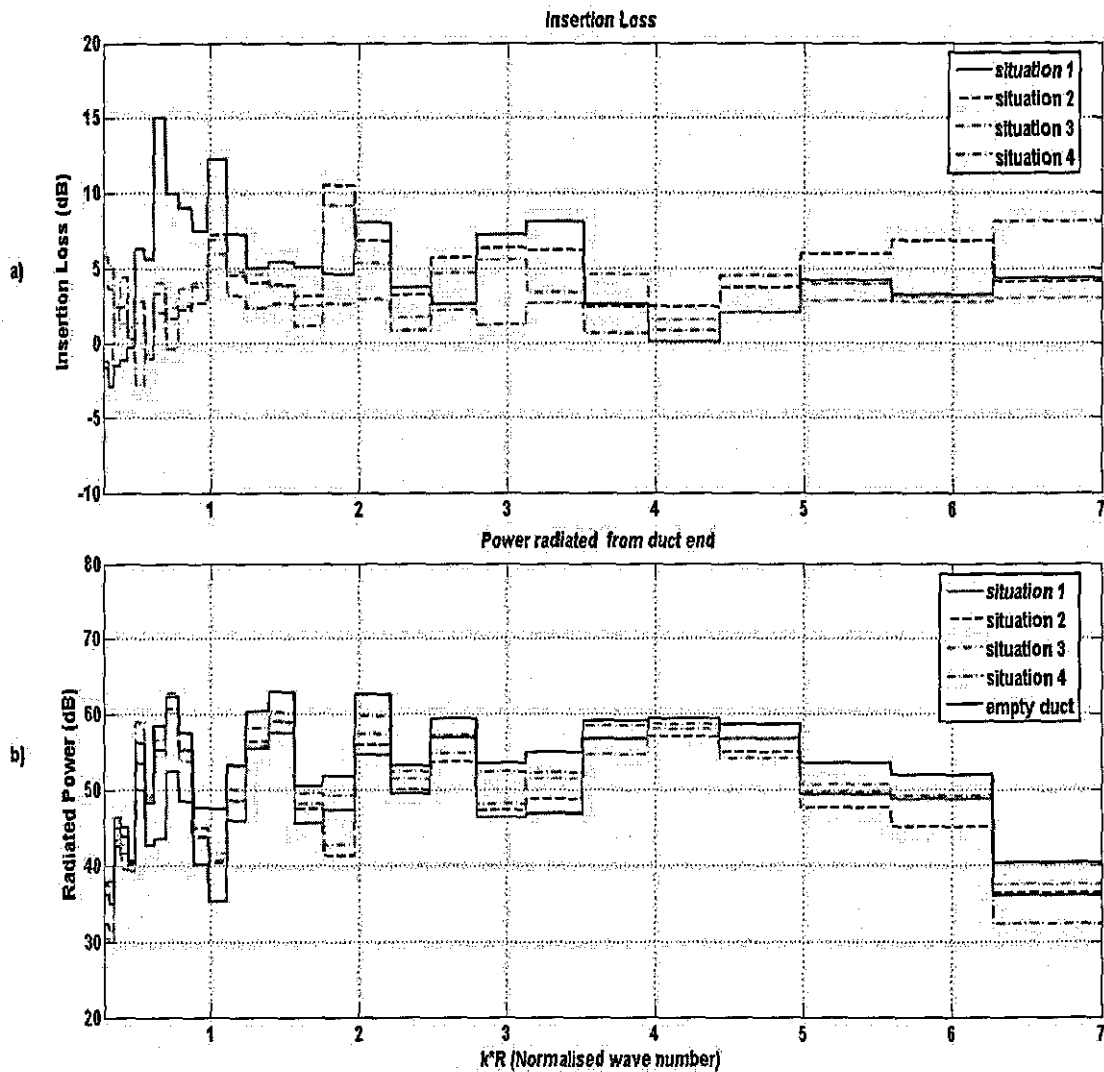


Fig 9.27 (I) Comparison of the insertion loss (IL) of four different situations

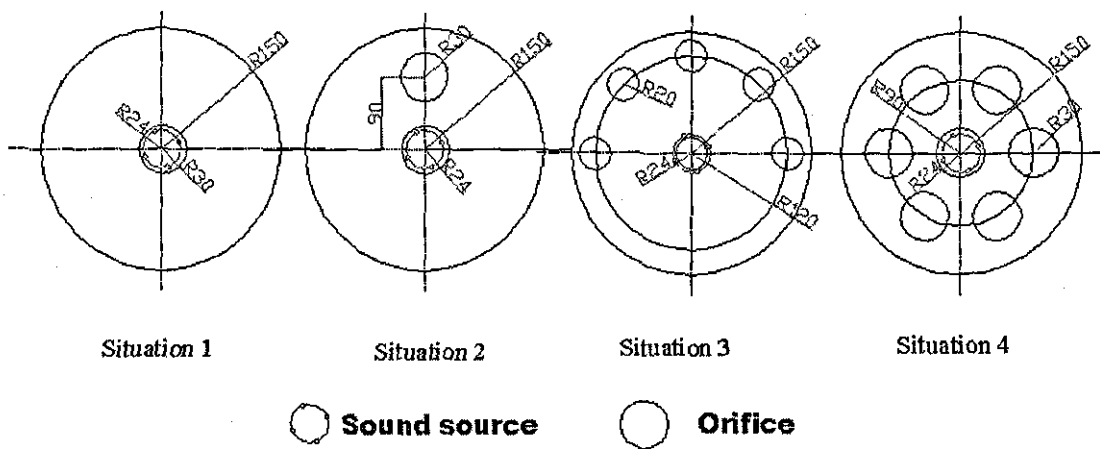


Fig 9.27 (II) Configurations of four source-orifices relationship situations

From this figure, it can be seen that

1. It is still hard to find some direct relationships between these insertion losses with the open area ratios, because there are many other items which can affect the insertion losses. However for most part of the normalized wave number range, the open area ratio does have a significant effect on the insertion losses. When $k^* R < 4$, the larger the open area ratio is, the less the insertion losses it causes.
2. When the axially-symmetric higher-order mode (0, 2) cuts on, the insertion losses caused by the single concentric orifice situation is the smallest, and then the axially-symmetric situation (situation 4) and then axially-unsymmetric situation 3, and situation 2. This also shows not only the open area playing an important role in the insertion losses, but also the configurations of those orifices.

From the analysis made in this chapter, combining the radiated powers with the insertion losses for different configurations of the apertures in the device, it can be seen that normally the smaller the open area of the orifice is, the larger the insertion loss it causes. Also for all the situations shown in this chapter, if the sound source is concentric to the main duct, in the normalized wave number range $k^* R < 4$, the single concentric orifice situation (Situation 1 in Fig 9.27 (II)) has the greatest effect on the insertion loss; while in the in the normalized wave number range $k^* R > 4$, the two asymmetric placed eccentric orifices situation (Situation 3 in Fig 9.26 (II)) has the greatest effect on the insertion loss. If the sound source is eccentric to the main duct, in most normalized wave number range between $1 < k^* R < 7$, the single eccentric orifice situation (Situation 1 in Fig 9.23 (II)) has greatest effect on the insertion loss, while the six symmetric eccentric orifices plus one concentric situation (Situation 4 in Fig 9.24 (II)) has least effect on it.

9.5 Discussion

In this chapter, the errors for the powers radiated out of the duct and the insertion losses are not discussed. This is because it is hard to get the actual values for the powers radiated out of the duct, and then it is difficult to get the actual values for the insertion losses for different situations. One can get the powers radiated out of the duct through

the measurement, however this is a time and labour consuming work and no measurement methods can give perfect results, because there are always some errors inherent in the measurement methods (equipment errors, the measurement position errors, the integrating errors, etc). Through the analysis made in Chapter 6 and Chapter 8, one knows that there are some errors for those amplitudes obtained by this model. However those errors are quite similar scaled and considered to be acceptable. So it is assumed the powers obtained from those amplitudes are also similar scaled and acceptable. Especially for the insertion losses, which are relative values other than absolute ones (W_I/W_{II}), some errors brought by the same model can be cancelled.

From the study presented in this chapter, it can be seen that the radiated power is an effective approximate lumped parameter for the study of the effects of the aperture devices. One can just treat the whole acoustic system as a black box and use this time and space independent parameter to study the performances of different aperture devices. Through the analysis of the distribution of the radiated powers between different modes, the approximate lumped-parameter model constructed in this chapter is considered to be acceptable and effective in the study of the acoustic properties for simple aperture devices in circular duct in the higher normalized wave number range.

Also combining the analysis of the radiated power with the analysis of the insertion losses, one can successfully separate the performance of the aperture device from the performance of the main duct and also separate the effects of the configuration of the orifices from the effects of the sound source location in higher normalized wave number range. So these two parameters are considered to be applicable for the study of the higher-order mode propagation in circular ducts.

Through the comparison of both the powers and the insertion losses for different situations, it can also be seen that there are many factors which can affect these two parameters, such as, the location of the sound source, the open area ratio, the configurations of those orifices in the device (number of the orifices and comparative positions of those orifices (especially the presence and absence of a concentric orifice)). Other factors are not mentioned in this chapter, such as the total length of the main duct,

the thickness of the aperture device, the distance between the source end and the aperture devices. However these factors are considered in the procedure of the model construction and are not so important as those factors which are discussed in this chapter. So by adjusting these factors, one can adjust the effects of that simple aperture device exerted on the whole in-duct field.

Chapter 10 Conclusions and discussion

10.1 Conclusions

The aim of the current investigation is to establish a generic approach to allow the separation of the performance of the aperture device from the performance of the circular duct across a wide normalized wave number range. So at first the lumped-parameter model (acoustical two-ports system model) is tested in the plane wave region. Through the demonstration, it is confirmed that this model can work properly for the duct without a simple aperture device present, as well as the duct with a simple aperture device present in the plane wave region. From the results for orifices with different diameters shown in Chapter 2, it is easy to see that the smaller the open area of the orifice is, the larger the error it caused in the estimated impedances. Also in this chapter, two measurement methods, the hard screen method and the two-different-inputs method are tested and compared. Through the comparison, the hard screen method is found to be an inaccurate method due to inherent practical problems. However, the two-different-inputs method is shown to be an effective way for the lumped parameters measurement.

However due to the cross-coupling effects that occur between higher-order modes at the end of the duct or any discontinuities in the duct, the lumped-parameter model is not applicable for the higher-order mode propagation in the duct. So an approximate lumped parameter model is proposed and aimed to extend the applicable frequency range to cover several higher-order mode propagation. In this model, every single mode is treated as an approximate lumped parameter. So an effective way to decompose the in-duct acoustic field into the sum of different single modes is necessary.

Although many experimental methods have been previously studied for the decomposition of the higher-order mode propagation in circular ducts, most of them have common disadvantages, such as the requirement of significant number of independent measurement positions, and the availability only for the decomposition

of the circumferential higher-order modes. So other effective methods are required. In this project, one theoretical decomposition method is proposed and studied.

The decomposition of the in-duct acoustic field means the acquisition of the unknown amplitudes of the propagating higher-order modes in the duct. The experimental decomposition methods obtain the amplitudes through enough measurements carried out in different positions. However the theoretical decomposition methods obtain the amplitudes through the seeking of the solution for a group of independent equations which are obtained from the descriptions of the boundary conditions.

So in Chapter 3, a description of the open end duct boundary condition is given. Based on the description, the generalized impedances Z_{mL} and complex reflection coefficients R_{mL} are obtained. From the analysis of the reflection coefficients, the relationships between incident wave amplitudes A_{mn} and the reflected wave amplitudes B_{mn} are established. In Chapter 4, two types of widely used sound source (plane wave source and point source) are introduced and the descriptions of both boundary conditions are also given.

Based on the descriptions of the boundary conditions, in Chapter 5 and Chapter 6, the independent equation groups for the duct without a simple aperture device present are established and the solutions are also obtained. Through the results shown in these two chapters, it can be seen that although there are some errors between the predicted results and direct measurements (normally less than 10% of direct measurements), the amplitudes of the higher-order modes obtained by this theoretical decomposition method are considered to be acceptable. Through the analysis presented in these two chapters, it can be seen that this theoretical decomposition method works well in the decomposition of the in-duct acoustic field for the duct without a simple aperture device present.

Then in Chapter 7 and Chapter 8, the simple aperture device is added to the in-duct field and the descriptions for the interfaces between the main duct and the aperture device are presented. Combining these descriptions with those for the open end and

the sound source, a group of independent equations is established and the solution is also obtained. With the presence of the simple aperture device, the in-duct acoustic field can be divided into the before orifice field and the after orifice field. Also through the comparison of the theoretically calculated results with the directly measured results, the amplitudes of the higher-order modes for both the before orifice field and the after orifice field obtained by this theoretical decomposition method are considered to be acceptable. Through the analysis presented in these two chapters, it also can be seen that this theoretical decomposition method works well in the decomposition of the in-duct acoustic field for the duct with a simple aperture devices present.

Then in Chapter 9, after successfully decomposing the in-duct acoustic field into the sum of different single mode and the obtaining of the amplitudes of different modes propagating in the duct, the power radiated out of the duct is taken as an approximate parameter to describe the effects of different simple aperture devices on the in-duct field. Through the analysis of the total radiated power and the powers of different modes, the effects of different simple aperture devices on the distribution of the total radiated power between different modes are obtained. It is found that not only the location of the sound source in the plane transverse to z -axis has an effect on the higher-order modes distribution in the duct, but also the configuration of the orifices in the aperture device affects the distribution of the higher-order modes in the duct. Especially it is found that the concentric orifice has a significant effect on the in-duct acoustic field. From the analysis, it can be seen that the powers radiated from the end of the duct, especially the powers radiated in the form of different modes, can be used in the approximate lumped-parameter model.

After knowing the power radiated from the end of the duct for different situations, another parameter, the insertion loss (IL) is adopted to show the effects of different aperture devices. Through the comparison of the insertion losses for different source-orifices situations, it can be seen that the effects of the simple aperture devices on the insertion losses are not very significant. At most normalized wave number range the insertion loss is about 5 dB or even less. However from the changes of the insertion loss at different normalized wave number range, the effects of the different

configurations of the orifices in the simple aperture device are obtained. From the results presented, it can be seen that the insertion loss can be chosen as a parameter to describe the effects of the aperture device on the in-duct acoustic field even in the higher normalized wave number range.

Through the analysis made in the previous nine chapters, it is demonstrated that the model which combines those three boundaries' descriptions together to achieve the in-duct acoustic field decomposition is effective. Based on the decomposition of the in-duct field, one can easily reconstruct the in-duct field both for the before orifice field and the after orifice field and analyze the effects of different simple aperture devices.

Numerous previous works have been done on analysis of aperture devices in ducts, most of the work deals only with the performance of the aperture device in the plane wave propagation range. However by adopting this model, this range can be easily expanded from the plane wave region ($k * R < 1.84$) to an even wider normalized wave number range (in this investigation, the wider normalized wave number range has been extended to $k * R < 7.2$, which is four times the plane wave range and includes 16 propagating higher-order modes). In this normalized wave number range, a better understanding of the performance of the simple aperture device on the in-duct acoustic field is obtained.

Also by adopting this model, one can study the performance of the simple aperture device of nearly any thickness (not a hard screen) and any configurations of the circular orifices quite easily. By just inputting those different parameters, such as the number of the orifices, the thickness of the device, and the location and radius of each orifice into this model, one can get those amplitudes needed for the reconstruction and performance comparison.

So this model provides a generic approach for the decomposition of the in-duct field (without and with simple aperture devices), as well as a generic approach to study the performance of the simple aperture device on the in-duct acoustic field in the higher normalized wave number range.

10.2 Discussion and future research suggestions

In the investigation, the coupling effects that occur at the end of the duct have been discussed and through the developed analysis, the cross-coupling effects between different modes are obtained. However the coupling effects happen not only at the open end, but also at the boundaries between the sound source and the main duct, as well as the main duct and the simple aperture device. These coupling effects, including the cross-coupling effects between different modes and the cross-coupling effects between different orifices in the simple aperture device, are important for the understanding of what exactly are happening at those boundaries. Although these cross-coupling effects are considered and included in the model construction and calculation, they are not fully understood and clearly expressed and separated. So in any future investigations, attention should be focused on these coupling effects. By understand these coupling effects; one can have an even clearer view on the behavior of different simple aperture devices.

Also in this investigation, attention is not given to the position of the simple aperture device in the main duct, especially when this simple aperture device is located in the near field zone of the open end ($L < R$) or just at the open end. If the simple aperture device is located at that position, it is quite difficult to measure those acoustic properties for the after orifice field. However for many engineering problems, some simple aperture devices are installed in that position. So in future investigations, attention can also be given to this situation.

Another aspect, which is worthy for future research, is the style of the open end of the duct. In this investigation, only the duct with infinite flanged termination situation is studied. Other situations, such as the un-flanged termination situation, the un-flanged duct with specific thickness situation and the axis of the duct is not vertical to the flanged termination situation, are also widely adopted in the engineering works. So the coupling effects that happen at the end of the duct for these situations should also be studied in the higher normalized wave number range.

References

1. F. P. Mechel, *Formulas of Acoustics*, 2002.
2. L. E. Kinsler, A. R. Frey, A. B. Coppens and J. V. Sanders, *Fundamentals of Acoustics (Fourth edition)*, John Wiley & Sons Inc, 2000.
3. M. L. Munjal, *Acoustics of Ducts and Mufflers with application to exhaust and ventilation system design*, John Wiley & Son, 1987.
4. A. D. Pierce, *Acoustics: An introduction to its physical principles and application*, McGraw-Hill book company, 1981.
5. C. M. Harris, *Handbook of noise control (second edition)*, McGraw-Hill Book Company, 1979.
6. I. Malecki, *Physical foundations of technical acoustics*, Pergamon Press, 1969.
7. P. M. Morse and K. U. Ingard, *Theoretical acoustics*, McGraw-Hill Book Company, 1968.
8. S. N. Rschevkin, *A course of lectures on the theory of sound*, 1963.
9. G. N. Watson, *A treatise on the theory of Bessel functions* Cambridge University Press, 1958.
10. H. Levine and J. Schwinger, "On the radiation of sound from an unflanged circular pipe," *Physical Review*, vol. 73 (4), pp. 383-406, 1948.
11. Y. Ando, "On the sound radiation from semi-infinite circular pipe of certain wall thickness," *Acoustica*, vol. 22, pp. 219-225, 1969/70.
12. A. N. Norris and I. C. Sheng, "Acoustic radiation from a circular pipe with an infinite flange," *J. Sound Vib.*, vol. 135(1), pp. 85-93, 1989.
13. A. Selamet, Z. L. Ji and R. A. Kach, "Wave reflections from duct terminations," *J. Acoust. Soc. Am*, vol. 109(4), pp. 1304-1311, April. 2001.

14. X. X. Chen, X. Zhang, C. L. Morfey and P. A. Nelson, "A numerical method for computation of sound radiation from an unflanged duct," *J. Sound Vib.*, vol. 270, pp. 573-586, 2004.
15. E. Z. William, "Generalized radiation impedances and reflection coefficients of circular and annular ducts," *J. Acoust. Soc. Am.*, vol. 54(6), pp. 1667-1673, 1973.
16. P. Joseph and C. L. Morfey, "Multimode radiation from an unflanged, semi-infinite circular duct," *J. Acoust. Soc. Am.*, vol. 105(5), pp. 2590-2600, May. 1999.
17. N. Amir, H. Matzner and S. Shtrikman, "Acoustics of a flanged cylindrical pipe using singular basis functions," *J. Acoust. Soc. Am.*, vol. 107(2), pp. 714-724, Feb. 2000.
18. F. J. Fahy, *Sound intensity (second edition)*, London: Elsevier Applied Science, 1989.
19. J. Y. Chung, "Cross-spectral method of measuring acoustic intensity without error caused by instrument phase mismatch," *J. Acoust. Soc. Am.*, vol. 64(6), pp. 1613-1616, Dec. 1978.
20. J. Y. Chung and D. A. Blaser, "Transfer function method of measuring in-duct acoustic properties. I. Theory," *J. Acoust. Soc. Am.*, vol. 68(3), pp. 907-913, Sept. 1980.
21. J. Y. Chung and D. A. Blaser, "Transfer function method of measuring in-duct acoustic properties. II. Experiment," *J. Acoust. Soc. Am.*, vol. 68(3), pp. 914-921, Sept. 1980.
22. H. bodén and M. Åbom, "Influence of errors on the two-microphone methods for measuring acoustic properties in ducts," *J. Acoust. Soc. Am.*, vol. 79(2), pp. 541-548, Feb. 1986.

23. J. Dalmon and A. Bruneau, "Acoustic impedance measurement: plane-wave and first helical mode contributions," *J. Acoust. Soc. Am*, vol. 91(5), pp. 3026-3033, May. 1992.
24. D. H. Keefe, R. Ling and J. C. Bulen, "Method to measure acoustic impedance and reflection coefficient," *J. Acoust. Soc. Am*, vol. 91(1), pp. 470-485, Jan. 1992.
25. B. F. G. Katz, "Method to resolve microphone and sample location errors in the two-microphone duct measurement method," *J. Acoust. Soc. Am*, vol. 108(5), pp. 2231-2237, Nov 2000.
26. S. Jang and J. Ih, "On the multiple microphone method for measuring in-duct acoustic properties in the presence of mean flow," *J. Acoust. Soc. Am*, vol. 103(3), pp. 1520-1526, Mar. 1998.
27. J. P. Dalmont, "Acoustic impedance measurement, Part I: a review " *J. Sound Vib.*, vol. 243 (3), pp. 427-439, 2001.
28. J. P. Dalmont, "Acoustic impedance measurement, Part II: A new calibration method," *J. Sound Vib.*, vol. 243 (3), pp. 441-459, 2001.
29. S. Jang and J. Ih, "On the selection of loads in the multi-load method for measuring the acoustic source parameters of duct systems," *J. Acoust. Soc. Am*, vol. 111(3), pp. 1171-1176, March. 2002.
30. B. D. Mugridge, "The measurement of spinning acoustic modes generated in an axial flow fan" *J. Sound Vib .*, vol. 10, pp. 227-246, 1969.
31. P. Harel and M. Perulli, "Measurement, in a duct, of the space-structure of the discrete-frequency noise generated by an axial compressor" *J. Sound Vib .*, vol. 23(4), pp. 487-506, 1972.
32. M. Akoum and J. Ville, "Measurement of the reflection matrix of a discontinuity in a duct," *J. Acoust. Soc. Am*, vol. 103(5), pp. 2463-2468, May. 1998.

33. C. J. Moore, "Measurement of radial and circumferential modes in annular and circular fan ducts," *J. Sound Vib.*, vol. 62 (2), pp. 235-256, 1979.
34. E. J. Kerschen and J. P. Johnston, "A modal separation measurement technique for broadband noise propagating inside circular ducts," *J. Sound Vib.*, vol. 76 (4), pp. 499-515, 1981.
35. M. Åbom, "Modal decomposition in ducts based on transfer function measurements between microphone pairs," *J. Sound Vib.*, vol. 135 (1), pp. 95-114, 1989.
36. J. Ville and F. Foucart, "Experimental setup for measurement of acoustic power dissipation in lined ducts for higher order modes propagation with air mean-flow conditions," *J. Acoust. Soc. Am.*, vol. 114(4), pp. 1742-1748, Oct 2003.
37. K. A. Mulholland and H. D. Parbrook, "Transmission of sound through apertures of negligible thickness," *J. Sound Vib.*, vol. 5(3), pp. 499-508, 1967.
38. M. Salikuddin, "Acoustic behavior of orifice plates and perforated plates with reference to low-frequency sound absorption," *J. Sound Vib.*, vol. 139(3), pp. 361-381, 1990.
39. K. H. Jun and H. J. Eom, "Acoustic scattering from a circular aperture in a thick hard screen," *J. Acoust. Soc. Am.*, vol. 98(4), pp. 2324-2327, Oct. 1995.
40. J. L. Horner, R. Lyons and B. A. T. Petersson, "Approximations for modal coupling in scattered fields from orifices," *J. Acoust. Soc. Am.*, vol. 108(2), pp. 488-493, Aug. 2000.
41. J. L. Horner, R. Lyons and B. A. T. Petersson, "An approximate methods for determining the maximum amplitude of higher-order duct modes," *J. Acoust. Soc. Am.*, vol. 110(1), pp. 80-85, Jul. 2001.
42. J. S. Seo, H. J. Eom and H. S. Lee, "Acoustic scattering from two circular apertures in a thick hard plane," *J. Acoust. Soc. Am.*, vol. 107(5), pp. 2338-2343, May. 2000.

43. A. Sadamoto and Y. Tsubakishita and Y. Murakami, "Sound attenuation in circular duct using slit-like short expansion of eccentric and/or serialized configuration" *J. Sound Vib.*, vol. 277, pp. 987-1003, 2004.
44. K. S. Peat, "The acoustic impedance at the junction of non-coaxial cylindrical ducts," *Journal of Low Frequency Noise and Vibration*, vol. 11, pp. 114-123, Nov. 1992.
45. A. Selamet and P. M. Radavich, "The effect of length on the acoustic attenuation performance of concentric expansion chambers: An analytical, computational and experimental investigation" *J. Sound Vib.*, vol. 201 (4), pp. 407-426, 1997.
46. A. Selamet and Z. L. Ji, "Acoustic attenuation performance of circular expansion chambers with single-inlet and double -outlet" *J. Sound Vib.*, vol. 229 (1), pp. 3-19, 2000.
47. A. Selamet and Z. L. Ji, "Acoustic attenuation performance of circular expansion chambers with offset inlet/outlet: I. analytical approach" *J. Sound Vib.*, vol. 213 (4), pp. 601-617, 1998.
48. A. Selamet and Z. L. Ji, and P. M. Radavich, "Acoustic attenuation performance of circular expansion chambers with offset inlet/outlet: II. Comparison with experimental and computational studies" *J. Sound Vib.*, vol. 213 (4), pp. 619-641, 1998.
49. A. Selamet and Z. L. Ji, "Circular asymmetric Helmholtz resonators" *J. Acoust. Soc. Am*, vol. 107(5), pp. 2360-2369, May 2000.
50. A. D. Sahasrabudhe, M. L. Munjal and S. A. Ramu, "Analysis of inertance due to the higher order mode effects in a sudden area discontinuity" *J. Sound Vib.*, vol. 185 (3), pp. 515-529, 1995.
51. N. S. Dickey, A. Selamet and M. S. Ciray, "An experimental study of the impedance of perforated plates with grazing flow," *J. Acoust. Soc. Am*, vol. 110(5), pp. 2360-2370, Nov. 2001.

52. S. Lee and J. Ih, "Empirical model of the acoustic impedance of a circular orifice in grazing mean flow," *J. Acoust. Soc. Am*, vol. 114(1), pp. 98-113, July. 2003.
53. J. C. Wendoloski, "Sound absorption by an orifice plate in a flow duct," *J. Acoust. Soc. Am*, vol. 104(1), pp. 122-132, July. 1998.
54. A. S. JR. and W. W. Soroka, "Sound transmission through rectangular slots of finite depth between reverberant rooms," *J. Acoust. Soc. Am*, vol. 47(1), pp. 5-11, 1970
55. G. W. Johnston and K. Ogimoto, "Sound radiation from a finite length unflanged circular duct with uniform axial flow. I. Theoretical analysis," *J. Acoust. Soc. Am*, vol. 68(6), pp. 1858-1870, Dec. 1980.
56. G. W. Johnston and K. Ogimoto, "Sound radiation from a finite length unflanged circular duct with uniform axial flow .II. Computed radiation characteristics," *J. Acoust. Soc. Am*, vol. 68(6), pp. 1871-1882, Dec. 1980.
57. P. O. A. L. Davies, "The design of silencers for internal combustion engines," *J. Sound Vib.*, vol. 1 (2), pp. 185-201, 1964.
58. C. L. Morfey, "Sound transmission and generation in ducts with flow," *J. Sound Vib.*, vol. 14 (1), pp. 37-55, 1971.
59. C. L. Morfey, "Rotating pressure patterns in ducts: their generation and transmission," *J. Sound Vib.*, vol. 1, pp. 60-87, 1964.

Appendix B: Phase match of the microphone pair in the measurement

In order to achieve the accurate measurement of the phase information, the phase match is carried out for the microphone pair used in the measurement and the procedure is given as below:

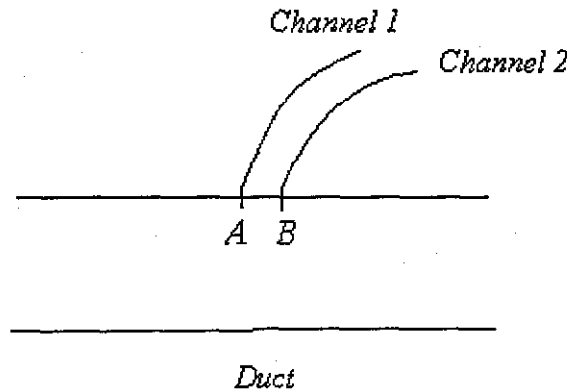


Fig B.1 The set-up for phase match of microphone pair

1. As shown in Fig B.1, two positions *A* and *B* are taken along the wall of the duct. A microphone, cable and an input channel of data acquisition unit consist of Channel 1 and another microphone, cable and an input channel of data acquisition unit consists of Channel 2.
2. So if the acoustic field in the duct is a constant one, then the actual phases of the acoustic pressures at *A* and *B* are also constant and nominated as φ_A and φ_B . The actual phases of the Channel 1 and Channel 2 are also constant and independent of the measurement position, so the phases of the two channels are nominated as φ_1 and φ_2 .
3. At first, place Channel 1 at position *A*, the measured phase of acoustic pressure at position *A* should be $\varphi_A + \varphi_1$; place Channel 2 at position *B*, the measured phase of acoustic pressure at position *B* should be $\varphi_B + \varphi_2$. So the phase difference between two channels is measured and can be expressed as:

$$\Delta\varphi_1 = (\varphi_A + \varphi_1) - (\varphi_B + \varphi_2);$$
4. Then place Channel 2 at position *A*, the measured phase of acoustic pressure at position *A* should be $\varphi_A + \varphi_2$; place Channel 1 at position *B*, the measured phase

of acoustic pressure at position B should be $\varphi_B + \varphi_1$. So the phase difference between two channels is measured and can be expressed as:

$$\Delta\varphi_2 = (\varphi_B + \varphi_1) - (\varphi_A + \varphi_2);$$

5. Add these two phase difference together, one can get

$$(\varphi_1 - \varphi_2) = (\Delta\varphi_1 + \Delta\varphi_2)/2$$

Which is the phase difference between Channel 1 and Channel 2.

6. Then in the following measurement work, this difference is taken away from the measured phase difference between Channel 1 and Channel 2, and the actual phase difference between two measurement positions is obtained.

7. The same procedure is carried out between Channel 3 and Channel 4, one can get

$$(\varphi_3 - \varphi_4) = (\Delta\varphi_3 + \Delta\varphi_4)/2$$

8. Channel 1 and Channel 2 consist of one microphone pair and Channel 3 and Channel 4 consist of another microphone pair.

9. Also the same procedure is carried out between Channel 1 and Channel 3, one can get

$$(\varphi_1 - \varphi_3) = (\Delta\varphi_5 + \Delta\varphi_6)/2$$

After doing the phase match described above, one can removed the phase difference between any two channels and the actual phase difference between two measurement positions are obtained.

Appendix C: Derivation of pressure continuity boundary condition

For pressure continuity condition between the small duct and the main duct, there is

$$P_{SA} + P_{SB}|_{z=-L} = P_A + P_B|_{z=-L} \quad (\text{over } S_1). \quad (\text{C.1})$$

Multiplying both sides of this equation by $J_t(k_{r,t,s}^I r_1) e^{-jt\varphi}$ and integrating over the small duct region, one can get

$$\begin{aligned} & \int_0^{2\pi R_1} \int_0^0 ((SA_{01} e^{jkL} + SB_{01} e^{-jkL}) \\ & + \sum_{n=2}^{\infty} (SA_{0n} e^{jk_{z,0,n}^I L} + SB_{0n} e^{-jk_{z,0,n}^I L}) J_0(k_{r,0,n}^I r_1) \\ & + \sum_{m=1}^{\infty} \sum_{n=1}^{\infty} J_m(k_{r,m,n}^I r_1) [(SA_{mn}^+ e^{jk_{z,m,n}^I L} + SB_{mn}^+ e^{-jk_{z,m,n}^I L}) e^{-jm\varphi} \\ & + (SA_{mn}^- e^{jk_{z,m,n}^I L} + SB_{mn}^- e^{-jk_{z,m,n}^I L}) e^{jm\varphi}]) J_t(k_{r,t,s}^I r_1) e^{-jt\varphi} r_1 dr_1 d\varphi \\ & = \int_0^{2\pi R_2} \int_0^0 ((A_{01} e^{jkL} + B_{01} e^{-jkL}) \\ & + \sum_{n=2}^{\infty} (A_{0n} e^{jk_{z,0,n}^H L} + B_{0n} e^{-jk_{z,0,n}^H L}) J_0(k_{r,0,n}^H r) \\ & + \sum_{m=1}^{\infty} \sum_{n=1}^{\infty} J_m(k_{r,m,n}^H r) [(A_{mn}^+ e^{jk_{z,m,n}^H L} + B_{mn}^+ e^{-jk_{z,m,n}^H L}) e^{-jm\theta} \\ & + (A_{mn}^- e^{jk_{z,m,n}^H L} + B_{mn}^- e^{-jk_{z,m,n}^H L}) e^{jm\theta}]) J_t(k_{r,t,s}^I r_1) e^{-jt\varphi} r_1 dr_1 d\varphi. \end{aligned} \quad (\text{C.2})$$

In which SA_{mn}^+ , SA_{mn}^- , SB_{mn}^+ and SB_{mn}^- are amplitudes of higher-order modes in the small duct; A_{mn}^+ , A_{mn}^- , B_{mn}^+ and B_{mn}^- are amplitudes of higher-order modes in the main duct. $k_{z,m,n}^I$ and $k_{r,m,n}^I$ represent the wave numbers along z -axis and r direction in the small duct; $k_{z,m,n}^H$ and $k_{r,m,n}^H$ represent the wave numbers along z -axis and r direction in the main duct.

According to equation below,

$$\int_0^{2\pi} e^{jm\varphi} d\varphi = \begin{cases} 0 & (m \neq 0) \\ 2\pi & (m = 0). \end{cases} \quad (\text{C.3})$$

For $t = 0, s = 1$, there is

$$J_0(k_{r,0,1}^I r_1) e^{-j0\varphi} = 1. \quad (\text{C.4})$$

So applying equation (C.4) and equation (C.3) into equation (C.2), it can be rewritten as

$$\begin{aligned}
 & 2\pi \int_0^{R_1} (SA_{01}e^{jkl} + SB_{01}e^{-jkl})r_1 dr_1 \\
 & + 2\pi \int_0^{R_1} \sum_{n=2}^{\infty} (SA_{0n}e^{jk_{z,0,n}^I L} + SB_{0n}e^{-jk_{z,0,n}^I L}) J_0(k_{r,0,n}^I r_1) r_1 dr_1 \\
 & = \int_0^{R_1} \int_0^{2\pi} (A_{01}e^{jkl} + B_{01}e^{-jkl}) r_1 dr_1 d\varphi \\
 & + \int_0^{R_1} \int_0^{2\pi} \sum_{n=2}^{\infty} (A_{0n}e^{jk_{z,0,n}^II L} + B_{0n}e^{-jk_{z,0,n}^II L}) J_0(k_{r,0,n}^II r) r_1 dr_1 d\varphi \\
 & + \int_0^{R_1} \int_0^{2\pi} \sum_{m=1}^{\infty} \sum_{n=1}^{\infty} ((A_{mn}^+ e^{jk_{z,m,n}^II L} + B_{mn}^+ e^{-jk_{z,m,n}^II L}) e^{-jm\theta} + \\
 & \quad (A_{mn}^- e^{jk_{z,m,n}^II L} + B_{mn}^- e^{-jk_{z,m,n}^II L}) e^{jm\theta}) J_m(k_{r,m,n}^II r) r_1 dr_1 d\varphi .
 \end{aligned} \tag{C.5}$$

The relationship of Bessel function is given below,

$$\int_0^R r J_0(kr) dr = \frac{R}{k} J_1(kR) \tag{C.6}$$

And the Graf's addition theorem of Bessel function,

$$J_m(\mu r) e^{-jm\theta} = \sum_{p=-\infty}^{\infty} J_{m+p}(\mu \delta_1) J_p(\mu r_1) e^{-j(p\varphi + m\theta_0)}, \tag{C.7}$$

in which, r and θ are coordinates for the main duct coordinate system, r_1 and φ are coordinates for the small duct coordinate system, δ_1 and θ_0 are the coordinate original points of the small duct in the main duct coordinate system. The relationship between these two coordinates is shown in Fig C.1.

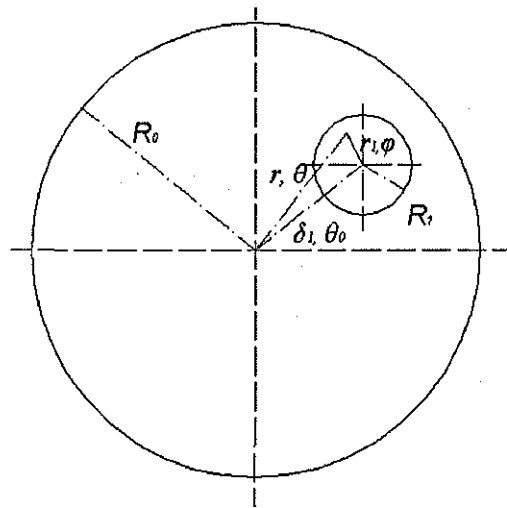


Fig C.1 The configuration of the main duct and the small duct coordinate

Applying equation (C.7) to the right side of the equation (C.5)

$$\begin{aligned}
 & 2\pi \int_0^{R_1} (SA_{01}e^{jkl} + SB_{01}e^{-jkl})r_1 dr_1 \\
 & + 2\pi \int_0^{R_1} \sum_{n=2}^{\infty} (SA_{0n}e^{jk_{z,0,n}^I L} + SB_{0n}e^{-jk_{z,0,n}^I L}) J_0(k_{r,0,n}^I r_1) r_1 dr_1 \\
 & = \int_0^{R_1} \int_0^{2\pi} (A_{01}e^{jkl} + B_{01}e^{-jkl}) r_1 dr_1 d\varphi \quad (C.8) \\
 & + \int_0^{R_1} \int_0^{2\pi} \sum_{n=2}^{\infty} (A_{0n}e^{jk_{z,0,n}^I L} + B_{0n}e^{-jk_{z,0,n}^I L}) J_0(k_{r,0,n}^I \partial_1) J_0(k_{r,0,n}^I r_1) r_1 dr_1 d\varphi \\
 & + \int_0^{R_1} \int_0^{2\pi} \sum_{m=1}^{\infty} \sum_{n=1}^{\infty} (((A_{mn}^+ e^{jk_{z,m,n}^I L} + B_{mn}^+ e^{-jk_{z,m,n}^I L}) e^{-jm\theta_0} + (A_{mn}^- e^{jk_{z,m,n}^I L} + B_{mn}^- e^{-jk_{z,m,n}^I L}) e^{jm\theta_0}) \\
 & \quad J_m(k_{r,m,n}^I \partial_1) J_0(k_{r,m,n}^I r_1)) r_1 dr_1 d\varphi .
 \end{aligned}$$

Then applying equation (C.6) into equation (C.8), one can get,

$$\begin{aligned}
 & SA_{01}e^{jkl} + SB_{01}e^{-jkl})R_1/2 \\
 & = (A_{01}e^{jkl} + B_{01}e^{-jkl})R_1/2 \\
 & + \sum_{n=2}^{\infty} (A_{0n}e^{jk_{z,0,n}^I L} + B_{0n}e^{-jk_{z,0,n}^I L}) \frac{1}{k_{r,0,n}^I} J_0(k_{r,0,n}^I \partial_1) J_1(k_{r,0,n}^I R_1) \quad (C.9) \\
 & + \sum_{m=1}^{\infty} \sum_{n=1}^{\infty} (((A_{mn}^+ e^{jk_{z,m,n}^I L} + B_{mn}^+ e^{-jk_{z,m,n}^I L}) e^{-jm\theta_0} + (A_{mn}^- e^{jk_{z,m,n}^I L} + B_{mn}^- e^{-jk_{z,m,n}^I L}) e^{jm\theta_0}) \\
 & \quad \frac{1}{k_{r,m,n}^I} J_m(k_{r,m,n}^I \partial_1) J_1(k_{r,m,n}^I R_1)).
 \end{aligned}$$

Which is identical to equation (4.11).

For $t = 0, s = 2, 3, \dots, \infty$, still applying equation (C.3) and equation (C.7) to equation (C.2), there is

$$\begin{aligned}
 & 2\pi \int_0^{R_1} (SA_{01}e^{jkl} + SB_{01}e^{-jkl})r_1 J_0(k_{r,0,s}^I r_1) dr_1 \\
 & + 2\pi \int_0^{R_1} \sum_{n=2}^{\infty} (SA_{0n}e^{jk_{z,0,n}^I L} + SB_{0n}e^{-jk_{z,0,n}^I L}) J_0(k_{r,0,n}^I r_1) J_0(k_{r,0,s}^I r_1) r_1 dr_1 \\
 & = \int_0^{2\pi} \int_0^{R_1} (A_{01}e^{jkl} + B_{01}e^{-jkl}) J_0(k_{r,0,s}^I r_1) r_1 dr_1 d\varphi \quad (C.10) \\
 & + \int_0^{2\pi} \int_0^{R_1} \sum_{n=2}^{\infty} (A_{0n}e^{jk_{z,0,n}^I L} + B_{0n}e^{-jk_{z,0,n}^I L}) J_0(k_{r,0,n}^I \partial_1) J_0(k_{r,0,n}^I r_1) J_0(k_{r,0,s}^I r_1) r_1 dr_1 d\varphi \\
 & + \int_0^{2\pi} \int_0^{R_1} \sum_{m=1}^{\infty} \sum_{n=1}^{\infty} (((A_{mn}^+ e^{jk_{z,m,n}^I L} + B_{mn}^+ e^{-jk_{z,m,n}^I L}) e^{-jm\theta_0} + (A_{mn}^- e^{jk_{z,m,n}^I L} + B_{mn}^- e^{-jk_{z,m,n}^I L}) e^{jm\theta_0}) \\
 & \quad J_m(k_{r,m,n}^I \partial_1) J_0(k_{r,m,n}^I r_1) J_0(k_{r,0,s}^I r_1)) r_1 dr_1 d\varphi .
 \end{aligned}$$

Using the integral relations of Bessel function

$$\int_0^R r J_m(\lambda r) J_m(\mu r) dr = \begin{cases} \frac{R}{\lambda^2 - \mu^2} [\mu J_m(\lambda R) J'_m(\mu R) - \lambda J_m(\mu R) J'_m(\lambda R)] & (\lambda \neq \mu) \\ \frac{R^2}{2} \left\{ (J'_m(\lambda R))^2 + \left(1 - \frac{m^2}{\lambda^2 R^2}\right) (J_m(\lambda R))^2 \right\} & (\lambda = \mu). \end{cases} \quad (\text{C.11})$$

Also applying equation (C.6) to equation (C.10), one can get,

$$\begin{aligned} & (SA_{0s} e^{jk_{z,0,s}^I L} + SB_{0s} e^{-jk_{z,0,s}^I L}) J_0(k_{r,0,s}^I R_1) R_1 / 2 \\ &= \sum_{n=2}^{\infty} (A_{0n} e^{jk_{z,0,n}^I L} + B_{0n} e^{-jk_{z,0,n}^I L}) \frac{k_{r,0,n}^I}{k_{r,0,s}^I - k_{r,0,n}^I} J_0(k_{r,0,n}^I \delta_1) J'_0(k_{r,0,n}^I R_1) \\ &+ \sum_{m=1}^{\infty} \sum_{n=1}^{\infty} ((A_{mn}^+ e^{jk_{z,m,n}^I L} + B_{mn}^+ e^{-jk_{z,m,n}^I L}) e^{-jm\theta_0} + (A_{mn}^- e^{jk_{z,m,n}^I L} + B_{mn}^- e^{-jk_{z,m,n}^I L}) e^{jm\theta_0}) \\ &\quad \frac{k_{r,m,n}^I}{k_{r,0,s}^I - k_{r,m,n}^I} J_m(k_{r,m,n}^I \delta_1) J'_0(k_{r,m,n}^I R_1). \end{aligned} \quad (\text{C.12})$$

Which is identical to equation (4.12).

For $t = 1, 2, \dots, \infty, s = 1, 2, \dots, \infty$, applying equation (C.3) to equation (C.2), there is,

$$\begin{aligned} & \int_0^{2\pi R_1} \int_0^{\infty} \sum_{m=1}^{\infty} \sum_{n=1}^{\infty} (SA_{mn}^- e^{jk_{z,m,n}^I L} + SB_{mn}^- e^{-jk_{z,m,n}^I L}) J_m(k_{r,m,n}^I r_1) J_t(k_{r,t,s}^I r_1) e^{j(m-t)\varphi} r_1 dr_1 d\varphi \\ &= \int_0^{2\pi R_1} \int_0^{\infty} (A_{01} e^{jkL} + B_{01} e^{-jkL}) J_t(k_{r,t,s}^I r_1) e^{-jt\varphi} r_1 dr_1 d\varphi + \\ & \int_0^{2\pi R_1} \int_0^{\infty} \sum_{n=2}^{\infty} (A_{0n} e^{jk_{z,0,n}^I L} + B_{0n} e^{-jk_{z,0,n}^I L}) J_0(k_{r,0,n}^I r) J_t(k_{r,t,s}^I r_1) e^{-jt\varphi} r_1 dr_1 d\varphi \\ & \int_0^{2\pi R_1} \int_0^{\infty} \sum_{m=1}^{\infty} \sum_{n=1}^{\infty} (((A_{mn}^+ e^{jk_{z,m,n}^I L} + B_{mn}^+ e^{-jk_{z,m,n}^I L}) e^{-jm\theta} + (A_{mn}^- e^{jk_{z,m,n}^I L} + B_{mn}^- e^{-jk_{z,m,n}^I L}) e^{jm\theta}) \\ & \quad J_m(k_{r,m,n}^I r) J_t(k_{r,t,s}^I r_1) e^{-jt\varphi} r_1 dr_1 d\varphi. \end{aligned} \quad (\text{C.13})$$

Then applying equation (C.3) and Graf's addition theorem of Bessel function (C.7) to equation (C.13), one can get

$$\begin{aligned} & \int_0^{2\pi R_1} \int_0^{\infty} \sum_{m=1}^{\infty} \sum_{n=1}^{\infty} (SA_{mn}^- e^{jk_{z,m,n}^I L} + SB_{mn}^- e^{-jk_{z,m,n}^I L}) J_m(k_{r,m,n}^I r_1) J_t(k_{r,t,s}^I r_1) e^{j(m-t)\varphi} r_1 dr_1 d\varphi \\ &= \int_0^{2\pi R_1} \int_0^{\infty} (A_{01} e^{jkL} + B_{01} e^{-jkL}) J_t(k_{r,t,s}^I r_1) e^{-jt\varphi} r_1 dr_1 d\varphi + \end{aligned}$$

$$\int_0^{2\pi} \int_0^{R_1} \sum_{n=2}^{\infty} (A_{0n} e^{jk_{z,0,n}^H L} + B_{0n} e^{-jk_{z,0,n}^H L}) J_0(k_{r,0,n}^H \delta_1) J_t(k_{r,0,n}^H r_1) J_t(k_{r,t,s}^I r_1) r_1 dr_1 d\varphi \quad (C.14)$$

$$\int_0^{2\pi} \int_0^{R_1} \sum_{m=1}^{\infty} \sum_{n=1}^{\infty} (((A_{mn}^+ e^{jk_{z,m,n}^H L} + B_{mn}^+ e^{-jk_{z,m,n}^H L}) J_{m-1}(k_{r,m,n}^H \delta_1) J_{-t}(k_{r,m,n}^H r_1) e^{-jm\theta_0} \\ + (A_{mn}^- e^{jk_{z,m,n}^H L} + B_{mn}^- e^{-jk_{z,m,n}^H L}) J_{m+1}(k_{r,m,n}^H \delta_1) J_t(k_{r,m,n}^H r_1) e^{jm\theta_0}) \\ J_t(k_{r,t,s}^I r_1)) r_1 dr_1 d\varphi .$$

Finally applying integral relations of Bessel function (C.11) to equation (C.14), there is

$$(SA_{ts}^- e^{jk_{z,t,s}^I L_3} + SB_{ts}^- e^{-jk_{z,t,s}^I L_3}) (1 - \frac{t^2}{k_{r,t,s}^I{}^2 R_1^2}) J_t(k_{r,t,s}^I R_1) R_1 / 2 \\ = \sum_{n=2}^{\infty} (A_{0n} e^{jk_{z,0,n}^H L_3} + B_{0n} e^{-jk_{z,0,n}^H L_3}) J_t(k_{r,0,n}^H \delta_1) (\frac{k_{r,0,n}^H}{k_{r,t,s}^I{}^2 - k_{r,0,n}^H{}^2}) J_t'(k_{r,0,n}^H R_1) \\ + \sum_{m=1}^{\infty} \sum_{n=1}^{\infty} (((A_{mn}^+ e^{jk_{z,m,n}^H L_3} + B_{mn}^+ e^{-jk_{z,m,n}^H L_3}) (-1)^t J_{m-1}(k_{r,m,n}^H \delta_1) e^{-jm\theta_0} \\ + (A_{mn}^- e^{jk_{z,m,n}^H L_3} + B_{mn}^- e^{-jk_{z,m,n}^H L_3}) J_{m+1}(k_{r,m,n}^H \delta_1) e^{jm\theta_0}) \\ (\frac{k_{r,m,n}^H}{k_{r,t,s}^I{}^2 - k_{r,m,n}^H{}^2}) J_t'(k_{r,m,n}^H R_1)) . \quad (C.15)$$

Which is identical to equation (4.13).

Multiplying both sides of equation (C.1) with $J_t(k_{r,t,s}^I r_1) e^{jm\varphi}$ and integrating over the small duct region, following the procedure from equation (C.13) to equation (C.15), one can get, for $t = 1, 2, \dots, \infty, s = 1, 2, \dots, \infty,$

$$(SA_{ts}^+ e^{jk_{z,t,s}^I L} + SB_{ts}^+ e^{-jk_{z,t,s}^I L}) (1 - \frac{t^2}{k_{r,t,s}^I{}^2 R_1^2}) J_t(k_{r,t,s}^I R_1) R_1 / 2 \\ = \sum_{n=2}^{\infty} (A_{0n} e^{jk_{z,0,n}^H L} + B_{0n} e^{-jk_{z,0,n}^H L}) J_t(k_{r,0,n}^H \delta_1) (\frac{k_{r,0,n}^H}{k_{r,t,s}^I{}^2 - k_{r,0,n}^H{}^2}) J_t'(k_{r,0,n}^H R_1) \\ + \sum_{m=1}^{\infty} \sum_{n=1}^{\infty} (((A_{mn}^+ e^{jk_{z,m,n}^H L} + B_{mn}^+ e^{-jk_{z,m,n}^H L}) J_{m+t}(k_{r,m,n}^H \delta_1) e^{-jm\theta_0} \\ + (A_{mn}^- e^{jk_{z,m,n}^H L} + B_{mn}^- e^{-jk_{z,m,n}^H L}) (-1)^t J_{m-t}(k_{r,m,n}^H \delta_1) e^{jm\theta_0}) \\ (\frac{k_{r,m,n}^H}{k_{r,t,s}^I{}^2 - k_{r,m,n}^H{}^2}) J_t'(k_{r,m,n}^H R_1)) . \quad (C.16)$$

Which is identical to equation (4.14).

Appendix D: Derivation of velocity continuity boundary condition

For the velocity continuity condition between the small duct and the main duct, there is

$$v_{SA} + v_{SB} \Big|_{z=-L} = v_A + v_B \Big|_{z=-L} \quad (\text{over } S_1) , \quad (\text{D.1})$$

$$v_A + v_B \Big|_{z=-L} = 0 \quad (\text{over } (S - S_1)) . \quad (\text{D.2})$$

In which S is the cross sectional area of the main duct, S_1 is the cross sectional area of the source duct.

Multiplying both equation (D.1) and (D.2) by $J_t(k_{r,t,s}^{II} r) e^{-jt\theta}$, integrating equation (D.1) over the small duct region and (D.2) over other region, adding them together, one can obtain the following,

$$\begin{aligned} & \int_0^{2\pi R_1} \int_0^0 ((SA_{01} e^{jkL} - SB_{01} e^{-jkL}) \\ & + \sum_{n=2}^{\infty} \frac{k_{z,0,n}^I}{k} (SA_{0n} e^{jk_{z,0,n}^I L} - SB_{0n} e^{-jk_{z,0,n}^I L}) J_0(k_{r,0,n}^I r_1) \\ & + \sum_{m=1}^{\infty} \sum_{n=1}^{\infty} (\frac{k_{z,m,n}^I}{k} J_m(k_{r,m,n}^I r_1) [(SA_{mn}^+ e^{jk_{z,m,n}^I L} - SB_{mn}^+ e^{-jk_{z,m,n}^I L}) e^{-jm\varphi} \\ & + (SA_{mn}^- e^{jk_{z,m,n}^I L} - SB_{mn}^- e^{-jk_{z,m,n}^I L}) e^{jm\varphi}])) J_t(k_{r,t,s}^{II} r) e^{-jt\theta} r_1 dr_1 d\varphi \\ & = \int_0^{2\pi R_0} \int_0^0 ((A_{01} e^{jkL} - B_{01} e^{-jkL}) \\ & + \sum_{n=2}^{\infty} \frac{k_{z,0,n}^{II}}{k} (A_{0n} e^{jk_{z,0,n}^{II} L} - B_{0n} e^{-jk_{z,0,n}^{II} L}) J_0(k_{r,0,n}^{II} r) \\ & + \sum_{m=1}^{\infty} \sum_{n=1}^{\infty} (\frac{k_{z,m,n}^{II}}{k} J_m(k_{r,m,n}^{II} r) [(A_{mn}^+ e^{jk_{z,m,n}^{II} L} - B_{mn}^+ e^{-jk_{z,m,n}^{II} L}) e^{-jm\theta} \\ & + (A_{mn}^- e^{jk_{z,m,n}^{II} L} - B_{mn}^- e^{-jk_{z,m,n}^{II} L}) e^{jm\theta}])) J_t(k_{r,t,s}^{II} r) e^{-jt\theta} r dr d\theta . \end{aligned} \quad (\text{D.3})$$

In which SA_{mn}^+ , SA_{mn}^- , SB_{mn}^+ and SB_{mn}^- are amplitudes of higher-order modes in the small duct; A_{mn}^+ , A_{mn}^- , B_{mn}^+ and B_{mn}^- are amplitudes of higher-order modes in the main duct.

$k_{z,m,n}^I$ and $k_{r,m,n}^I$ represent the wave numbers in the small duct; $k_{z,m,n}^{II}$ and $k_{r,m,n}^{II}$ represent the wave numbers in the main duct.

According to equation below,

$$\int_0^{2\pi} e^{jm\varphi} d\varphi = \begin{cases} 0 & (m \neq 0) \\ 2\pi & (m = 0) \end{cases} \quad (D.4)$$

For $t = 0, s = 1$, there is

$$J_0(k_{r,0,1}^{\text{II}} r) e^{-j0\theta} = 1. \quad (D.5)$$

Applying equation (D.4) and equation (D.5) to equation (D.3), it can be rewritten as

$$\begin{aligned} & \int_0^{R_1} (SA_{01} e^{jkL} - SB_{01} e^{-jkL}) r_1 dr_1 \\ & + \sum_{n=2}^{\infty} \frac{k_{z,0,n}^{\text{I}}}{k} (SA_{0n} e^{jk_{z,0,n}^{\text{I}} L} - SB_{0n} e^{-jk_{z,0,n}^{\text{I}} L}) J_0(k_{r,0,n}^{\text{I}} r_1) r_1 dr_1 \\ & = \int_0^{R_0} (A_{01} e^{jkL} - B_{01} e^{-jkL}) r dr + \sum_{n=2}^{\infty} \frac{k_{z,0,n}^{\text{II}}}{k} (A_{0n} e^{jk_{z,0,n}^{\text{II}} L} - B_{0n} e^{-jk_{z,0,n}^{\text{II}} L}) J_0(k_{r,0,n}^{\text{II}} r) r dr. \end{aligned} \quad (D.6)$$

According to the relationship of Bessel function

$$\int_0^R r J_0(kr) dr = \frac{R}{k} J_1(kR) \quad (D.7)$$

The relationship between those two coordinates is shown in Fig C.1.

Applying equation (D.7) to equation (D.6), one can get,

$$(SA_{01} e^{jkL} - SB_{01} e^{-jkL}) R_1^2 = (A_{01} e^{jkL} - B_{01} e^{-jkL}) R_0^2. \quad (D.8)$$

Which is identical to equation (4.15).

For $t = 0, s = 2, 3, \dots, \infty$, still applying equation (D.4) to equation (D.3), there is

$$\begin{aligned} & \int_0^{2\pi} \int_0^{R_1} (SA_{01} e^{jkL} - SB_{01} e^{-jkL}) r_1 J_0(k_{r,0,s}^{\text{II}} r) dr_1 d\varphi \\ & + \int_0^{2\pi} \int_0^{R_1} \sum_{n=2}^{\infty} \frac{k_{z,0,n}^{\text{I}}}{k} (SA_{0n} e^{jk_{z,0,n}^{\text{I}} L} - SB_{0n} e^{-jk_{z,0,n}^{\text{I}} L}) J_0(k_{r,0,n}^{\text{I}} r_1) J_0(k_{r,0,s}^{\text{II}} r) r_1 dr_1 d\varphi + \\ & \int_0^{2\pi} \int_0^{R_0} \sum_{m=1}^{\infty} \sum_{n=1}^{\infty} ((SA_{mn}^+ e^{jk_{z,m,n}^{\text{I}} L} - SB_{mn}^+ e^{-jk_{z,m,n}^{\text{I}} L}) e^{-jm\varphi} + (SA_{mn}^- e^{jk_{z,m,n}^{\text{II}} L} - SB_{mn}^- e^{-jk_{z,m,n}^{\text{II}} L}) e^{jm\varphi}) \\ & \quad \frac{k_{z,m,n}^{\text{I}}}{k} J_m(k_{r,m,n}^{\text{I}} r_1) J_0(k_{r,0,s}^{\text{II}} r)) r_1 dr_1 d\varphi \\ & = \int_0^{2\pi} \int_0^{R_0} (A_{01} e^{jkL} - B_{01} e^{-jkL}) J_0(k_{r,0,s}^{\text{II}} r) r dr d\theta \\ & + \int_0^{2\pi} \int_0^{R_0} \sum_{n=2}^{\infty} \frac{k_{z,0,n}^{\text{II}}}{k} (A_{0n} e^{jk_{z,0,n}^{\text{II}} L} - B_{0n} e^{-jk_{z,0,n}^{\text{II}} L}) J_0(k_{r,0,n}^{\text{II}} r) J_0(k_{r,0,s}^{\text{II}} r) r dr d\theta. \end{aligned} \quad (D.9)$$

Using the integral relations of Bessel function

$$\int_0^R r J_m(\lambda r) J_m(\mu r) dr = \begin{cases} \frac{R}{\lambda^2 - \mu^2} [\mu J_m(\lambda R) J'_m(\mu R) - \lambda J_m(\mu R) J'_m(\lambda R)] & (\lambda \neq \mu) \\ \frac{R^2}{2} \left\{ (J'_m(\lambda R))^2 + \left(1 - \frac{m^2}{\lambda^2 R^2}\right) (J_m(\lambda R))^2 \right\} & (\lambda = \mu). \end{cases} \quad (D.10)$$

Also using the Graf's addition theorem of Bessel function to the left of equation (D.9),

$$J_m(\mu r) e^{-jm\theta} = \sum_{p=-\infty}^{\infty} J_{m+p}(\mu \delta_1) J_p(\mu r_1) e^{-j(p\varphi + m\theta_0)}. \quad (D.11)$$

One can get equation below,

$$\begin{aligned} & (SA_{01} e^{jkL} - SB_{01} e^{-jkL}) \frac{R_1}{k_{r,o,s}^{II}} J_0(k_{r,o,s}^{II} \delta_1) J_1(k_{r,o,s}^{II} R_1) \\ & + \sum_{n=2}^{\infty} \left(\frac{k_{z,0,n}^I}{k} (SA_{0n} e^{jk_{z,0,n}^I L} - SB_{0n} e^{-jk_{z,0,n}^I L}) \right. \\ & \quad \left. \frac{R_1 k_{r,o,s}^{II}}{k_{r,0,n}^I{}^2 - k_{r,o,s}^{II}{}^2} J_0(k_{r,o,s}^{II} \delta_1) J_0(k_{r,0,n}^I R_1) J'_0(k_{r,o,s}^{II} R_1) \right) \\ & + \sum_{m=1}^{\infty} \sum_{n=1}^{\infty} \left(\frac{k_{z,m,n}^I}{k} ((SA_{mn}^+ e^{jk_{z,m,n}^I L} - SB_{mn}^+ e^{-jk_{z,m,n}^I L}) + (SA_{mn}^- e^{jk_{z,m,n}^I L} - SB_{mn}^- e^{-jk_{z,m,n}^I L})) \right. \\ & \quad \left. \frac{R_1 k_{r,o,s}^{II}}{k_{r,m,n}^I{}^2 - k_{r,o,s}^{II}{}^2} J_m(k_{r,o,s}^{II} \delta_1) J_m(k_{r,m,n}^I R_1) J'_m(k_{r,o,s}^{II} R_1) \right) \\ & = \frac{k_{r,o,s}^{II}}{k} (A_{0s} e^{jk_{z,o,s}^{II} L} - B_{0s} e^{-jk_{z,o,s}^{II} L}) \frac{R_0^2}{2} J_0^2(k_{r,o,s}^{II} R_0). \end{aligned} \quad (D.12)$$

Which is identical to equation (4.16).

For $t = 1, 2, \dots, \infty, s = 1, 2, \dots, \infty$, applying equation (D.4) to equation (D.3), it can be written as,

$$\begin{aligned} & \int_0^{2\pi} \int_0^{R_1} (SA_{01} e^{jkL} - SB_{01} e^{-jkL}) J_1(k_{r,t,s}^{II} r) e^{-jm\theta} r_1 dr_1 d\varphi \\ & + \int_0^{2\pi} \int_0^{R_1} \sum_{n=2}^{\infty} \frac{k_{z,0,n}^I}{k} (SA_{0n} e^{jk_{z,0,n}^I L} - SB_{0n} e^{-jk_{z,0,n}^I L}) J_0(k_{r,0,n}^I r_1) J_1(k_{r,t,s}^{II} r) e^{-jm\theta} r_1 dr_1 d\varphi \\ & + \int_0^{2\pi} \int_0^{R_1} \sum_{m=1}^{\infty} \sum_{n=1}^{\infty} (((SA_{mn}^+ e^{jk_{z,m,n}^I L} - SB_{mn}^+ e^{-jk_{z,m,n}^I L}) e^{-jm\varphi} + (SA_{mn}^- e^{jk_{z,m,n}^I L} - SB_{mn}^- e^{-jk_{z,m,n}^I L}) e^{jm\varphi}) \\ & \quad \frac{k_{z,m,n}^I}{k} J_m(k_{r,m,n}^I r_1) J_1(k_{r,t,s}^{II} r) e^{-jm\theta} r_1 dr_1 d\varphi \\ & = \int_0^{2\pi} \int_0^{R_0} \sum_{m=1}^{\infty} \sum_{n=1}^{\infty} (((A_{mn}^+ e^{jk_{z,m,n}^I L} - B_{mn}^+ e^{-jk_{z,m,n}^I L}) e^{-jm\theta} + (A_{mn}^- e^{jk_{z,m,n}^I L} - B_{mn}^- e^{-jk_{z,m,n}^I L}) e^{jm\theta}) \\ & \quad \frac{k_{z,m,n}^{II}}{k} e^{-jm\theta} J_m(k_{r,m,n}^{II} r) J_1(k_{r,t,s}^{II} r) r dr d\theta. \end{aligned} \quad (D.13)$$

Then applying the Graf's addition theorem of Bessel function (D.11) to the left of equation (D.13), one can get

$$\begin{aligned}
 & \int_0^{2\pi R_1} \int_0^{2\pi R_1} (SA_{01} e^{jkL} - SB_{01} e^{-jkL}) J_t(k_{r,t,s}^{II} \partial_1) J_0(k_{r,t,s}^{II} r_1) e^{-jt\theta_0} r_1 dr_1 d\varphi \\
 & + \int_0^{2\pi R_1} \int_0^{2\pi R_1} \sum_{n=2}^{\infty} \frac{k_{z,o,n}^I}{k} (SA_{0n} e^{jk_{z,o,n}^I L} - SB_{0n} e^{-jk_{z,o,n}^I L}) J_0(k_{r,o,n}^I r_1) J_t(k_{r,t,s}^{II} \partial_1) J_0(k_{r,t,s}^{II} r_1) e^{-jt\theta_0} r_1 dr_1 d\varphi \\
 & + \int_0^{2\pi R_1} \int_0^{2\pi R_1} \sum_{m=1}^{\infty} \sum_{n=1}^{\infty} ((SA_{mn}^+ e^{jk_{z,m,n}^I L} - SB_{mn}^+ e^{-jk_{z,m,n}^I L}) J_{-t}(k_{r,t,s}^{II} r) J_{m-t}(k_{r,t,s}^{II} \partial_1) e^{-jt\theta_0} \\
 & \quad + (SA_{mn}^- e^{jk_{z,m,n}^I L} - SB_{mn}^- e^{-jk_{z,m,n}^I L}) J_t(k_{r,t,s}^{II} r) J_{m+t}(k_{r,t,s}^{II} \partial_1) e^{jm\theta_0}) \\
 & \quad \frac{k_{z,m,n}^I}{k} J_m(k_{r,m,n}^I r) r_1 dr_1 d\varphi \\
 & = \int_0^{2\pi R_0} \int_0^{2\pi R_0} \sum_{m=1}^{\infty} \sum_{n=1}^{\infty} ((A_{mn}^+ e^{jk_{z,m,n}^I L} - B_{mn}^+ e^{-jk_{z,m,n}^I L}) e^{-jm\theta} + (A_{mn}^- e^{jk_{z,m,n}^I L} - B_{mn}^- e^{-jk_{z,m,n}^I L}) e^{jm\theta}) \\
 & \quad \frac{k_{z,m,n}^{II}}{k} e^{-jt\theta} J_m(k_{r,m,n}^{II} r) J_t(k_{r,t,s}^{II} r) r dr d\theta.
 \end{aligned} \tag{D.14}$$

Finally applying the integral relations of Bessel function (D.10) to equation (D.14), there is

$$\begin{aligned}
 & (SA_{01} e^{jkL} - SB_{01} e^{-jkL}) e^{-jt\theta_0} J_t(k_{r,t,s}^{II} \delta_1) \frac{R_1}{k_{r,t,s}^{II}} J_1(k_{r,t,s}^{II} R_1) \\
 & + \sum_{n=2}^{\infty} \left(\frac{k_{z,o,n}^I}{k} (SA_{0n} e^{jk_{z,o,n}^I L} - SB_{0n} e^{-jk_{z,o,n}^I L}) e^{-jt\theta_0} \right. \\
 & \quad \left. J_t(k_{r,t,s}^{II} \delta_1) \frac{R_1 k_{r,t,s}^{II}}{k_{r,o,n}^I - k_{r,t,s}^{II}} J_0'(k_{r,t,s}^{II} R_1) J_0(k_{r,o,n}^I R_1) \right) \\
 & + \sum_{m=1}^{\infty} \sum_{n=1}^{\infty} ((SA_{mn}^+ e^{jk_{z,m,n}^I L} - SB_{mn}^+ e^{-jk_{z,m,n}^I L}) (-1)^m J_{t-m}(k_{r,t,s}^{II} \delta_1) \\
 & \quad + (SA_{mn}^- e^{jk_{z,m,n}^I L} - SB_{mn}^- e^{-jk_{z,m,n}^I L}) J_{m+t}(k_{r,t,s}^{II} \delta_1)) \\
 & \quad \frac{k_{z,m,n}^I}{k} \left(\frac{R_1 k_{r,t,s}^{II}}{k_{r,m,n}^I - k_{r,t,s}^{II}} \right) J_m'(k_{r,t,s}^{II} R_1) J_m(k_{r,m,n}^I R_1) e^{-jt\theta_0} \\
 & = \frac{k_{z,t,s}^{II}}{k} (A_{ts}^- e^{jk_{z,t,s}^{II} L} - B_{ts}^- e^{-jk_{z,t,s}^{II} L}) \frac{R_0^2}{2} \left(1 - \frac{t^2}{k_{r,t,s}^{II} R_0^2} \right) J_t^2(k_{r,t,s}^{II} R_0).
 \end{aligned} \tag{D.15}$$

Which is identical to equation (4.17).

Multiplying both equations (D.1) and (D.2) by $J_t(k_{r,t,s}^{II} r) e^{jt\theta}$ and integrating equation (D.1) over the small duct region and (D.2) over other region, then adding them together, following the procedure from equation (D.13) to equation (D.15), one can get,

$$\begin{aligned}
 & (SA_{01} e^{jkL} - SB_{01} e^{-jkL}) e^{jt\theta_0} J_t(k_{r,t,s}^{II} \delta_1) \frac{R_1}{k_{r,t,s}^{II}} J_1(k_{r,t,s}^{II} R_1) \\
 & + \sum_{n=2}^{\infty} \left(\frac{k_{z,o,n}^I}{k} (SA_{0n} e^{jk_{z,o,n}^I L} - SB_{0n} e^{-jk_{z,o,n}^I L}) e^{jt\theta_0} \right. \\
 & \quad \left. J_t(k_{r,t,s}^{II} \delta_1) \frac{R_1 k_{r,t,s}^{II}}{k_{r,o,n}^I - k_{r,t,s}^{II}} J_0(k_{r,t,s}^{II} R_1) J_0(k_{r,o,n}^I R_1) \right) \\
 & + \sum_{m=1}^{\infty} \sum_{n=1}^{\infty} \left[(SA_{mn}^+ e^{jk_{z,m,n}^I L} - SB_{mn}^+ e^{-jk_{z,m,n}^I L}) J_{m+t}(k_{r,t,s}^{II} \delta_1) \right. \\
 & \quad \left. + (SA_{mn}^- e^{jk_{z,m,n}^I L} - SB_{mn}^- e^{-jk_{z,m,n}^I L}) (-1)^m J_{t-m}(k_{r,t,s}^{II} \delta_1) \right] \\
 & \quad \frac{k_{z,m,n}^I}{k} \left(\frac{R_1 k_{r,t,s}^{II}}{k_{r,m,n}^I - k_{r,t,s}^{II}} \right) J_m(k_{r,t,s}^{II} R_1) J_m(k_{r,m,n}^I R_1) e^{jt\theta_0} \\
 & = \frac{k_{z,t,s}^{II}}{k} (A_{ts}^+ e^{jk_{z,t,s}^{II} L} - B_{ts}^+ e^{-jk_{z,t,s}^{II} L}) \frac{R_0^2}{2} \left(1 - \frac{t^2}{k_{r,t,s}^{II} R_0^2} \right) J_t^2(k_{r,t,s}^{II} R_0).
 \end{aligned} \tag{D.16}$$

Which is identical to equation (4.18).

Appendix E: The procedure to calculate the amplitudes of the pressures by using reference measurement results (point source)

The measurements work in this investigation can be divided into two groups, which are: reference measurements and direct measurements. The direct measurement results are used to compare with the theoretical calculated results (predictions) obtained by the model calculation. The reference measurement results are used to calculate the amplitudes of acoustic properties in the duct. According to the experimental set-up shown in Fig 7.3, the two reference measurement positions are randomly chosen at position 1 ($0.15m(100\%R), 0, -2.33m(-74.3\%L)$) and position 2 ($0.15m(100\%R), 3*\pi/4, -1.5m(-50\%L)$). The reason to use two reference measurements is given in Section 5.4.2. The procedure of the application of the reference measurements is given as below using the plane wave source as an example:

1. In equation (5.12) or equation (7.32), let the amplitude of the volume velocity U to be unity, then substitute the coordinate of the reference position 1 into matrix X of this equation, it is possible to get the relative amplitudes of A_{mn}, B_{mn} for duct without a simple aperture situation or $A_{mn}, B_{mn}, \dots, F_{mn}$ for duct with a simple aperture device situation. Substituting these relative amplitudes and coordinate of the reference point into equation (5.1), it is possible to get the relative acoustic pressure at that reference point.
2. Comparing this relative acoustic pressure with the actual pressure (reference measurement), it is possible to get the ratio between the relative acoustic pressure and actual pressure (P_{act}/P_{comp}). This ratio should be equal to the actual amplitude of the volume velocity U .
3. Applying the procedure 1-2 to the reference measurement position 2, it is possible to get another group of the actual amplitude volume velocity U .
4. Taking the average of these two volume velocity as the actual amplitude of the volume velocity and substituting this actual amplitude into equation (5.12) or equation (7.32) again, the real values of the amplitudes, such as A_{mn}, B_{mn} for duct without a simple aperture device or $A_{mn}, B_{mn}, \dots,$ and F_{mn} for duct with a simple aperture device, are obtained.

5. Substituting these real amplitudes and the coordinates of the direct measurement points into acoustic pressure equation (5.1), it is possible to get the theoretical calculated acoustic pressures (predictions) at the direct measurement points. Comparing these calculated pressures (predictions) with those directly measured pressures (direct measurements), one can check the errors of the theoretical calculations.

For the duct without a simple aperture device situation, just following the procedure (1-5), it is possible to get the calculated results and then decompose the in duct acoustic field through two reference measurement results.

For the duct with a simple aperture device situation, the acoustic pressures for the before orifice field can be obtained by following the same procedure (1-5). For the after orifice field, there are two different groups of situations. For situations other than those two specific situations proposed in Chapter 7, one can still obtain the acoustic pressures by using the same procedure (1-5) and the reference measurements presented above.

However for those two specific situations, another two reference measurement positions, which are located at position 3 ($0.15m(100\%R), 0, -0.12m(-4\%L)$) and position 4 ($0.15m(100\%R), 2 * \pi / 3, -0.20m(-6.67\%L)$) respectively in the after orifice field, are taken. So for the after orifice field calculation, in the procedure 1-5, substituting position 1 and position 2 with position 3 and position 4, following the same procedure, it is possible to get the calculated results for the after orifice field.

Appendix F: The procedure to calculate the amplitudes of the pressures by using reference measurement results (plane wave source)

The measurements work in this investigation can be divided into two groups, which are: reference measurements and direct measurements. The direct measurement results are used to compare with the theoretical calculated results (predictions) obtained by the model calculation. The reference measurement results are used to calculate the amplitudes of acoustic properties in the duct. According to the experimental set-up shown Fig 8.2, the two reference measurement positions are randomly chosen at position 1 $(0.15m(100\%R), 0, -2.33m(-74.3\%L))$ and position 2 $(0.15m(100\%R), 3*\pi/4, -1.5m(-50\%L))$. The reason to use two reference measurements is given in Section 5.4.2. The procedure of the application of the reference measurements is given as below:

1. In equation (6.3) or equation (8.2), let the amplitude of the incident wave in the source duct (SA_{01}) to be unity, then substitute the coordinate of the reference position 1 into matrix X of this equation, it is possible to get the relative amplitudes of SB_{01} , A_{mn} , B_{mn} for duct without a simple aperture device situation or SB_{01} , A_{mn} , B_{mn} , ..., F_{mn} for duct with a simple aperture device situation. Substituting these relative amplitudes and coordinate of the reference point into acoustic pressure equation (5.1), it is possible to get the relative acoustic pressure at that reference point.
2. Comparing this relative acoustic pressure with the actual pressure (reference measurement), it is possible to get the ratio between the relative acoustic pressure and actual pressure (P_{act} / P_{comp}). This ratio should be equal to the actual amplitude of the incident wave in the source duct (SA_{01}).
3. Applying the procedure 1-2 to the reference measurement position 2, it is possible to get another actual amplitude of the incident wave in the source duct (SA_{01}).
4. Taking the average of these two SA_{01} as the actual amplitude of the incident wave in the source duct and substituting this actual amplitude into equation (6.3) or

equation (8.2) again, the real values of the amplitudes, such as SB_{01} , A_{mn} , B_{mn} for duct without a simple aperture device or SB_{01} , A_{mn} , B_{mn} ..., and F_{mn} for duct with a simple aperture device, are obtained.

5. Substituting these real amplitudes and the coordinates of the direct measurement points into acoustic pressure equation (5.1), it is possible to get the theoretically calculated acoustic pressures (predictions) at the direct measurement points. Comparing the calculated pressures (predictions) with the directly measured pressures (direct measurements), one can check the errors of the theoretical calculations.

For the duct without a simple aperture device situation, just following the procedure (1-5), it is possible to get the calculated results and then decompose the in duct acoustic field through two reference measurement results.

For the duct with a simple aperture device situation, the acoustic pressures for the before orifice field can be obtained by following the same procedure (1-5). For the after orifice field, there are two different groups of situations. For situations other than those two specific situations proposed in Chapter 8, one can still obtain the acoustic pressures by using the same procedure (1-5) and the reference measurements presented above.

However for those two specific situations, another two reference measurement positions, which are located at position 3 ($0.15m(100\%R), 0, -0.12m(-4\%L)$) and position 4 ($0.15m(100\%R), 2 * \pi / 3, -0.20m(-6.67\%L)$) respectively in the after orifice field, are taken. So for the after orifice field calculation, in the procedure 1-5, substituting position 1 and position 2 with position 3 and position 4, following the same procedure, one can get the calculated results for the after orifice field.



